Role of ATM in the repair of blocked DNA double-strand breaks

Realizada en CABIMER
(Departamento de Biología del Genoma)

Memoria presentada por
Alejandro Álvarez Quilón

Para optar al grado de Doctor en
Biología Molecular y Biomedicina
3 Febrero 2017

Dirigida por
Felipe Cortés Ledesma

Tutor
Andrés Aguilera López

B

ABSTRACT

Ataxia telangiectasia (A-T) is caused by loss-of-function mutations in the ATM (Ataxia Telangiectasia mutated) kinase, and represents a paradigm for cancer predisposition and neurodegenerative syndromes linked to deficiencies in the DNA-damage response (DDR). The role of ATM as a key regulator of signalling following DNA double-strand breaks (DSBs) has been dissected in extraordinary detail, but the impact of this process on DSB repair still remains controversial; while ATM-deficient cells and organisms are hypersensitive to DSB-inducing agents, they display only subtle repair defects. Here, we develop novel genetic and molecular tools to modulate the structure of DSB ends and demonstrate that ATM is indeed required for efficient and accurate DSB rejoining, but exclusively when the ends are irreversibly blocked. We therefore identify the nature of ATM involvement in DSB repair, presenting blocked DNA ends as a possible pathogenic trigger of A-T.

RESUMEN

La Ataxia telangiectasia (A-T) es un síndrome causado por mutaciones de pérdida de función en la kinasa ATM (Ataxia Telangiectasia mutated). A-T representa el paradigma de los síndromes caracterizados por predisposición a cáncer y neurodegeneración asociados a deficiencias en la respuesta a daño en el ADN. La función de dicha proteína como regulador principal en la señalización celular en respuesta a roturas de doble cadena en el ADN se ha definido en detalle, aunque aún se desconoce el impacto que provoca en su reparación. Mientras que la deficiencia de ATM causa una alta sensibilidad a agentes que inducen roturas de doble cadena, no se han detectado grandes defectos en la reparación de estas lesiones. En esta Tesis se desarrollan nuevos métodos moleculares y genéticos para modificar la estructura de los extremos de las roturas de doble cadena en el ADN. Mediante estas técnicas se demuestra que ATM es esencial para la correcta reparación de roturas de doble cadena, pero exclusivamente cuando los extremos de éstas están bloqueados. De esta manera identificamos la función de ATM en la reparación de roturas de doble cadena y sugerimos que los extremos bloqueados en el ADN pueden ser la causa de la Ataxia-telangiectasia.

INDEXES

TABLE OF CONTENTS

FIGURES INDEX

TABLES INDEX

ABBREVIATIONS

A-T	Ataxia-telangiectasia
AOA1	Ataxia with oculomotor apraxia type 1
AOA4	Ataxia with oculomotor apraxia type 4
ATLD	A-T like disorder
ATM	Ataxia-telangiectasia Mutated
ATR	Ataxia Telangiectasia And Rad3-Related Protein
bp	Base pair
c-NHEJ	core Non-homologous end joining
CC	Cleavage complex
CGH	Comparative genomic hybridization
CNS	Central Nervous System
CSR	Class-switch Recombination
DAPI	4',6-diamino-2-fenilindol
DDR	DNA Damage Response
DN	Double negative
DNA	Deoxyribonucleic acid
DNA-PK	DNA-dependent protein kinase
DNA-PKcs	DNA-dependent protein kinase catalytic subunit
DP	Double positive
DSB	Double-strand break
dsDNA	double-stranded DNA
EDTA	Ethylenediaminetetraacetic acid
GFP	Green fluorescent protein
HDAC4	Histone deacetylase 4
HR	Homologous recombination
Ig	Immunoglobulin
IR	Ionizing radiation
LET	Linear energy transfer
Lys	Lysine
MEFs	Mouse embryonic fibroblasts

MMEJ	Microhomology-mediated end joining
MRN	MRE11-RAD50-NBS1 complex
NHEJ	Non-homologous end joining
nt	Nucleotide
PCR	Polymerase chain reaction
PIKK	Phosphatidylinositol 3-kinase-related kinases
Rb	Retinoblastoma
RNA	Ribonucleic acid
ROS	Reactive oxygen species
RS-SCID	Radiation-sensitive severe combined immunodeficiency
rSAP	Recombinant shrimp alkaline phosphatase
RSS	Recombination signal sequence
SCID	Severe combined immunodeficiency
Ser	Serine
SLOPE	Selective Labelling Of Protein-blocked Ends
SP	Single positive
SSB	Single-strand break
ssDNA	Single-stranded DNA
TCR	T-cell receptor
TDP	Tyrosyl-DNA-phosphodiesterase
TDP1	Tyrosyl-DNA-phosphodiesterase 1
TDP2	Tyrosyl-DNA-phosphodiesterase 2
TdT	Terminal nucleotide transferase
Thr	Threonine
TOP1	Topoisomerase 1
TOP1cc	Topoisomerase 1 cleavage complex
TOP2	Topoisomerase 2
TOP2cc	Topoisomerase 2 cleavage complex
VZ-SVZ	Ventricular and Subventricular zones

I. INTRODUCTION

I. INTRODUCTION

1. DNA Damage

The discovery of DNA as the cellular component responsible for the storage of genetic information marks a turning point in the molecular biology field. Initially, DNA was considered as a highly stable molecule. However, researchers promptly realised that DNA was largely susceptible to spontaneous decay and it frequently suffers damage (Lindahl 1993). It is estimated that each cell in the human body suffers tens of thousands of lesions per day (De Bont & van Larebeke 2004; Vilenchik & Knudson 2003). To overcome this threat, cells have developed complex mechanisms of repair, which efficiently revert DNA damage and minimize the adverse outcomes of these lesions (Lindahl & Wood 1999; Ciccia & Elledge 2010). Unfortunately, DNA repair is not always efficient, and unrepaired damage can accumulate under certain conditions (Altieri et al. 2008). For instance, when the DNA repair machinery is impaired, or when tissues confront high levels of damage, lesions in the DNA may scape cellular control. In consequence, these alterations in the genetic material threaten the correct functioning of cells by causing a large number of deleterious outcomes, ranging from mutations and epigenetic changes, to gross rearrangement of chromosomes. Eventually, accumulation of DNA damage can impair essential functions, leading to uncontrolled cell division, premature cell death and aging (Freitas & De Magalhães 2011; Surova & Zhivotovsky 2013; Jackson & Loeb 2001). Therefore, DNA damage is considered as a key determinant in human disease, being a hallmark in cancer, neurodegenerative processes and several congenital syndromes.

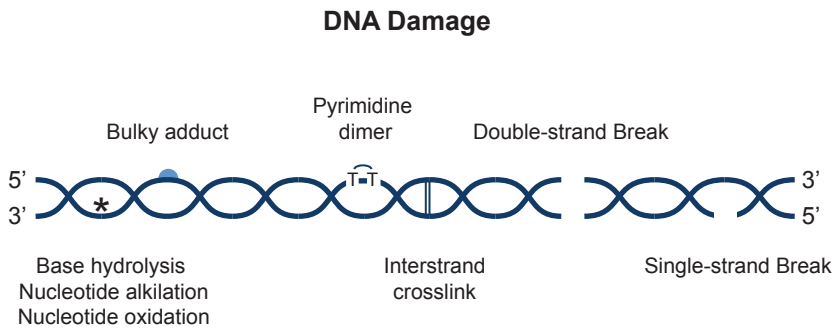

Figure 1: Types of DNA damage. Different type of lesions can alter DNA structure. Alkylation and oxidation of nucleotides, hydrolysis of bases or interstrand crosslink and pyrimidine dimers are commonly found. Chemicals can also interact with the DNA molecule forming bulky adducts altering DNA structure. Single-strand breaks (SSBs) and double-strand breaks (DSBs) interrupt continuity of the DNA backbone.

1.1. DNA Double-strand Breaks

DNA can suffer different types of damage (Figure 1). On one hand, the chemical structure of canonical nucleotides can be altered, either in the ribose or in the nitrogenous base. Indeed, we can find a plethora of these modifications; base hydrolysis, oxidation and alkylation of nucleotides or bulky adduct formation, pyrimidine dimers or interstrand covalent bonds, amongst others (Marnett 2000). On the other hand, the strand continuity of the DNA backbone can be interrupted. Within this type of lesion, the most frequent are single-strand breaks (SSBs), which are generated when one strand of the double helix is broken (Caldecott 2008). Thus, the continuity and structure of the molecule is not compromised, since an intact copy is maintained in the complementary strand, which is used as template for accurate repair. However, cells face situations in which both of the two strands of the helix are broken. Thus, double-strand breaks (DSBs) present

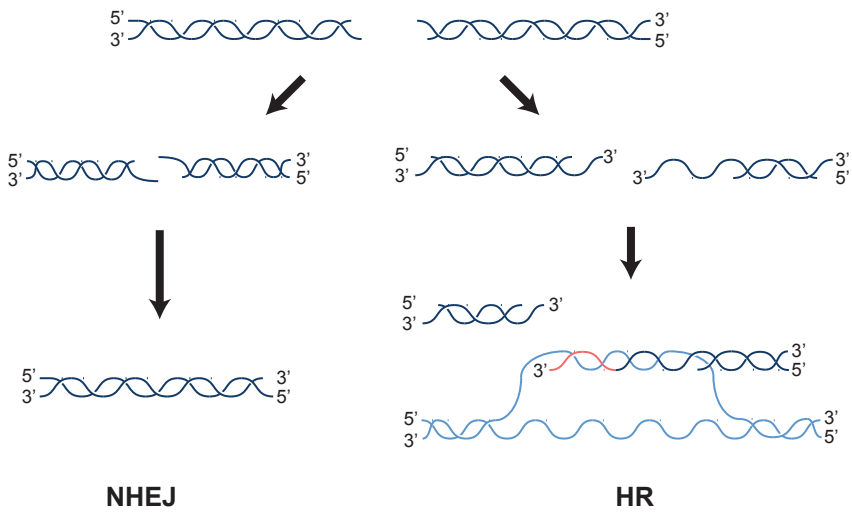

Figure 2: Pathways for the repair of DSBs in mammalian cells. DSBs are repaired by non-homologous end joining (NHEJ) pathway by direct ligation of DNA ends (left). In the homologous recombination (HR) pathway (right), DNA ends are resected by 5' strand degradation and newly formed 3' protruding ends invade a homologous sequence, which is used as template for repair.

a huge threat to cells, since the continuity of the DNA molecule is lost. On top of this, cells cannot rely on a complementary strand to directly copy the genetic information, increasing the likelihood of mutations.

1.2. DSB repair in mammalian cells

To avoid DSB accumulation, there are two conceptually different ways in which these lesions can be repaired: by undergoing the direct ligation of the ends or by using a DNA template to copy and restore genetic information. Based on this, the two main pathways in mammals are non-homologous end joining (NHEJ) and homologous recombination

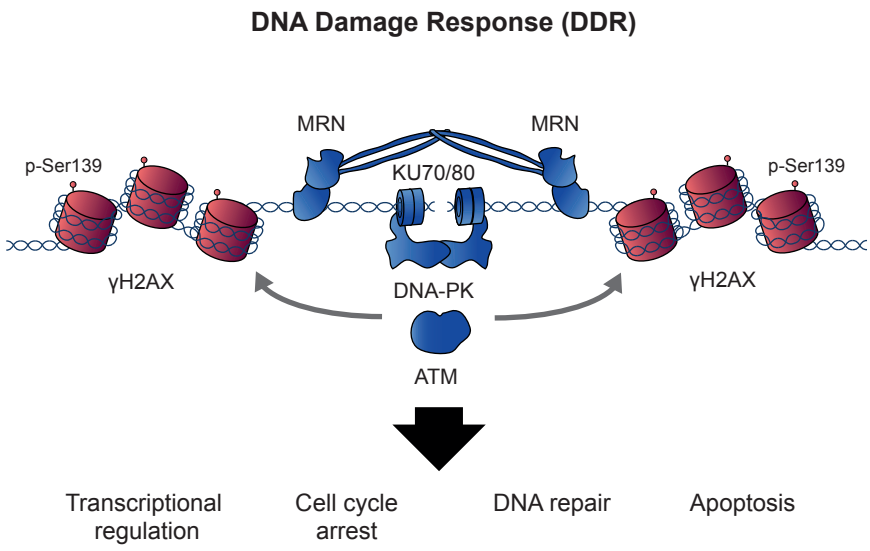

Figure 3: DNA damage response (DDR). DNA double strand-breaks are detected by KU70/80 heterodimer and the MRN complex. KU70/80 associated with DNA ends recruits DNA-PK catalytic subunit (DNA-PKcs) forming the DNA-PK holoenzyme. This, in collaboration with ATM activation triggers the DDR signalling cascade. MRN complex collaborate to tether DSB ends and to maintain ATM active in the vicinity of DSBs. This leads to H2AX phosphorylation in Ser139 (γH2AX), promoting the recruitment of downstream factors. The DDR modulates important cellular functions such as transcriptional regulation, cell cycle arrest, repair of the lesion, and apoptosis.

(HR), respectively (Thompson 2012). As can be seen in Figure 2, while NHEJ directly ligates the ends of a DSB and is active throughout most of the cell cycle, HR requires a template to proceed, and preferentially uses sister chromatids which are only available during S/G2 cell cycle phases (Rothkamm et al. 2003). NHEJ machinery detects and tethers DSB ends, promoting their joining by a final step of ligation. Importantly, it can promote repair of numerous types of termini, but the use of homology is always restricted to 1-4 base pairs. Conversely, HR-repair requires a first step of resection, which trims the

5' ends of DSBs to generate large 3' protruding ends. This single-strand DNA (ssDNA) structure is essential for the steps of homology search and strand invasion of the template required for HR repair (for an extensive review see Mehte & Haber 2014). Alternatively, DSBs can be channelled through a backup pathway called microhomology-mediated end joining (MMEJ) (McVey & Lee 2008; Frit et al. 2014). For this, DSB ends are processed in a similar manner as in HR resection, but instead of using a homologous template to restore genetic information they are directly ligated. However, MMEJ uses larger regions of homology (5-25 bp), leading to deletions of the flanking sequence. MMEJ pathway is associated with complex chromosomal rearrangements and abnormalities such as deletions, inversions and translocations. Nevertheless, to which extent MMEJ pathway physiologically contributes to DNA repair and its relevance is still a matter of debate (Sfeir & Symington 2015).

These repair pathways are integrated in the so-called DNA damage response (DDR), a network that orchestrates the direct repair of lesions, in coordination with the regulation of important cellular processes, such as cell cycle progression, gene transcription, and chromosome segregation (Figure 3) (Harper & Elledge 2007). This large-scale mechanism is associated with changes at all cellular levels, so a vast number of proteins and post-translational modifications are associated with the DDR (Polo & Jackson 2011). Traditionally, they have been classified in different groups depending on their function (Harrison & Haber 2006). There are sensor proteins that efficiently recognize specific lesions in DNA. These early factors activate transducer proteins, which in turn recruit mediators that exponentially amplify the signal. Eventually, effector proteins have

the capacity to carry out the repair of the lesions, activate cell cycle checkpoint, remodel the chromatin or interfere with other cellular processes involved. It is worth noting that despite general factors are involved in all types of DNA damage, specific proteins are also required depending on the nature of the damage and the cellular status. In the particular case of DSBs, they are rapidly detected by the KU70/80 heterodimer and MRE11-RAD50-NBS1 (MRN) complex; two factors which display great affinity for DNA ends (Downs & Jackson 2004; Williams et al. 2007). After DSB recognition, DNA-PKcs, ATM and ATR, three kinases of the hosphatidylinositol 3-kinase-related kinases (PIKK) family, can be recruited to sites of damage serving as transducers of the signal (Falck et al. 2005). Importantly, while DSB induction robustly activates ATM and DNA-PKcs, ATR specifically requires ssDNA for its activation (Falck et al. 2005; Shiotani & Zou 2009a). For this, ATR is activated when DSBs are resected and ssDNA regions are formed, channelling repair toward HR (Shiotani & Zou 2009b). ATR activation is not restricted to DSBs, since it is also activated upon replicative stress during proliferative stages of the cell cycle, sensing damage in replication forks (Ward & Chen 2001; Falck et al. 2005; Cimprich & Cortez 2008). Once they are active, ATR and ATM are crucial in the regulation of effector proteins such as CHK1, CHK2 and the tumour suppressor p53, which are crucial in the arrest of the cell cycle (Rouse & Jackson 2002). This allows cells to repair DNA before proceeding to the next stage in the presence of damage. Eventually, in the cases in which DNA damage proves to be irreparable, DDR participates in triggering apoptosis (Roos & Kaina 2013). This pathway is essential to remove potentially dangerous cells from the organism when DNA damage exceeds their repair capacity.

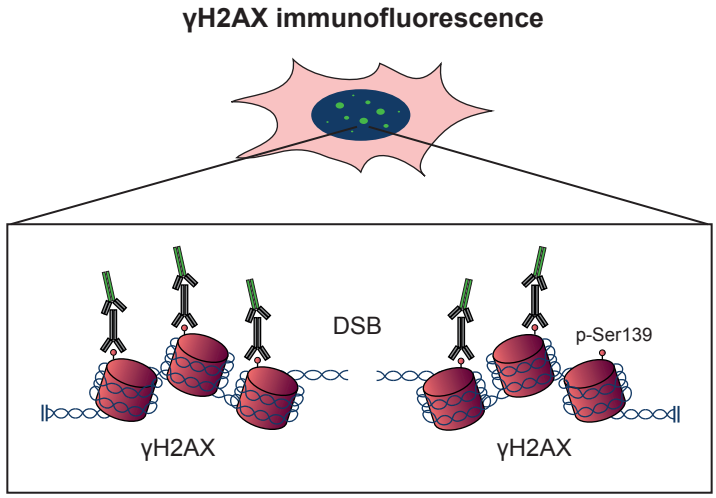

Figure 4: γH2AX immunofluorescence foci. Post-translational phosphorylation in Ser139 of histones H2AX, known as γH2AX, largely expands along megabases flanking DSBs. By performing immunofluorescence using γH2AX specific primary antibody and fluorochrome-conjugated secondary antibody, discrete foci can be observed under the microscope.

A relevant characteristic of DDR factors is their local accumulation in the vicinity of DSBs (Polo & Jackson 2011). Taking advantage of specific antibodies against these factors, discrete foci within the nuclei can be observed under the microscope by immunofluorescence techniques (Costes et al. 2010). Historically, this approach has helped researchers to analyse DSB induction and disappearance in cells and tissues under several experimental setups. Specifically, one of the most upstream events in DSB signalling is the redundant phosphorylation in Ser139 of histone variant H2AX (known as γH2AX), which can be carried out by ATM, ATR and DNA-PKcs (Firsanov et al. 2011). This post-translational modification has been used as a trustable DSB marker, since the amount of DSBs present in a particular cell has been proven to correlate with the number of discrete foci observed by immunofluorescence (Figure 4) (Kinner et al.

2008; Löbrich et al. 2010).

Beside its technical application in the study of DSB repair, γH2AX modification is physiologically relevant for the DDR. Indeed, this post-translational modification extends rapidly along megabases flanking both sides of a break, acting as a scaffold for a large number of downstream factors. Amongst them, MRN-complex member NBS1, 53BP1 and BRCA1 are functionally relevant proteins that form irradiation-induced foci (Bekker-Jensen & Mailand 2010; Shroff et al. 2004; Ünal et al. 2004). These factors are critical for DSB repair even when they do not posses any enzymatic activity, since their recruitment would dictate the preferential repair pathway that will operate in a specific lesion (Chapman et al. 2012; Panier & Boulton 2014). The physiological importance of the recruitment of DDR factors is supported by a detailed dissection of numerous knockout mouse model and cells derived from human patients (Celeste et al. 2002; Barlow et al. 1996; Lou et al. 2006). These have unveiled several outcomes of an inefficient DDR, such as increased genome instability and hypersensitivity to DSB inducing agents (Franco et al. 2006; Craig H Bassing et al. 2002). Moreover, this can lead to infertility and immunodeficiency, two processes in which HR and NHEJ pathways have key roles respectively. Thus, these observations support the notion that DSB repair and the DDR are two closely adjusted mechanisms that rely on a large number of factors, and which have to be precisely controlled to avoid deleterious outcomes for cells and organisms.

1.3. Non-homologous end joining (NHEJ)

In mammalian cells, the NHEJ is the major pathway for the repair of DSBs.

Indeed, it has been proven to operate throughout the cell cycle (Rothkamm et al. 2003), being specifically relevant during G0/G1, when HR is largely inactive (Huertas et al. 2008). In addition, it contributes to a significant fraction of DSB repair even during S and G2 phases, when HR reaches its maximum activity (Mao et al. 2008). Typical NHEJ pathway can be divided into different steps (Figure 5) (Davis & Chen 2013). First of all, DSBs are efficiently recognized by the ring-shaped heterodimer formed by KU70 and KU80. Then, DSB ends are bridged and stabilized when DNA-PKcs is recruited to form the DNA-PK complex. This promotes the inward translocation of the KU70/80 ring and DNA-PKcs kinase becomes active, phosphorylating itself and other downstream factors. The exact role that DNA-PKcs phosphorylation cascade plays in NHEJ is still a matter of debate, but DNA-PKcs autophosphorylation seems to be a required step

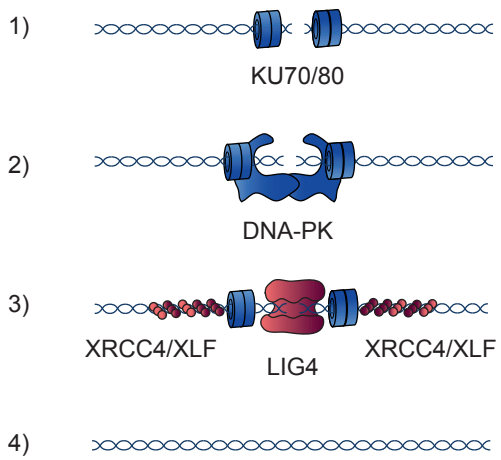

Figure 5: The Non-homologous end joining (NHEJ) pathway. First, DSBs are recognized by the ring-shaped KU70/80 heterodimer. DNA-PK catalytic subunit (DNA-PKcs) is recruited and activated, translocating KU70/80 ring inward the break. This forms the DNA-PK holoenzyme that phosphorylates several downstream factors. Finally, DNA-PK suffers conformational changes allowing XRCC4/XLF filament to form and the recruitment of Ligase IV, which ligates DNA ends.

for NHEJ to proceed (Lees-Miller & Meek 2003). Finally, helped by accessory factors such as XLF/Cernunnos, XRCC4 and PAXX proteins, DNA Ligase IV is recruited to catalyse the ligation of the (Mahaney et al. 2012; Ochi et al. 2015), how NHEJ factors disengage when DSB repair is completed or ligation is unfeasible is still unknown. It has been proposed that KU80 is polyubiquitilated and degraded by the proteasome to release the ring from the rejoined DNA molecule (Postow 2011; Feng & Chen 2012). However, recent work has described that p97/VCP can promote structural changes in KU70/80 to release the ring from DNA (van den Boom et al. 2016)

Importantly, the precise chemical structure that terminal nucleotides of DSBs display are highly influential for NHEJ, since DNA Ligase IV enzyme requires compatible ends harbouring a 5' phosphate and a 3' hydroxyl groups for its activity (Lindahl & Barnes 1992). Thus, when DSB termini display aberrant structures that block DSB ends, they cannot be directly joined (Povirk 2012). There are to ways in which this can be bypassed (Figure 6). First, cells posses enzymatic activities that can directly convert these structures into ligatable ends. This does not compromise the nucleotide sequence, and we have termed this process as *unblocking*. Conversely, a more general pathway called *processing* can remove chemical modifications from DSB termini by nucleotide trimming. Beside the specific chemical structure, NHEJ is also influenced by the compatibility between DSB ends. Indeed, it is highly efficient in the rejoining of DSB ends with complementary ssDNA overhangs, but it can also proceed with DSBs harbouring incompatible overhangs and blunt ends (Smith et al. 2001; Raghavan & Raman 2004; Gu et al. 2007). For this, NHEJ accessory proteins carry out end processing

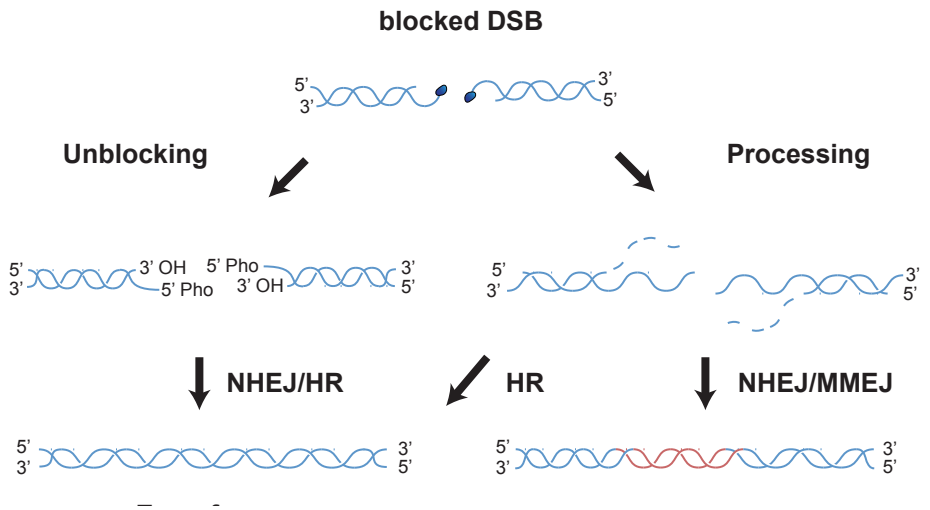

Figure 6: Unblocking and processing of DSBs. Unblocking pathways directly convert ends into 5' phosphate and 3' hydroxyl but the nucleotide sequence remains intact, promoting error-free repair (left). Processing can also facilitate blocked DSBs repair by removing aberrant structures from DNA ends by nucleotide trimming (right). This pathway can lead to error-prone repair when non-templated repair pathways such as NHEJ or MMEJ are used.

until ligatable termini are generated (Strande et al. 2012). Thus, single-stranded overhangs and blunt ends can be trimmed by nucleases, and ssDNA gaps that are newly formed can be filled by DNA polymerases (Budman et al. 2007). In this regard, the nuclease Artemis and Polymerases μ and λ have been demonstrated to contribute to the efficiency of NHEJ (Riballo et al. 2004; Ramsden 2011; Malyarchuk et al. 2013). Interestingly, biochemical characterization of Artemis has revealed different enzymatic activities that can support DSB end unblocking and processing, such as 5'-3' exonuclease activity on single-stranded DNA and endonuclease activity in the ssDNA/dsDNA junction of single-strand overhangs (Chang & Lieber 2016).

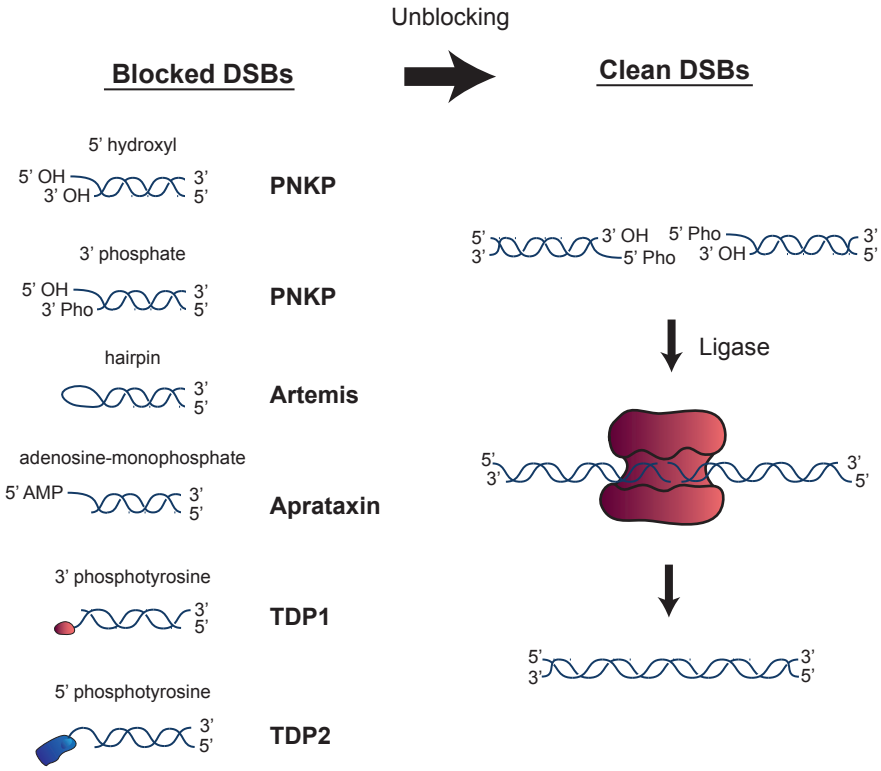

Figure 7: Structure of DNA ends and unblocking enzymes. DSB termini can be blocked by numerous chemical structures in vivo. Several unblocking enzymes are present in mammalian cells and efficiently convert these structures in clean 5' phosphate and 3' hydroxyl DSB termini (left). These clean DSBs can be in theory, directly repaired with the only enzymatic activity of a ligase (right).

1.4. Relevance of DSB end structure

As mentioned above, DSB repair mechanisms are conditioned by the chemical structure that DNA molecules present at their termini. Thus, if a DSB harbours clean ends, which are 5' phosphate (5' Pho) and 3' hydroxyl (5' OH), in theory, they can be

rejoined with the only enzymatic activity of a ligase (Figure 7). In contrast to clean DSBs, there are some situations in which cells can encounter blocked DSBs harbouring aberrant structures at their ends (Povirk 2012). Indeed, a large number of different chemical structures have been described to impede efficient repair. Thus, as advanced previously, cells rely on two alternative pathways that can convert blocked ends into clean termini before they can be ligated). First of all, cells count on a wide variety of unblocking enzymes that directly catalyse the removal of specific aberrant structures from ends (Strande et al. 2012). Thus, each type of structure can count with one or several dedicated enzymatic activities to modify a particular type of blocked DSB. Importantly, the unblocking process does not compromise the nucleotide sequence. In contrast to this situation, when cells do not possess unblocking enzymes for a specific structure, DSBs have to be processed by nucleotide trimming upstream of the ends (Figure 6). If a non-templated repair pathway such as NHEJ is used, processing could lead to mutations and gain or loss of nucleotides in the joining site. Thus, unblocking activities are remarkably important when DSBs are channelled through NHEJ-dependent repair. Consistently, there are a vast number of unblocking enzymes that have been linked to DSB repair, including TDP1, TDP2, PNKP, Aprataxin, Ku and Artemis (Figure 6). Each of these factors efficiently detects and removes specific chemical blockages in DNA ends, facilitating DSB repair by NHEJ. Nonetheless, in contrast to NHEJ, HR invariably requires processing of 5' strand to generate resected 3' ends (Huertas 2010). Thus, blockages in the 5' termini have negligible impact on this pathway (Liao et al. 2016).

2. Sources of DNA Double-strand Breaks

It is estimated that an average human cell suffers around ten DSBs per day. The incidence of this type of damage in the DNA is largely minor if compared with other type of lesions. However, due to the great impact that DSBs display on cellular and physiological homeostasis is key to understand how they arise during human life. It is important to mention that despite DSBs being considered a serious threat for human physiology, there are crucial physiological processes such as gametogenesis and lymphocyte development that directly rely on the induction of endogenously programmed DSB for their correct function (Lam & Keeney 2015; Bednarski & Sleckman 2012; Stavnezer et al. 2008). Thus, in these special cases, organisms must activate enzymes that induce DSBs in a controlled environment. In addition to this, there are other multiple factors that can increase the incidental induction of DSBs (Mills et al. 2003).

2.1. Programmed DNA Double-strand Breaks

Gametogenesis generates haploid cells that are ready to form offspring. During this process, meiotic recombination is essential to increases genetic variation in populations and to ensure the efficient segregation of chromosomes (Baudat et al. 2013). For this, during prophase I stage of meiosis, homologous chromosomes associate forming a tetrad or bivalent, composed by four chromatids. Then, a precise number of DSBs are induced by the SPO11 recombinase in random sites along chromosomes. These

are blocked DSBs, since SPO11 protein remains covalently bound to the 5' termini of the DNA. Importantly, these lesions are channelled through a HR-dependent repair (Lam & Keeney 2015). For this, DSBs are resected and 3' protruding ends can invade homologous chromosomes that are in close proximity in the bivalent. This mechanism is key for meiotic recombination, since HR can be modulated to favour the formation of crossovers, which facilitates proper chromosome segregation and eventually promotes the interchange of genetic information between different parental chromosomes, generating unique combinations of gametes (Longhese et al. 2009). Consistently, human syndromes that are caused by mutations in genes involved in HR repair may display infertility, and polymorphisms in DSB repair genes carried by healthy individuals have been associated with impaired fertility (Cooke & Saunders 2002; Ji et al. 2013).

Another example of programmed DSBs in mammals is the induction of cleavage during T and B lymphocyte development. Induction of DSBs and their repair account for the highly diverse repertoire of immunoglobulins (Igs) and T cell receptors (TCR) that supports diversification of immune cells to recognize and adapt to new pathogens (Schatz & Swanson 2011). There are two different mechanisms in which programmed DSBs are induced, the rearrangement of TCR and Igs by V(D)J recombination in immature lymphocytes (Craig H. Bassing et al. 2002), and the isotype switching of the constant region of Igs in mature activated B-cells, induced by class switch recombination (CSR) (Stavnezer et al. 2008). In similar ways, both processes require DSB induction and a proficient NHEJ pathway for its completion. In fact, defects in c-NHEJ efficiency or a decrease in its accuracy, lead to immunodeficiency and/or lymphoma predisposition,

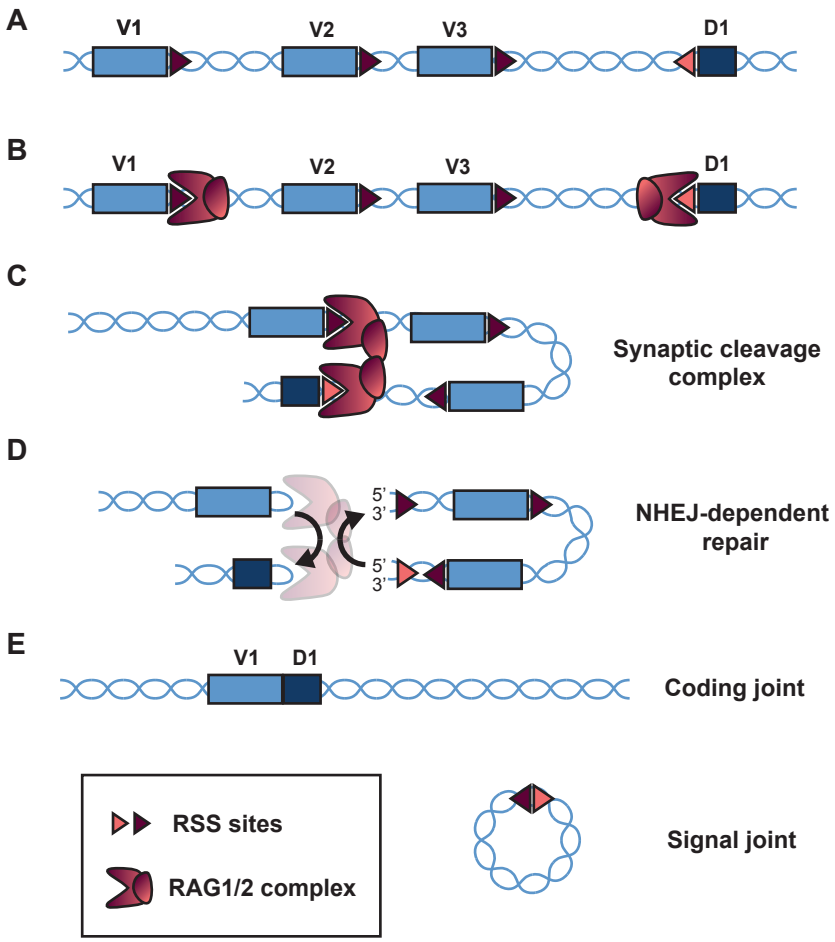

Figure 8: V(D)J recombination during lymphocyte maturation. A) T-cell receptor and Immunoglobulin genes contain arrays of different V, D and J coding segments, flanked by recombination signal sequences (RSS). **B)** RAG1/2 recombinase recognizes two different RSS sequences amongst the V, D or J segments. **C)** It brings genomic regions together forming the synaptic cleavage complex. **D)** It promotes DNA cleavage in each RSS, forming two DSBs. Each of them is formed by a hairpin structure in the coding end, and a blunt-end in the signal end. **E)** NHEJ pathway joins the two blunt-ends forming a circular extrachromosomal signal joint. Artemis endonuclease catalyzes the opening of the hairpin-ends, licensing them for NHEJ repair. This results in a lymphocyte precursor with a specific combination of single V, D and J regions rearranged together.

respectively (Bassing & Alt 2004). T cell receptor (TCR) or Immoglobulin (Ig) genes contain an array conformed by several different coding variable (V), diversity (D) and joining (J) segments, which are flanked by recombination signal sequences (RSS). In early stages of T and B lymphocyte maturation, V(D)J recombination rearranges a single combination of V, J, and in some cases, D segments in a random fashion (Craig H. Bassing et al. 2002; Zhang & Swanson 2008). At the molecular level, the mechanism that underlies V(D)J recombination is highly complex, but extensive multidisciplinary studies have been performed along decades to elucidate the steps involved (for an extensive review see (Craig H. Bassing et al. 2002)). To initiate the process RAG1/2 recombinase recognizes RSS sites adjacent to a pair of coding segments (Figure 8) (Schatz & Swanson 2011). Then, it brings these chromosomal sites together forming what is called the synaptic complex, and eventually promotes the cleavage of the DNA precisely in the RSS sequence. Due to its special catalytic mechanism, RAG1/2 recombinase generates two DBS, and each of them is formed by a hairpin-end, adjacent to the coding segment, and a blunt end, adjacent to the RSS site (McBlane et al. 1995). Therefore, two types of DSBs are induced, two blunt and clean ends and two blocked by a hairpin structure. The two blunt ends are joined together by core NHEJ machinery (KU70/80, DNA-PKcs, XLF, XRCC4 and DNA Ligase IV). This yields what is known as signal joints, forming extrachromosomal circles of RSS sequences ligated. The two hairpin-ends remaining are ligated together to form what is known as the coding join. In addition to c-NHEJ, repair of coding ends requires a previous step of hairpin opening. This is carried out by the endonuclease Artemis, which beyond its general role in processing can act as an unblocking enzyme for this type of DSBs (Kurosawa & Adachi 2010; Moshous et

al. 2001). Thus, upon DNA repair by NHEJ, two different coding sequences out of the multiple possibilities are joined. Importantly, Artemis does not cleave at the hairpin-apex (Chang & Lieber 2016). Due to this, it generates overhangs in which nucleotides are added by terminal nucleotide transferase (TdT) and DNA polymerases μ and λ (Thai & Kearney 2005; Weill & Reynaud 2008). This step is key to introduce sequence variations that will be eventually transcribed and translated in the final protein product, resulting in the large variability in antigen-binding domains of Igs and TCRs (Gauss & Lieber 1996).

2.2. Incidental DNA Double-strand Breaks

Beside programmed physiological processes, there are numerous ways in which DSBs may arise in cells (Mills et al. 2003). They can be induced either by exogenous or endogenous sources. Probably, for its importance for cancer treatment and the study of DNA repair, ionizing radiation (IR) has been the paradigm of an exogenous source of DSBs. When IR passes through cells, it modifies the chemical structure of the molecules by inducing intermediary radical ions, free radicals and excited states. This affects several cellular components, such as lipid membranes, proteins, nucleic acids, etc. Nevertheless, due to the importance for cellular homeostasis, DNA molecule is especially vulnerable. IR induces multiple types of DNA damage, such as nucleotide modifications, SSB and DSBs, leading to oncogenic mutations and cell death (Ward 1988). However, due to its capacity to promote cell death specifically in highly proliferating cells, low energy radiation such as X- or γ-rays, are commonly used in radiotherapy for cancer treatment. There are other

types of radiation that present higher energy deposition rates, which is termed high LET (Linear Energy Transfer). For instance, α-particles present in outer space or produced by radon gas and uranium^{238} emitters are high LET. This type of radiation induces a larger number of complex and clustered damage in the DNA molecule, displaying a higher number of mutations and increasing its oncogenic potential (Hada & Georgakilas 2008). It is worth mentioning that DSBs induced by IR are largely heterogeneous. Terminal nucleotides can harbour a plethora of aberrant structures that differs from the canonical nucleotides, and clustered lesions can be present near DNA ends. The likelihood of the induction of more complex or blocked DSBs precisely correlates with increasing LET. On top of this, IR-induced DSBs can contain 5' overhang, 3' overhang, and rarely blunt ends. Besides IR, there are other important exogenous sources of DSB induction, such as the exposure to chemicals that directly interfere with the DNA molecule, or the presence of enzymes with endonuclease activity, such as restriction enzymes. In addition, agents that normally induce SSBs can produce DSBs when two of these lesions arise in close proximity in a random manner.

Endogenous processes also contribute in a large extent to the cellular formation of DSBs. For instance, DNA replication can indirectly generate DSBs when it proceeds through SSB lesions (Kuzminov 2001; Cortés-Ledesma & Aguilera 2006). Therefore, there are important factors that largely contribute to SSB induction, and indirectly to DSB formation, such as the oxidative attack of reactive oxygen species (ROS) to the DNA molecule, or the abortive action of Topoisomerase 1. It is estimated that amongst the large number of SSB that are accumulated in human cells, at least 1% scape cellular

control, being converted in DSBs in each cell division (Vilenchik & Knudson 2003). Additionally, other endogenous enzymatic activities that are key for DNA metabolism and cellular function present a direct source of DSB induction. Indeed, the catalytic action of topoisomerase 2 (TOP2) requires the cleavage of both strands of the double helix to promote topological changes. In normal conditions, the resealing of the cleavage is largely favoured. However, in certain situations, such as the presence of nearby DNA lesions, or the exposure to specific chemical agents, topoisomerase 2 normal activity is impaired and it can lead to the induction of DSBs (Deweese & Osheroff 2009). Since TOP2 abortive action is of the utmost importance to our work, this process will be dissected in detail.

3. DNA Topoisomerases

DNA in its relaxed state assumes the B conformation; a right-handed helix in which each turn is 34 Å and it is formed by 10 base pairs (Richmond & Davey 2003). If stretched out, the 3 billions base pairs (bp) contained in each human cell would measure approximately two meters long. Since it has to be packed within the cellular nucleus, an intricate compartment of just around 6 μm of diameter, DNA has to wind tightly around histones and adopt different topological states (Cavalli & Misteli 2013). Furthermore, when DNA is subject to metabolic processes such as replication, transcription and chromosomal segregation, it suffers torsional stress or supercoiling, and it can usually be found tangled, knotted and catenated (Gilbert & Allan 2014). These constraints are normally removed by topoisomerases, enzymes that allow changes of topology by

inducing transient cleavages in the DNA (for an extensive review see (Pommier et al. 2016). Indeed, topoisomerases are essential proteins that have been found in every form of life studied to date. Chemically, their catalytic activity is based on a nucleophilic attack performed by an oxygen molecule of a tyrosine residue, which cleaves DNA in the phosphate backbone. Importantly, this phosphate group remains transiently attached to the catalytic tyrosine of the protein by a covalent phosphotyrosine bond, and this is used to allow DNA topology to be conveniently changed. Based on the structure and their mechanism of action, they can be classified into type I and II, and each of them in subfamilies A and B. While type I topoisomerases cleave only one strand of the DNA, type II requires ATP hydrolysis to promote the transport of an intact DNA molecule

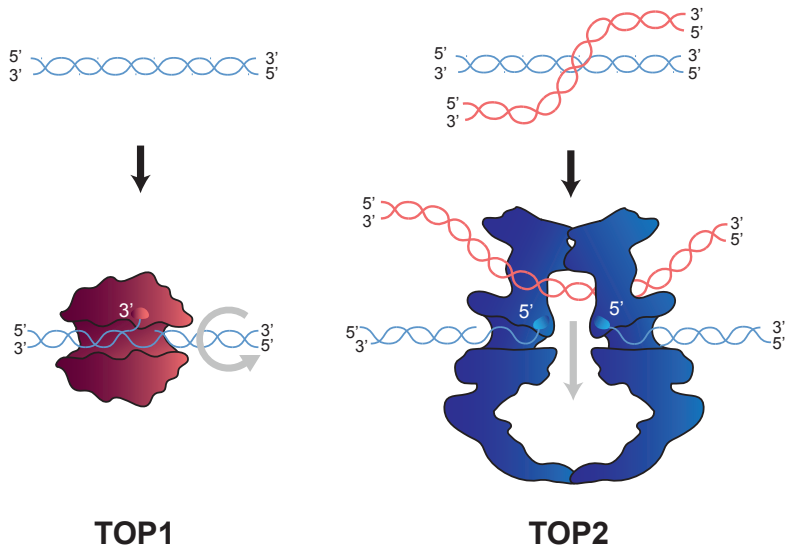

Figure 9: Main topoisomerase activities in mammals. Topoisomerase 1 (TOP1) introduces a cleavage in a single strand of the double helix, allowing DNA to rotate along its axis. TOP1 remains covalently bound to the 3' end of the DNA by its catalytic tyrosine (left). Topoisomerase 2 (TOP2) homodimer induces the simultaneous cleavage of both strands of the double helix. The gap formed is used to pass another segment of DNA. TOP2 remains covalently bound to 5' DNA ends by the catalytic tyrosine residues (right).

through a cleavage induced in both strands of another segment of DNA (Figure 9). Type IA topoisomerases display specific cleaving polarity, remaining attached to the 5' end of the DNA, while type IB remain bound to 3' ends. In the case of type IIA and IIB, they also display 5' cleaving polarity, these subfamilies being differentiated by structural considerations.

Humans express several different topoisomerases, which carry out specific tasks during a large range of physiological processes, such as replication, transcription, chromosomal segregation and DNA repair. Representative members of the different families are TOP3α and TOP3β (type IA), TOP1 and mitochrondrial TOP1 (type IB) and two isoforms of type IIA topoisomerases, α and β (termed TOP2A and TOP2B). To point out the importance of these enzymes, deletions of any of their orthologous in rodents lead to lethality. Indeed, homozygous mutations in *Top1*, *Top2a*, and *Top3a* genes lead to defects in early stages of embryo development, and *Top2b* and *Top3b* mutant mice die shortly after birth (Morham et al. 1996; St. Pierre et al. 2002; Yang et al. 2000; Kwan & Wang 2001; Li & Wang 1998)

TOP2A and TOP2B share many similarities but they have separate nuclear functions. While TOP2A is essential for cell proliferation and it is almost absent in differentiated cells, TOP2B activity is important for the removal of topological constraints generated by the RNA polymerase machinery (Pommier et al. 2016). TOP2B is essential for neural differentiation and brain development. Increasing evidences suggest that TOP2B has alternative specific roles. TOP2B has been shown to regulate transcriptional

status of precise genes controlled by different stimuli. In this regard, its activity has been linked to the transcriptional regulation in response to hormones, such as estrogen and androgen (Haffner et al. 2010; Bong-Gun et al. 2006). Moreover, it has been described that TOP2B activity controls early response gene expression, which are key for synapse formation, neurite outgrowth and the maintenance of the balance between excitatory and inhibitory synapses in the adult central nervous system (Madabhushi et al. 2015).

3.1. Topoisomerase 2 and DNA Double-strand Breaks

Due to the singularities of type II topoisomerases, which cleave simultaneously in both strands of the double helix, their activity has been considered as a double-edged sword (Nitiss 2009). Thus, TOP2 catalytic cycle is a tightly regulated process. First of all, a TOP2 homodimer interacts with an intact region of DNA and then, it captures another DNA segment (Figure 10). TOP2 catalytic sites induce the simultaneous cleavage of both strands of the double helix in the first DNA molecule. The gap created is used to pass the previously captured DNA segment through, and after this transaction, TOP2 ensures the correct joining of the cleavage by religating DNA ends and releases the transported segment. Therefore, through this mechanism DNA molecules can be untangled, unknotted and decatenated. If the two segments of DNA involved in the process belong to the same molecule, this process also allows removal of supercoiling.

Importantly, there is a crucial intermediate during this catalytic cycle termed the cleavage complex (TOP2cc), in which DNA is cleaved in both strands and each subunit of

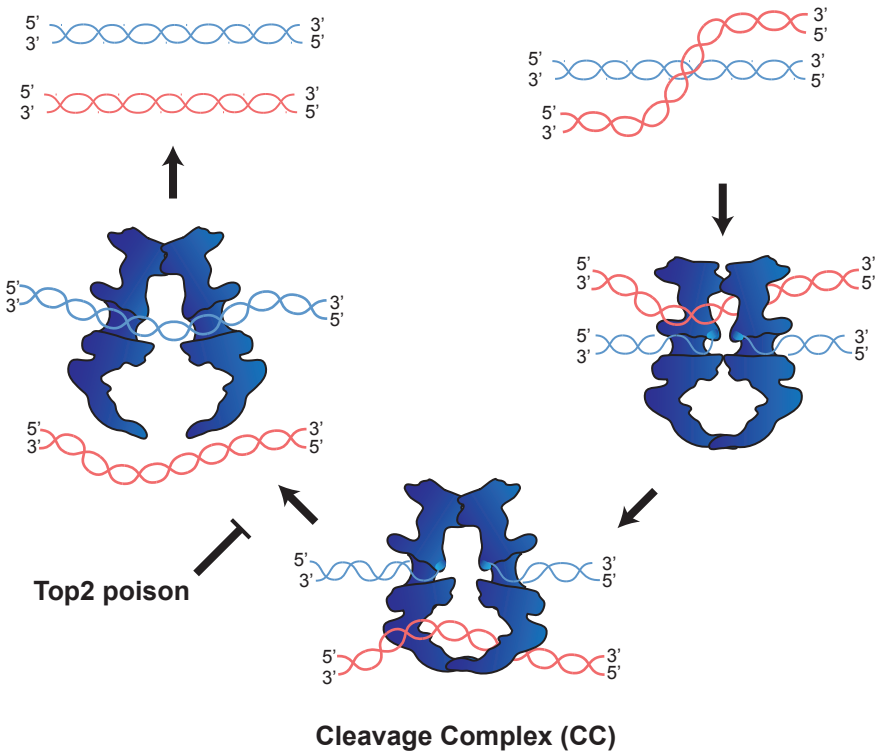

Figure 10: Catalytic cycle of Topoisomerase 2. TOP2 homodimer interacts with an intact DNA molecule and captures another segment. Then, it promotes the cleavage of both strands of the double-helix forming the cleavage complex (TOP2cc), in which each subunit of TOP2 is covalently linked to 5′ phosphate ends by the catalytic tyrosine residues. The gap created is used to pass through the captured DNA segment. Finally, TOP2 ensures the religation of the cleavage and the other fragment is released. TOP2-poisons can stabilize the TOP2cc state.

TOP2 is covalently linked to the 5' phosphate ends by the catalytic tyrosine. The cleavage complex is normally a short-term intermediate, since the topoisomerase rapidly joins the ends as the DNA segment has been passed through the gap. However, the exposure to chemicals known as TOP2-poisons, or the presence of nearby lesions in the DNA, can stabilize TOP2cc (Deweese & Osheroff 2009). These intermediates are considered an obstacle for DNA metabolism, since as long as the protein remains covalently attached

to the DNA molecule, genetic information cannot be accessed properly. Thus, if the transcription machinery and replication forks encounter a cleavage complex, TOP2 protein is signalled for degradation by the 26S proteasome (Zhang et al. 2006) (Figure 11). This leads to disassembly of the TOP2 homodimer, and in consequence a DSB is newly formed. It is important to remark that if TOP2-poison is removed before TOP2 degradation proceeds, TOP2cc reverts and the enzyme can continue with its normal catalytic cycle. However, once that a DSB is in fact produced after TOP2 degradation, it is detected and signalled by the DNA damage response machinery. Transcription-generated DSBs are more dependent on the proteasome for DDR signalling. In any case, DDR signalling cascade proceeds in an indistinguishable manner compared to DSB induced by IR or other known damaging agent (Sunter et al. 2010). Therefore, γH2AX histone modification expands in the regions adjacent to the lesion. Nevertheless, TOP2-induced DSBs are intrinsically different in structure, since they are characterised by harbouring a peptide adduct resulting of the proteosomal degradation of TOP2, which is covalently bound to each 5' end of the DNA by a tyrosyl-phosphodiester bond. Therefore, they are considered blocked DSBs, and in consequence unblocking by a 5' tyrosyl-DNA-phosphodiesterase (5'TDP) activity or end processing must take place to ensure the repair of these lesions.

It is worth noting that the amount of DSBs induced by TOP2 poisons depends on its activity, which is extremely high in proliferative cells (Heck et al. 1988). Based on this, TOP2-poisons have been commonly used as antineoplastic drugs in the treatment of a broad range of tumours, including malignant lymphomas, sarcomas, leukemias, and

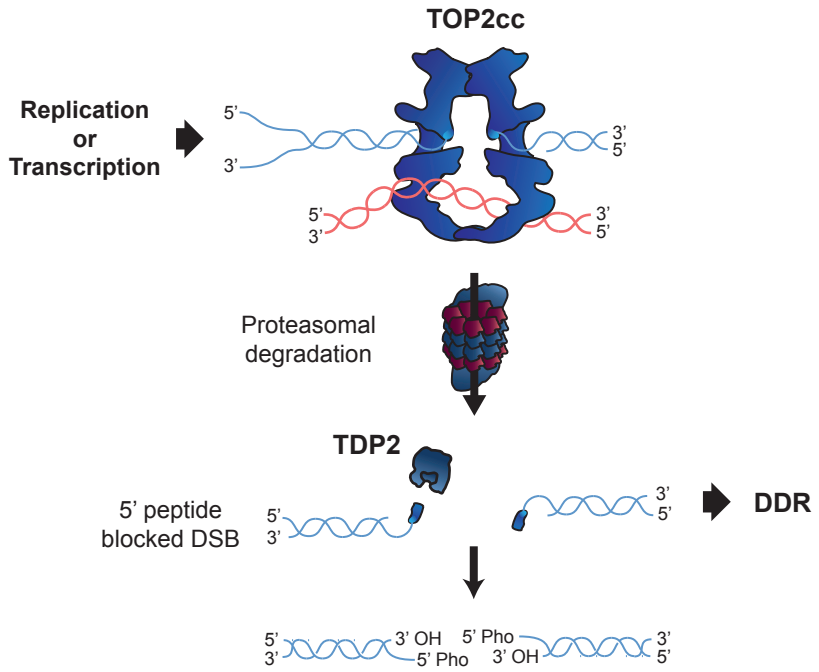

Figure 11: Induction of DSBs by the abortive activity of Topoisomerase 2. If ongoing replication or transcription encounters a TOP2cc, TOP2 homodimer is signalled and degraded by the 26S proteasome. Degradation of TOP2cc leads to the formation of a irreversible DSB characterized by peptide adducts covalently bound to 5' DNA ends by a phosphotyrosine bond, which lead to the activation of the DNA damage response. TDP2 promotes the unblocking of 5' phosphotyrosines, converting them into clean 5' phosphate and 3' hydroxyl DSBs.

lung, ovarian, breast and testicular cancers (Pommier et al. 2010). However, similarly to other chemotherapeutic agents, TOP2-targeting drugs are only partially selective for tumour cells, resulting in unwanted toxicity in normal tissues. Thus, therapy-associated chromosome translocations linked to secondary leukemias have been described as a consequence of TOP2 induced DSB by these chemotherapeutical agents (Pendleton et al. 2014). Consistently, breakpoints in some of these translocations have been correlated

with preferential sites of TOP2 activity (Lovett et al. 2001). Therefore, the study of the molecular mechanism underlying TOP2 activity and the repair of DSBs induced by its abortive action is essential, not just for the understanding of cellular mechanisms, but also for important issues in human health.

Amongst the large number of TOP2-poisons that have been developed up to date, we can find etoposide (VP-16), teniposide (VM-26), and DNA intercalators such as doxorubicin and amsacrine (m-AMSA). These molecules inhibit DNA religation step of TOP2 catalytic cycle, after TOP2cc is formed. Additionally, other molecules such as quinolones, ellipticines, azatoxins, and the natural flavonoid genistein increase the likelihood of the formation of TOP2cc (Pommier et al. 2010). Remarkably, beside their clinical relevance in cancer treatment, these molecules have been widely used as DSB inducing agents in the study of DNA repair, since they have demonstrated a high capacity to induce breakage. Due to its specificity, fast kinetics in TOP2cc induction and solubility, etoposide has been probably the most used TOP2-poison in the DNA repair field up to date. Nevertheless, it is worth mentioning that on top of DSBs, etoposide has been described to generate SSBs (Muslimovic et al. 2011).

3.2. Tyrosyl-DNA-phosphodiesterase 2 (TDP2)

The enzyme Tyrosyl-DNA-phosphodiesterase 1 (TDP1), a member of the Phospholipase D family, was described to remove 3'-phosphotyrosines, 3'-phosphoglycolates and 3'-nucleosides from SSB termini (Connelly & Leach 2004).

TDP1 activity has been shown to account for the repair of TOP1-induced damage, since degradation of TOP1 cleavage complexes generates SSBs characterized by 3' phosphotyrosines. Moreover, TOP1 activity can also induce DSB preferentially during S-phase, since DNA replication machinery converts 3' blocked SSBs into DSBs. Under this condition, TDP1 has been proposed to promote efficient NHEJ of 3' phosphotyrosine blocked DSBs (Heo et al. 2015). Moreover, 5'TDP activity was described in Sacharomyces cerevisae TDP1 ortholog and human TDP1 overexpression conferred cellular resistance upon etoposide exposure, suggesting a possible role of TDP1 in the repair of TOP2-induced damage. However, mammalian TDP1 showed a marked preferential polarity in 3' over 5' phosphotyrosines (Nitiss et al. 2006). Thus, whether TDP1 activity was physiologically relevant for the repair of TOP2-induced damage remained unclear. In 2009, a genetic screening revealed Tyrosyl-DNA-phosphodiesterase 2 (TDP2) as a novel human enzyme that displayed a clear 5' tyrosyl-DNA-phosphodiesterase activity. Consistently, the conversion of 5'-phosphotyrosyl DSB substrates into 5'-phosphate termini by cellular extracts, totally relied on the presence of TDP2 protein (Cortés-Ledesma et al. 2009). For this, TDP2 was proposed as the only physiologically relevant human enzyme capable of unblock TOP2-induced DSBs.

TDP2 is a protein of 47 kDa that belongs to $Mg2^{+}/Mn^{2+}$-dependent family of phosphodiesterases, and it seems to have appeared in higher eukariotes, since no yeast ortholog has been found. It has been proposed that TDP2 is a multitask protein, and its functions might go beyond DNA repair (Chunyang Li et al. 2011). Indeed, before its enzymatic activity was identified, TDP2 was known as TTRAP (TRAF and TNF

receptor-associated protein) (Xu et al. 2008; Zhou et al. 2013). Thus, it had been suggested that TDP2 could interfere with cell survival and immune response by inhibiting NFκB activation. Simultaneously, TDP2 was also named EAPII (ETS1-Associated Protein II) since it was identified as an interactor of ETS1, a transcription factor linked with tumorigenesis and metastasis (Pei et al. 2003; C. Li et al. 2011). Finally, TDP2 has been linked to viral infection by several independent laboratories. On one hand, TDP2 has been reported to interact with HIV-1 integrase, which facilitates viral integration (Zhang et al. 2009). If this function of TDP2 relies on its enzymatic activity remains unclear. In the other hand, TDP2 activity has been described to impact on hepatitis B persistent reservoirs, by allowing the formation of closed circle circularization of the viral genome after the removal of the P protein, which is covalently attached by a tyrosyl-phosphodiester bond (Königer et al. 2014). In a similar manner, TDP2 has been identified as the responsible for the removal of the small viral protein (VPg) from picornavirus RNA genome (Virgen-slane et al. 2012). This enzymatic activity, termed VPg unlinkase, is essential during viral replication for the removal of VPg cap, which is covalently attached to the 5'-end of the viral genomic RNA via a phosphotyrosyl bond.

In any case, the repair of TOP2-induced DSBs seems to be the leading function of TDP2, and extensive work has been performed at the cellular level to unveil its mechanism of action (Zeng et al. 2011; Gómez-Herreros et al. 2013; Ledesma et al. 2009; Gómez-Herreros et al. 2014). In early experiments, TDP2 activity has been demonstrated to account for the unblocking of 5' phosphotyrosines harboured by dsDNA using cellular extracts. In addition, purified recombinant TDP2 has shown to display 5' tyrosyl-DNA-

phosphodiesterase activity even at low protein concentrations. Consistently with these in vitro results, TDP2 has been described to facilitate the efficient repair of TOP2-induced DSBs in human and avian cells, preventing them from their deleterious consequences (Ledesma et al. 2009; Zeng et al. 2011; Gómez-Herreros et al. 2014). TDP2-depleted A539 human cell line and TDP2–deficient DT40 avian cells have been shown to be hypersensitive to TOP2-poison exposure, showing a negligible effect upon other DSB inducing agents, such as ionizing radiation and methylmethane sulphonate (Gómez-Herreros et al. 2013; Zeng et al. 2011; Ledesma et al. 2009). Based on the epistatic relation between KU70 deletion over TDP2 deficiency in promoting survival upon etoposide exposure, it has been suggested that TDP2 participates in the NHEJ repair pathway (Gómez-Herreros et al. 2013). In addition to the cellular characterization, structural and biochemical details of TDP2 enzymatic activity have been precisely described in recent work (Schellenberg et al. 2012; Shi et al. 2012). Moreover, to address the physiological implications of TDP2 deficiency in the entire organism, a mouse model has been developed (Gómez-Herreros et al. 2013). *Tdp2*$^{-/-}$ mice are born in mendelian proportions and lack any gross spontaneous phenotype. Nonetheless, TDP2-deficient mice show a marked hypersensitivity upon etoposide injections, displaying lymphoid toxicity, intestinal damage, and increased genome instability in the bone marrow compared to wild-type mice.

Homozygous mutations in *TDP2* have been described to be the cause of a newly identified cogenital syndrome, characterised by diverse neural defects encompassing mental disability, seizures and ataxia (Gómez-Herreros et al. 2014).

Blood extracts prepared from these patients showed a total absence of 5' TDP activity, and lymphoblastoid cells displayed DSB repair deficiency and hypersensitivity upon etoposide exposure. Importantly, TDP2 absence has been proposed to impacts on TOP2-dependent transcriptional regulation. Consistently, depletion of TDP2 in human cellular model deregulates the expression of androgen-receptor target genes, which are normally regulated by TOP2 activity. Moreover, brains obtained from the TDP2 mouse model displayed transcriptional deregulation, particularly in a set of genes that are crucial for neural development and maintenance, a subset of which depend on TOP2B. However, the impact of TDP2 loss on rodent central nervous system is largely minor when compared to human. Nonetheless, taking these observations altogether, TDP2 activity seems to contribute to the efficient TOP2-dependent transcriptional regulation in mammals. Thus, TDP2 can be considered a crucial factor in human physiology, but the extent of its implication would require further investigation.

4. Double-strand Break Repair and Human Health

DSBs are one of the most dangerous types of lesions that can arise in DNA. Thus, considering the large number of physiological processes in which DSBs are involved, it is not surprising that when repair is suboptimal, it can directly leads to severe biological consequences such as sporadic cancer incidence, neurodegeneration and aging (Vilenchik & Knudson 2003; Jeppesen et al. 2011). In fact, if just a single DSB remains unrepaired, it can lead to cell death and apoptosis, being determinant in tissue homeostasis. For instance, considering that the human brain contains billions of neurons,

neural development requires high rates of cellular proliferation to achieve an adequate cellular mass. During this phase, cells are particularly sensitive to DSBs. If a high number of these cells present unrepaired breaks, massive cell loss leads to developmental delay or failures (Reynolds & Stewart 2013). In a similar manner, if significant cell loss due to unrepaired DNA damage occurs in adult tissues with low self-renewal capacity, cells are not efficiently substituted. Consistently, cell death due to unrepaired DNA damage in adult central nervous system (CNS) has been proven to be a hallmark of several neurodegenerative processes (Jeppesen et al. 2011).

On top of this, if DBSs are not repaired properly, it increases the probability to generate mutations and chromosomal rearrangements (Mills et al. 2003). In each organism, cell death is precisely balanced with proliferation to preserve a constant number of cells in tissues and organs (Roos et al. 2015). However, a wide range of mutations, chromosomal fusions and translocations often alter gene expression, activating oncogenes or disabling tumour suppressors. This in turn can lead to uncontrolled cell proliferation, promoting neoplastic transformation (Khanna & Jackson 2001; Helleday et al. 2014). Thus, unfaithful DSB repair is considered one of the hallmarks of cancer. Additionally, genome instability produced by DSB repair malfunction directly contributes to tumour heterogeneity and clonal evolution, which are key steps in cancer metastasis and drug resistance.

Mutations in DSB repair genes have been linked to a large variety of human syndromes (McKinnon & Caldecott 2007). Overall, they are congenital disorders

characterized by a combination of immune deficiency, developmental delay, infertility, central nervous system defects and/or cancer proneness. Importantly, each set of features displayed by individuals carrying mutations in a unique DNA repair gene gives us insights of the physiological function of the protein encoded. Extensive work has been done in mouse models to elucidate the link between DSB repair and disease (Nordstrand et al. 2007). Nevertheless, rodent models do not always recapitulate every human feature and cellular approaches with cells isolated from patients have been key to dissect the molecular implications of these mutations.

4.1. c-NHEJ Syndromes

One of the most remarkable syndromes linked to DSB repair is the radiosensitivity and severe combined immunodeficiency (RS-SCID) (Christopher C. Dvorak 2010). These patients are characterized by reduced or absent circulating lymphocytes, combined with severe hypersensitivity to IR or radiomimetic agents. Individuals frequently present mutations in single genes, normally related to the NHEJ pathway. These mutations often result in the impairment at different stages of the NHEJ pathway, which correlates with the severity of the symptoms observed.

As mentioned above, NHEJ is essential for the efficient repair of IR-induced DSBs and RAG1/2-dependent cleavage during V(D)J recombination. Consistently, mutations in genes such as *LIG4* (encoding DNA ligase IV), *XLF* (XLF), *PRKDC* (DNA-PKcs) and *DCLRE1C* (Artemis) have been found in patients suffering from

RS-SCID (Woodbine et al. 2014). Curiously, mutations in other c-NHEJ factors such as KU70/80 or XRCC4 have not been found up to date. Null mutations in genes such as *LIG4* and *XRCC4* in mice are embryonic lethal (Barnes et al. 1998; Gao et al. 1998) and RS-SCID patients linked to *LIG4* mutations are hypomorphic (Chistiakov 2010), and mutations that totally abolish Ligase IV activity have not been found yet. Altogether, these observations suggest that mutations in c-NHEJ underlie the profound immunodeficiency of these patients, but curiously, only mutations that partially reduce NHEJ are compatible with embryonic development.

Indeed, in addition to immune system defects, a fraction of RS-SCID patients display developmental or growth delay, dysmorphic facial characteristics and congenital microcephally (Buck et al. 2006; O'Driscoll et al. 2001; Woodbine et al. 2013). It has been suggested that a defective NHEJ repair during development can underlie these severe features. Importantly, these phenotypes are present when RS-SCID is caused by mutations in c-NHEJ genes but not in Artemis, which is key for V(D)J hairpin opening and end processing, but it is accessory for general NHEJ (Moshous et al. 2001). Supporting this notion, developmental defects are totally absent in non-radiosensitive SCID patients, a similar human syndrome characterised by mutations in RAG1/2 genes (Notarangelo et al. 2016). In these cases, individuals present defective V(D)J due to the absence of cleavage in TCR and Ig genes, but they show proficient NHEJ repair upon IR exposure. Therefore, these observations strongly suggest that defects in c-NHEJ are the underlying cause of the defects in CNS development in RS-SCID patients. Nonetheless, while the role of NHEJ in V(D)J recombination has been dissected in detail, the impact

of defective NHEJ in neural development is less clear.

Despite the specific role of LIG4 in DSB repair by NHEJ, no other role in the repair of other type of lesions has been reported to date. Mouse models for LIG4 syndrome display microcephaly, and they have served to provide insights in the role of NHEJ during neural development. Indeed, *LIG4* null embryos die during E8-16.5 due to a p53-dependent apoptotic pathway, which suggests that DSBs may be endogenously arising during brain development, and NHEJ pathway is required for its correct repair (Frank et al. 2000). Curiously, embryonic neuronal stem and progenitor cells that are located in the ventricular and sub-ventricular zones (VZ-SVZ) undergo rapid cell divisions from developmental stage E8 to E16.5, which are key to achieve an accumulation of enough stem cells to eventually differentiate to neurons (Sun & Hevner 2014). It has been suggested that during this highly proliferative stage, DSBs are likely to arise in high amounts due to replicative stress. However, several other factors that can induce lesions during the critical stage of neuronal development have been proposed. On top of this, neural precursors have been shown to display hypersensitive apoptosis in response to DNA damaging agents, apoptosis being triggered with twenty-fold less DSBs than in adult brain cells (Barazzuol et al. 2015). Therefore, neural development is considered a critical process in which efficient repair mechanisms are highly required to avoid the deleterious outcomes of DSBs.

4.2. Other DNA Break-related Syndromes

Besides c-NHEJ factors, there are other human syndromes linked to DSB repair factors. Ataxia-telangiectasia (A-T) and ATLD (A-T like disorder) are two rare syndromes characterized by progressive cerebellar ataxia amongst other common features, such as radiosensitivity, immunodeficiency, cancer predisposition and infertility. For the importance to this work A-T will be dissected in further detail. ATLD syndrome is caused by mutations in the MRE11 gene, which encodes for MRE11, the nuclease component of the MRN complex (Taylor et al. 2004). Apparently, DSBs have been proposed to be the molecular trigger underlying ATLD, since the MRN complex is required for the repair of these lesions specifically. Nijmegen breakage syndrome, which is caused by a truncation in the *NBS1* gene, other member of the MRN complex, displays microcephaly, dysmorphic cranium, growth retardation, impaired sexual maturation and immunodeficiency (Digweed & Sperling 2004). Seckel-syndrome, which is caused by mutations in the gene encoding for ATR displays microcephaly, facial dystrophy and growth retardation (Driscoll et al. 2004). Since ATR plays an essential role in cellular tolerance to replicative stress apart from DSB repair, defective replication seem to be the determinant factor for the development of this disease.

Additionally, there are other syndromes linked to mutations in DNA repair genes characterized by microcephaly and other neural defects. Mutations in genes that have been described as accessory for the NHEJ pathway have been also linked to human syndromes. Mutations in *APTX* (Aprataxin) cause ataxia with oculomotor apraxia type 1 (AOA1), characterised by childhood onset of slowly progressive cerebellar ataxia, followed by oculomotor apraxia and a severe motor neuropathy (Date et al. 2001). Mutations in

PNKP (PNKP) have been linked with a wider range of neurological disorders, ranging from congenital microcephaly to oculomotor apraxia type 4 (AOA4) (Shen et al. 2010; Bras et al. 2015). Furthermore, specific mutations in *TDP1* gene are the cause of a neurodegenerative disorder known as spinocerebellar ataxia with axonal neuropathy (SCAN1) (Caldecott 2008). Interestingly, this set of diseases display a wide range of neurological features but with no overt immunodeficiency, neither phenotypes in other organs. Despite the fact that APRTX, PNKP and TDP1 can promote unblocking of DSBs, they display a primary role in SSB repair. For all of this, it has been suggested that blocked SSBs could be the molecular trigger underlying the neural features in these particular syndromes.

These observations altogether suggests that defects in DNA break repair may trigger a wide range of neurological features, ranging from deficient neural development to progressive neurodegeneration. However, it is not still clear whether some of these syndromes are caused by the accumulation of DSB, or other type of damage contributes to them. It is important to remark that mutations that totally impair NHEJ or HR have not been found in humans, suggesting that these are essential pathways and their total lack leads to embryonic lethality.

5. Ataxia-telangiectasia (A-T)

Since its identification, Ataxia telangiectasia (A-T) has been the paradigm of human inherited disease related to the DDR (Lavin 2008; McKinnon 2012). Indeed,

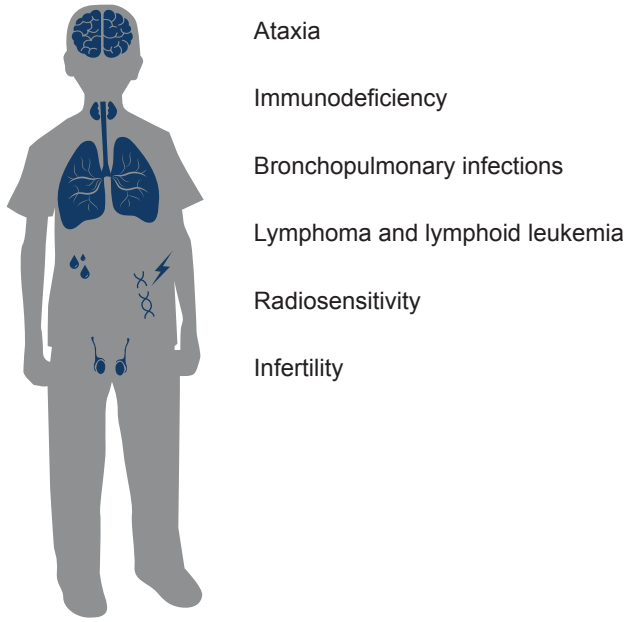

Figure 12: Ataxia Telangiectasia (A-T) syndrome. Individuals carrying homozygous mutations in ATM gene are characterized by multisystem failures such as, cerebellar ataxia, immunodeficiency, high incidence of bronchopulmonary infections, predisposition to lymphomas and leukemia, radiosensitivity and infertility.

spontaneous chromosomal instability and a profound hypersensitivity to DSB-inducing agents in cells derived from A-T patients, differentiate this syndrome from other spinocerebellar ataxias (Taylor et al. 1975). In 1995, positional cloning experiments defined mutations in ataxia-telangiectasia mutated (*ATM*) gene as the responsible for the A-T syndrome (Savitsky et al. 1995). Since then, several different mutations have been identified (Concannon & Gatti 1997; Sasaki et al. 1998; Chun & Gatti 2004). Up

to date, whether defective DSB-repair is the trigger of the clinical pathology, or it resides in an alternative function of ATM is still a matter of debate.

5.1. A-T Human Syndrome

A-T disease is associated with multi-systemic features, affecting development and maintenance of the brain, gonads and immune system (Figure 12). Primarily, A-T is an early-onset progressive neurodegenerative disorder, in which patients are born with no overt symptoms (Chun & Gatti 2004). At an age of 2-3 years, progressive ataxia starts to develop. Extensive loss of movement control becomes observable as a loss of balance (ataxia), slurred speech (dysarthria), and difficulties to regulate fine eye movements (oculomotor apraxia) and voluntary muscle contraction (dyssynergia). As a consequence, patients normally require the use of a wheelchair in the first decade of life. Importantly, a wide range in the severity of these features has been observed, negatively correlating with the residual levels of ATM activity (Verhagen et al. 2012; Taylor et al. 2015). A-T neurodegeneration is mainly restricted to the cerebellum, in which Purkinje and granule cells seem to be specially affected (Thomas O. Crawford 1998). Why these cell-types are particularly sensitive to ATM-deficiency is still unknown, but it has been proposed that the lower apoptotic threshold in these cell-types upon DNA damage induction could partially account for their loss. Other possibilities such as the lack of compensatory repair pathways in these particular cells have been also considered (Barzilai 2010).

During the last decades, supportive and symptomatic treatments have progressively

increased lifespan of patients with A-T during the last decades (Luciana Chessa 2016), which it varies greatly amongst individuals, presenting a median survival of 25 years, with some reported cases reaching the 50's (Crawford et al. 2006). The major cause of death in A-T is pulmonary failure, which is often caused by sinopulmonary infections due to primary immunodeficiency (McGrath-Morrow et al. 2010). Indeed, individuals present lymphocytopenia, characterized by lower numbers of circulating CD4+ or CD8+ single

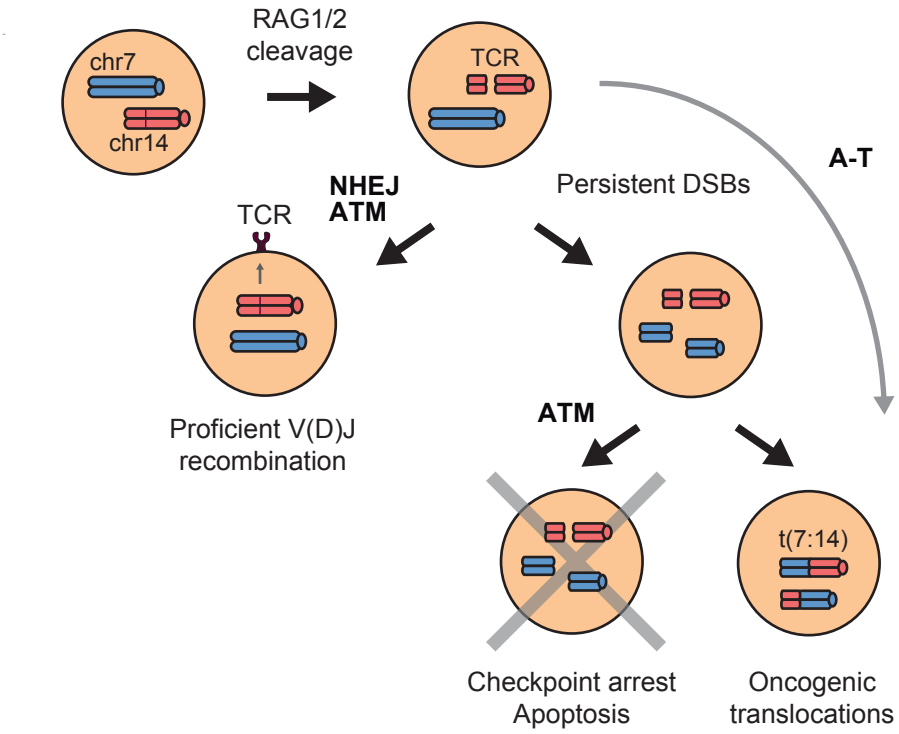

Figure 13: Model to explain oncogenic translocations linked to lymphoid malignancies in A-T. During T-cell development programmed DSBs are induced by RAG1/2 in TCR loci. ATM is crucial for the correct repair of these lesions by the NHEJ machinery. If DSBs induced by RAG1/2 or by other sources arise during this process, ATM triggers cell cycle arrest to allow DNA repair. Loss of ATM increases the likelihood of lymphocyte proliferation in cells carrying persistent DSBs, which potentially generate gross chromosomal rearrangements and oncogenic translocations.

positive (SP) mature T-cells (Nowak-Wegrzyn et al. 2004). Cancer is the second cause of death, with roughly a third of the cases developing tumours, which are mainly (85%) lymphomas and lymphocytic leukemias, with a total absence of myeloid tumours (Taylor 1996). Amongst them, acute T-cell lymphoblastic leukemia and adult T-cell leukemia are frequent. Nonetheless, the exact contribution of ATM loss to these processes is still under debate. It has been proposed that inaccurate repair of RAG1/2-induced DSBs can underlie T-cell neoplasia in A-T. Additionally, defective cell cycle checkpoint arrest in the presence of unrepaired damage can also contribute to oncogenic development.

Recurrent chromosomal rearrangements in A-T lymphomas have been previously described in detail (Taylor 1996). Interestingly, clonal translocations clustering in TCR and immunoglobulin genes are frequently present. Typically, translocation and inversion involving chromosome 7 and 14, presenting breakpoints situated at ch.14q11 (TCRα/δ gene), ch.7q35 (TCRβ), and ch.7p14 (TCRγ) have been described. In fact, accumulation of unrepaired DSBs within these loci have been described to substantially contribute to the formation of oncogenic translocations (Figure 13) (Zheng 2013). Moreover, breakpoints in the *TCR* genes have been found in translocations with known oncogenes, such as *TCL1* and *MTCP*. However, other recurrent clonal translocations that have been identified do not cluster in *TCR* or *Ig* genes, suggesting that a pathway independent of V(D)J recombination must underlie these rearrangements. Different mechanisms have been proposed to explain how DSBs can arise during T-cell development in sites that normally should not undergo RAG1/2 cleavage (Roth 2003). One possibility to explain DSBs arising in non-TCR sites is the erroneous RAG1/2-dependent cleavage in cryptic

recombination signal sequence (RSS) (Lewis et al. 1997). These cryptic RSS sites resemble a true RSS, in terms of sequence and chromatin status, but they are not adjacent to an antigen receptor or immunoglobulin gene. Therefore, RAG1/2 recombinase can cleave in these sites at a lower frequency compared to TCR and Igs loci. If they are located within oncogenes and tumour supressors, DSBs arising in these regions are dangerous, presenting a potential source of neoplastic changes in the genome. Indeed, cleavage of RAG1/2 in cryptic RSS has been observed along the genome, and it has been proposed to underlie some of the translocations found in other types of T-cell lymphomas. Another mechanism that can contribute to translocations is the occurrence of DSBs during periods of rapid cellular proliferation (Callen et al. 2007). ATM deficiency would contribute to accumulation of these replication-dependent DSBs within lymphocytes due to a defective cell cycle checkpoint arrest. In any case, other alternative mechanisms in which DSBs may arise in lymphocytes have not been addressed yet.

5.2. A-T Mouse Model

ATM mouse models have served to understand important issues about the etiology of A-T. ATM-deficient mice recapitulate many features of the human syndrome, including susceptibility to lymphoid tumours, primary immunodeficiency, infertility, radiosensitivity and smaller body size (Barlow et al. 1996). However, this model does not recapitulate the striking neurodegenerative phenotype of A-T patients (Lavin 2013). *Atm*$^{-/-}$ mice present a median survival ranging from 100 to 350 days, depending on the genetic background (Genik et al. 2014). These animals normally

succumb to massive thymic lymphomas, which largely expand in the chest cavity, leading to breathing difficulties and eventually to death. These tumours are mainly composed by CD4+CD8+ double positive clonal T-cells, but also CD4+ or CD8+ single positives have been described. Translocations involving chromosome 14, with breakpoints in the *Tcra/d* genes with amplifications of its upstream region are frequently found, with a large number of tumours presenting the clonal translocation t(12:14) (Zha et al. 2010). This particular oncogenic translocation depends on the enhancer of the *Tcrd* gene (Eδ) for its formation, since they are absent in $Atm^{-/-}E\delta^{-/-}$ mice (Jiang et al. 2015). This suggests that it is specifically formed during recombination of the *Tcrd* (TCRδ) gene. Other complex rearrangements involving chromosome 19, which contains Pten tumour suppressor, telomeric regions of chromosome 12, which includes *Tcl1* oncogene and *Bcl11b* tumor suppressor, or chromosome 2, which contain *Notch1* oncogene, have been also described in $Atm^{-/-}$ thymic lymphomas.

One important observation is the fact that rodent models carrying ATM-deletion or C-terminal RAG2-deletion, display similar outcomes in terms of T-cell oncogenesis. Both mutations lead to genome instability and complex chromosomal rearrangements after RAG1/2 cleavage during V(D)J recombination. In fact, ATM and the C-terminus of RAG2 have been demonstrated to contribute to post-cleavage complex stabilization, restraining DSB repair to c-NHEJ in the coding joints (Deriano et al. 2011; Chaumeil et al. 2013). Indeed, $Atm^{-/-}$ lymphocytes tend to form illegitimate hybrid join formation, characterised by nucleotide loss and the addition of palindromic and non-templated nucleotides (Bredemeyer, Huang, et al. 2008). In any case, lymphoma incidence caused

by ATM deficiency does not seem to rely completely in V(D)J recombination process, since tumour predisposition in ATM-deficient mice is not supressed by *Rag1* or *Rag2* deletion (Petiniot et al. 2002). Nevertheless, translocations involving TCRα/δ locus do depend on RAG1/2 cleavage, since they are not found in $Atm^{-/-}Rag1^{-/-}$ or in $Atm^{-/-}Rag2^{-/-}$. This altogether, strongly suggests that rearrangements in the TCR, while increasing tumorigenic potential, are not the only requirement for thymic lymphoma development. For this, it is essential to explore alternative mechanisms that contribute to neoplastic development in A-T disease.

5.3. Ataxia-Telangiectasia Mutated (ATM) protein

The Ser/Thr kinase ATM controls several cellular processes by modulating protein phosphorylation. This 360 kDa protein belongs to the PI3K-like kinases family (PIKKs), which includes DNA-PKcs, ATR, TRRAP, SMG1 and mTOR. These enzymes are usually involved in the cellular response to different stresses, being crucial in cellular homeostasis (Lempiäinen & Halazonetis 2009). Like ATR and DNA-PKcs, ATM preferentially phosphorylates specific targets on serine or threonine residues, followed by a glutamine, which is known as the S/T-Q motif (Kastan & Lim 2000). Up to date, numerous proteins have been defined as ATM substrates in vitro and in vivo. Proteomic screens revealed more than a thousand putative ATM substrates, encompassing different cellular processes such as gene expression, cell cycle control, chromatin organization, stress responses, cellular metabolism and DNA damage amongst others (Shiloh & Ziv 2013).

Structurally, ATM presents its active PI3K-like domain, located in its carboxy-terminus, a FAT domain (conserved in FRAP and TRRAP), a FATC domain (FAT C-terminal) and several HEAT domains, important for protein-protein specific interactions. ATM is normally found as inactive homodimers, which in response to specific stress, changes its spatial localization and become active in its monomeric form. In addition, numerous post-translational modifications have been described to modulate ATM activity (Paull 2015). It has been described three in trans autophosphorylation sites, Ser-367, Ser-1893 and Ser-1981, which are important for activation of human ATM. However, abrogation of these three sites showed to be dispensable for its activation in the rodent counterpart (Daniel et al. 2008). Other post-translational modifications, such as TIP60-mediated acetylation at Lys-3016, are particularly important for the early trigger of ATM activation.

DSBs are probably the genotoxic lesion that activates ATM most robustly. However, after decades of study, the exact mechanism in which ATM senses these lesions remains elusive. Despite DNA ends being required for its full activation, other factors such as changes in chromatin status could be sufficient for the early stages (You et al. 2007; Kim et al. 2009). The MRN complex does not seem necessary for initial activation, but it has been described as crucial for maintaining ATM association to DSBs, since removal of any member of the complex or impeding ATM interaction with NBS1 impairs its retention in DSB-induced foci (Uziel et al. 2003). In addition to DSBs, ATM has been proposed to sense oxidative stress, since it becomes active after disulphide-crosslinked

dimer formation upon oxidation. Consistently, ATM-deficient cells have been described to display hypersensitivity to oxidative agents (Guo et al. 2010). However, the biological significance of this pathway and its impact in A-T disease remains elusive.

The role of ATM in modulating the DDR upon genotoxic agents has been well dissected in the past (Iliakis et al. 2003). In fact, it is considered as an apical factor in the G1/S and G2/M checkpoints, which prevent cells from respectively undergoing replication of the DNA or proceeding into mitosis in the presence of damage. As mentioned above, in response to ionizing radiation, ATM phosphorylates Chk2 and p53. This event is key for the G1/S arrest, since activation of Chk2 promotes Cdc25A phosphorylation and its subsequent degradation by the 26S proteasome. Finally, reduced levels of Cdc25A results in the accumulation of the unphosphorylated form of Cdk2, which is incapable of initiating replication and promoting the firing of replication origins. Simultaneously, p53 is also activated by specific ATM-dependent phosphorylation in its Ser-15, and progressively, by Chk2-dependent phosphorylation in Ser-20, which contributes to the full activation of the pathway. These events promote p53 stabilization within the nucleus, by blocking its nuclear export and its subsequent proteasomal degradation in the cytoplasm. Increased levels of p53 in the nucleus favour its role as transcriptional activator, triggering the expression of several target genes, such as p21. These factors altogether inhibit Cdk2/CyclinE-dependent progression to S phase. On top of this, p21 also contribute to maintain S phase-genes repressed by inhibiting Cdk4-CyclinD kinase activity. This reduces Retinoblastoma (Rb) phosphorylated form, which is key for the release of E2F, an important transcriptional activator of these S-phase genes.

Additionally, the G2/M checkpoint is an essential halt that avoid cells to enter mitosis when DNA is damaged (Löbrich & Jeggo 2007). Indeed, deficiencies in G2/M checkpoint lead to embryonic lethality in several mouse models. Moreover, cells lacking this arrest display chromosomal rearrangements and breaks upon DSB induction. Similar to the G1/S checkpoint, ATM is a keystone in the G2/M checkpoint arrest. ATM is strongly activated upon DSBs induction in G2, and its activity has been proposed to modulate end resection of the breaks. This step, which generates ssDNA patches, efficiently activates ATR kinase, which phosphorylates Chk1, another essential effector of the G2/M checkpoint. On top of this, in a similar manner as in G1, ATM phosphorylates Chk2. Finally phosphorylated forms of Chk1 and Chk2 interfere with Cdk1-CyclinB, avoiding mitotic entry. Therefore, the absence of ATM contributes to unregulated cell cycle progression in the presence of DSBs, potentially leading to mutations and chromosomal rearrangements that can lead to uncontrolled cell growth or cellular collapse.

Nonetheless, besides the contribution of ATM to cell cycle checkpoint arrest, other functions have also been described. Indeed, one of the issues that remain most controversial is that, despite the profound radiosensitivity displayed by AT cells, the ATM role on the repair of DSBs is still unclear. Early works demonstrated that AT cells accumulate only a small fraction (≈15%) of persistently unrepaired DSBs induced by IR exposure (Foray et al. 1997; Kühne et al. 2004). This mild, but consistent, repair defect was observed in G1 and G2 cell cycle stages, ruling out a possible effect of checkpoint

deregulation. Importantly, Artemis endonuclease was described as the downstream factor of ATM responsible for this repair defect (Riballo et al. 2004). Since a fraction of the IR-induced DSBs contains aberrant structures in their termini, it was proposed that ATM could specifically promote the repair of breaks with more complex structures. Therefore, Artemis-dependent nucleolitic trimming, controlled by ATM phosphorylation, would allow the processing of the breaks that cannot be directly ligated by c-NHEJ. However, due to the technical impossibility to induce homogeneous population of molecularly controlled blocked DSBs, the validation of the model was challenging at that moment. Ever since, alternative functions of ATM in DSB repair have been proposed.

IR induces DSBs randomly along the genome. Thus, a fraction of these lesions will be located in high dense heterochromatin regions. ATM has been proposed to contribute specifically to the repair of heterochromatin-associated DSBs. In this regard, ATM induces heterochromatin decompaction in the vicinity of these DSBs. For this, ATM kinase is required for KAP1 (KRAB-associated protein 1) phosphorylation (Goodarzi et al. 2010). This modification leads to KAP1-dependent changes in the chromatin status, allowing repair to proceed in these lesions. Other ATM downstream factors such as 53BP1, RNF8, RNF168 and MDC1 have also been proposed to be essential for the repair of heretochromatin-associated DSBs (Noon et al. 2010). Curiously, according to the role of ATM in changing chromatin status, it has been suggested that ATM can deregulate gene expression through interfering with histone deacetylase 4 (HDAC4) (Li et al. 2012). This HDAC4-dependent regulation of gene expression seems to be essential for neuronal function, and could underlie to some extent A-T neurological features. It is

important to mention that this role of ATM in transcriptional regulation seems largely independent of DNA damage signalling or repair. Recent work has also linked ATM activity with the clustering of multiple DSB in repair foci upon AsiSI restriction enzyme cleavage (Caron et al. 2015a). Curiously, ATM inactivation has shown a negligible impact on the repair rate of these lesions. It is important to mention that AsiSI enzyme generates compatible and clean DSBs that can be easily religated by the repair machinery.

5.4. Interplay of ATM and DNA-PKcs in the Repair of Double-strand Breaks

DNA-PKcs, with a molecular weight of approximately 460 kDa, is one of the largest kinases within the PI3K-like kinase family (Dobbs et al. 2010). Although DNA-PKcs is not conserved in lower eukaryotes, the kinase activity of DNA-PKcs is required in mammalian cells for efficient NHEJ. Structurally, it shares several common features with ATM, such as the C-terminal kinase domain, which is flanked by a FAT and FATC domains, and numerous HEAT domains in its N-terminal region. Interestingly, several redundant roles have been described for ATM and DNA-PKcs kinases within the DNA damage response upon DSB induction. However, their regulation and the functional implications of their loss largely differ. In fact, while the role of ATM in DSB repair remains still unclear, DNA-PKcs has been described as a key member in c-NHEJ pathway. Consistent with this, mutations in DNA-PKcs and chemical agents that specifically inhibit its kinase activity have been described to cause marked DSB repair defects and radiosensitivity under several experimental conditions.

The DNA-PK holoenzyme is formed when KU70/80 heterodimeric ring associates to DSB ends, promoting the recruitment and activation of the DNA-PK catalytic subunit (Gottlieb & Jackson 1993). Despite the fact that DNA-PKcs has been described to phosphorylate a high number of substrates in vitro and in vivo, the validation and relevance of these modifications under physiological conditions are still a matter of debate. Until present, the most characterized phosphorylation substrate has been by far DNA-PKcs itself (Stiff et al. 2004; Uematsu et al. 2007). Indeed, it has been described to suffer a large number of phosphorylations in in a large number of residues. The kinase activity and autophosphorylation have been demonstrated to be important for the efficient repair and cell survival upon the exposure to DSB-inducing agents. At the molecular level, it has been postulated that two DNA-PKcs molecules can autophosphorylate each other in trans when they are confronted in DSB end synapses during NHEJ (Reddy et al. 2004; Meek et al. 2007). This autophosphorylation leads to the dissociation of DNA-PKcs from DSB ends, resulting in decreased kinase activity of the DNA-PK holoenzyme (Chan & Lees-Miller 1996). Thus, inactive DNA-PKcs remains associated to DSB ends, preventing access to other required repair factors.

Several phosphorylation clusters have been mapped in DNA-PKcs. Nonetheless, up to date, the most functionally relevant are the ABCDE and PQR (Meek et al. 2007). ABCDE phosphorylation cluster encompasses the residues Thr-2609, Ser-2612, Thr-2620, Ser-2624, Thr-2638, Thr-2647, and the PRQ the serine residues 2023, 2029, 2041, 2053 and 2056. Single alanine mutations in these residues displayed negligible effect in NHEJ capacity. However, combined mutations in all the residues of PQR or ABCDE

displayed different levels of radiosensitivity (Cui et al. 2005; Ding et al. 2003) Curiously, in contrast to the milder effect observed in the PQR mutant, combined mutations in the six residues of the ABCDE confer a profound sensitivity to IR exposure, which was even more pronounced than null mutations. At the molecular level, the major defect exhibited by ABCDE and PQR mutants was a disruption in DNA end processing capacity by the NHEJ pathway (Meek et al. 2008). In contrast, normal kinase activity, interaction with KU70/80 and recruitment to DSB sites were not affected. Nevertheless, while ABCDE phosphorylation seems to promote end processing, activation of the PRQ cluster leads to joining events with excessive nucleotide loss. Thus, it has been proposed that phosphorylation of these clusters are tightly regulated to modulate end protection and processing of DSBs. In this way, while ABCDE phosphorylation is key for end trimming, PQR phosphorylation limits end processing. Following DSB end synapse, multiple phosphorylation events can control DNA-PKcs conformational changes, allowing the recruitment of downstream processing enzymes and to the ligase complex (Meek et al. 2008). Structure of DSB termini condition DNA-PKcs activation, ranging from low by blunt-end and hairpin-end, to most active in the case of 3' and 5' overhangs (Hammarsten et al. 2000). Thus, different DSB ends would require specific DNA-PKcs phosphorylation steps to modulate end protection, processing and eventual repair by the NHEJ pathway.

Nevertheless, to which extent PQR and ABCDE clusters are exclusively phosphorylated by DNA-PKcs itself is unclear. In this regard, it has been suggested that Ser-2056 phosphorylation in the PQR cluster is indeed an autophosphorylation site,

while both DNA-PKcs and ATM seem to contribute to the phosphorylation of Thr-2609 in the ABCDE cluster (Chen et al. 2007). Additionally, ABCDE phosphorylation was described to be essential for the Artemis-dependent endonuclease activity, important for end processing during NHEJ (Goodarzi et al. 2006). Thus, it has been proposed that the role of ATM in the repair of DSB could be mediated by the phosphorylation of DNA-PKcs to activate Artemis.

II. OBJECTIVES

II. OBJECTIVES

Due to the relevance of DSBs for human physiology, the understanding of the molecular mechanisms that govern their repair is key. Importantly, the chemical structure present at DSB ends is highly influential for their repair, since it conditions the enzymatic activities and pathways required for an efficient repair. Nonetheless, the study of the repair of blocked DSBs has been largely impeded due to the technical incapacity to induce homogeneous populations of breaks. Based on previous work, we hypothesized that we can take advantage of TOP2-induced DSBs and TDP2 to control DNA end structure in cells and mouse models. For this, further characterization of the physiological activity of TDP2 in mammalian cells, and the validation of our theoretical approach, are required.

Mutations in the *ATM* gene cause the rare syndrome Ataxia-Telangiectasia. Despite the fact that ATM protein plays a central role in the DNA damage response upon DSB induction, and that several of the phenotypes have been linked to defects in DSB repair, the exact molecular trigger of this devastating disease remains elusive. Previous findings suggest the possibility of ATM being important for the repair of DSBs that present terminal blockages. Therefore, we aimed to demonstrate if the specific chemical structure present at DSB ends is a determinant factor in the requirement of ATM for their repair. This would put forward blocked DSBs as a possible trigger of A-T symptomatology.

Thus, the objectives of this Thesis are the following:

1. Determine how the chemical structure of DNA ends influences the repair of DSBs
   1.1. Characterize the biochemical activity of TDP2
   1.2. Develop a genetic tool to induce homogeneous populations of blocked and clean DSBs

2. Determine the contribution of ATM to the repair of blocked DSBs in mammals
   2.1. Evaluate repair in ATM-deficient cells upon clean or blocked DSB-induction
   2.2. Characterize the cellular impact of ATM loss upon clean or blocked DSB-induction

3. Analyse the impact of TOP2-induced DSBs for the symptomatology of Ataxia-Telangiectasia
   3.1. Study the contribution of ATM to the repair of blocked DSBs in a rodent model
   3.2. Determine the impact of spontaneous TOP2-induced damage in an ATM mouse model

III. RESULTS

III. RESULTS

1. TDP2 is the major 5'-TDP activity and creates ligatable DSBs

The discovery of TDP2 as the first 5'-tyrosyl-DNA-phosphodiesterase (5'-TDP) activity raised the possibility of it being an important factor in the repair of TOP2-induced damage and, therefore, in the clinical response to TOP2 poisons (Ledesma et al. 2009). To determine the impact of TDP2 loss on TOP2-induced DNA damage in mammals, we took advantage of a previously generated mouse in which the first three exons of *Tdp2* plus the 5'-UTR were deleted. For this, primary mouse embryonic fibroblast (MEF) cells were isolated from wildtype and TDP2-deficient mice (*Tdp2*$^{-/-}$).

To test if *Tdp2* deletion abolishes 5'-TDP activity, radiolabelled oligonucleotide duplexes containing 5' phosphotyrosine (5'-Tyr) moieties were incubated with protein extracts prepared from wildtype and *Tdp2*$^{-/-}$ primary MEFs. Then, samples were subject to polyacrylamide gel electrophoresis. Through this methodology, the conversion of 5'-Tyr to 5' phosphate (5'-Pho) termini can be observed as a mobility shift. Wild-type samples showed a marked 5'-TDP activity in blunt-end 5'-Tyr substrates, as can be observed by the appearance of a lower band corresponding to 5'-Pho moieties (Figure 14A). On the contrary, TDP activity was totally abolished in *Tdp2*$^{-/-}$ extracts. This confirms the effective inactivation of TDP2 in mutant rodent cells. Consistently with previous work performed in avian DT40 and A549 TDP2-depleted cells, our result extends the conclusion of TDP2 being the only physiologically relevant 5' -TDP activity in rodent primary cells.

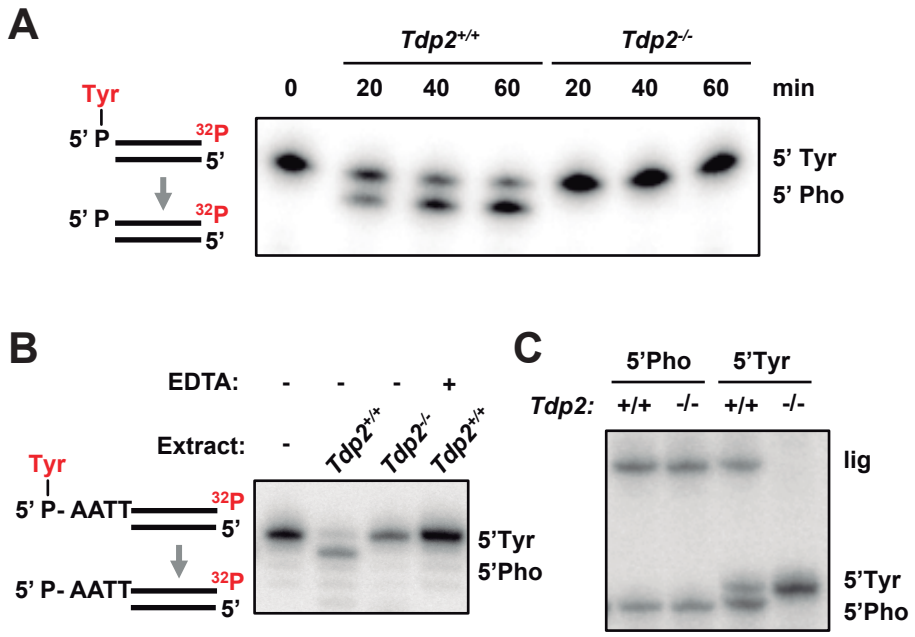

Figure 14: Deletion of Tdp2 in primary MEFs abolishes 5′-TDP activity. (A) DNA duplex substrate harbouring a 5′ phosphotyrosine blunt end was incubated during the indicated times with 1.5 µg cellular extracts from *Tdp2*$^{+/+}$ or *Tdp2*$^{-/-}$ primary MEFs. **(B)** Duplex substrate harbouring a 5' phosphotyrosine self-complementary overhang end was incubated with 10 µg cellular extract from *Tdp2*$^{+/+}$ and *Tdp2*$^{-/-}$ transformed MEFs for 2 h in the presence or absence of 50 mM EDTA. Migration of the 5′ phosphotyrosine (5' Tyr) to 5' phosphate (5' Pho) is indicated. **(C)** 5′ phosphate (5' Pho) and 5′ phosphotyrosine (5' Tyr) substrates were incubated for 1.5 h with 3.3 µg cellular extract from Tdp2+/+ and *Tdp2*$^{-/-}$ transformed MEFs as in "A", but in the presence of recombinant TDP2 and T4 ligase. Migration of ligation (lig) product is indicated.

Previous work has described that TOP2 introduce two staggered nicks at 4 bp of distance (Pommier et al. 2016). Therefore, taking into consideration the biochemical mechanism of TOP2 cleavage, we anticipated that DSBs induced by this specific pathway would not harbour blunt-ends, but 5' compatible overhangs. Thus, we speculated that if TDP2 account for the physiological unblocking of TOP2-induced damage, it

would be highly active over this type of substrates. TDP2 activity would reconstitute complementary *clean* DSBs (5' phosphate and 3' hydroxyl termini), which would be an ideal substrate for ligation by NHEJ. For this, we recapitulated the previous experiment but using substrates harbouring 5'-Tyr in 4 bp overhangs. Consistently, cell extracts prepared from wild-type cells display high activity on these substrates, and was completely absent in *Tdp2*$^{-/-}$ (Figure 14B). EDTA-mediated chelation of Mg^{2+}, which is essential for TDP2 function but dispensable for other unblocking enzymes such as TDP1, completely eliminated 5'-TDP activity in wild type MEF extracts (Gao et al. 2012).

We could predict that upon TDP2 activity, repair of TOP2-induced lesions would accurately preserve DNA sequence, suggesting the possibility of error-free NHEJ. To test this hypothesis, we examined whether TDP2 action at 5'-Tyr substrates creates termini that can be directly joined with the single activity of a ligase. Indeed, addition of T4 DNA Ligase in reactions containing wildtype MEF extracts resulted in the additional appearance of a product of 46-nt, indicative of the completion of repair without the loss of a single nucleotide. However, this product was not observed if reactions contained cell extract from *Tdp2*$^{-/-}$ MEFs, confirming that DNA ligation was dependent on TDP2 activity (Figure 14C).

Furthermore, to analyse ligation of DSBs directly catalysed by cell extracts, we generated linear plasmids by PCR amplification with primers harbouring 5' phosphate (5'-Pho) or 5' phosphotyrosine (5'-Tyr) moieties. This linear dsDNA simulates chromosomal DSBs, due to the larger length (6.7 kb) compared with substrates

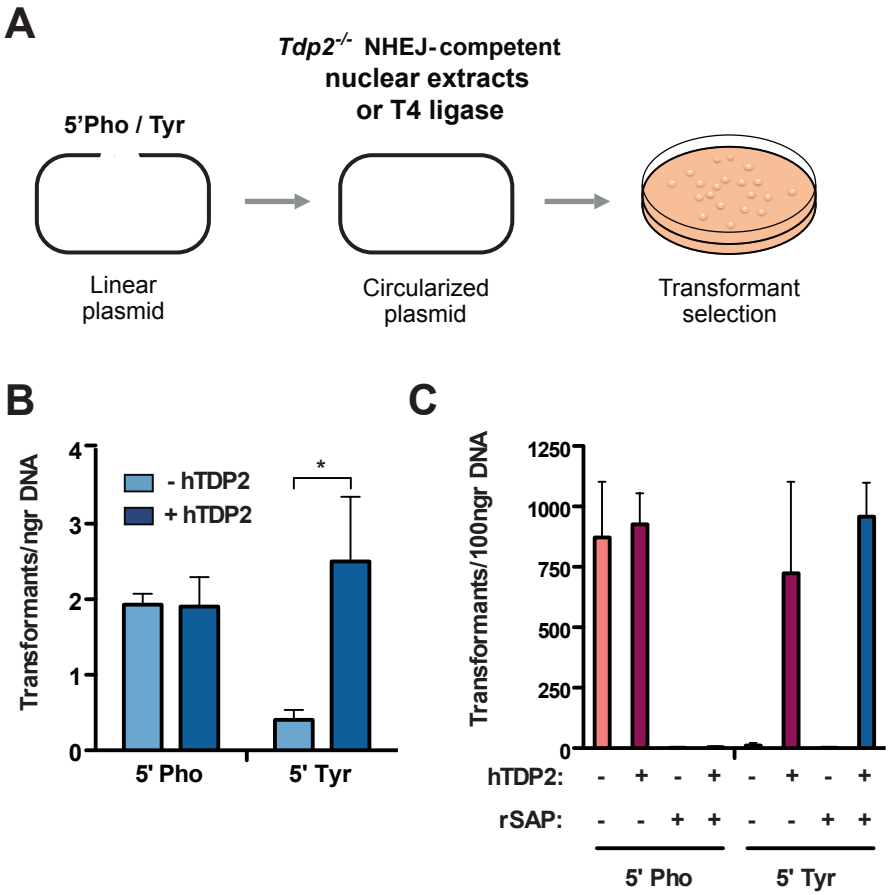

Figure 15: Recombinant TDP2 facilitates NHEJ by reconstituting 'clean' DSBs in vitro. (A) Scheme of the in vitro plasmid circularization assay. **(B)** Circularization efficiency of linear 5' Tyr and 5' Pho plasmids catalysed by nuclear extracts prepared from Tdp2-/- transformed MEFs in the presence and absence of recombinant human TDP2. Average ± s.e.m. of three independent experiments is shown. Statistical significance by Two-way ANOVA test with Bonferroni post-test is indicated (*P≤0.05; **P≤0.01; ***P≤0.001). **(C)** Same as in "B", but substrates were pre-incubated in the presence or absence of Shrimp Alkaline Phosphatase (rSAP). After heat-inactivation of rSAP, circularization was performed by T4 ligase.

employed previously (27 bp) (Seluanov et al. 2004). The incubation of these substrates with NHEJ-competent nuclear extracts results in plasmid circularization events, which were scored as kanamycin-resistant colonies following bacterial transformation (Figure 15A). Nuclear extracts from *Tdp2*$^{-/-}$ MEFs efficiently circularized linear plasmids with 5'-Pho ends, but not 5'-Tyr counterparts (Figure 15B). This difference was lost upon addition of recombinant human TDP2 (hTDP2) to the reaction, confirming the TDP2–dependent nature of the repair by NHEJ of this type of lesions. Additionally, in order to test whether TDP2 activity reconstitutes clean DSBs, both plasmids were pre-incubated with Shrimp Alkaline Phosphatase (rSAP). In order to avoid dephosphorylation of the newly formed 5'-Pho by TDP activity, rSAP was heat inactivated prior to TDP2 and T4 ligase addition to the reactions. Since 5'-Pho termini are required for ligation, pre-incubation with rSAP abolished circularization of the 5'-Pho plasmid (Figure 15C). On the contrary, 5'-Tyr moieties protected ends from dephosphorylation by rSAP, licensing plasmids for ligation when hTDP2 was specifically present in the reactions.

Collectively, our data suggest that TDP2 supports the only physiologically relevant 5'-TDP activity in mammalian cells. Its activity facilitates the accurate repair of 5' phosphotyrosine blocked DSBs, by generating 5' phosphate termini that can proceed to direct ligation, supporting the notion that TDP2 can allow error-free NHEJ of TOP2-induced DNA damage.

2. TDP2 promotes efficient repair of TOP2-induced DSBs by removing

covalently bound peptides.

Based on the fact that TDP2-deficiency abolishes 5'-TDP activity in cells, we speculated that upon exposure to TOP2-poisons, tyrosine residues or peptide adducts would remain covalently linked to DNA at the sites of TOP2-induced lesions that have not been unblocked or processed yet. Indeed, we aimed to develop a methodology to specifically measure protein-blocked DSBs, which we have termed SLOPE (Selective Labelling Of Protein-blocked Ends). SLOPE is based on a previously described assay that has been used to identify genomic regions of TOP2 cleavage (Haffner et al. 2010). Essentially, following isolation of genomic DNA after extensive Proteinase K treatment, TOP2-blocked DSBs will harbour covalently bound tyrosines. Biotin is then conjugated to these residues by a specific chemical reaction. Based on the selective reactivity of activated N-Hydroxysuccinimide (NHS) esters of biotin with primary amino groups ($-NH_2$) contained in side chain of lysine (K) residues and the N-terminus of polypeptides. Finally, the amount of biotin conjugated is measured in dot-blot assays, and used as an indicator of protein covalently linked to DNA. To detect irreversible TOP2-blocked DSBs resulting from etoposide treatment but not cleavage complexes, cells are incubated in the absence of the drug to allow cleavage complex reversal before DNA isolation. As can be seen in Figure 16A, incubation of wildtype MEFs with etoposide did not detectably change the amount of protein covalently linked to DNA compared with untreated samples, while a clear and significant increase was observed in *Tdp2*$^{-/-}$ cells. These results demonstrate that, upon etoposide treatment, protein-blocked DSBs accumulate in TDP2-deficient cells.

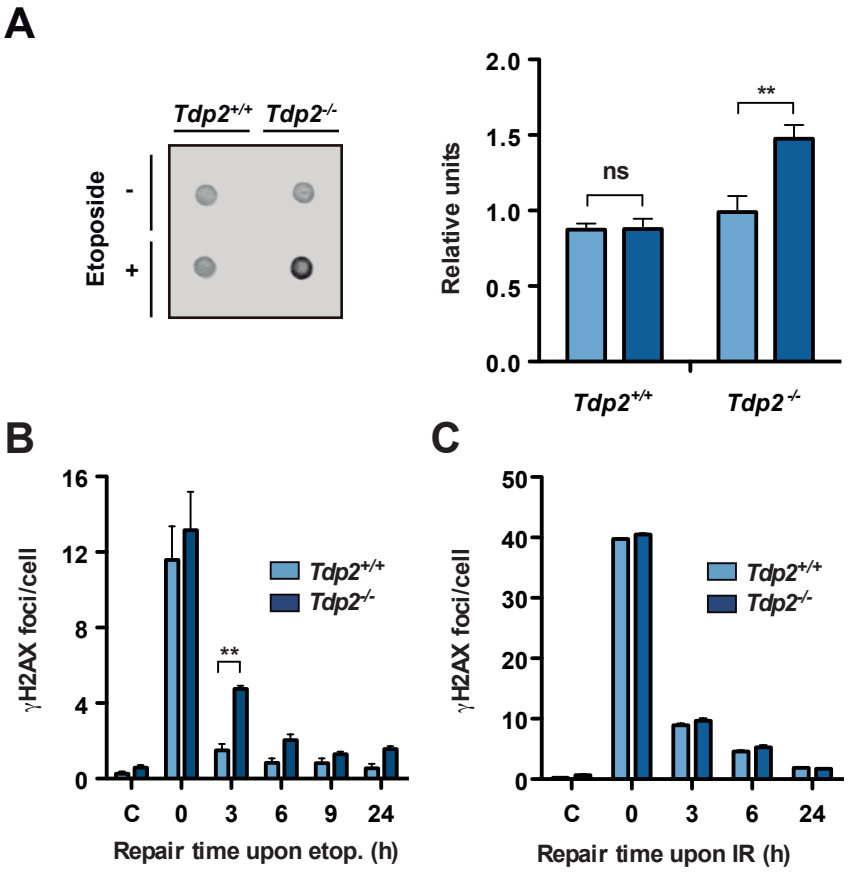

Figure 16: TDP2 removes peptide adducts and promote efficient repair of TOP2-induced DSBs. (A) Representative image of SLOPE assay (left) and quantification (right) performed in *Tdp2*$^{+/+}$ and *Tdp2*$^{-/-}$ confluency-arrested primary MEFs. Average±s.e.m. Signal from three independent experiments and statistical significance by two-way ANOVA test with Bonferroni post-test is shown (right) (*P≤0.05; **P≤0.01; ***P≤0.001). **(B)** γH2AX foci induction after 30 min 10 μM etoposide treatment and repair at different times following drug removal in confluency arrested *Tdp2*$^{+/+}$ and *Tdp2*$^{-/-}$ primary MEFs. Average±s.e.m. signal from three independent experiments and statistical significance by two-way ANOVA test with Bonferroni post-test is shown (*P≤0.05; **P≤0.01; ***P≤0.001). **(C)** Same than in B but cells were exposed to 2 Gy γ-irradiation.

Our previous results suggest that TDP2 can facilitate error-free NHEJ by removing

5'- phosphotyrosines from DSBs. Thus, we next analysed the importance of TDP2 in the repair of DSBs generated by TOP2 poisons in mammalian cells. To address this, we measured DSB repair at different time-points after 30 min of etoposide treatment in wild-type and *Tdp2*$^{-/-}$ primary MEFs. For this we performed immunofluorescence of the Ser139-phosphorylated form of H2AX (γH2AX), which forms foci that accurately correlate with the amount of DSBs present in cells. Since TOP2 activity is subject to cell cycle variations, cells were confluency arrested in G0 to avoid discrepancies in DSB induction. On top of this, NHEJ is the only active pathway operating in quiescent cells. Interestingly, the rate of DSB repair was diminished in *Tdp2*$^{-/-}$ MEFs upon etoposide treatment (Figure 16B), consistent with the anticipated TDP2 function in the repair of TOP2-induced DSBs by NHEJ. In contrast to treatment with etoposide, which generates DSBs in which 5'-TDP activity is required, the rate of DSB repair was indistinguishable in *Tdp2*$^{-/-}$ compared to wildtype cells following γ-irradiation (Figure 16C). In summary, these results demonstrate that TDP2 is required for the efficient repair of TOP2-induced DSBs in mammalian cells.

3. ATM facilitates repair of TOP2-blocked but not clean DSBs

As mentioned above, we can use TOP2 poisons such as etoposide to induce DSBs that are homogeneous in structure. Therefore, we can modulate the ends of these DSBs by working in different genetic backgrounds (Figure 17A). 3' hydroxyl and 5' phosphate clean ends will be formed in cells containing TDP2 activity, while breaks with a peptide block on 5' ends will accumulate in TDP2-deficient cells. Following this rationale, we

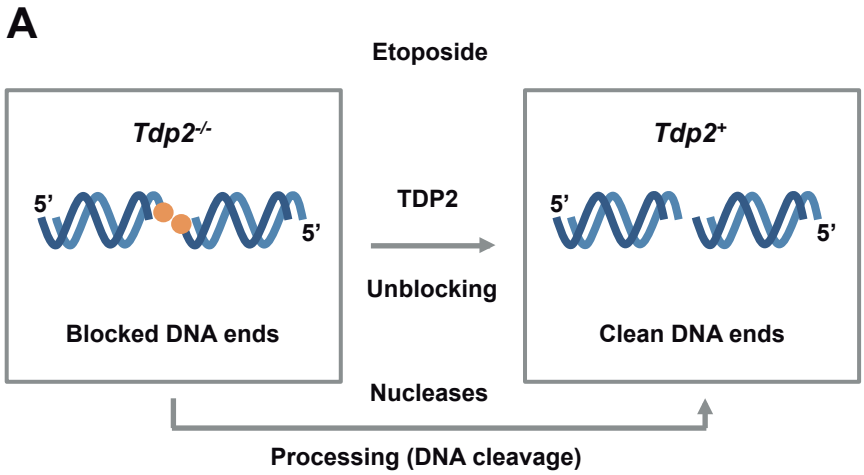

Figure 17: TDP2 determines end structure of TOP2-induced DSBs. Scheme of the strategy used to generate DSBs with specific structure. Etoposide exposure induces TOP2-mediated DSBs that are blocked by 5' peptide adducts. In wildtype cells, TDP2 activity can efficiently unblock these lesions. Conversely, in TDP2-deficient background all DSBs are blocked, requiring DNA cleavage and processing by nucleases for their repair.

can use this genetic system to control the chemical structure present in DSBs, being extraordinarily adequate for the study of the repair of blocked DSBs.

Since ATM was previously proposed to have a role in DSB-end processing (Riballo et al. 2004), we decided to apply the experimental setup described above to analyse the impact of its loss on the repair of either clean or blocked DSBs. For this, we measured DSB repair following the time course of γH2AX foci disappearance in G0 primary MEFs after etoposide treatment (See Figure 16B). We observed that the absence of ATM caused a marked reduction in the intensity of etoposide-induced γH2AX foci (Figure 18A, upper). This is not surprising given the key role of ATM in H2AX phosphorylation

in response to DSBs (Kastan & Lim 2000). However, in contrast to the intensity, the number of γH2AX foci induced was not affected, validating the use of this parameter as a DSB-scoring tool in our particular setup (Figure 18A, lower). As can be seen in Figure 19A, the absence of ATM did not affect the rate of DSB repair in *Tdp2*$^{+/+}$ background, consistent with previous observations, suggesting that ATM does not influence repair of clean DSBs. In contrast, a striking decrease in the repair rate was observed in the combined mutant *Tdp2*$^{-/-}$ *Atm*$^{-/-}$, with ~40% of the breaks remaining unrepaired even 24 h after damage induction (Figure 19B). This strongly suggests that ATM is crucial for the repair of DSB, specifically when they are blocked. Remarkably, it is the first time that such a severe repair defect is reported in ATM-deficient cells. Since *Tdp2*$^{+/+}$ cells were

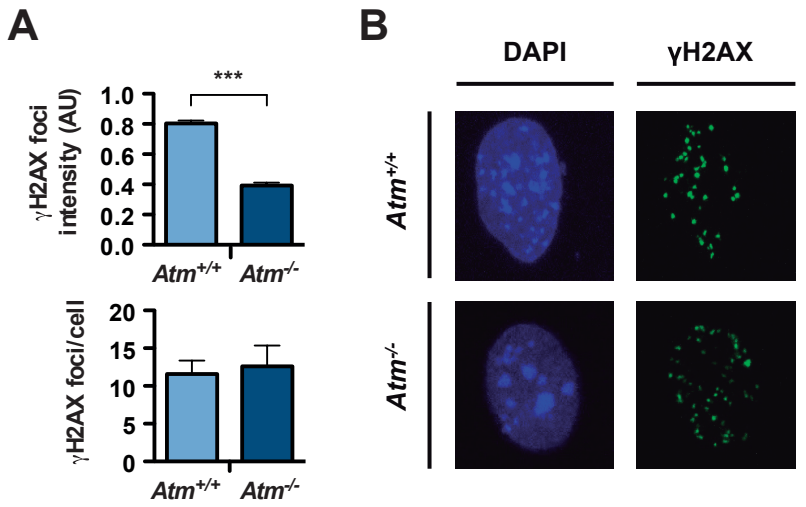

Figure 18: ATM does not affect the induction of DSBs generated by TOP2. (A) Average number per cell (upper) and intensity (lower) of γH2AX foci after 30 min 10 μM etoposide treatment in the indicated confluency arrested primary MEFs. Average±s.e.m. of three independent experiments and statistical significance by Mann-Whitney test is indicated (*P≤0.05; **P≤0.01; ***P≤0.001). **(B)** Representative images of γH2AX foci (green) and DAPI counterstain (blue) are shown.

indistinguishable from *Tdp2*$^{+/-}$ in ATM-deficient background, we can conclude that a single copy of *Tdp2* is sufficient to unblock TOP2-induced DSBs (Figure 20). Moreover,

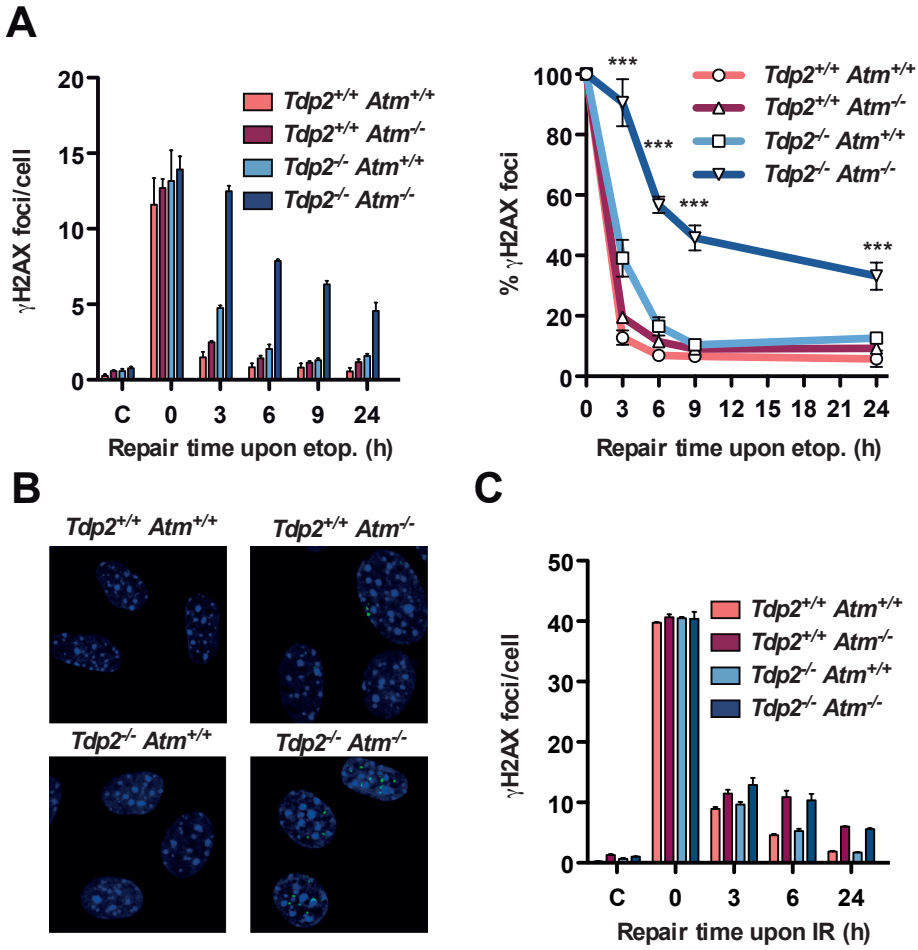

Figure 19: ATM facilitates repair of TOP2 blocked DSBs in confluency arrested MEFs. (A) γH2AX foci induction and disappearance upon 30 min treatment with 10 μM etoposide and different repair times in the indicated confluency arrested primary MEFs. Total number of foci (left) and percentage remaining (right) is shown. Average ± s.e.m. of at least three independent experiments is shown (left). Statistical significance by two-way ANOVA test with Bonferroni post-test is indicated (*P≤0.05; **P≤0.01; ***P≤0.001) (right). **(B)** Representative images of γH2AX foci (green) and DAPI counterstain (blue) for the 24 h repair time point. **(C)** Same as in 'A' but cells were exposed to 2Gy γ-irradiation.

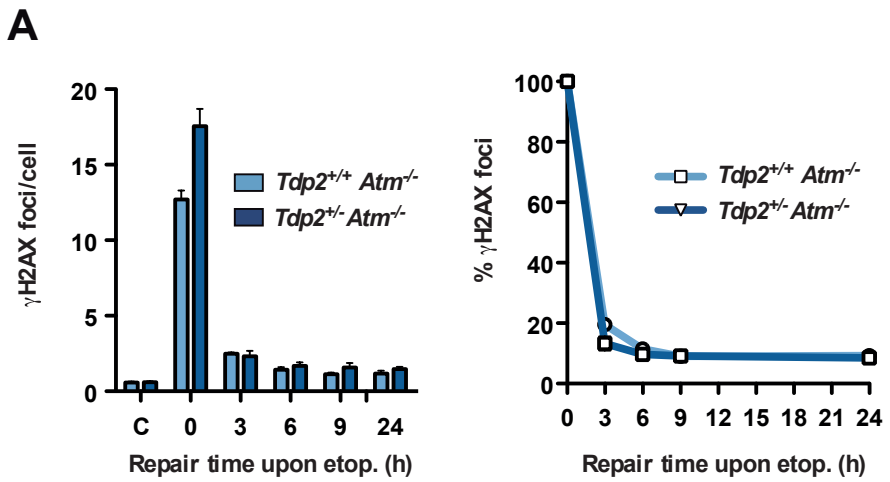

Figure 20: A single copy of TDP2 can promote efficient repair of TOP2-induced DSBs. (A) Comparison of DSB-repair efficiency between *Tdp2*$^{+/+}$ and *Tdp2*$^{+/-}$ cells in ATM-deficient background. γH2AX foci induction and disappearance upon 30 min treatment with 10 μM etoposide and different repair times in the indicated confluency arrested primary MEFs. Total number of foci (left) and percentage remaining (right) is shown. Average ± s.e.m. of at least three independent experiments is shown (left). Statistical significance by two-way ANOVA test with Bonferroni post-test is indicated (*P≤0.05; **P≤0.01; ***P≤0.001) (right).

the synergistic defect of TDP2 and ATM deletion was specific to TOP2-induced breaks, not being observed with ionizing radiation (Figure 19C). Consistent with previous work, repair of only ~10% of the breaks relies on ATM upon IR exposure, independently of the TDP2 status.

Based on this end structure-specific function of ATM, we tested whether there was differential activation upon clean or blocked DSB-induction. For this we monitored autophosphorylation of ATM in Ser-1981 (Bakkenist & Kastan 2003). Interestingly, ATM was activated to similar extent in wildtype and TDP2-deficient background

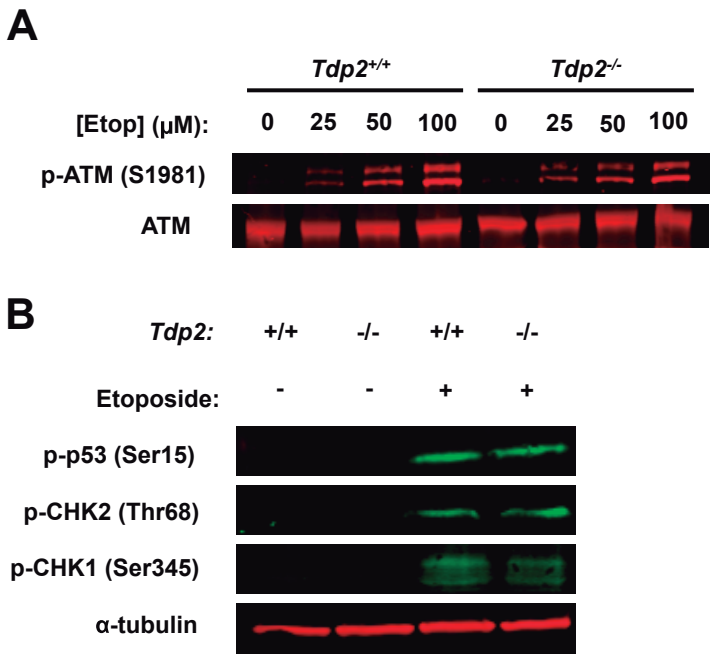

Figure 21: Equivalent DDR signalling in wild-type and TDP2-deficient cells. **(A)** ATM activation monitored by immunoblot of S1981 phosphorylation, after 30 min incubation with etoposide of *Tdp2*$^{+/+}$ and *Tdp2*$^{-/-}$ confluency arrested primary MEFs. Total ATM was used as a loading control. **(B)** p53, CHK2 and CHK1 activation, was monitored by immunoblot of phosphorylation in the indicated residues, after 30 min incubation of *Tdp2*$^{+/+}$ and *Tdp2*$^{-/-}$ confluency arrested primary MEFs with 100μM etoposide. α-Tubulin was used as a loading control.

upon increasing doses of etoposide exposure (Figure 21A). Next, we addressed if its downstream factors involved in the DNA damage response (DDR) were differentially activated in similar conditions. We previously observed that γH2AX signalling in response to etoposide strongly relies on ATM (Figure 18), but its deficiency only has an impact on repair in the absence of TDP2. Consistently with this independence between signalling and repair, ATM and downstream checkpoint factors, such as p53, CHK1 and

Chk2 were equally activated in *Tdp2*$^{+/+}$ and *Tdp2*$^{-/-}$ cells upon etoposide exposure (Figure 21).

To confirm the synergism between TDP2 and ATM in the repair of etoposide-induced DSBs, we repeated the analysis using chemical inhibition of ATM, instead of deletion (Figure 22). Consistently, incubation with the ATM inhibitor KU55933 diminished the repair rate of TOP2-induced DSBs, but specifically in *Tdp2*$^{-/-}$ background. Since chemical inhibition abolishes ATM activity but the protein is still present, this result demonstrates that the role of ATM in the repair of blocked DSBs depends on its

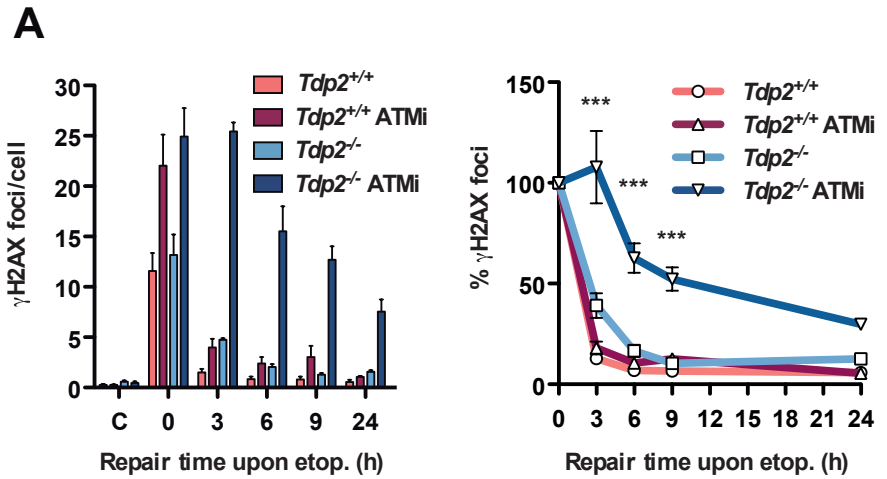

Figure 22: ATM kinase activity is important for the repair of TOP2 blocked DSBs (A) γH2AX foci induction and disappearance upon 30 min treatment with 10 μM etoposide and different repair times in the indicated confluency arrested primary MEFs incubated or not with 10μM ATMi. Total number of foci (left) and percentage remaining (right) is shown. Average ± s.e.m. of at least three independent experiments is shown (left). Statistical significance by two-way ANOVA test with Bonferroni post-test is indicated (*P≤0.05; **P≤0.01; ***P≤0.001) (right).

function as kinase. On top of this, it rules out possible artefacts caused by heterogeneity in MEFs.

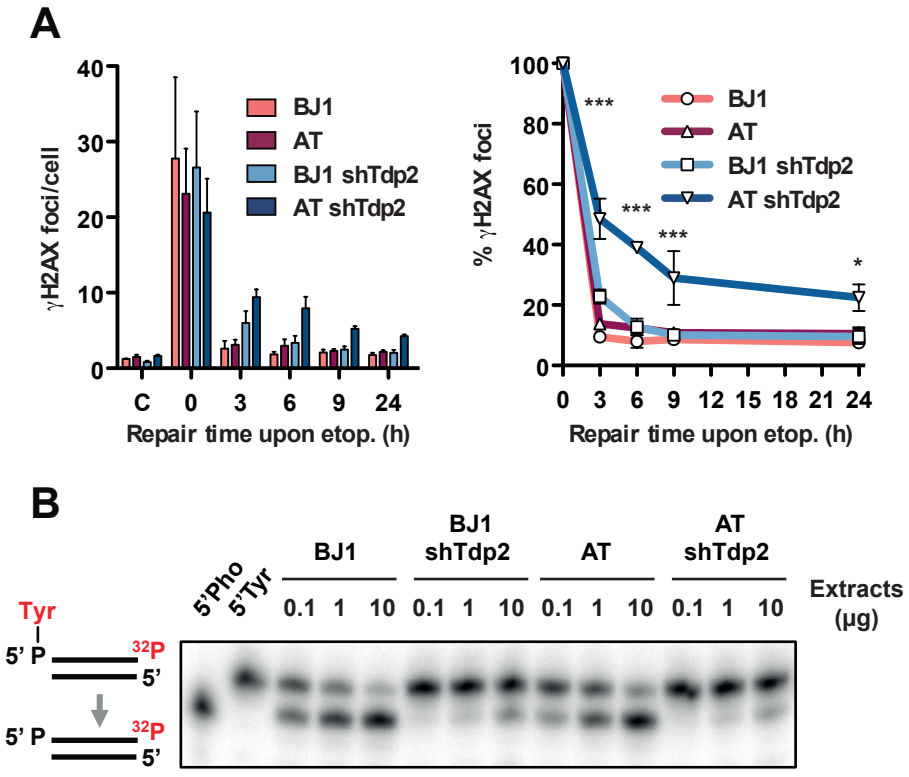

Figure 23: ATM facilitates repair of TOP2 blocked DSBs in human cells (A) γH2AX foci induction and disappearance upon 30 min treatment with 20 μM etoposide and different repair times in primary fibroblast derived from A-T patients (AT) and wildtype controls (BJ1) depleted (shTDP2) or not for TDP2. Total number of foci (left) and percentage remaining (right) is shown. Average ± s.e.m. of at least three independent experiments is shown (left). Statistical significance by two-way ANOVA test with Bonferroni post-test is indicated (*P≤0.05; **P≤0.01; ***P≤0.001) (right). **(B)** A duplex substrate harbouring a 5' phosphotyrosine blunt end was incubated for 2h with increasing concentration of the indicated cellular extracts. Migration of the 5' phosphotyrosine (5' Tyr) and 5' phosphate (5' Pho) is shown.

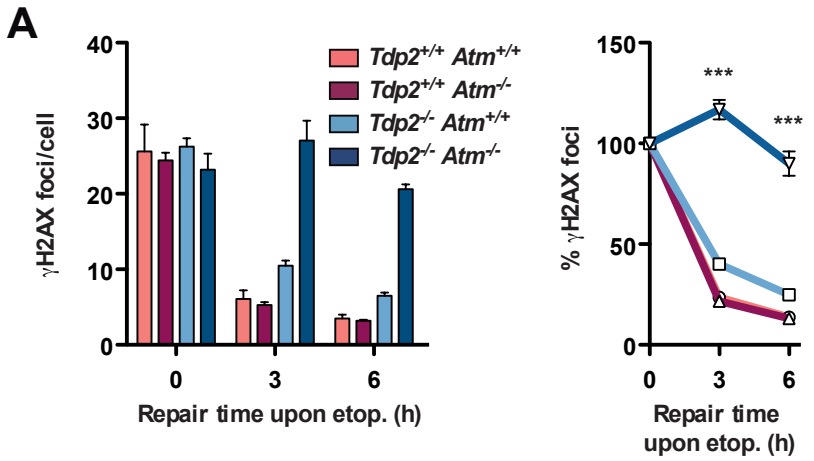

Figure 24: ATM facilitates repair of TOP2 blocked DSBs in G1 cells. (A) γH2AX foci induction and disappearance upon 30 min treatment with 20 μM etoposide and different repair times in the indicated G1 primary MEFs. Total number of foci (left) and percentage remaining (right) is shown. Average ± s.e.m. of at least three independent experiments is shown (left). Statistical significance by two-way ANOVA test with Bonferroni post-test is indicated (*P≤0.05; **P≤0.01; ***P≤0.001) (right).

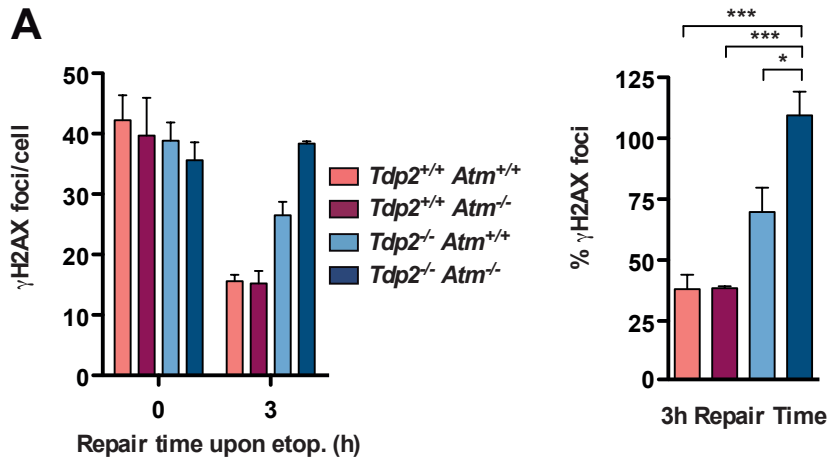

Figure 25: ATM facilitates repair of TOP2 blocked DSBs in G2 cells. (A) γH2AX foci induction and disappearance upon 30 min treatment with 20 μM etoposide and different repair times in the indicated G2 primary MEFs. Total number of foci (left) and percentage remaining (right) is shown. Average ± s.e.m. of at least three independent experiments is shown (left). Statistical significance by two-way ANOVA test with Bonferroni post-test is indicated (*P≤0.05; **P≤0.01; ***P≤0.001) (right).

Next, we extended our results to human by using confluency-arrested primary fibroblasts derived from A-T patients. A similar DSB-repair defect was observed when AT cells were depleted for TDP2, and not in neither wild type nor non-depleted controls (Figure 23A). However, in this case the effect was milder compared to previous results figure 19A, perhaps due to an incomplete knockdown of TDP2, as determined by a ~10% residual 5'-TDP activity (Figure 23B). Finally, as can be seen in Figure 24 and Figure 25, the synergistic repair defect observed between TDP2 and ATM deficiency upon etoposide, was not restricted to quiescent cells, since it was also observed in cycling cells (both in G1 and G2). Overall, this set of results constitutes strong evidence for an involvement of ATM in DSB repair, but specifically when DSBs are blocked, being extensive to rodent and human cells. Moreover, we can conclude that the mechanism underlying this phenotype directly relies on ATM kinase activity.

4. ATM function in blocked DSB repair on the chromatin status

In the currently accepted model, ATM is specifically required to repair DSBs associated to heterochromatin regions. It has been proposed to promote heterochromatin decompaction, facilitating access to the repair machinery. Despite TOP2 activity being enriched in highly transcribed euchromatin regions, we aimed to test if ATM function in the repair of blocked lesions was related with its role in heterochromatin-associated DSBs. For this, we decided to analyse by three-dimensional confocal microscopy, the location of etoposide-induced γH2AX foci with respect to heterochromatin in *Tdp2*$^{-/-}$ *Atm*$^{-/-}$ confluency-arrested primary MEFs (Figure 26). As expected, none of the γH2AX

foci induced with etoposide colocalized within highly dense chromocenters and only 15.45% (34 out of 220 foci scored) were located at less than 0.4 µm from its boundaries (Figure 26A), which we considered to be heterochromatin associated. In these same

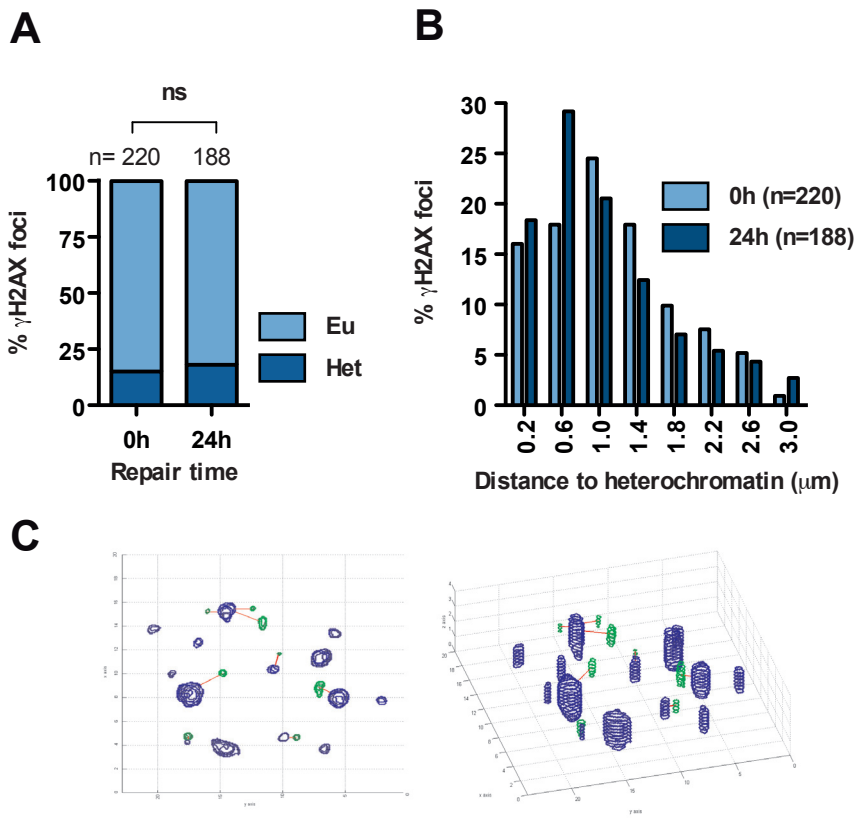

Figure 26: Unrepaired TOP2-blocked DSBs are not associated with heterochromatin. Confluency-arrested *Tdp2*$^{-/-}$*Atm*$^{-/-}$ primary MEFs were treated 30 min 10µM etoposide. (A) Percentage of γH2AX foci that are located within heterochromatin (Het) or euchromatin (Eu) following 0 and 24 h repair after treatment. A cut-off distance of 0.4 µM from the centroid of each focus to the nearest euchromatin/ heterochromatin boundary was applied. Statistical significance by Chi Square test is indicated. **(B)** Distribution of distances between γH2AX foci and heterochromatin as determined above. Bins of 0.4 µm centred on the indicated distance were used for representation. **(C)** Example of the automatic calculation of distances between γH2AX foci (green) and densely DAPI-stained chromocenters (blue) used for the data shown above. Both a z-stack projection (left) and a 3D reconstitution (right) are shown.

conditions, a significantly higher percentage of the breaks (~40%) required ATM activity for their repair (see Figure 19A), indicating that the chromatin status of a TOP2-induced DSB is not a major determinant of ATM requirement for repair. Furthermore, if ATM loss would impair just heterochromatin-associated DSBs repair, an increase in the percentage of foci in close proximity to this regions would be expected as repair proceeds. However, the overall distribution of heterochromatin-associated foci was not significantly changed following 24h of repair (Figure 26B), with the vast majority of unrepaired foci (81.92%) being located within euchromatin (Fig.26A). Therefore, we conclude that the involvement of ATM in the repair of TOP2-blocked DSBs is largely independent of its role in facilitating repair of heterochromatin associated-DSBs.

5. ATM facilitates repair of blocked-DSBs preserving DNA sequence

TOP2-blocked DSBs represent only one type of many possible blockages occurring in vivo. We therefore aimed to confirm the involvement of ATM in the repair of blocked DSBs using a TOP2-independent system, in which structure of DNA ends could be molecularly controlled. We started by searching for a 5' modification that could block DNA ends in vitro. We found that 5' biotin (5'-Bio) was not removed from duplex oligonucleotides in vitro by HEK293T cellular extracts, while a clear 5'-TDP activity was observed under the same conditions (Figure 27). Therefore, we decided to use this 5'-Bio modification to block ends of the pEGFP-Pem1 system. This system has been widely used as a measure of NHEJ repair, since reconstitution of GFP expression occurs when linear plasmids are recircularized after transfection in mammalian cells (Figure 28A).

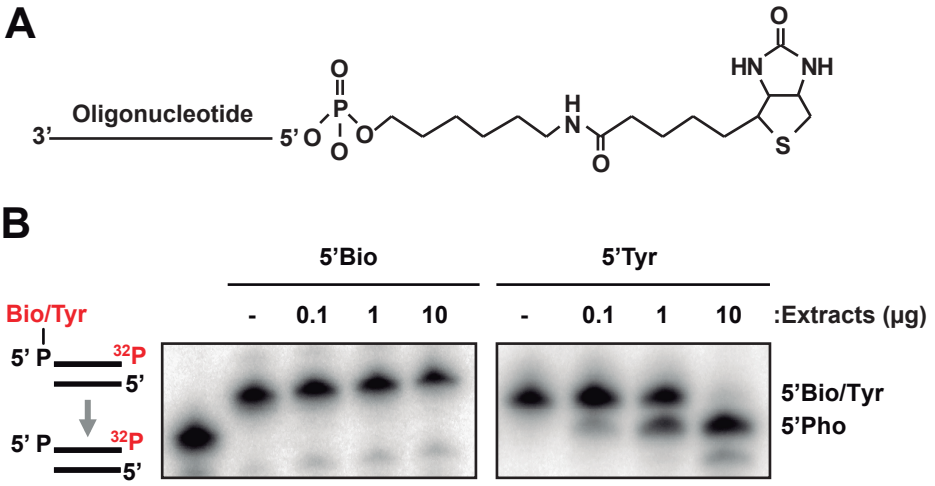

Figure 27: 5'-biotin blocks DSB ends. (A) Scheme of the structure of the 5'-biotin modification used. **(B)** Duplex substrates harbouring a 5'-biotin (5'Bio) or a 5'-tyrosine (5'Tyr) blunt end were incubated with the indicated concentration of HEK293T cellular extracts for 2 h. Migration of the 5' biotin, 5' tyrosine and 5' phosphate (5'Pho) is indicated.

Using PCR-mediated amplification using primers with different 5' termini, we were able to generate DNA substrates that harboured either clean 5'-phosphates (5'-Pho) or blocked 5'-biotins (5'-Bio). This was confirmed by streptavidin-mediated pull-down, in which only the linear plasmids containing 5' biotin termini were isolated (Figure 28B).

Taking advantage of this experimental setup, as can be seen in figure 29A, repair of pEGFP-Pem1 plasmids containing clean 5'-Pho was not significantly affected by incubation of HEK293T cells with an ATM inhibitor, as measured by either percentage of GFP-expressing cells (Figure 29A, left) or the total accumulated fluorescence intensity (Figure 29A, right). In contrast, repair of 5' biotin linear DNA was significantly decreased by ATM inhibition, regardless of the quantification method used. As an additional control,

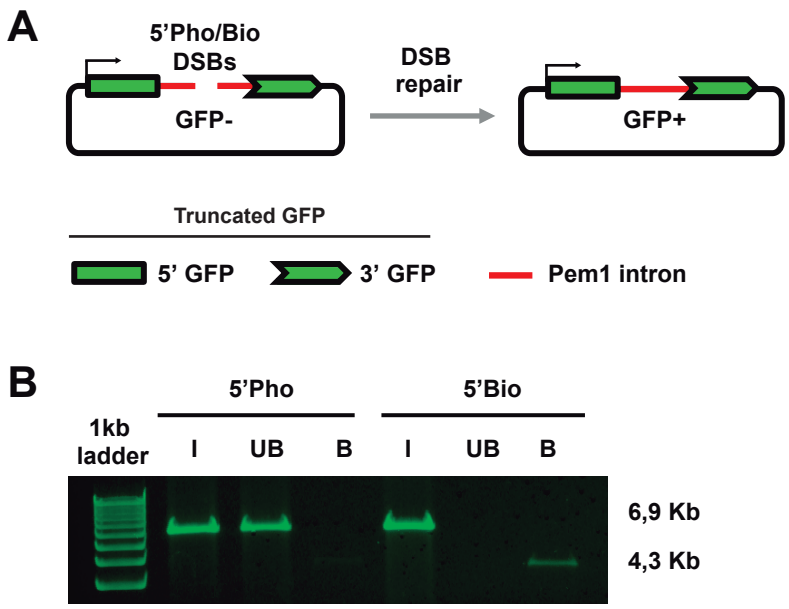

Figure 28: pEGFP-Pem1 system can be modified to measure blocked DSB repair. **(A)** Scheme of the system harbouring 5′ phosphate or 5′ biotin ends (left) and a truncated form of the GFP gene. The expected repair product yields GFP expresion (right). Pem1 intro allows insertions and deletions in the joining site without disrupting GFP expression. **(B)** Validation of the substrates used. Each substrate was incubated with streptavidin-coated magnetic particles. Input (I), unbound (UB) and bound (B) fractions are shown.

we found that ATM was not required to repair a 5' hydroxyl (5'-OH) modification, that should not result in end blockage due to the presence of PNKP enzyme, which convert 5'-OH into 5'-Pho (Figure 29B). Therefore, by using a molecularly defined system, we confirmed that the absence of ATM kinase activity impedes the efficient repair of blocked DSBs.

Additionally, we analysed not just the quantity, but also the quality of repair. For this, we amplified a minimum of 46 individual events for each condition by bacterial

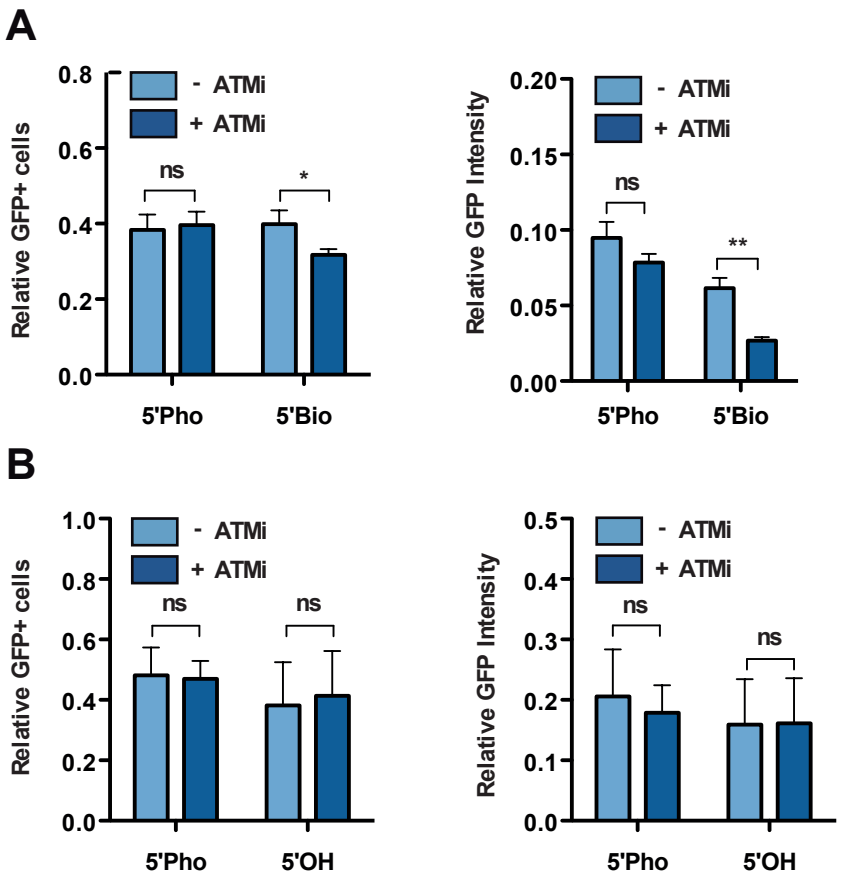

Figure 29: : ATM facilitates repair of biotin-blocked DSBs (A) HEK293T cells were transfected in the presence or absence of 10 μM ATM inhibitor with the substrates described in figure 28, and analysed by FACS for GFP-positive cells (left) and average GFP intensity (right). In both cases, data are relative to transfection with a control pEGFP-Pem1 circular plasmid. Average±s.e.m. of four independent experiments and statistical significance by two-way ANOVA with Bonferroni post-test is shown (*P≤0.05; **P≤0.01; ***P≤0.001). **(B)** Same as "A" but cells were transfected with linear plasmids containing 5′ phosphate or 5′ hydroxyl ends.

cloning. Single repair events were subject to restriction analysis to measure losses in the DNA sequence (Figure 30). It is important to mention that blockage in DSB termini decreased repair accuracy per se, independently of ATM status. However, ATM inhibition

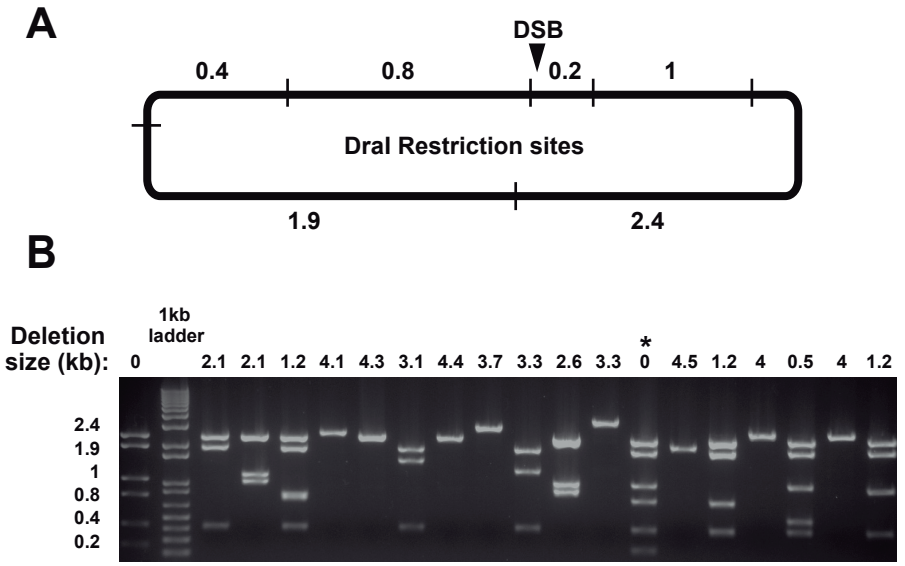

Figure 30: Deletion analysis of plasmids rescued from transfected HEK293T cells (A) DraI restriction map of re-circularized pEGFP-Pem1 plasmid. The DSB site is indicated (arrow). **(B)** Representative repair events rescued from cells treated with ATMi and transfected with 5' biotin substrates previously used in Figure 29. Single repair events were analysed by agarose gel electrophoresis after DraI endonuclease enzyme digestion. Deletion size calculated for each individual clone is indicated. Control of pEGFPPem1 re-circularized plasmid is shown (lane 1). Asterisk indicates a clone without detectable deletion.

had negligible impact on the quality of 5'-Pho DSB repair. On the contrary, when 5'-Bio plasmids were assayed, a marked decrease (from 20% to 5%) in the percentage of repair events not carrying detectable loss of sequence was observed (Figure 31A). Nonetheless, in the clones showing DNA loss, the average size of deleted sequence was unchanged by ATM inhibition (Figure 31B). This demonstrates that ATM prevents excessive sequence loss from DNA ends, which suggest an involvement in the regulation of blocked DSB end processing.

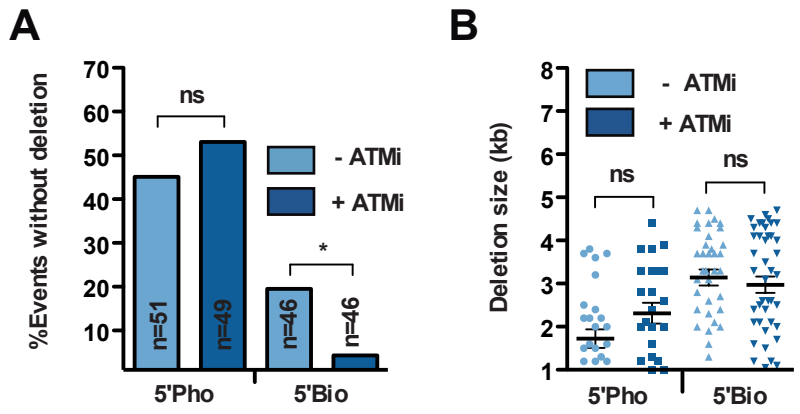

Figure 31: ATM protects degradation of biotin-blocked DSB ends (A) Percentage of plasmid-repair events not associated with detectable sequence loss. Statistical significance by Chi Square test is shown (*P≤0.05; **P≤0.01; ***P≤0.001). **(B)** Distribution of the size in single repair events that contained deletions. Average±s.e.m. and statistical significance by Kruskal-Wallis test with Dunn's post-test are indicated.

6. ATM function on blocked DSBs has consequences for the cell

The incapacity to properly repair even a single DSB can lead to cell death and/or genome rearrangements. It is therefore conceivable that the ATM loss could have a drastic impact in cells upon TOP2-induced DSBs, aggravated when DSBs are blocked. To test this hypothesis, we exploited our genetic approach to address the cellular implications of ATM loss upon 'clean' against 'blocked' TOP2-induced damage.

For this, cell survival in response to increasing doses of etoposide was measured by clonogenic assay. We observed that Atm deletion in transformed MEFs had a negligible effect on etoposide sensitivity in *Tdp2*$^{+/+}$ background. In contrast, sensitivity of *Tdp2*$^{-/-}$ cells, which was mild at low doses of etoposide, was significantly increased by ATM

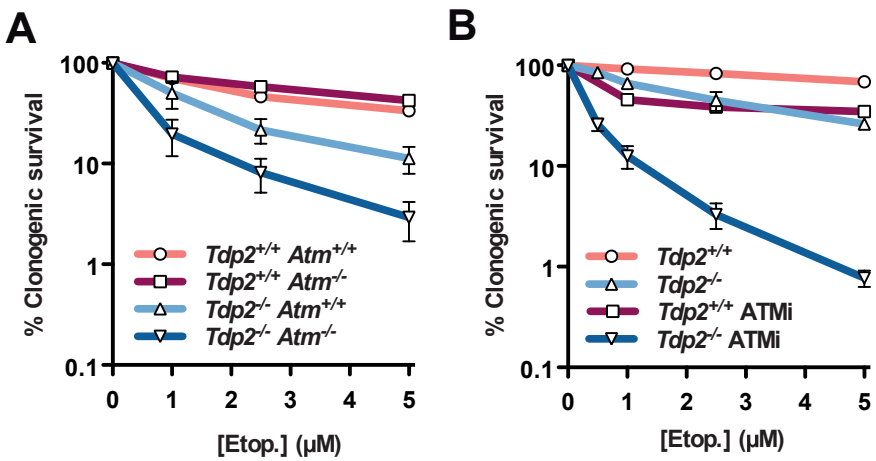

Figure 32: ATM promotes survival upon induction of blocked DSBs. (A) Clonogenic survival of the indicated transformed MEFs following acute treatment with the indicated concentrations of etoposide. Average±s.e.m. of at least three independent experiments is shown. **(B)** As above, with or without incubation with 10 μM ATM inhibitor.

loss, correlating with the observed synergistic repair defect of combined TDP2 and ATM loss (Figure 32A). An even larger effect was observed if ATM inhibition was used instead of deletion (Figure 32B), confirming the requirement of the kinase activity of ATM, and ruling out differences caused by heterogeneity intrinsic to the MEFs or the cellular transformation process. Furthermore, the difference observed between deletion and chemical inhibition suggests a possible negative effect of inactive ATM, consistent with previous observations of the lethality of the catalytic dead ATM knock-in mice compared to *Atm* complete deletion (Yamamoto et al. 2012).

Furthermore, we addressed the impact of ATM deficiency on genome integrity following etoposide treatment in *Tdp2*$^{+/+}$ and *Tdp2*$^{-/-}$ transformed MEFs. First, we monitored micronuclei formation, which arise from the missegregation of chromosomes

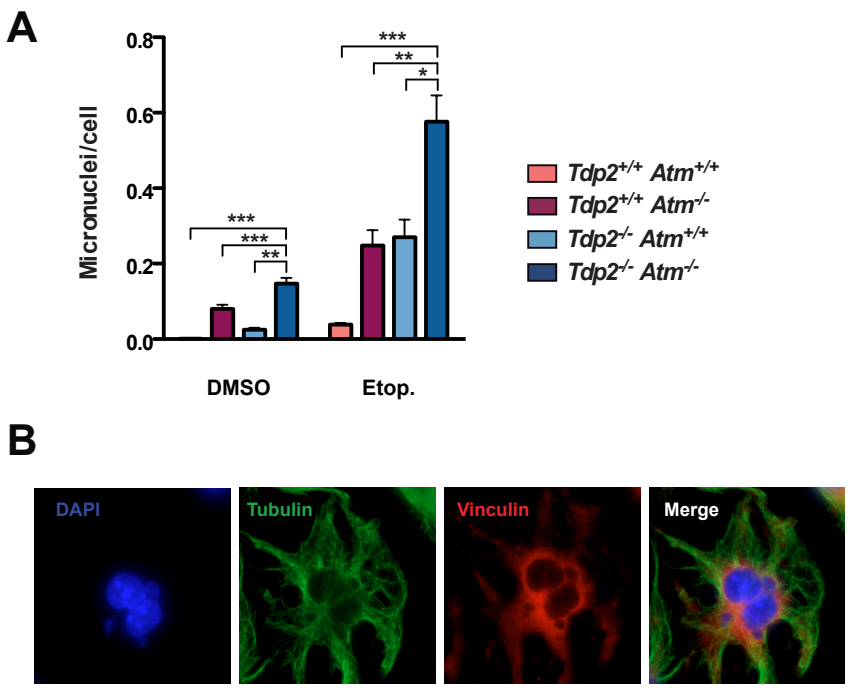

Figure 33: ATM promotes the maintenance of genome integrity upon induction of blocked DSBs. (A) Micronuclei scored in the indicated binucleated transformed MEFs following acute treatment with 2.5 μM etoposide (30 min). Histogram bars (left) represent the average±s.e.m. of n≥600 cells from three independent experiments. Statistical significance by one-way ANOVA with Bonferroni post-test is indicated (*P≤0.05; **P≤0.01; ***P≤0.001). **(B)** Representative image of a treated *Tpd2*$^{-/-}$*Atm*$^{-/-}$ cell containing multiple micronuclei. Tubulin (green), vinculin (red), DAPI (blue) and merge staining are shown.

or acentric chromosomal fragments, and it is a well-established indicator of genome instability (Fenech 2000). To restrict our analysis to micronuclei arising due to the etoposide treatment applied, cytokinesis was blocked with cytochalasin B and only binucleated cells were scored (Figure 33). Independent deletion of either *Atm* or *Tdp2* caused an increase in etoposide-induced micronuclei. Interestingly, the levels were further increased when both genes were simultaneously deleted, doubling the frequency

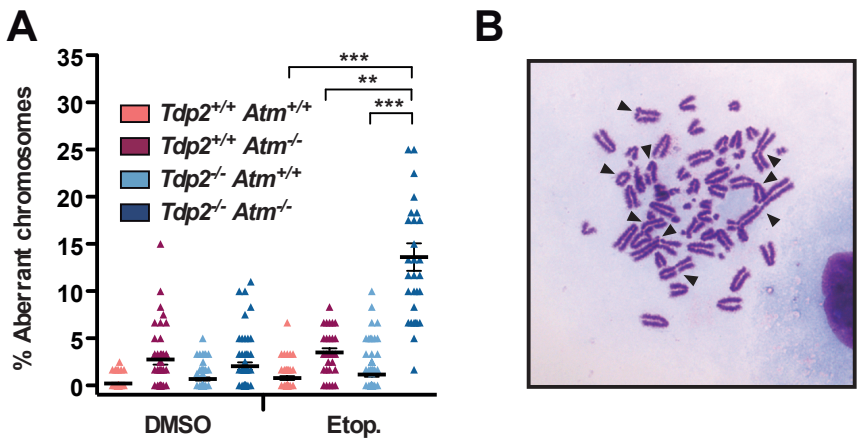

Figure 34: ATM protects cells from chromosomal abnormalities induced by blocked DSBs. (A) Chromosomal aberrations (both break and exchange type) following acute treatment with 2.5 μM etoposide (30 min). Plot shows the number of aberrations per 100 chromosomes from individual metaphase spreads obtained in at least 6 independent experiments. Average±s.e.m. and statistical significance by Kruskal-Wallis test with Dunn's post-test is indicated (*P≤0.05; **P≤0.01; ***P≤0.001). **(B)** Representative image of a *Tpd2*$^{-/-}$*Atm*$^{-/-}$ metaphase containing multiple chromosomal aberrations (arrows).

observed in either single mutant. It is worth noting that the frequency observed corresponds to extremely high levels of instability, with many of the cells displaying multiple micronuclei, a qualitative difference compared with single mutants. To extend the analysis on genome instability, we scored chromosomal aberrations in metaphase spreads (Figure 34). Following etoposide treatment, *Tdp2*$^{-/-}$*Atm*$^{-/-}$ cells displayed a marked increase in the number of chromosomal aberrations observed. A wide variety of aberration types were observed, including breaks, radial chromosomes and fusions. On average, these cells showed a striking 15% aberrant chromosomes, which represent a 7.5-fold and 3-fold increase when compared to single *Tdp2*$^{-/-}$*Atm*$^{-/-}$ mutants, respectively. Altogether, these results demonstrate that ATM promotes cell survival and maintains genome integrity upon blocked DSBs.

Tdp2$^{-/-}$ *Atm*$^{-/-}$ mice recapitulate the cellular phenotype

Considering that ATM deficiency has a striking impact on cells upon blocked DSBs induction, we hypothesized that this type of lesions could have severe physiological consequences in a complex organism such as mouse. To test this, mice originated from *Tdp2* and *Atm* double heterozygote crosses (*Tdp2*$^{+/-}$*Atm*$^{+/-}$ x *Tdp2*$^{+/-}$*Atm*$^{+/-}$) were generated. They were born with no detectable gross abnormality and in normal mendelian proportions (Figure 35A).

In order to determine the impact of TDP2 and ATM loss upon TOP2-induced damage, adult mice (8 wk) homozygous for *Tdp2* and *Atm* deleted alleles were subject to a single intraperitoneal injection of etoposide (25 mg/kg). As can be seen in Figure 35B, *Tdp2*$^{-/-}$*Atm*$^{-/-}$ double-knockout mice showed a severe hypersensitivity upon etoposide exposure, suffering a progressive weight loss reaching a 15% loss after 6 days, when animals were sacrificed. Histopathological analysis revealed marked villous atrophy in the small intestinal mucosa as the likely cause of the drastic weight loss (Figure 35C). In contrast, etoposide injections have negligible effect in either wildtype or ATM-deficient mice, and only a mild weight loss and intestinal atrophy was observed in *Tdp2*$^{-/-}$ animals. These results suggest a protective role of ATM against adverse effects of etoposide in vivo, but just when TDP2 is absent. For this, we can conclude that the phenotype of etoposide sensitivity observed in cells is consistently recapitulated in mice.

A

Genotype	Observed	Expected
Tdp2$^{+/+}$*Atm*$^{+/+}$	24	32
Tdp2$^{+/+}$*Atm*$^{+/-}$	70	75
Tdp2$^{+/+}$*Atm*$^{-/-}$	27	32
Tdp2$^{+/-}$ *Atm*$^{+/+}$	58	64
Tdp2$^{+/-}$ *Atm*$^{+/-}$	152	130
Tdp2$^{+/-}$ *Atm*$^{-/-}$	69	65
Tdp2$^{-/-}$ *Atm*$^{+/+}$	27	32
Tdp2$^{-/-}$ *Atm*$^{+/-}$	60	65
Tdp2$^{-/-}$ *Atm*$^{-/-}$	31	32
Total	518	

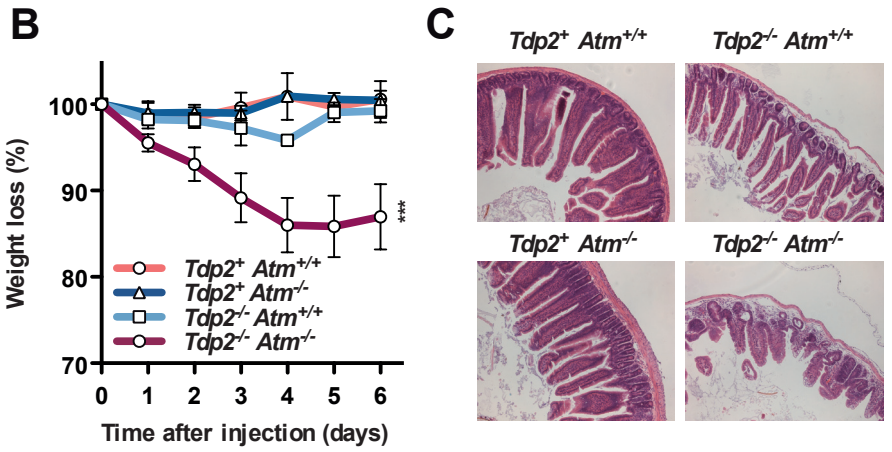

Figure 35: ATM loss confers hypersensitivity to blocked DSB induction in mice. **(A)** Genotypes of the progeny of crosses between *Tdp2/Atm* double-heterozygote mice expected by mendelian proportions and observed are shown. **(B)** Body weight of 8-week old mice cohorts intraperitoneally injected with a single dose of etoposide (25mg/kg). Average ± s.e.m. of the percentage of initial body weight from 5 mice and statistical significance by Two-way ANOVA with Bonferroni post-test are shown (*P≤0.05; **P≤0.01; ***P≤0.001). **(C)** Representative images of hematoxylin-eosin stained jejunum slices obtained 6 days after etoposide exposure.

In previous work, in addition to intestinal damage, etoposide injections resulted in elevated splenic and thymic atrophy in *Tdp2*$^{-/-}$ mice compared to wildtype (Gómez-

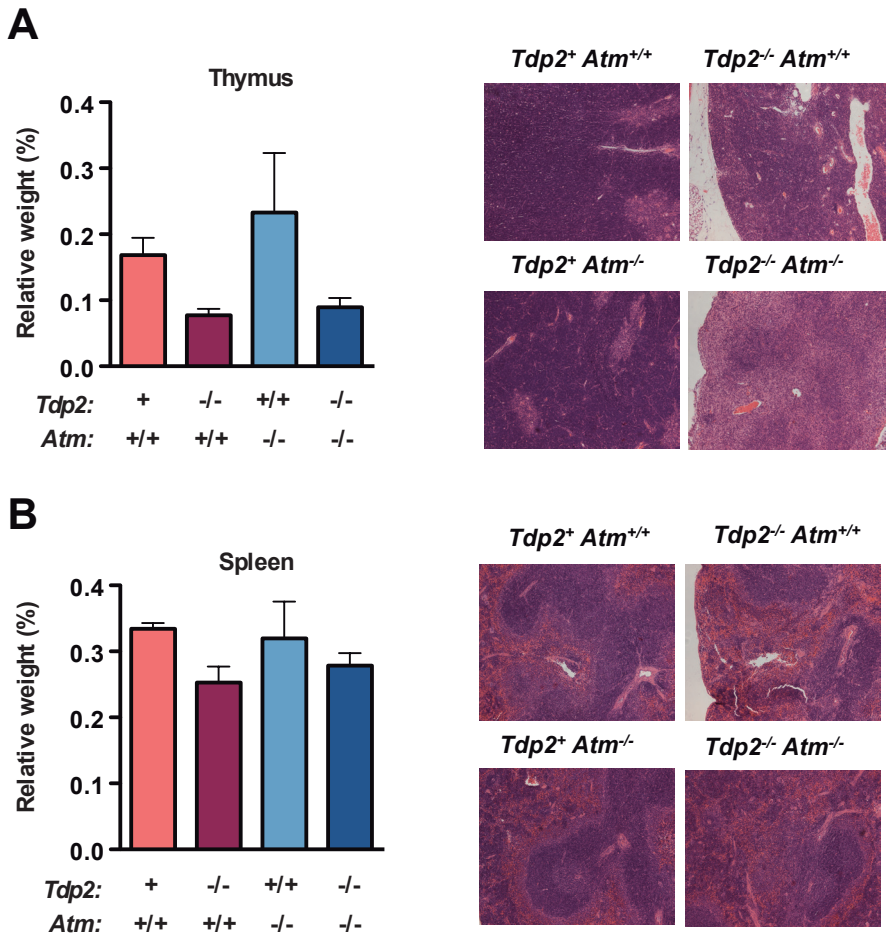

Figure 36: ATM loss does not affect thymus or spleen upon blocked DSB induction
(A) Weight of thymus from mice sacrified in Figure 21 was measured (left). Average ± s.e.m. is indicated. Representative images of hematoxylin-eosin stained tissue slices are shown (right). **(B)** Same as in "A" but for spleen tissue was analysed.

Herreros et al. 2013). Consistently, histological analysis of thymus and spleen in TDP2-deficient animals revealed a reduction in weight and cellular content (Figure 36). This effect was milder compared to higher etoposide dose and remarkably more pronounced

in thymus than in spleen (note the low density of dark-stained nuclei (Figure 36A, right). However, we observed a negligible effect of ATM inactivation in these particular tissues.

7. *Tdp2*$^{-/-}$*Atm*$^{-/-}$ mice display elevated mortality due to an increased incidence of thymic lymphoma

Based on our previous results, we can propose blocked DSBs as a potential threat to ATM-deficient animals. Indeed, we wondered whether this type of damage could underlie some of the symptoms of the A-T syndrome. We reasoned that if TOP2 damage underlies any of the phenotypes observed in ATM mouse model, inactivation of TDP2 would largely aggravate it.

Mice carrying homozygous deletion of Atm alleles were previously reported to be smaller in size (Barlow et al. 1996). For this, the body weight of male mice was measured 4 weeks after birth. As expected, *Atm*$^{-/-}$ mice showed a significant decrease in size compared to wildtype. On the contrary, deletion of Tdp2 did not aggravate the decreased size characteristic of Atm mice (Figure 37A). Nonetheless, when cellular growth index was measured in primary MEF cultures, *Tdp2*$^{-/-}$*Atm*$^{-/-}$ cells showed a marked reduction in proliferation compared with single mutants (Figure 37B), suggesting that TOP2-damage arises spontaneously, impacting on cell growth ex vivo.

Since inactivation of both genes has negligible effect during development, we decided to analyse their life span. For this, weight and general health status was monitored

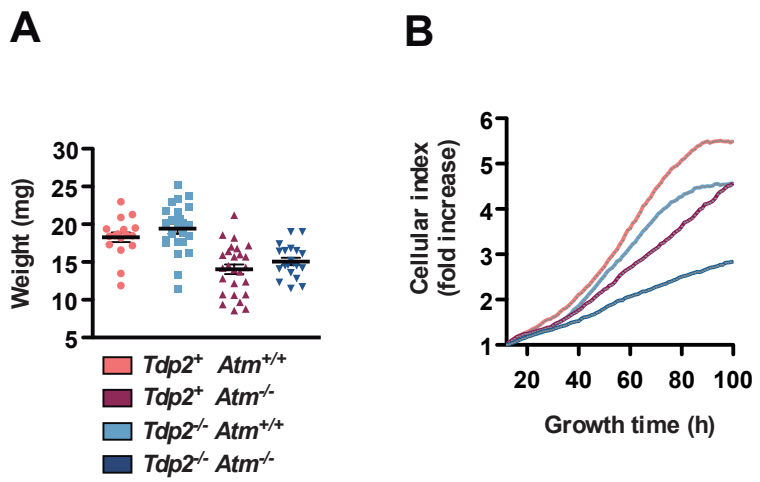

Figure 37: The effect of TDP2 and ATM deficiency on cellular and mouse growth. **(A)** Weight of at least 20 male mice of the indicated genotypes 4-weeks after birth. **(B)** Cellular growth index was measured hourly during 3 days in the indicated genotypes of primary MEFs.

weekly in a minimum of 20 mice per genotype, until reaching the experimental endpoint of 720 days (Figure 38A). ATM-deficient mouse model is characterized by an acute mortality within the first year of life, with a large number of animals developing massive thymic tumours. They succumb to disease since fast-growing T-cell lymphomas lead to lung collapse (Figure 38B, right). Consistent with this, we observed that ATM-deficient animals showed an increased death rate compared to wildtype. Strikingly, this was largely aggravated by Tdp2 inactivation, since *Tdp2*$^{-/-}$*Atm*$^{-/-}$ showed a median survival of 140 days, contrasting with 307 days in the case of *Tdp2*$^{+}$*Atm*$^{-/-}$ mice (Figure 38A). Furthermore, *Tdp2* and *Atm* double-knockout mice showed an increased incidence of thymic lymphoma compared with Atm single mutants, increasing from 43 % to 72 % the likelihood of developing this type of tumour during the first year of life (Figure 38B).

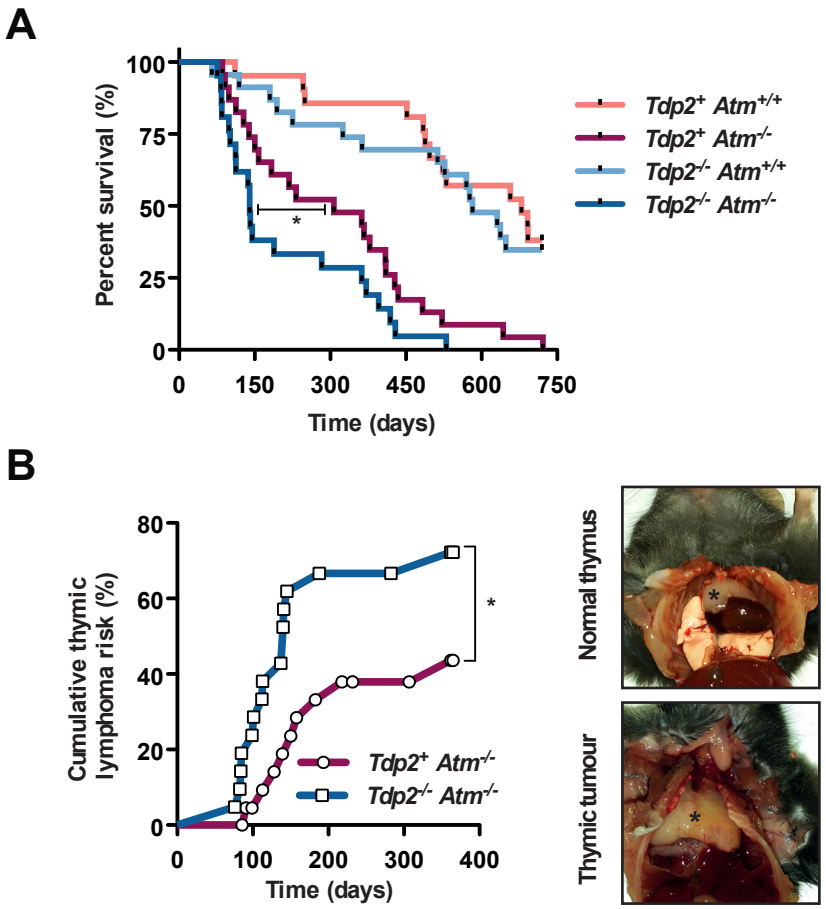

Figure 38: *Tdp2 Atm* homozygous mutant mice suffer increased incidence of thymic lymphoma. (A) Kaplan-meier survival curve of wild-type, *Tdp2*$^{+}$*Atm*$^{-/-}$, *Tdp2*$^{-/-}$*Atm*$^{-/-}$ and *Tdp2*$^{-/-}$*Atm*$^{-/-}$ mice. At least 20 animals per genotype were included in the analysis. **(B)** Representation of the cumulative risk to develop thymic lymphoma of the indicated mice (left). Statistical significance by Wilcoxon test of survival or thymic lymphoma risk is indicated (*P≤0.05; **P≤0.01; ***P≤0.001). Representative image of a thymic turmour compared to a healthy thymus (right).

Thus, we considered the possibility of TOP2 induced damage being a major determinant during A-T lymphomagenesis.

A

	Tdp2^{+} *Atm*$^{-/-}$	*Tdp2*$^{-/-}$ *Atm*$^{-/-}$
CD4-CD8-	1.98 ± 0.90	1.74 ± 0.54
CD4+CD8-	3.36 ± 1.54	3.20 ± 0.59
CD4-CD8+	1.22 ± 0.22	1.30 ± 0.40
DP	93.44 ± 0.22	93.76 ± 2.48

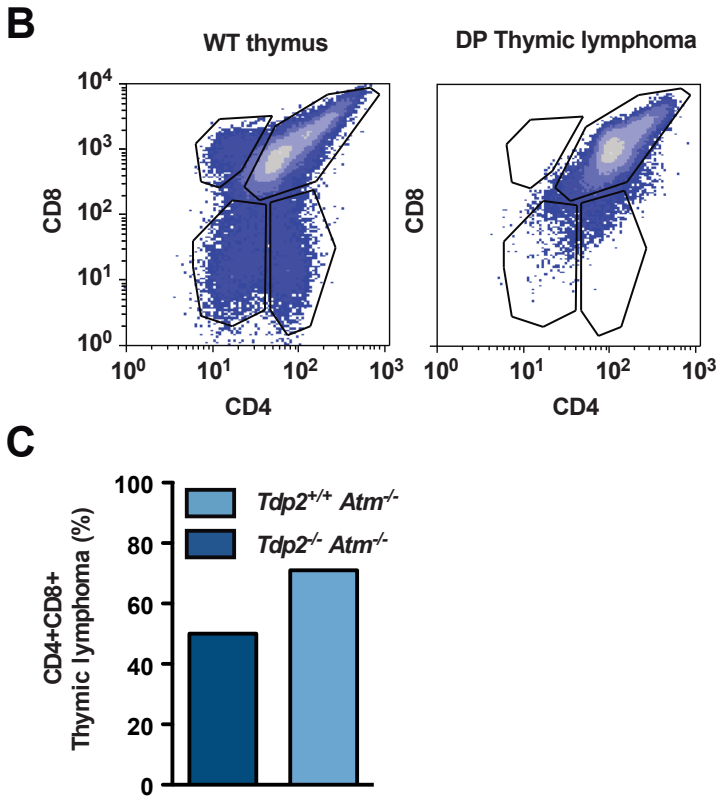

Figure 39: Characterization of *Tdp2*$^{-/-}$*Atm*$^{-/-}$ lymphomas. (A) Representation of the mean ± s.e.m of the percentage of precursors (double negative, DN), immature CD4+CD8+ (double-positive, DP), or mature CD4+CD8- and CD4-CD8+ (simple-positive, SP) T-lymphocytes. **(B)** FACs profile of T-lymphocytes extracted from a representative normal thymus (left) or a thymic tumour (right). X and Y axis represent CD4 and CD8 signal respectively. **(C)** Representation of the percentage of tumours composed by immature CD4+CD8+ lymphocytes in the indicated genotypes.

Atm$^{-/-}$ mice were reported to display decreased number in mature CD4 and CD8 single positive T-lymphocytes. Thus, we first tested if TDP loss affects the distribution. We found that double-knockout mice did not show differential distribution of T-lymphocyte populations in healthy thymus compared to *Tdp2*$^{+}$*Atm*$^{-/-}$ mice. Then, thymic lymphomas were further characterized. Fundamentally, tumours isolated from double-knockout and *Atm*$^{-/-}$ mice were formed by immature double-positive (DP) T-lymphocytes (Figure 39). In order to evaluate genomic instability in these tumours, we analyse copy number variation in the genome of cancerous cells by performing a Comparative Genomic Hybridization (CGH). Through this assay, deletions and duplications along the genome of tumour cells can be detected (Michels et al. 2007), and these regions of instability have been proven to correlate within breakpoints of oncogenic translocations. Thus, we compared instability hotspots along the genome of 6 double-knockout and 2 *Atm*$^{-/-}$ thymic tumours (Figure 40). Interestingly, we found several recurrent hotspots of instability along the genome of *Tdp2*$^{-/-}$*Atm*$^{-/-}$ mice. A marked instability in the telomeric region of chromosome 12 was observed in 6 out of 6 mice. In a similar manner, trisomy of chromosome 15 was also observed in every tumour analysed. Consistently with the contribution of V(D) J recombination to clonal translocations previously described in A-T malignancies, 4 out of 6 displayed instability along the chromosome 14, with breakpoints located in the *Tcrad* gene. Other genomic regions displaying increased instability were found, such as chromosome 19 (2 out of 6), in which *Pten* tumor suppressor is located, telomeric region of chromosome 5 (2 out of 6) and chromosome 2 and 6, with breaking points mapping in *Notch1* tumour suppressor or immunoglobulin genes respectively (1 out of 6). ATM-deficient tumours showed instability in the same regions that were observed in double-

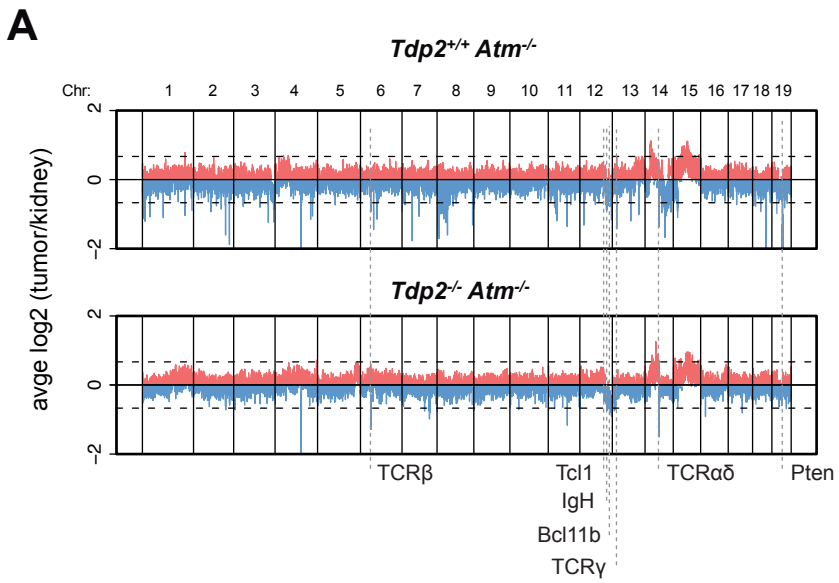

Figure 40: CGH analysis of *Tdp2*$^{-/-}$*Atm*$^{-/-}$ thymic lymphomas. (A) Each tumor sample was hybridized and analyzed using kidney DNA as control. The Y axis represents amplification/deletion index (sum of Log2 tumor/kidney ratio of all tumors analyzed). Significant copy number variations are defined by Log2 tumor/kidney > 0.66 (black dashed line). The amplification score at each probe location is plotted in red and deletion score is plotted in blue. Location of important genes in which copy number variation has been previously described is indicated.

knockout tumours. Importantly, every breakpoint and instability hotspot observed in our analysis were described in previous characterization of the ATM-deficient mouse model (Zha et al. 2010). Thus, our result suggests that TDP2 loss does not alter the location and distribution of chromosomal breakage that induces oncogenic translocations of thymic malignancies in *Atm*$^{-/-}$ mice. This, together with the marked increase in the incidence of thymic lymphomas observed in double-knockout mice compared to single *Atm* deletion, suggests that TOP2 could participate in the neoplastic changes described in A-T.

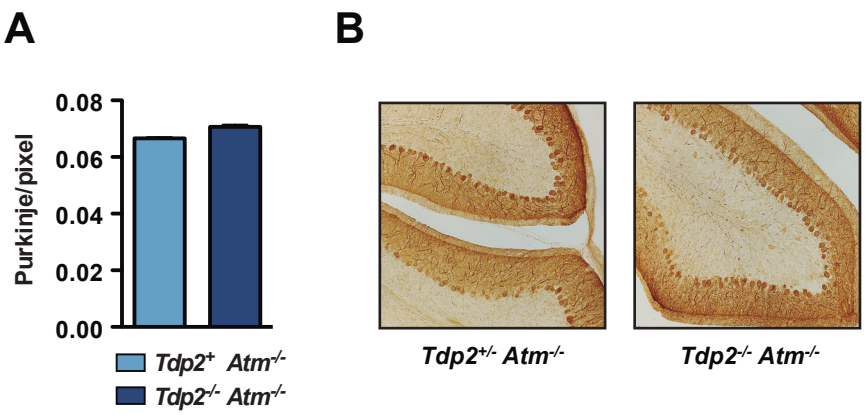

Figure 41: *Tdp2*$^{-/-}$*Atm*$^{-/-}$ mice do not show cerebellar neurodegeneration. (A) Purkinje cellular density observed by calbindin immunohistochemistry on sagital vibratome sections of cerebellums obtained from *Tdp2*$^{+}$*Atm*$^{-/-}$ and *Tdp2*$^{-/-}$*Atm*$^{-/-}$ 8-weeks old mice. At least three independent individuals per genotype were analyzed. **(B)** Representative images of cerebellum.

ATM-deficient mice recapitulate the majority of A-T symptoms, with the exception of the progressive Purkinje cell loss leading to cerebellar ataxia. It is important to mention that the lack of an adequate animal model for this particular feature has traditionally impeded the study of the most debilitating symptom of A-T. Therefore, we tested whether TDP2 inactivation influences cerebellum integrity in 8-week mice. We did not observe any reduction in Purkinje cell density in cerebellar tissues when double-knockout were compared with single ATM-deficient animals (Figure 41). Moreover, animals that were subject to lifespan analysis (Figure 38A) did not show any gross deficiency in motor skills at any point of the experiment. It is important to remark that TOP2-induced damage as a trigger of cerebellar ataxia in A-T disease cannot rule out by these results, since the mouse model has proved to be an inadequate model for neurodegeneration in numerous DDR-related diseases.

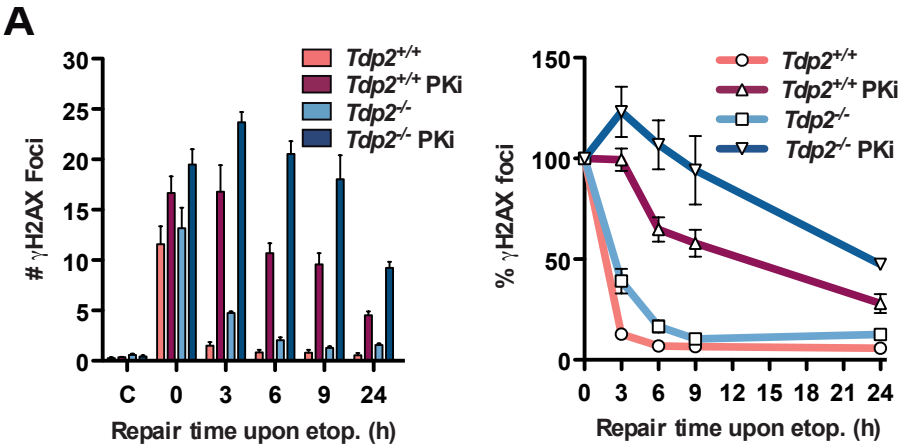

Figure 42: DNA-PKcs activity mediates repair of TOP2-induced DSBs (A) γH2AX foci induction and disappearance upon 30 min treatment with 10 μM etoposide and different repair times in the indicated confluency arrested primary MEFs incubated or not with 10 μM DNA-PKi. Total number of foci (left) and percentage remaining (right) is shown. Average ± s.e.m. of at least three independent experiments is shown (left). Statistical significance by two-way ANOVA test with Bonferroni post-test is indicated (*P≤0.05; **P≤0.01; ***P≤0.001) (right).

8. DNA-PKcs activity and ATM redundantly promote repair of blocked-DSBs.

DNA-PKcs and ATM are enzymes that belong to the same PI3K-like kinase family. They have been reported to modulate the DNA damage response upon DSB-induction, and redundant and non-redundant functions have been described. Therefore, we decided to test if DNA-PKcs was implicated in the repair of blocked DSBs. For this, we decided to test how inactivation of DNA-PKcs would impact TOP2-induced DSB repair in wildtype and TDP2-deficient backgrounds. As above, we followed the time course of γH2AX foci disappearance after etoposide treatment in G0 primary MEFs (Figure 42). As previously reported, wildtype cells showed accumulation of unrepaired

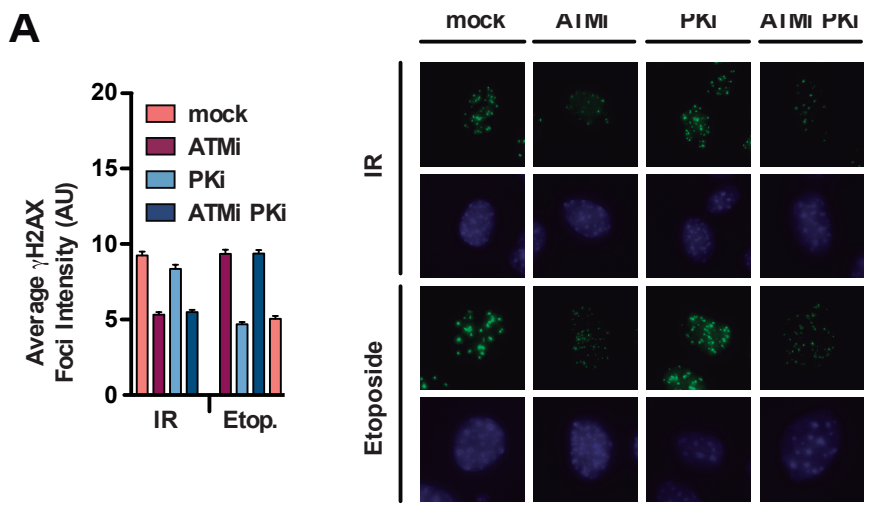

Figure 43: Induction of γH2AX foci upon ATM and DNA-PKcs inactivation (A) Average foci intensity of γH2AX foci after 30 min 10 μM etoposide treatment in confluency arrested primary MEFs incubated with ATMi, DNA-PKi and the combination of both inhibitors (left).

foci when DNA-PKcs activity was inhibited, according to its general role in NHEJ. Interestingly, DNA-PKcs inactivation showed a further DSB repair defect in *Tdp2*$^{-/-}$ cells compared with the wildtype. These points out the specific requirement of DNA-PKcs in blocked DSB repair, suggesting an additional role in processing beyond its general function in NHEJ.

Since these kinases have been reported to be responsible for the redundant phosphorylation of H2AX (Burma et al. 2001; Stiff et al. 2004), we analysed γH2AX foci induction upon irradiation and etoposide exposure in the presence of ATM and DNA-PKcs inhibitors (Figure 43). Consistently with previous results, we observed that γH2AX formation is largely dependent on ATM kinase, since foci intensity was largely reduced by ATM inhibition. Nevertheless, DNA-PKcs inhibition by itself or in combination

with ATM inactivation, showed a negligible impact on γH2AX foci intensity. Therefore, we validated the use of γH2AX foci scoring to measure DSB repair in conditions in which both kinases are inactivated.

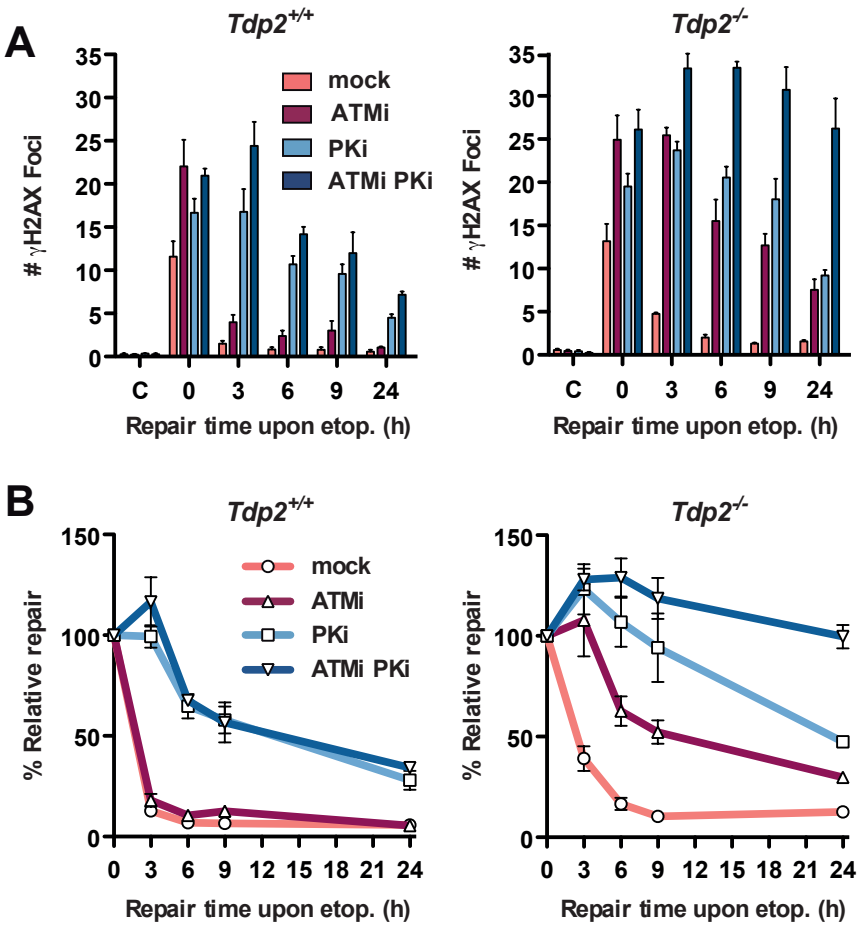

Figure 44: ATM and DNA-PKcs kinase activities redundantly promote the repair of TOP2-induced blocked DSBs (A) γH2AX foci induction and disappearance upon 30 min treatment with 10 μM etoposide and different repair times in wild-type confluency arrested primary MEFs incubated or not with 10 μM ATMi, DNA-PKi or the combination of both inhibitors. Total number of foci (upper) and percentage remaining (lower) is shown. Average ± s.e.m. of at least three independent experiments is shown (left). Statistical significance by two-way ANOVA test with Bonferroni post-test is indicated (*P≤0.05; **P≤0.01; ***P≤0.001) (right). **(B)** Same in "A" but with *Tdp2*$^{-/-}$ MEFs.

To determine the interaction between ATM and DNA-PKcs in the repair of TOP2-induced damage, we followed the time course of γH2AX foci disappearance after etoposide treatment, combining ATM and DNA-PKcs chemical inhibition. As can be seen in Figure 44A, inhibiting ATM had a negligible effect in the repair of clean DSB, even when DNA-PKcs was inactivated. Strikingly, in TDP2-deficient cells, the combination of both inhibitors showed a marked repair defect compared with single inactivation (Figure 44B). Moreover, in cells carrying deletions in Atm and inactive DNA-PKcs, TDP2 deficiency results in the complete abrogation of DSB repair (Fig.45A). Curiously, under *Atm* deletion and the chemical inhibition of DNA-PK, γH2AX foci formation was absent at 30 min after etoposide exposure (Fig.45B), but foci could be proficiently scored at 9h after etoposide removal.

In any case, to avoid artefacts due to the indirect measure of DSBs in conditions in which γH2AX foci induction was impaired, we performed the neutral comet assay (Figure 45C). This approach is based in the direct measure of DSBs, by comparing the electrophoretic mobility of the DNA contained in the nuclei of single cells embedded in agarose (Olive & Banath 2006). We did not observe differential comet signal in *Tdp2*$^{-/-}$ *Atm*$^{-/-}$ MEFs when they were incubated or not with DNA-PKcs inhibitor, confirming that similar number of DSBs are induced by etoposide exposure. This result validates γH2AX foci scoring performed in Figure 45A as an efficient measure of DSB repair. On top of this, after 12 hours of etoposide withdrawal, inhibition of DNA-PKcs combined with ATM-deficiency totally impaired DSB repair, consistent with our previous result.

Based on our observations, we anticipated that impairment of both, ATM and DNA-PKcs activity, would lead to severe consequences for cell integrity upon blocked DSB exposure. Thus, cell survival was monitored by clonogenic assay in response to

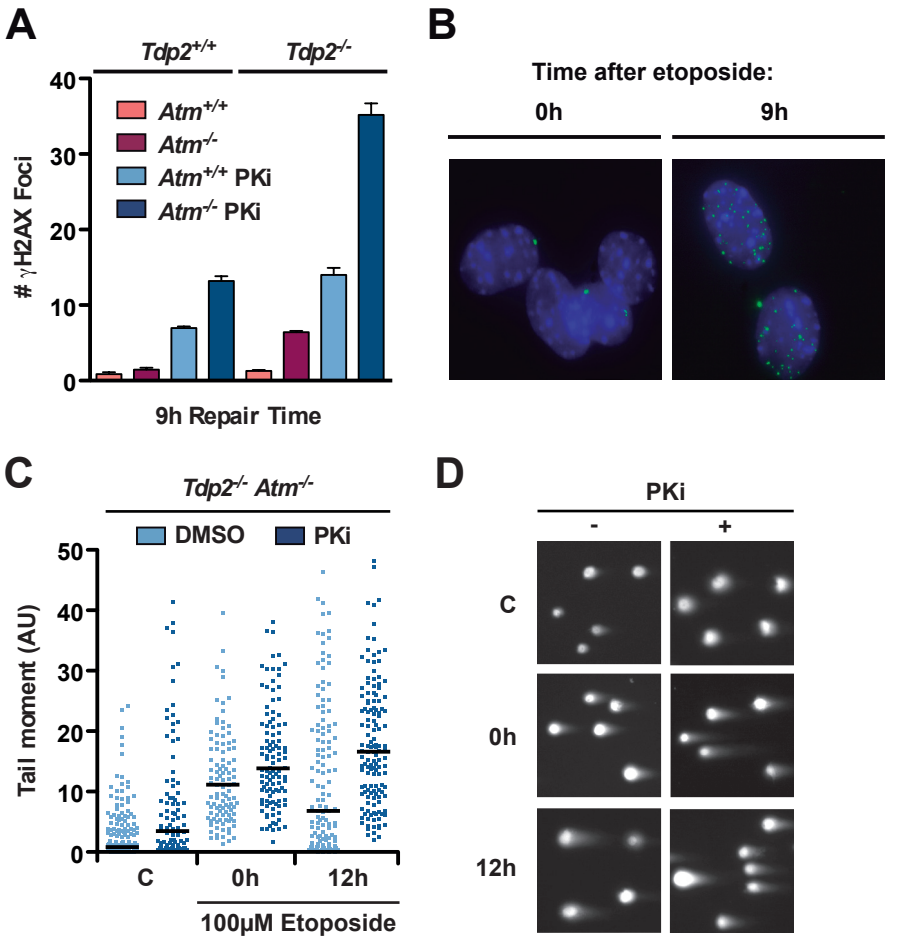

Figure 45: DNA-PKcs inactivation aggravates ATM deletion repair defect to TOP2-induced blocked DSBs. (A) γH2AX foci after 9 h following drug removal (30 min 10 μM etoposide) in the indicated genotypes of confluency arrested primary MEFs incubated or not with 10 μM of DNA-PKcs inhibitor. **(B)** Representative images of γH2AX foci (green) and DAPI counterstain (blue) for the induction (0 h) and 9 h repair time point in *Tdp2*$^{-/-}$ *Atm*$^{-/-}$ cells upon DNA-PKcs inhibition are shown. **(C)** Neutral comet assay in confluency arrested primary MEFs incubated 1 h 100 μM etoposide treatment and 12 h repair point (left). A representative image is shown (right).

increasing doses of etoposide in wildtype and *Tdp2*$^{-/-}$ transformed MEFs (Figure 46). Combined ATM and DNA-PKcs inactivation resulted in etoposide sensitivity compared to single inhibition, even in wild-type background (Figure 46A). Nevertheless, a largely aggravated hypersensitivity to etoposide was observed in TDP2-deficient background when ATM and DNA-PKcs were simultaneously inactivated, even at lower doses of etoposide (Figure 46B). This altogether suggests that ATM and DNA-PKcs encompasses two redundant pathways to protect cell integrity upon DSBs, but they are especially important for the survival upon blocked DSBs.

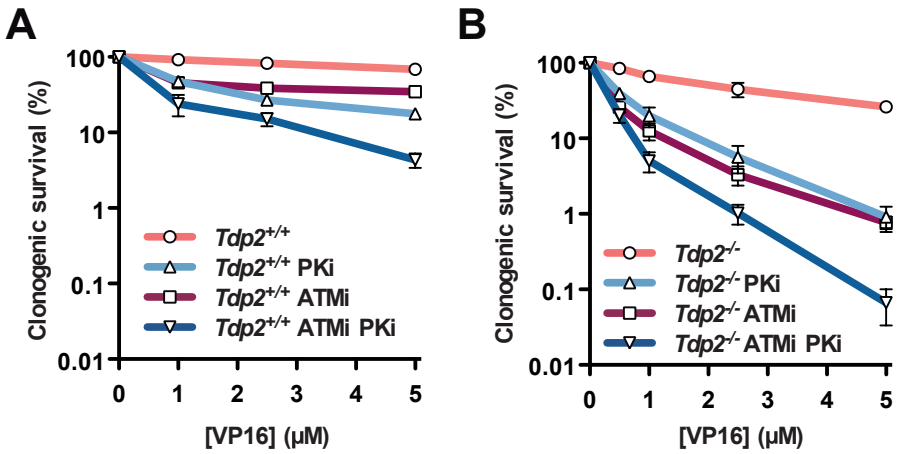

Figure 46: ATM and DNA-PKcs redundantly promote survival upon induction of blocked DSBs. (A) Clonogenic survival of wild-type transformed MEFs following acute treatment with the indicated concentrations of etoposide. Cells were incubated or not with 10 μM ATM, DNA-PKcs or the combination of both inhibitors. **(B)** As above, but *Tdp2*$^{-/-}$ transformed MEFs were used.

IV. DISCUSSION

IV. DISCUSSION

The study of the mechanisms that repair damaged DNA and safeguard the genetic information has provided essential knowledge of how living cells function. Since researchers pointed out the inherent instability in the chemistry of DNA, and its reactivity with numerous chemical and physical agents, the study of DNA repair has served to make a qualitative leap in scientific, clinical, technological and even social issues. Of particular interest, we can mention the contribution to unveil the cause of important human diseases (McKinnon & Caldecott 2007). In this regard, defective DNA repair mechanisms have been demonstrated to predispose individuals to aging, cancer proneness or to suffer congenital syndromes. In addition, since DNA repair capacity largely affect the response to cytotoxic treatments commonly used against cancer, discerning how repair pathways can be modulated to specifically induce tumour death is decisive (Melorose et al. 2008). On top of this, besides the contribution in disease treatment, it is worth mentioning that DNA repair field has also helped to develop important biotechnological advances, ranging from daily-used laboratory techniques, to the most innovative procedures of genome editing and next generation sequencing. Therefore, understanding at the molecular level the rules that govern DNA repair attaches the utmost importance.

1. Molecular role of TDP2 and its physiological implications

TOP2 activity is keystone in DNA metabolism, since it removes topological constraints generated by transcription and replication, and facilitates chromosomal

segregation. Importantly, previous work has also linked TOP2 with transcriptional regulation of important genes during human development. On top of this, TOP2 activity and its trapping in cleavage complexes promoted by TOP2-poisons has been an effective approach to treat several types of oncogenic malignancies over decades. For all of this, the mechanisms of how TOP2 induces DNA damage and how these lesions are repaired are of particular interest for cellular and molecular biologist, as well as clinicians.

In this work, we have dissected the enzymatic activity of TDP2, confirming that it is the only relevant 5'-tyrosyl-DNA-phosphodiesterase activity in mammalian cells, consistently with previous results obtained in avian DT40 cells and human cell lines. However, TDP1 had been proposed to undergo the removal of 5' phosphotyrosine blockages from DNA ends, collaborating in the repair of TOP2-induced DSBs. This was based on a weak 5'-TDP activity of human TDP1 recombinant protein, resistance of TDP1 overexpressing cells to etoposide treatment and the physiological 5'-TDP activity described in Saccharomyces cerevisiae TDP1 (Nitiss et al. 2006). Nonetheless, we have not detected any residual 5'-TDP activity in *Tdp2*$^{-/-}$ cellular extracts or in wildtype extracts in the presence of Mg^{2+} chelator EDTA, suggesting that TDP1 activity, which is Mg^{2+}-independent (Murai et al. 2012), cannot compensate TDP2 deficiency. Moreover, alternative work has not found evidence for an increased etoposide sensitivity or repair defect of *Tdp1/Tdp2* deleted cells compared to single TDP2-deficient cells (Zeng et al. 2012). It is important to mention, that in contrast to *TDP1*, there is no obvious *TDP2* ortholog in yeast. Hence, we can speculate that while *Saccharomyces cerevisiae* TDP1 can display both activities efficiently, TDP2 could have appeared later in

evolution, restricting TDP1 to a more specialized 3' TDP activity in higher eukaryotes. Furthermore, previous work has proposed that TDP2 activity promotes the repair of TOP2-induced DSBs in mammalian cells, based on its preference for 5'-phosphotyrosyl termini in blunt dsDNA, compared to single-stranded 5' termini or 5' termini at single-strand breaks (Ledesma et al. 2009). It is worth mentioning that TOP2 cleavage is characterized by four-based staggered nicks in the DNA backbone, that can potentially produce DSBs harbouring 5' phosphotyrosine overhangs (Liu et al. 1983). Consistently, we have observed that TDP2 promotes the efficient cleavage of 5' phosphotyrosines harboured in 4 bp overhangs, consistent with a physiological role of TDP2 in the repair of TOP2-induced lesions. On top of this, our data strongly suggests, that the biochemical mechanism of TDP2 unblocks TOP2-induced DSBs without loss of a single nucleotide, generating 5' phosphate complementary overhangs. The result of this reaction largely facilitates the direct ligation of these DSBs by the NHEJ machinery. Consistent with a role of TDP2 in NHEJ pathway, *KU70* has been described to be epistatic over *TDP2* for etoposide sensitivity. Nevertheless, whether TDP2 can act independently or it requires the association with NHEJ factors under physiological conditions is still unclear. In this regard, direct interaction between c-NHEJ proteins and TDP2 have not been described so far. In any case, TDP2 displays the most adequate enzymatic activity to ensure error-free ligation of TOP2-induced DSBs. In theory, it was anticipated that TDP2 activity would be crucial when NHEJ is the only active pathway.

Although TDP2 loss slows down the repair of DSBs, they are eventually repaired even in quiescent cells when NHEJ is the only active pathway. This suggests

that alternative mechanisms must be operating. In theory, the absence of TDP2 forces TOP2-induced DSBs to undergo processing, since this is the only mechanism that can remove 5'-peptide adducts to allow ligation. In consequence, DSB ends must be trimmed by nucleases. It is important to keep in mind that 5' overhang trimming potentially leads to sequence loss, since DNA polymerases cannot reconstitute the original sequence, due to its characteristic 5' to 3' polymerization polarity (Ramsden 2011). Thus, despite TDP2-independent pathways must be operating to repair TOP2-induced lesions, they are potentially mutagenic. Indeed, it has been described that TDP2-deficient cells suffer increased genome instability upon TOP2-poison exposure (Gómez-Herreros et al. 2013). It would be essential to analyse in the future at the nucleotide level, the consequence of TDP2 loss upon TOP2-induced damage. Nonetheless, this is technically challenging, since TOP2 activity is normally enriched in certain regions of the genome, but it does not cleave in a sequence specific manner (Madabhushi et al. 2015). In consequence, the lack of TOP2-induced DSB specific sites has impeded this analysis under physiological conditions. Thus, new approaches should be developed to address this issue.

Mutagenic DNA repair has been proven to contribute to cancer development and progression. Therefore, it is tempting to think that TDP2 loss would present a potential source of genome instability and neoplastic changes. Thus, TDP2 is a factor that must be taken into account in cancer development, progression and treatment. To address the implication of TDP2 in cancer, incidence of tumours in lifespan experiments should be carried out in TDP2 mouse model. In addition, TDP2 must be considered a determinant factor in cancer treatment, especially when patients are treated with TOP2-

poisons (Pommier et al. 2010). We can anticipate that TDP2 inactivation will sensitize tumour cells to TOP2-poison chemotherapy. Indeed, to explore this possibility, catalytic inhibitors that block TDP2 activity have been described recently and they are under characterization for their adequateness for clinical trials (Marchand et al. 2016; Kossmann et al. 2016; Kankanala et al. 2016; P. Hornyak et al. 2016) However, it is important to consider that based on our findings, inactivation of TDP2 could channel DSB-repair to error-prone pathways, which can potentiate the development of treatment-associated secondary leukemias (Pendleton et al. 2014).

TOP2B plays an essential role in the removal of topological constraints allowing efficient transcription, being determinant for the expression of neural development and long genes (Li et al. 2014; Lyu et al. 2006; Nur-E-Kamal et al. 2007; King et al. 2013). Beside its role in topological modulation, increasing evidence supports the notion that human TOP2B also modulates the expression of specific genes in response to certain stimuli. Indeed, TOP2B activity in promoters has been proposed to regulate the expression of certain genes in response to hormones, such as estrogen and androgen, amongst other stimuli (Haffner et al. 2010; Bong-Gun et al. 2006). In a similar manner, recent work has proposed that TOP2B activity mediates the expression of early-response gene in neurons (Madabhushi et al. 2015). Curiously, it has been proposed that the transcriptional regulation mediated by TOP2B relies on the induction of physiological DSBs (Bunch et al. 2015). Nevertheless, how this mechanism is regulated in order to modify gene transcriptional status is still unknown. In any case, efficient DSB repair machinery would be crucial for maintaining genome integrity in transcribed regions.

Interestingly, depletion of TDP2 was shown to greatly reduced gene expression of AR-regulated genes in a cellular system, suggesting that TDP2 contributes to this mechanism (Gómez-Herreros et al. 2014). However, further work needs to be performed to measure the extent of TDP2 contribution in early-response genes regulation in adult brain. Another important issue is that recent work has linked mutations in TDP2 that abolish the enzymatic activity with a congenital syndrome characterized by severe neural deficiencies (Gómez-Herreros et al. 2014). These neural features seem to be caused by deregulation of TOP2-dependent transcription of important genes for neural development and homeostasis. Altogether, these observations points toward TDP2 as a crucial factor for TOP2-mediated regulation of the transcriptional landscape, and which loss may have severe consequences in human health.

Finally, it is worth mentioning that the exact contribution of TDP2 to HR pathway remains unclear. Nonetheless, we can anticipate that the presence of 5' blockages would have a negligible impact on HR pathway, since in this repair pathway DSBs normally undergo processing of the 5' strand. In this regard, it has been reported that TDP2 loss lead to channelling TOP2-induced DSBs through HR repair, suggesting that TDP2 activity is restricted to NHEJ pathway (Gómez-Herreros et al. 2013). Consistently, the combination of TDP2 depletion and BRCA2 deficiency, a factor that promotes HR repair, displayed synergistic hypersensitivity upon etoposide exposure, suggesting that TDP2 operates in a HR-independent manner. Curiously, Spo11 initiates meiotic recombination by inducing DSBs in a similar manner as Topoisomerase 2, remaining attached by a covalent phosphotyrosine bond to the 5' ends (Lam & Keeney 2015;

Neale et al. 2005). During this process, homologous chromosomes are confronted in the bivalent and DSBs are channelled towards HR repair (Gao et al. 2014). Whether TDP2 can cleave SPO11 complexes in vivo is still unclear. We can speculate that based on the requirement of TOP2cc degradation to allow TDP2 unblocking activity, intact Spo11 would be refractory to TDP2 activity. Importantly, this would ensure that processing of 5' strand and repair by HR is the preferential pathway operating during gametogenesis. In any case, it is tempting to think that TDP2 activity would be modulated in different physiological processes, depending on the requirement for 5' end unblocking.

2. Molecular role of ATM in the repair of blocked DNA double-strand breaks

Historically, the study of how the chemical structure of DSB ends affects the repair process has been impeded by the inability to induce homogeneous lesions. The majority of DNA damaging agents used for this purpose generates a vast number of heterogeneous chemical structures. IR has been widely used as a tool for the study of DNA repair, but it produces a plethora of nucleotide and base modifications, and generates a combination of SSBs and DSBs (Ward 1988; Hagen 1994). By chance, a small fraction of these breaks would harbour a damaged base blocking the termini. On top of this, higher-energy radiation has been also used for the study of blocked DSB, since it increases the likelihood to generate clustered DSB with aberrant structures at their termini (Brenner & Ward 1992). However, the heterogeneity of lesions generated in the DNA molecule impedes the interpretation of the results obtained through this approach. There are more molecularly controlled systems that have shed some light on

the process of blocked DSB-repair. For instance, V(D)J recombination, which relies on the cleavage of RAG1/2 recombinase in specific loci during lymphocyte development, generates at the same time two types of DSBs, a hairpin blocked DSB in the coding end, and a clean blunt-ended DSB in the signal end. This has allowed researchers to analyse the contribution of NHEJ factors in the repair of each type of DSB. Several in vitro and in vivo systems have been developed for the study of this process, being determinant in immunology research (Ramsden et al. 1997; Bredemeyer, Helmink, et al. 2008). However, tools that rely on RAG1/2 cleavage have also shown disadvantages for the study of blocked DSB repair, since they only operate in G1 lymphocytes and display characteristic and peculiarities that are specific of the V(D)J recombination process.

For all these reasons, we aimed to develop a novel approach to analyse the contribution of different factors to the repair of blocked DSBs. In the present work, we have successfully defined genuine methodology to induce homogeneous population of blocked or clean DSBs depending on the genetic background (Figure 17). Importantly, we have proven that several experimental setups can be proficiently assayed in different cells and animal models. Nonetheless, it stands to reason that this system relies on TOP2-activity, and therefore, TOP2 singularities and modulation along different conditions must be taken into consideration.

Since ATM identification, numerous laboratories have carried out extensive research to elucidate its molecular role and impact on human pathology. Presumably, due to the overwhelming number of processes in which it is involved and the numerous proteins that

are regulated by its kinase activity, it has been extremely complex to integrate every facet of ATM. In any case, its deficiency has been consistently demonstrated to impact just on a small fraction of DSB repair in cells. Therefore, two subpopulations of DSBs, according to their ATM dependency or independency, could be considered. Our work demonstrates that to some extent, this division might be based on the structural heterogeneity of the ends induced by DNA-damaging agents. Indeed, we have demonstrated that ATM does not influence the repair of clean DSBs, which present 5' phosphate and 3' hydroxyl termini, or in DSBs that can be directly unblocked. Consistently, alternative studies with different approaches such as the cleavage with restriction enzymes in certain regions of the genome have described similar results (Caron et al. 2015b). In contrast to clean DSBs, ATM activity is crucial to facilitate the repair of blocked DSBs, preventing from their deleterious outcomes. Therefore, we have contributed to the understanding of the molecular role of ATM in the repair of DSBs.

Curiously, ATM inhibition seems to sensitize cells to blocked DSBs to a greater extent than ATM deletion. This suggests that the presence of inactive ATM could inhibit DSB repair, probably in a dominant negative fashion, while ATM loss allows the repair by redundant pathways. This is consistent with the observation that *Atm*$^{-/-}$ mice are viable, in contrast to the embryonic lethality displayed by mice expressing a kinase-dead mutant form of ATM (Yamamoto et al. 2012). In addition, our data strongly suggests that ATM action in blocked DSBs is largely independent on the previously reported role of ATM in facilitating repair of heterochromatin-associated lesions. Our results, while they can be interpreted as conflicting with the previous model, are indeed

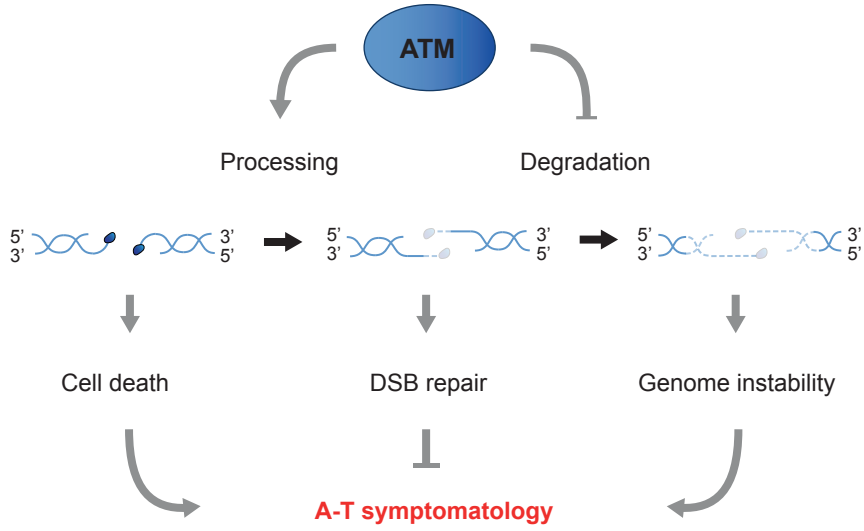

Figure 47: Model for ATM involvement in blocked DSB repair. ATM promotes processing and inhibits excessive degradation of blocked DSBs to ensure correct repair. Processing is essential to remove blockages from DNA ends and to avoid cell death induced by unrepaired DSBs. At the same time, ATM ensures that end trimming is the minimum necessary for repair, avoiding excessive degradation. This protects cells from genomic instability associated to deletions and gross chromosomal rearrangements. In the absence of ATM, increased cell death and genome instability can trigger the development of A-T symptomatology.

a demonstration of a broader role of ATM in the repair of any kind of complex lesion in which repair is suboptimal. In this context, ATM would be crucial for any DSB that is not directly ligated by the DSB repair machinery. Beside this, recent work has suggested that ATM also promotes higher-order chromatin organization, ensuring association in repair clusters of multiple DSBs induced by restriction enzymes, but this not seem to affect the repair process (Caron et al. 2015b).

Unfortunately, the exact molecular mechanism of ATM in blocked DSBs still

remained elusive. Nevertheless, our results allow us to propose two possibilities that are not mutually exclusive (Figure 47). On one hand, ATM kinase activity may promote end processing by regulating the action of factors required for this process, such as endonucleases or DNA polymerases. On the other hand, beyond its role in facilitating the processing of blocked DSBs, it may preserve genome integrity, by ensuring that DSB ends undergo the minimum processing required for repair. This controlled processing would be crucial to avoid excessive end degradation that can lead to error-prone repair and gross chromosomal rearrangements.

In theory, there are several possible known nucleases that can be taken into consideration. However, it is important to remark that multiple enzymes might be downstream of ATM and account for DSB processing when they cannot be efficiently unblocked. For instance, Artemis and the MRN complex have been previously shown to contribute to the repair of TOP2-induced DSBs (Quennet et al. 2011; Kühne et al. 2004). Consistently, Artemis has been shown to promote processing of DSB during NHEJ pathway by its endonuclease activity, operating on 5' single-stranded overhangs (Chang & Lieber 2016; Goodarzi et al. 2006). Interestingly, its endonuclease activity preferentially cleaves on the ssDNA/dsDNA junction. Thus, in theory, it would be capable to trim 5' blocked ends generated by TOP2-abortive activity with a minimum loss of nucleotides. On top of this, Artemis has proven required for fully efficient NHEJ repair, using diverse damaging agents. Importantly, fibroblasts carrying mutations in Artemis, display a similar repair defect compared to ATM-deficient cells upon IR exposure (Riballo et al. 2004). Indeed, ATM deficiency was shown to be epistatic over

Artemis-deficiency, suggesting that ATM could be in some way modulating its activity. Nonetheless, ATM has been proven to phosphorylate Artemis, but this seems to be dispensable for DSB repair (Goodarzi et al. 2006). For all of these, it would be crucial to analyse the exact contribution of Artemis in the repair of blocked DSBs under our specific experimental conditions.

In addition to Artemis-dependent processing, which is restricted to a few nucleotides away from the ends, the MRN complex can act hundreds of nucleotides upstream of the DSB termini (Garcia et al. 2012). MRN complex activity is crucial for HR repair, since it can initiate resection of DSBs generating 3' protruding ends. For this, it promotes endonuclease cleavage upstream of the DSB termini, followed by a 3' to 5' exonuclease activity. Thus, in principle, the MRN complex could also facilitate the removal of a 5' blockage. Consistent with this possibility, the interplay between the MRN complex and ATM in regulating DSB repair has been widely reported. Indeed, every single component of the MRN complex can be phosphorylated by ATM, and ATM full activation upon DSB-induction seems to require its interaction with the MRN complex through NBS1 (Lavin et al. 2015; Difilippantonio et al. 2007). On top of this, ATM has been proposed as a modulator of the processing activity of MRN (Kijas et al. 2015). Thus, it would be essential to test if the ATM-dependent pathway for the repair of blocked DSBs relies on the MRN complex nuclease activity. In any case, it will be necessary to carry out further work to elucidate to which extent Artemis or the MRN complex are contributing to the repair of TOP2-induced DSBs in the absence of TDP2, and how they are regulated by the ATM kinase activity.

As mentioned above, it is also tempting to speculate that ATM could inhibit excessive degradation of DSBs. In quiescent cells (G1/G0), processing activity must be closely regulated to avoid long-range resection of DSB ends, since sister chromatids are not present during these cell cycle stages to be used as template for HR. Under these conditions, NHEJ is the preferential repair pathway, but MMEJ pathway, which requires MRN processing, could also contribute to the repair of this type of lesions in the absence of an unblocking activity (Sfeir & Symington 2015). It is tempting to think that ATM could be responsible for the inhibition of long-range resection when the MRN complex initiates degradation of DNA ends. A possible candidate would be Exo1 exonuclease, which promotes extensive degradation of ends to channel DSBs to a HR-dependent repair (Bolderson et al. 2010). Nevertheless, there are other possible factors in the DDR that are controlled by ATM activity and could prevent long-range resection. ATM-dependent formation of γH2AX has been demonstrated to be essential for the recruitment of downstream factors, such as MDC1, 53BP1 and BRCA1 (Bekker-Jensen & Mailand 2010). They have been suggested to be crucial choice of repair pathway, controlling to which extent DSBs are processed. Since ATM is the major contributor to the early wave of γH2AX phosphorylation upon DSB induction, a decrease in γH2AX formation adjacent to the lesions could lead to unprotected DSB ends. Consistent with this hypothesis, cells and mice lacking H2AX present increased genome instability upon DSB-induction in numerous experimental setups (Celeste et al. 2002). Indeed, blocked DSBs generated during V(D)J recombination are largely degraded in a MRN-dependent manner in the absence of Artemis and H2AX (Helmink et al. 2011). In a

similar manner, we can propose that, TDP2-deficiency would force TOP2-induced DSBs to be processed and in the absence of ATM-dependent formation of large γH2AX regions, MRN complex and other nucleases could promote excessive degradation of ends, leading to error-prone repair, gross chromosomal rearrangements or accumulation of unrepaired DSBs. Nevertheless, future experiments must be performed to clarify the exact contribution of each of these factors to the increased genomic instability linked to ATM-deficiency upon the induction of blocked DSBs.

Up to date, several redundant and non-redundant roles of ATM and DNA-PKcs have been reported. However, the precise function of these kinases in DSB repair is still a matter of debate. Both are efficiently activated by DSB induction, and they share numerous common substrates. However, they also support distinct functions and their impairment implies different outcomes for cells and organisms. While *ATM* deletion leads to nearly normal repair rate, and an accumulation of a fraction of permanently unrepaired DSBs, DNA-PKcs absence largely slows down repair but not completing repair (Goodarzi et al. 2010). Notably, in both cases, DSB induction leads to the accumulation of illegitimate joining events that are highly deleterious. Strikingly, we have found that ATM and DNA-PKcs encompass two pathways that redundantly promote blocked DSB repair in mammalian cells. In the absence of both activities, cells show a marked sensitivity upon this type of lesions, probably due to a total lack of repair. Indeed, such a striking repair defect has been only observed in *Lig4*$^{-/-}$ quiescent cells upon IR exposure. Further dissection of downstream factors that function in each pathway would be particularly interesting.

While we have observed a negligible effect of ATM absence in clean DSB repair,

DNA-PKcs inactivation has shown a significant accumulation of unrepaired DSBs. This is consistent with previous evidence of DNA-PKcs kinase activity being important for NHEJ. Nevertheless, the repair defect was exacerbated when the termini were blocked, suggesting that DNA-PKcs kinase activity, in addition to the role in the end joining process itself, is specifically required for the correct processing of blocked lesions. Our experiments have been performed using chemical inhibition of DNA-PKcs and dominant negative effects due to the presence of inactive protein attached to DSB ends cannot be ruled out. Thus, it would be important in the future to carry out experiments in DNA-PKcs-deficient background. In any case, two distinct pathways seem to operate in cells for the repair of blocked DSBs, differentially regulated by ATM or DNA-PKcs kinase activities. Therefore, it is tempting to speculate that in conditions in which ATM is absent, DNA-PKcs would compensate for the removal of these lesions. Interestingly, combined absence of ATM and DNA-PKcs have been shown to lead to embryonic lethality in mice (Gurley & Kemp 2001). This has been explained as a synthetic lethality effect produced by the accumulation of DSBs characteristic of a DNA-PKcs deficiency, on top of the impairment in cell cycle checkpoints caused by *Atm* deletion. However, since these two proteins distinctly control the only two pathways for the repair of blocked DSBs, we hypothesize that accumulation of blocked DSBs could to some extent underlie the severity the phenotype observed in the combined absence of ATM and DNA-PK.

The formation of the DNA-PK complex at DSBs has been described as a key step for end tethering and protection, end processing and repair pathway choice. In this regard, the modulation of DNA-PKcs activity and its structure is key during the

repair process. For this, DNA-PKcs suffers conformational changes that are modulated by the phosphorylation of functionally different clusters, such as the ABCDE and the PQR (Meek et al. 2008). Previous work has described the importance of the kinase activity of DNA-PKcs and its posttranslational changes upon the exposure to DSB-inducing agents. Thus, it is tempting to think that a tightly adjusted phosphorylation status along the repair process is essential. In the present work we have described the importance of ATM and DNA-PKcs activities in the repair of DSBs that specifically harbour a blockage in their termini. Thus, we can hypothesize that ATM and DNA-PKcs modulate precisely the status of DNA-PK phosphorylation, and this is key for the correct repair of blocked DSBs, since they rely on processing to ensure ligation. It has been proposed that the PQR cluster is autophosphorylated in trans, and this leads to end protection, reducing nucleotide loss in joining events. Additionally, this phosphorylation seems to contribute to an open conformation of DNA-PKcs, allowing the access of the ligase complex to complete the NHEJ process. Conversely, phosphorylation in the ABCDE cluster seems to be carried out by DNA-PKcs or ATM redundantly (Chen et al. 2007), facilitating end processing. In this regard, Artemis endonuclease activity seems to rely on the phosphorylation of the ABCDE cluster (Goodarzi et al. 2006). Therefore, we can hypothesize that in the presence of blocked DSBs generated by TOP2 abortive action, redundant phosphorylation of the ABCDE could be key to promote limited end processing by Artemis or other downstream nucleases. Consistent with this, ATM and DNA-PKcs kinase activities display redundant roles for the repair of blocked DSBs in our particular experimental setup. It will be crucial to dissect the specific contribution of each phosphorylation events that facilitate the repair of blocked DSBs.

3. Physiological implications of ATM function in the repair of blocked double-strand breaks

Our results strongly support the notion that ATM is critical in minimizing the deleterious outcomes of blocked DSBs, not just in cells, but also in the context of the entire organism. Consistent with this, ATM has been described to contribute to different processes in which blocked DSB repair is crucial, and which have a direct impact in A-T. First, during V(D)J recombination in lymphocyte development, ATM promotes the stability and correct repair of RAG1/2 induced DSBs. Importantly, the impairment of the correct joining of coding ends leads to DSB accumulation during lymphocyte development, underlying the immunodeficiency and increased lymphoma incidence observed in A-T patients. Specifically, ATM activity is key for protecting coding ends, which are hairpin blocked, from degradation and promoting their faithful joining. In contrast, ATM loss does not affect the joining of signal ends, which are clean blunt ends (Bredemeyer et al. 2006). Secondly, meiotic recombination involves the repair of DSBs harbouring SPO11 protein covalently bound to its 5' end. Indeed, the impairment of this process has been reported to be the cause of sterility in A-T individuals, since ATM directly influence SPO11-dependent DSB induction and repair during gametogenesis (Lange et al. 2011; Garcia et al. 2015).

Several alternative roles that are independent of TOP2 abortive activity have been attributed to TDP2 in the past (Chunyang Li et al. 2011). Nevertheless, no gross spontaneous phenotypes have been observed until present in TDP2-deficient mice. Thus,

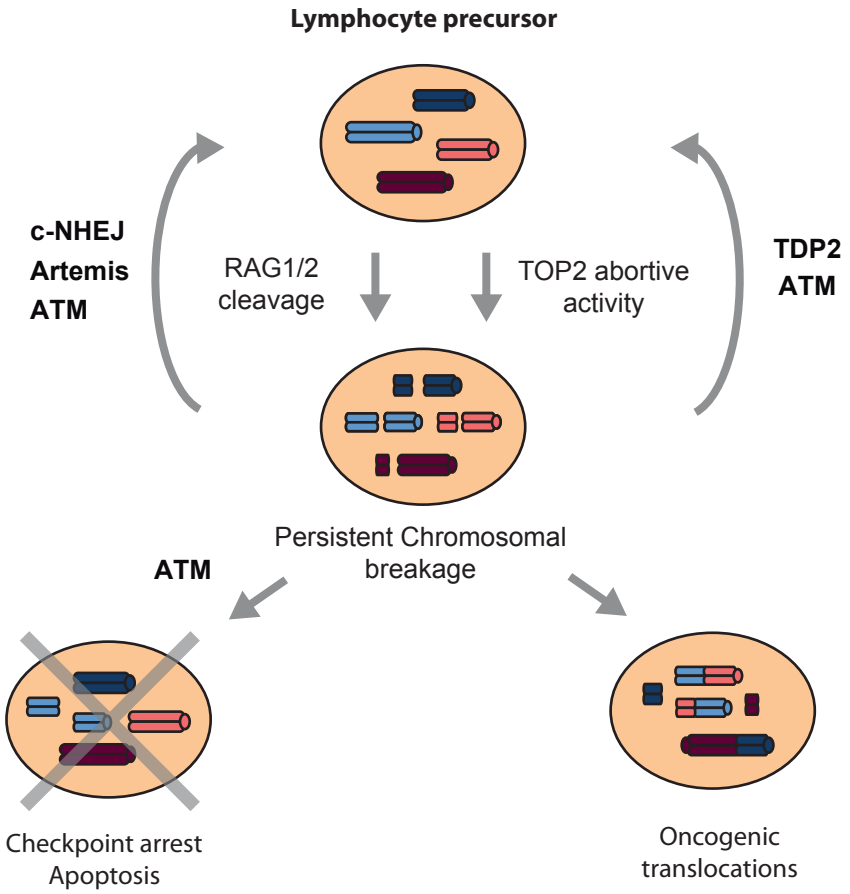

Figure 48: Model for the molecular trigger of thymic lymphomas in A-T. During lymphocyte maturation DSBs arise by RAG1/2 cleavage in order to promote V(D)J recombination. c-NHEJ machinery in collaboration with Artemis and ATM ensures the repair of these lesions. In addition, TOP2-dependent transcriptional regulation can induce DSBs, which requires TDP2 and ATM for their correct repair. In the absence of both, persistent DSBs accumulate. ATM is also required for cell cycle arrest and apoptosis upon DSB-induction. In the absence of ATM, immature lymphocytes can proliferate with persistent chromosomal breakage induced by RAG1/2 and TOP2 activity, increasing the likelihood of unfaithful repair of DSBs that underlie the induction of oncogenic translocation.

based on the specificity of TDP2 in the unblocking of DSB blocked by 5' peptide adducts, we anticipated that any aggravation of the features displayed by the ATM mouse model

by the absence of TDP2, would uncover TOP2 abortive action as a possible trigger of A-T symptoms. Remarkably, we have found that *Tdp2/Atm* double-knockout mice are more likely to suffer thymic malignancies, compared to ATM-deficient animals. Thus, it is tempting to speculate that TOP2 could be a potential source of chromosomal breakage during lymphocyte development, increasing the likelihood of the appearance of oncogenic translocations in A-T patients. This spontaneous source of DSBs, combined with an increase of unfaithful repair, cell-cycle arrest impairment and defective DDR characteristic of ATM deficiency would alllow lymphocytes with a high number of mutations and oncogenic translocations to develop, leading to a higher incidence of thymic lymphoma.

These findings opened two possible scenarios. On one hand, TOP2 abortive action could increase chromosomal breakage in sites that are distinct to the break points described in ATM tumours. On the other hand, TOP2 cleavage could directly increase the likelihood of breakage in specific sites that spontaneously occurs in A-T malignancies. Based on the analysis of the spatial distribution of instability sites along the genome in $Tdp2^{+/+}Atm^{-/-}$ and $Tdp2^{-/-}Atm^{-/-}$ tumours, we can conclude that chromosomal breakage is occurring in similar regions in both genetic backgrounds. This suggests that oncogenic translocations previously described in A-T could be, at least in part, triggered by mechanisms that are dependent on TOP2. Thus, we propose a model in which TOP2-abortive activity is a determinant factor in the appearance of lymphoid leukemia in A-T (Figure 48).

Interestingly, ATM-deficient mice that cannot undergo V(D)J recombination still develop thymic malignancies but translocations do not involve TCR or immunoglobulin genes. Therefore, other source of DSBs, alternative from RAG1/2 cleavage, must be driving this oncogenic translocation. In this regard, TOP2 abortive action could account for chromosomal breakage that is not dependent on RAG1/2 cleavage. However, it is also possible that TOP2 activity influences V(D)J recombination, since this process relies on structural rearrangement of the chromatin, RAG1/2 cleavage complex formation and post-cleavage stabilization to ensure DNA repair. Thus, this process could generate high levels of topological stress, increasing TOP2 activity and the likelihood to be trapped in *TCR* and *Ig* genes.

It is important to mention that, to our knowledge, lymphocytes are the only cell lineage suffering the consequences of TDP2 and ATM combined deficiency in our experimental setup. This could be explained by the incapacity of other phenotypes to arise due to the early mortality of these mice. Nonetheless, double-knockout mice reaching above 520 days did not show any gross feature. Up to date, the determinant factor that underlies neurodegeneration in A-T, the most devastating characteristic of the syndrome, remains elusive. In this regard, ATM-deficient mouse models do not recapitulate the profound neural phenotype observed in A-T patients, which has greatly impeded its study. Remarkably, a recent porcine model of ataxia telangiectasia has been shown to reproduce neurological features and motor deficits of human A-T (Beraldi et al. 2015). This suggests that important interspecies differences may exist concerning the homeostasis of the neural system. We can also hypothesize that the likelihood of

appearance of lesion that underlie A-T neural defects are lower in mice, or independent pathways could efficiently compensate for their repair in the central nervous system. In addition, intrinsic differences during neural development, increased longevity of humans, or exposure to environmental sources of DNA damage, may account for these differences. Nevertheless, we aimed to analyse a possible role of blocked DSBs as the molecular trigger of neurodegeneration in A-T syndrome. Therefore, we tested if loss of TDP2 could uncover a possible effect of TOP2-induced damage in the central nervous system of ATM-deficient mice. Despite the fact that no overt neurological phenotype was observed in *Tdp2* and *Atm* double-knockout mice, we cannot rule out the possibility of TOP2-induced damage as a determinant factor in triggering A-T neurodegenerative symptoms in human, since there are multiple examples of rodent models that do not recapitulate neural defects. Moreover, it is important to bear in mind that TOP2-abortive activity represents just a single example of how blocked DSBs may arise in vivo, and there are several alternative sources of DSB carrying different blocking structures in their ends. Thus, further work must be performed to elucidate if blocked DSBs are indeed the cause of the progressive neurodegeneration of A-T disease.

V. CONCLUSIONS

V. CONCLUSIONS

1. TDP2-deficient mouse cells lack observable 5'-tyrosyl-DNA-phosphodiesterase activity in vitro

2. TDP2 activity facilitates the religation of 5' phosphotyrosine DNA substrates *in vitro*

3. Covalently-bound peptides accumulate on the DNA upon the exposure to TOP2 poisons in TDP2-deficient primary MEFs

4. ATM facilitates repair of TOP2-induced DSBs in human and rodent cells, specifically in the absence of TDP2

5. ATM function in the repair of TOP2-induced DSBs is heterochromatin independent

6. ATM function promotes cell survival and genome integrity in TDP2-deficient MEFs upon TOP2-induced DSBs

7. ATM function prevents loss of DNA sequence in extrachromosomal 5'-blocked DSBs in human cells

8. DNA-PKcs function in the repair of TOP2-induced DSBs is increased in the absence of TDP2

9. DNA-PKcs activity and ATM redundantly promote repair of TOP2-induced

DSBs in the absence of TDP2

10. ATM confers resistance to TOP2-poison exposure in mice, specifically in the absence of TDP2

11. *Tdp2*$^{-/-}$ *Atm*$^{-/-}$ mice display elevated mortality due to an increased incidence of thymic lymphoma compared to ATM-deficient mice

12. Lymphomas in *Tdp2*$^{-/-}$ *Atm*$^{-/-}$ double mutant mice are characterized by genome instability events that are similar to *Tdp2*$^{+/+}$ *Atm*$^{-/-}$ single

VI. MATERIALS AND METHODS

VI. MATERIALS AND METHODS

1. Cell culture procedures

1.1. Cell lines and primary cell culture

Cells were maintained in HEPA class 100 incubators (Thermo) at 37 ºC and 5% CO2.

Primary MEFs were isolated from embryos at day 13 p.c. and cultured at 3% O2 in Dubelcco's Modified Eagle's Medium (DMEM) supplemented with penicillin, streptomycin, 2 mM L-Glutamine, 15% FCS and non-essential aminoacids. All experiments were carried out between P1 and P5.

Transformed MEFs were maintained in DMEM supplemented with penicillin, streptomycin, 2 mM L-Glutamine and 10% FCS. MEFs were transformed by retroviral delivery of T121, a fragment of the SV40 large T antigen that antagonizes the three Rb family members but not p53 (Saenz Robles et al. 1994). After 20 passages under puromycine selection single clones that efficiently grew were selected.

HEK293T and U2OS cells were maintained at 37˚C, 5% CO2 in DMEM supplemented with penicillin, streptomycin, 2 mM L-Glutamine and 10% FCS.

A-T (Coriell's Repository GM05823D) and BJ1 primary fibroblasts were cultured at 37˚C, 5% CO2, in DMEM supplemented with penicillin, streptomycin, 2mM L-Glutamine and 15% FCS. Cells were maintained in HEPA class 100 incubators (Thermo) at 37 ºC and 5% CO2.

1.2. Lentivirus production and infection

To produce lentiviral particles containing vector expressing shRNA, $3.5x10^6$ HEK293T cells growing in 100-mm plates were transfected by calcium phosphate protocol with a mixture composed by 15 μg of either pLKO.1-puro-Tdp2-2 (clone TRCN0000003072, SIGMA) or empty control pLKO.1-puro (SIGMA), 10 μg of p8.91 (plasmid containing viral capsid genes) and 5 μg of pVSVG (plasmid containing viral envelope genes). Growing medium was recovered after 48 h, and viral particles were isolated from cells using 0.45 μm polyvinylidene difluoride (PVDF) filters (SLHV035RS, Millex®-HV, Millipore). Then, viral particles were concentrated by centrifugation for 1 hour and 30 min at 22.000 rpm at 4 ºC in a Beckman-coulter Optima L-100K Ultracentrifuge. Finally, viruses were resuspended in DMEM and stored at -80 ºC.

For infection, lentiviral particles were added to cells in DMEM supplemented with 4 μg/ml hexadimethrine bromide (H9268, Sigma). For titration U2OS cells were infected with serial dilutions of lentiviral particles. After 72 h, $2x10^3$ cells were seeded for duplicate in 100 mm dishes and selected in puromycine (1 μg/ml). Multiplicity of infection (MOI) was calculated based on the amount of puromycine resistant cells measured by the clonogenic survival assay. Finally, $0.5x10^6$ A-T human primary fibroblasts and wild-type BJ1 primary fibroblasts growing in 100 mm dishes were infected with MOI-1. After 3 days cells were selected in puromycin (1 μg/ml) for 7 days before assays were performed.

2. Molecular biology procedures

2.1. 5'-TDP activity *in vitro*

2.1.1. Radiolabeled substrates production

Substrates were generated by mixing *5'Y-blunt* and *Blunt.Rev.Comp.* oligonucleotides for blunt-ended, and *5'Y-overhang* and *Overh.Rev.Comp.* for 4 bp 5' overhang. 40 pmoles of oligonucleotides containing 5' phosphotyrosines and 20 pmoles of *Blunt.Rev.Comp* or *Overh.Rev.Comp.* were mixed in a total volume of 50 μl, heated at 95 ºC and cool down at 2 ºC/min rate.

Annealed DNA duplexes contained 5'-AG-3' overhangs. This was used for 3' fill in by Klenow polymerase (Takara) for 1 h at 37 ºC in the presence of [α-32P]-dCTP for radiolabelling, and 50 μM ddTTP that protect 3' ends from degradation by exonucleases. 5'-Y-AATT-3' overhangs could not be filled in, since dATP was not present in reactions. Unincorporated [α-32P]-dCTP was removed by illustra MicroSpin G-25 Columns (GE Healthcare).

2.1.2. Cell extract for *in vitro* reactions

The indicated cells were grown in 100 mm dishes and were collected by trypsinization. They were washed twice in PBS and the pellet was lysed by mild sonication in Lysis Buffer (40 mM Tris–HCl, pH 7.5, 100 mM NaCl, 0.1% Tween-20, 1 mM DTT) supplemented with 1 mM PMSF and protease inhibitor cocktail (Sigma). Extracts were clarified by centrifugation 10 min at 16500 g 4°C. Finally, protein concentration was measured with Bradford reagent (Sigma) and samples were aliquoted, frozen in liquid nitrogen and transferred to -80ºC for long-term storage.

2.1.3. 5'TDP reactions

Reactions contained 50 nM substrate, 80 μM competitor single-stranded oligonucleotide and the indicated amount of protein extract in a total volume of 6 μl Reaction Buffer (50 mM Tris-Cl, pH 7.5, 50 mM KCl, 1 mM MgCl2, 1 mM DTT,

100 μg/ml BSA). Additionally, to analyze ligation of substrates, reactions contained 5 units of T4 DNA ligase (Fermentas) and 1 mM ATP (Sigma). Reactions were stopped by the addition of Formamide Loading Buffer and boiling for 5 min at 95˚C. Samples were resolved in 7M Urea denaturing 20% polyacrylamide gel electrophoresis in 0.5x TBE buffer. Gels were analysed by phosphorimaging in a Fujifilm FLA5100 device (GE Healthcare).

2.2. Linear plasmid circularization assays

2.2.1. Substrate production

Substrates were generated by PCR-mediated amplification of plasmid pEGFP-Pem1-Ad2 with *5'P-NHEJ-Fw* and *5'P-NHEJ-Rv* primers, which harboured phosphate, or *5'Y-NHEJ-Fw* and *5'Y-NHEJ-Rv* containing phosphotyrosine moieties at 5' ends.

A high fidelity KOD Hot Start DNA Polymerase (Merck-Millipore) was used for PCR reaction. Template used for PCR was 0.2 ngr/μl of ScaI disgested pEGFP-Pem1-Ad2 (Seluanov et al. 2004). Primers were added at final concentration of 0.2 μM, dNTPs 2mM each, MgSO4 2mM, 2% DMSO (PCR grade) and 1U of HotStart KOD polymerase (Merck-Millipore) in 1x KOD polymerase buffer. PCR amplification was performed as following: 1x (95ºC 2 min), 35x (95ºC 20 s, 57.9ºC 10 s, 70ºC 3 min), 1x (70ºC 5 min). Substrates of the expected size were purified using Gel/PCR Purification Kits (Favorgen) in agarose 0.4% gel electrophoresis.

2.2.2. NHEJ-competent nuclear extracts

NHEJ-competent nuclear extracts were prepared from transformed MEFs in 3xT150 flasks at 90% of confluency. Cells were harvested and whased three times in

ice-cold PBS, and twice in buffer A (10 mM HEPES, pH 7.9; 1.5 mM MgCl2; 10mM KCl; 0,5 mM DTT and 0,2 mM PMSF) for 10'. Cells were lysed by homogenization (10 strokes with a type B pestle) and the nuclei were pelleted by centrifugation for 5' at 1500g at 4ºC. Nuclei were resuspended in one pellet volume of buffer C (20 mM HEPES, pH 7.9; 1.5 mM MgCl2; 0,42 M NaCl; 25% Glycerol; 0,6 mM KCl; 0,5 mM DTT and 0,2 mM PMSF) and incubated in rotation for 30' at 4ºC. Extracts were cleared by high speed centrifugation at 18000 g for 15 min at 4 ºC and supernatant was transfered to an Amicon Ultra-4 3k (Millipore) and spined at 4000 g for 30' at 4 ºC. Concentrated nuclear extracts were dyalized against 500 ml of buffer D (20 mM HEPES, pH 7.9; 20% Glycerol; 0,1 M Kcl; 0,2 mM EDTA; 0,2 mM PMSF and 0,5 mM DTT) for 4h at 4 ºC. Protein concentration was measured with Bradford reagent (Sigma) and extracts were finally fast-frozen in liquid nitrogen and stored at -80 ˚C.

2.2.3. In vitro plasmid circularization assay

For in vitro plasmid circularization using cellular nuclear extracts, reactions were performed by incubating 100 ng of each substrate with 7 μg of NHEJ-competent nuclear extracts for 6 h at 16˚C in NHEJ Buffer (50 mM Tris-HCl pH 7.5, 50 mM KCl, 1 mM DTT, 2 mM MgCl2, 1 mM ATP, 100 μg/ml BSA) in the presence or absence of 50 nM hTDP2 recombinant protein. Reactions were stopped by addition of EDTA (to a final concentration of 100 mM) and treated 30 min with Proteinase K (0.2 mg/ml). DNA was purified using FavorPrep GEL/PCR Purification Mini Kit (Favorgen) and transformed into MegaX DH10B T1 Electrocompetent Cells (Invitrogen). Positive transformants were selected by plating on LB agar plates containing kanamycin (25 μg/ml) and single colonies were manually counted to estimate religation efficiency.

For in vitro plasmid circularization using T4 Ligase, reactions were performed by incubating 400 ng of the indicated substrates in the presence or absence of 2 U of rSAP

(NEB) in 15 µl of 1x Cutsmart buffer (NEB) at 37 ºC for 1 h. To inactivate rSAP samples were incubated for 5 min at 65 ºC. The samples were incubated with 5 U of T4 Ligase (Fermentas) in the presence or absence of 50 nm hTDP2. The reaction was incubated for 6 h at 16 ºC in a buffer containing 50 mM Tris-HCl, 50 mM KCl, 1 mM DTT, 1 mM ATP, 5 mM MgCl2 and 100 µg/ml BSA. A final step of 30 min at 37 ºC adding EDTA to a final concentration of 100 mM and 0.2 mg/ml proteinase K, stopped the reaction. DNA was purified using FavorPrep GEL/PCR Purification Mini Kit (Favorgen) eluted in 20 µl of mili-Q water. 1 µl was used for DH5α transformation and transformants were selected by plating on LB agar plates containing kanamycin (25 µg/ml). Single colonies were manually counted to estimate religation efficiency.

2.3. Selective labelling of protein-blocked DNA ends (SLOPE)

Cells arrested in G0 were treated 30 min with 100 µM etoposide or vehicle (DMSO), and 30 min after drug removal (to allow reversal of cleavage complexes) genomic DNA was isolated with the DNeasy Blood and Tissue Kit (Qiagen), including the steps of proteinase K and RNAseA treatment as described by the manufacturer. Peptide residues that remain covalently linked to DNA were labelled with biotin by incubating 4 µg of gDNA with 1 µg/µl EDC (Sigma) and 6 mM amine-PEG3-biotin (Thermo Scientific) in 100 mM MES buffer pH 5.5 for 2 h rotating at room temperature. Then, in order to eliminate unreacted amine-PEG3-biotin DNA was purified by standard ethanol precipitation and resuspended in TE buffer. Finally, DNA was quantified using Nanodrop, and 500 ng were boiled and dotted on a Hybond-H+ (Amersham Bioscience) membrane and cross-linked with 70,000 µJ cm−2 UV. The membrane was blocked with Odyssey blocking buffer (LI-COR Biosciences) with 1% SDS, incubated with IRDye Streptavidin 800CW, 1/10,000 (LI-COR Biosciences) in the same buffer and washed (three times in TBS-0.1% Tween20). Dots were analysed and quantified in Odyssey CLx with ImageStudio Odyssey CLx Software. For the representation, the total signal in each

sample was related to an internal control using plasmid DNA.

2.4. DDR analysis by Western blot

Confluency-arrested primary MEFs were treatmed 30 min with the indicated concentration of etoposide, and resuspended on ice using a cell scraper. Cells were washed twice in cold PBS and the pellets were directly lysed in Laemli buffer by incubating them at 96 °C for 5 min. Protein concentration was measured by Pierce 660 nm Protein Assay with Ionic detergent compatibility reagent (Thermo Scientific). Thirty micrograms of sample were run in NuPAGE Tris-Acetate Mini gels 3–8% (Novex) and transferred to Immobilon-FL Transfer Membranes (Millipore) in a Mini-PROTEAN Tetra Cell System (Biorad) overnight applying 30 V at 4 ºC.

Membranes were blocked in Odyssey Blocking Buffer (LI-COR Biosciences) incubated with the indicated primary antibodies in Odyssey Blocking Buffer-0.1% Tween20 and washed (three times in TBS-0.1% Tween20). They were then incubated with the corresponding IRDye-conjugated secondary antibodies in Odyssey Blocking Buffer-0.1% Tween20 and washed (three times in TBS-0.1% Tween20 and 1 × in TBS buffer). Finally, membranes were analyzed in Odyssey CLx with ImageStudio Odyssey CLx Software.

The following primary antibodies were used at the indicated dilution: ATM (Sigma, MAT3-4G10/8), 1/1,000; ATM pS1981 (Cell Signaling, #4526), 1/1,000; p-CHK2 Thr68 (Cell Signaling, #2661), 1/1,000; p-p53 Ser15 (Cell Signaling, #9284), 1/1,000; p-CHK1 Ser345 (Cell Signaling, #2341), 1/1,000; α-tubulin (Sigma, T9026), 1/50,000.

3. Cell biology procedures

3.1. Immunofluorescence

Cells were grown on coverslips and treated as indicated. For DSB induction cells were treated with 10 μM etoposide for 30 min (Sigma) or exposed to 2 Gy of γ-radiation using a BIOBEAM GM 8000 (Gamma-Service Medical GmbH) emitter. For ATM and DNA-PK chemical inhibition, cells were incubated with 10 μM ATM inhibitor KU55933 (Tocris) or/and 10μM DNA-PKcs inhibitor NU7441 (Tocris) 30 min before DSB-induction until the experimental endpoint.

Cells were fixed 10 min in ice-cold methanol in the case of MEFs or 4% PFA-PBS in A-T and BJ1 human fibroblasts. Cells were then permeabilized (2 min in PBS-0.2% Triton X-100), blocked (30 min in PBS-5% BSA) and incubated with the required primary antibodies (1–3 h in PBS-1% BSA). Cells were then washed (three times in PBS-0.1% Tween 20), incubated for 30 min with the corresponding AlexaFluor-conjugated secondary antibodies (1/1,000 dilution in 1% BSA-PBS) and washed again as described above. Finally, they were counterstained with DAPI (Sigma) and mounted in Vectashield (Vector Labs). Primary antibodies were used at the indicated dilution: γH2AX (Millipore, 05-636)), 1/1,000; α-Tubulin (Abcam, ab18251), 1/2,000; Vinculin hVIN-1 (Sigma, V9131) 1/2,000.

When necessary to identify replicating cells, 5'-ethynyl-2'-deoxyuridine (EdU, Invitrogen) was added throughout treatment and repair at a final concentration of 10 mM. Click chemistry reaction was performed before standard Cyclin A immunofluoresncence and DAPI staining by incubating (30 min r.t.). For clickchemistry, 1 mM AlexaFluor-conjugated azide (Invitrogen) in reaction cocktail (100 mM TrisHCl pH 8.5, 1 mM CuSO4, 100 mM ascorbic acid) was added to the samples. For the analysis of G0/G1

confluency-arrested cells only Cyclin A negative cells were scored. For G2, as EdU was present (10 mM) during and after treatment, only Cyclin A positive cells without EdU incorporation were scored.

3.2. Microscopy analysis

Standard immunofluorescence assays were visualized using Leica DM6000 microscope and images were acquired using a Leica AF6000 image processing station. For DSB repair kinetic, γH2AX foci were manually scored (double-blind) in at least 40 cells preselected by DAPI staining for showing regular and standard nuclear morphology. At least three independent experiments were performed.

For heterochromatin and γH2AX foci spatial analysis a series of Z-sections (0.21mm step) were obtained using a Leica TCS-SP5 confocal microscope with a HCX PL APO 63x/ 1.40lBL objective. For image processing an in-house MATLAB R2012a based application was designed to segment nuclei images. For each nucleus, these series were segmented to obtain the number, position, intensity and volume values of γH2AX foci and heterochromatin (G and B components of the RGB image, respectively). The segmentation from the different sections was integrated to reconstitute the 3D information of each entire nucleus. Using this reconstitution, the distance between each focus and the nearest euchromatin/heterochromatin boundary in the 3D space was determined.

3.3. Plasmid circularization assays

Linear plasmids harbouring phosphate, hydroxyl or biotin (Sigma) moieties at 5' ends, were generated as described previously for in vitro circularization assays. For 5' phosphate linear plasmids *5'P-NHEJ-Fw* and *5'P-NHEJ-Fw,* for 5' biotin *5'B-NHEJ-*

Fw and *5'B-NHEJ-Fw,* and for 5'-hydroxyl *5'OH-NHEJ-Fw* and *5'OH-NHEJ-Fw,* pairs of primers were used. 1 μg of substrates were transfected into 0.25x10^6 HEK293T cells by using GeneJuice (Novagen) reagent following recommendations of the manufacturer. Cells were preincubated for 30 min with 10 μM ATMinhibitor KU55933 (Tocris) or vehicle (DMSO) before transfection. Cells were collected by trypsinization 16 hours later, and number of GFP positive cells, as well as GFP intensity was analysed using a BD FACSCalibur Flow Cytometer (342975, BD Biosciences).

To analyse individual repair events, DNA was isolated using QIAmp DNA mini kit (Qiagen) from cells treated as previously. Total DNA purified from these cells was transformed in MAX Efficiency DH10B Competent Cells (Invitrogen Positive transformants were selected by plating on LB agar plates containing kanamycin (25 μg/ml) and plasmid DNA was purified from single colonies. Sequence of single repair events were analysed by agarose gel electrophoresis after digestion with the restriction enzyme *Dra*I (Takara).

To validate the presence of 5' biotin in substrates, they were analysed by streptavidin-mediated precipitation. Dynabeads (10 μg) M-270 Streptavidin magnetic beads (Invitrogen) were prewashed (3 × in 5 mM Tris–HClpH 7.5, 0.5 mM EDTA in the presence of 1 M NaCl) and incubated with 100 ng of substrates for 1 h. Beads were then washed 4 times gradually decreasing NaCl concentration to 0. Finally, DNA fragments were eluted by 2 h incubation with *Bgl*II restriction enzyme (NEB). Input, unbound and bound DNA was analysed by agarose gel electrophoresis.

3.4. Clonogenic survival assays

Survival assays were carried out seeding 2,000 transformed MEFs in 100 mm dishes, in duplicate for each experimental condition. Cells were preincubated with 10 μM

ATM inhibitor KU55933 (Tocris), 10μM DNA-PKcs inhibitor NU7441 (Tocris) or vehicle (DMSO) for 1 h. The indicated concentration of etoposide (Sigma) was added and cells were incubated for additional 3 h. After a wash with PBS, fresh medium was added and cells were incubated for 10–14 days. Dishes were fixed and stained for colony scoring in Crystal Violet solution (0.5% Crystal violet in 20% ethanol). The surviving fraction at each dose was calculated by dividing the average number of visible colonies in treated versus untreated dishes.

3.5. Cytogenetic analysis

Micronuclei were analysed in transformed MEFs previously seeded onto coverslips. Following etoposide treatment, cytochalasin B (Sigma) was added at 4 μg/ml. 22 h post treatment, cells were fixed 10 min in methanol at -20ºC, and immunofluorescence was performed as previously described using antibodies against Tubulin and Vinculin, and stained with DAPI. To restrict the analysis to etoposide-induced micronuclei, only binucleated cells selected by visualization of the cytoplasm by Tubulin and Vinculin staining. They were manually scored for the presence of micronuclei by DAPI visualization.

Chromosomal aberrations were scored in Giemsa-stained metaphase spreads. Following treatment, recovery in fresh medium was allowed for 2 h, and demecolcine (Sigma) was added at a final concentration of 0.2 μg/ml. Four hours later, cells were collected by trypsinization, subjected to hypotonic shock for 1 h at 37 ˚C in 0.3 M sodium citrate, and fixed in 3:1 methanol:acetic acid solution. Cells were dropped onto acetic acid-humidified slides and stained 20 min in Giemsa-modified solution (5% v/v in H2O, Sigma). Samples were analyzed after permanent mounting in DEPEX.

3.6. Cellular index assay

Three independent sets of primary MEFs cells were analysed. 4000 cells were plated in E-plates 16 in duplicates and analised by the xCELLigence® RTCA DP (ACEA Bioscences). The instrument measures cellular proliferation by changes in impedance-based signals in real time.

4. Animal procedures

4.1. Ethics statement

All animal procedures were performed in accordance with European Union legislation and with the approval of the Ethical Committee for Animal Experimentation of the University of Seville and local Committee of Cabimer.

4.2. Animal maintenance

Double heterozygotes *Tdp2*$^{+/-}$ *Atm*$^{+/-}$ were obtained by the crossing of *Tdp2*$^{+/-}$ of an outbred 129Ola, CD1 and C57BL/6 background with 129/SvEv × NIH Black Swiss background *Atm*$^{+/-}$ mice. The colony was maintained by crossing double-heterozygotes, and littermates were used for experiments. Animals were housed in isolated cages with controlled ventilation trough HEPA-filters, kept under standard housing conditions (21±1°C with a photoperiod of 12:12 h), and manipulated in flow cabins. Sterile food pellets and water were available ad libitum.

Mice were genotyped using Phire Animal Tissue Direct PCR Kit (Thermo) following manufacturer instructions. For *Tdp2*, the indicated *TDP2-1*, *TDP2-2* and *TDP2-3* primers were used. This results in amplification of a 429 bp fragment from the

wild-type allele or 561 bp fragments from the mutant allele. In the case of *Atm*, *ATM-1*, *ATM-2* and *ATM-3* primers were used, resulting in amplification of a 160 bp fragment from the wild-type allele or 300 bp fragments from the mutant allele.

4.3. In vivo etoposide sensitivity

At 8 weeks of age, mice underwent intraperitoneal injection with 3 µl/g of body weight of either DMSO (vehicle control) or etoposide at 25 mg/ml in DMSO for a final dose of 25 mg/kg. Weight and general health status was monitored daily from the day of injection (inclusive). 6 days post-treatment mice were sacrificed by cervical dislocation and dissected for histopathological analysis. For this, organs were fixed in 4% paraformaldehyde for 2 days, embedded in paraffin, cut in 6 µm slices by microtome, stained with Hematoxylin-Eosin and visualized under the microscope.

4.4. Lifespan analysis

Minimum 20 mice per experimental condition were included in the analysis. Weight and general health status was monitored weekly. Animals were sacrificed by cervical dislocation and dissected for histopathological analysis in the case of showing a 20% loss of the maximum weight, the presence of a detectable tumor or signs of evident pain.

4.5. Lymphocyte analysis

Healthy thymus (4 weeks-old) or thymic lymphomas were extracted from mice, disgregated to single cells into EDTA-buffer and immunostained with anti-CD4-FITC (eBioscience, 17-0081-81, 1/500) and anti-CD8-APC (eBioscience, 11-0081-41, 1/500). Samples were fixed 10 min in 4%-paraformaldehyde for storage at 4 ºC. Intensity

was analysed using a BD FACSCalibur Flow Cytometer (342975, BD Biosciences).

4.6. Comparative Genomic Hybridization (CGH) analysis

For CGH, genomic DNA was purified from thymic tumours and kidney from *Tdp2*$^{+/+}$ *Atm*$^{-/-}$ or *Tdp2*$^{-/-}$ *Atm*$^{-/-}$ mice using DNeasy Blood and Tissue Kit (Qiagen) following recommendations of the manufacturer. 1 μg of genomic DNA from thymic lymphoma was profiled against 1 μg of matched normal kidney DNA from the same mouse. Processing, labelling and hybridization to Mouse Genome CGH Microarray 2x105K (G4425B-014699, Agilent) was performed at the Cabimer Genomic Facility. Data was processed using the package snapCGH within R (version 3.3.1) (Ewy & Sean 2016). Background correction was applied to fluorescence ratios of scanned images using the method 'minimum'. To compare hybridizations, normalization between arrays by the method 'scale' was performed. Finally, data was processed and ordered by the function 'processCGH', and fluorescence ratios were plotted using the R function 'plot' and the package Gviz (Smith et al. 2009). Thresholds for copy number alterations were set at log2 = ±0.6 for trisomy or hemizygous deletion.

4.7. Cerebellum histological analysis

Cerebellums were fixed in 4% paraformaldehyde, embedded in paraffin, and sagital 50 μm slices were obtained by vibratome. Immunohistochemistry was performed using anti-calbindin (D28K rabbit, CB-38a Swant, 1:5,000) primary antibody and Biotin-SP AffiniPure Goat Anti-Rabbit IgG (Jackson; 1:1,000) secondary antibody. Signal was developed using VECTASTAIN Elite ABC HRP Kit (Pk-6100, Vector Laboratories) and DAB (D4418-50SET, Sigma).

5. Statistical analysis

Statistical analysis was performed using GraphPad Prism software (GraphPad, San Diego, CA, USA).

6. Tables of materials

Cell name	Specie	Origin
primary MEFs	*Mus musculus*	Embryonic fibroblasts
BJ1	*Homo sapiens*	Primary skin fibroblasts
AT	*Homo sapiens*	Ataxia-telangiectasia primary fibroblasts
Transformed MEFs	*Mus musculus*	SV40-transformed embryonic fibroblasts
HEK293T	*Homo sapiens*	Embryonic kidney transformed cell line
U2OS	*Homo sapiens*	Osteosarcoma cell line

Table 1: Cells used in this Thesis.

Name	Sequence	5' end	From
5'Y-blunt	CTTCTCTTTCCAGGGCTATGT	5'-P-Y	MCRC
Blunt.Rev.Comp	AGACATAGCCCTGGAAAGAGAAG	5'-OH	Sigma
5'Y-overhang	AATTCTTCTCTTTCCAGGGCTATGT	5'-P-Y	MCRC
Overh.Rev.Comp	AGACATAGCCCTGGAAAGAGAAG	5'-OH	Sigma
5'P-NHEJ-Fw	AATTCTTCTCTTTCCAGGGCTATGT	5'-P	Sigma
5'P-NHEJ-Rv	AATTCATCCCCAGAAATGTAACTTG	5'-P	Sigma
5'Y-NHEJ-Fw	AATTCTTCTCTTTCCAGGGCTATGT	5'-P-Y	MCRC
5'Y-NHEJ-Rv	AATTCATCCCCAGAAATGTAACTTG	5'-P-Y	MCRC
5'B-NHEJ-Fw	AATTCTTCTCTTTCCAGGGCTATGT	5'-B	Sigma
5'B-NHEJ-Rv	AATTCATCCCCAGAAATGTAACTTG	5'-B	Sigma
5'OH-NHEJ-Fw	AATTCTTCTCTTTCCAGGGCTATGT	5'-OH	Sigma
5'OH-NHEJ-Rv	AATTCATCCCCAGAAATGTAACTTG	5'-OH	Sigma
TDP2-1	CCTTCATTACTTCTCGTAGGTTCTGGGTC	5'-OH	Sigma
TDP2-2	ACCCGCTCTTCACGCTGCTTCC	5'-OH	Sigma
TDP2-3	TACACCGTGCCATAATGACCAAC	5'-OH	Sigma
ATM-1	GACTTCTGTCAGATGTTGCTGCC	5'-OH	Sigma
ATM-2	CGAATTTGCAGGAGTTGCTGAG	5'-OH	Sigma
ATM-3	CCAGCTCATTCCTCCCACTCA	5'-OH	Sigma

Table 2: DNA Oligonucleotides used in this Thesis. 5'-P-Y (5' phosphotyrosine); 5'-OH (5' hydroxyl): 5'-P (5' phosphate) 5'-B (5' biotin); MCRC (Midland Certified Reagents Company)

Primary antibodies	Dilution	Obtained from	Specie
ATM	1/1,000	Sigma, MAT3-4G10/8	Mouse
ATM pS1981	1/1,000	Cell Signaling, #4526	Mouse
p-CHK2 Thr68	1/1,000	Cell Signaling, #2661	Mouse
p-p53 Ser15	1/1,000	Cell Signaling, #9284	Rabbit
p-CHK1 Ser345	1/1,000	Cell Signaling, #2341	Rabbit
α-tubulin	1/50,000	Sigma, T9026	Mouse
γH2AX	1/1,000	Millipore, 05-636	Mouse
α-Tubulin	1/2,000	Abcam, ab18251	Rabbit
Vinculin hVIN-1	1/2,000	Sigma, V9131	Mouse
anti-calbindin	1/5,000	D28K, CB-38a Swant	Rabbit
Cyclin A	1/500	Santa Cruz, sc-751	Rabbit
anti-CD4-FITC	1/500	eBioscience, 17-0081-81	Mouse
anti-CD8-APC	1/500	eBioscience, 11-0043-81	Mouse
Secondary			
IRDye 680RD goat anti-mouse IgG (H+L)	1/15,000	LI-COR, 926-68070	Goat
IRDye 800RD goat anti-rabbit IgG (H+L)	1/15,000	LI-COR, 926-32211	Goat
goat anti-mouse-AlexaFluor488	1/1,000	Jackson	Goat
goat anti-mouse-AlexaFluor594	1/1,000	Jackson	Goat
Biotin-SP AffiniPure Goat Anti-Rabbit IgG	1/1,000	Jackson, 111-065-003	Goat

Table 3: Antibodies used in this Thesis.

VII. BIBLIOGRAPHY

BIBLIOGRAPHY

Altieri, F. et al., 2008. DNA damage and repair: from molecular mechanisms to health implications. Antioxidants and redox signaling, 10(5), pp.891–937.

Bakkenist, C.J. & Kastan, M.B., 2003. DNA damage activates ATM through intermolecular autophosphorylation and dimer dissociation. Nature, 421(6922), pp.499–506.

Barazzuol, L. et al., 2015. Endogenous and X-ray-induced DNA double strand breaks sensitively activate apoptosis in adult neural stem cells. Journal of Cell Science, 128, pp.3597–3606.

Barlow, C. et al., 1996. Atm-deficient mice: a paradigm of ataxia telangiectasia. Cell, 86(1), pp.159–171.

Barnes, D.E. et al., 1998. Targeted disruption of the gene encoding DNA ligase IV leads to lethality in embryonic mice. Current Biology, 8(25), pp.1395–1398.

Barzilai, A., 2010. DNA damage, neuronal and glial cell death and neurodegeneration. Apoptosis, 15(11), pp.1371–1381.

Bassing, C.H. et al., 2002. Increased ionizing radiation sensitivity and genomic instability in the absence of histone H2AX. Proceedings of the National Academy of Sciences of the United States of America, 99(12), pp.8173–8.

Bassing, C.H. & Alt, F.W., 2004. The cellular response to general and programmed DNA double strand breaks. DNA Repair, 3(8–9), pp.781–796.

Bassing, C.H., Swat, W. & Alt, F.W., 2002. The mechanism and regulation of chromosomal V(D)J recombination. Cell, 109, pp.45–55.

Baudat, F., Imai, Y. & de Massy, B., 2013. Meiotic recombination in mammals: localization and regulation. Nature Reviews Genetics, 14(11), pp.794–806.

Bednarski, J.J. & Sleckman, B.P., 2012. Lymphocyte Development: Integration of DNA Damage Response Signaling. 1st ed., Elsevier Inc.

Bekker-Jensen, S. & Mailand, N., 2010. Assembly and function of DNA double-strand break repair foci in mammalian cells. DNA Repair, 9(12), pp.1219–1228.

Beraldi, R. et al., 2015. A novel porcine model of ataxia telangiectasia reproduces neurological features and motor deficits of human disease. Human Molecular Genetics, 24(22), pp.6473–6484.

Bolderson, E. et al., 2010. Phosphorylation of Exo1 modulates homologous recombination repair of DNA double-strand breaks. Nucleic Acids Research, 38(6), pp.1821–1831.

Bong-Gun, J. et al., 2006. A Topoisomerase IIb–Mediated dsDNA Break Required for Regulated Transcription. Science, 8888(June), pp.1798–1802.

De Bont, R. & van Larebeke, N., 2004. Endogenous DNA damage in humans: A review of quantitative data. Mutagenesis, 19(3), pp.169–185.

Bras, J. et al., 2015. Mutations in PNKP cause recessive ataxia with oculomotor apraxia type 4. American Journal of Human Genetics, 96(3), pp.474–479.

Bredemeyer, A.L., Huang, C.-Y., et al., 2008. Aberrant V(D)J recombination in ataxia telangiectasia mutated-deficient lymphocytes is dependent on nonhomologous DNA end joining. Journal of immunology (Baltimore, Md. : 1950), 181(4), pp.2620–5.

Bredemeyer, A.L. et al., 2006. ATM stabilizes DNA double-strand-break complexes during V(D)J recombination. Nature, 442(7101), pp.466–470.

Bredemeyer, A.L., Helmink, B.A., et al., 2008. DNA double-strand breaks activate a multi-functional genetic program in developing lymphocytes. Nature, 456(7223), pp.819–23.

Brenner, D.J. & Ward, J.F., 1992. Constraints on Energy Deposition and Target Size of Multiply Damaged Sites Associated with DNA Double-strand Breaks. International Journal of Radiation Biology, 61(6), pp.737–748.

Buck, D. et al., 2006. Cernunnos, a novel nonhomologous end-joining factor, is mutated in human immunodeficiency with microcephaly. Cell, 124(2), pp.287–299.

Budman, J., Kim, S.A. & Chu, G., 2007. Processing of DNA for nonhomologous end-joining is controlled by kinase activity and XRCC4/ligase IV. Journal of Biological Chemistry, 282(16), pp.11950–11959.

Bunch, H. et al., 2015. Transcriptional elongation requires DNA break-induced signalling. Nature Communications, 6, p.10191.

Burma, S. et al., 2001. ATM phosphorylates histone H2AX in response to DNA double-strand breaks. The Journal of biological chemistry, 276(45), pp.42462–42467.

Caldecott, K.W., 2008. Single-strand break repair and genetic disease. Nature reviews Genetics, 9(8), pp.619–631.

Callen, E. et al., 2007. ATM prevents the persistence and propagation of chromosome breaks in lymphocytes. Cell, 130(1), pp.63–75.

Caron, P. et al., 2015a. Non-redundant Functions of ATM and DNA-PKcs in Response to DNA Double-Strand Breaks. Cell Reports, 13(8), pp.1598–1609.

Caron, P. et al., 2015b. Non-redundant Functions of ATM and DNA-PKcs in Response to DNA Double-Strand Breaks. Cell Reports, 13(8), pp.1598–1609.

Cavalli, G. & Misteli, T., 2013. Functional implications of genome topology. Nature structural & molecular biology, 20(3), pp.290–9.

Celeste, A. et al., 2002. Genomic Instability in Mice Lacking Histone H2AX. Science, 296(May), pp.922–927.

Chan, D.W. & Lees-Miller, S.P., 1996. The DNA-dependent protein kinase is inactivated by autophosphorylation of the catalytic subunit. Journal of Biological Chemistry, 271(15), pp.8936–8941.

Chang, H.H.Y. & Lieber, M.R., 2016. Structure-Specific nuclease activities of Artemis and the Artemis: DNA-PKcs complex. Nucleic Acids Research, 44(11), pp.4991–4997.

Chapman, J.R. et al., 2012. BRCA1-associated exclusion of 53BP1 from DNA damage sites underlies temporal control of DNA repair. Journal of cell science, 125(Pt 15), pp.3529–34.

Chaumeil, J. et al., 2013. The RAG2 C-terminus and ATM protect genome integrity by controlling antigen receptor gene cleavage. Nature communications, 4, p.2231.

Chen, B.P.C. et al., 2007. Ataxia telangiectasia mutated (ATM) is essential for DNA-PKcs phosphorylations at the Thr-2609 cluster upon DNA double strand break. Journal of Biological Chemistry, 282(9), pp.6582–6587.

Chistiakov, D.A., 2010. Ligase IV syndrome. Advances in Experimental Medicine and Biology, 685(6), pp.175–185.

Christopher C. Dvorak, M.J.C., 2010. Radiosensitive Severe Combined Immunodeficiency Disease. , 30(1), pp.1–19.

Chun, H.H. & Gatti, R.A., 2004. Ataxia-telangiectasia, an evolving phenotype. DNA Repair, 3(8–9), pp.1187–1196.

Ciccia, A. & Elledge, S.J., 2010. Review The DNA Damage Response : Making It Safe to Play with Knives. Molecular Cell, 40(2), pp.179–204.

Cimprich, K.A. & Cortez, D., 2008. ATR: an essential regulator of genome integrity. Nature reviews. Molecular cell biology, 9(8), pp.616–27.

Concannon, P. & Gatti, R.A., 1997. Diversity of ATM gene mutations detected in patients with ataxia- telangiectasia. Human Mutation, 10(2), pp.100–107.

Connelly, J.C. & Leach, D.R.F., 2004. Repair of DNA covalently linked to protein. Molecular cell, 13(3), pp.307–316.

Cooke, H.J. & Saunders, P.T.K., 2002. Mouse models of male infertility. Nature reviews. Genetics, 3(10), pp.790–801.

Cortés-Ledesma, F. & Aguilera, A., 2006. Double-strand breaks arising by replication through a nick are repaired by cohesin-dependent sister-chromatid exchange. EMBO reports, 7(9), pp.919–926.

Cortés-Ledesma, F. et al., 2009. A human 5'-tyrosyl DNA phosphodiesterase that repairs topoisomerase-mediated DNA damage. Nature, 461(7264), pp.674–678.

Costes, S. V. et al., 2010. Spatiotemporal characterization of ionizing radiation induced DNA damage foci and their relation to chromatin organization. Mutation Research - Reviews in Mutation Research, 704(1–3), pp.78–87.

Crawford, T.O. et al., 2006. Survival probability in ataxia telangiectasia. Archives of disease in childhood, 91(7), pp.610–1.

Cui, X. et al., 2005. Autophosphorylation of DNA-Dependent Protein Kinase Regulates DNA End Processing and May Also Alter Double-Strand Break Repair Pathway Choice. Molecular and Cellular Biology, 25(24), pp.10842–10852.

Daniel, J.A. et al., 2008. Multiple autophosphorylation sites are dispensable for murine ATM activation in vivo. Journal of Cell Biology, 183(5), pp.777–783.

Date, H. et al., 2001. Early-onset ataxia with ocular motor apraxia and hypoalbuminemia is caused by mutations in a new HIT superfamily gene. Nature genetics, 29(2), pp.184–188.

Davis, A. & Chen, D., 2013. DNA double strand break repair via non-homologous end-joining. Translational Cancer Research, 2(3), pp.130–43.

Deriano, L. et al., 2011. The RAG2 C terminus suppresses genomic instability and lymphomagenesis. Nature, 471(7336), pp.119–123.

Deweese, J.E. & Osheroff, N., 2009. The DNA cleavage reaction of topoisomerase II: wolf in sheep's clothing. Nucleic acids research, 37(3), pp.738–748.

Difilippantonio, S. et al., 2007. Distinct domains in Nbs1 regulate irradiation-induced checkpoints and apoptosis. The Journal of experimental medicine, 204(5), pp.1003–1011.

Digweed, M. & Sperling, K., 2004. Nijmegen breakage syndrome: Clinical manifestation of defective response to DNA double-strand breaks. DNA Repair, 3(8–9), pp.1207–1217.

Ding, Q. et al., 2003. Autophosphorylation of the catalytic subunit of the DNA-dependent protein kinase is required for efficient end processing during DNA double-strand break repair. Molecular and Cellular Biology, 23(16), pp.5836–5848.

Dobbs, T.A., Tainer, J.A. & Lees-Miller, S.P., 2010. A structural model for regulation of NHEJ by DNA-PKcs autophosphorylation. DNA Repair, 9(12), pp.1307–1314.

Downs, J. a & Jackson, S.P., 2004. A means to a DNA end: the many roles of Ku. Nature reviews. Molecular cell biology, 5(5), pp.367–378.

Driscoll, M.O. et al., 2004. An overview of three new disorders associated with genetic instability : LIG4 syndrome , RS-SCID and ATR-Seckel syndrome. , 3, pp.1227–1235.

Ewy, M. & Sean, D., 2016. Statistical Genomics: Methods and Protocols.

Falck, J., Coates, J. & Jackson, S.P., 2005. Conserved modes of recruitment of ATM, ATR and DNA-PKcs to sites of DNA damage. Nature, 434(7033), pp.605–611.

Fenech, M., 2000. The in vitro micronucleus technique. Mutation Research - Fundamental and Molecular Mechanisms of Mutagenesis, 455(1–2), pp.81–95.

Feng, L. & Chen, J., 2012. The E3 ligase RNF8 regulates KU80 removal and NHEJ repair. Nature Structural & Molecular Biology, 19(2), pp.201–6.

Firsanov, D. V., Solovjeva, L. V. & Svetlova, M.P., 2011. H2AX phosphorylation at the sites of DNA double-strand breaks in cultivated mammalian cells and tissues. Clinical Epigenetics, 2(2), pp.283–297.

Foray, N. et al., 1997. Hypersensitivity of ataxia telangiectasia fibroblasts to ionizing radiation is associated with a repair deficiency of DNA double-strand breaks. International journal of radiation biology, 72(3), pp.271–83.

Franco, S. et al., 2006. H2AX prevents DNA breaks from progressing to chromosome breaks and translocations. Molecular Cell, 21(2), pp.201–214.

Frank, K.M. et al., 2000. DNA ligase IV deficiency in mice leads to defective neurogenesis and embryonic lethality via the p53 pathway. Molecular Cell, 5(6), pp.993–1002.

Freitas, A.A. & De Magalhães, J.P., 2011. A review and appraisal of the DNA damage theory of ageing. Mutation Research - Reviews in Mutation Research, 728(1–2), pp.12–22.

Frit, P. et al., 2014. Alternative end-joining pathway(s): Bricolage at DNA breaks. DNA Repair, 17, pp.81–97.

Gao, R. et al., 2012. Biochemical characterization of human tyrosyl-DNA phosphodiesterase 2 (TDP2/TTRAP): A Mg^{2+}/Mn^{2+}-dependent phosphodiesterase specific for the repair of topoisomerase cleavage complexes. Journal of Biological Chemistry, 287(36), pp.30842–30852.

Gao, R. et al., 2014. Proteolytic degradation of topoisomerase II (Top2) enables the processing of Top2-DNA and Top2-RNA covalent complexes by tyrosyl-DNA-phosphodiesterase 2 (TDP2). Journal of Biological Chemistry, 289(26), pp.17960–17969.

Gao, Y. et al., 1998. A critical role for DNA end-joining proteins in both lymphogenesis and neurogenesis. Cell, 95(7), pp.891–902.

Garcia, V. et al., 2012. Bidirectional resection of DNA double-strand breaks by Mre11 and Exo1. Nature, 479(7372), pp.241–244.

Garcia, V. et al., 2015. Tel1(ATM)-mediated interference suppresses clustered meiotic double-strand-break formation. Nature, 520, pp.114–118.

Gauss, G.H. & Lieber, M.R., 1996. Mechanistic constraints on diversity in human V(D)J recombination. Molecular and Cellular Biology, 16(1), pp.258–269.

Genik, P.C. et al., 2014. Strain background determines lymphoma incidence in Atm knockout mice. Neoplasia (New York, N.Y.), 16(2), pp.129–36.

Gilbert, N. & Allan, J., 2014. Supercoiling in DNA and chromatin. Current Opinion in Genetics and Development, 25(1), pp.15–21.

Gómez-Herreros, F. et al., 2013. TDP2-Dependent Non-Homologous End-Joining Protects against Topoisomerase II-Induced DNA Breaks and Genome Instability in Cells and In Vivo. PLoS Genetics, 9(3).

Gómez-Herreros, F. et al., 2014. TDP2 protects transcription from abortive topoisomerase activity and is required for normal neural function. Nature genetics, 46(5), pp.516–21.

Goodarzi, A.A. et al., 2006. DNA-PK autophosphorylation facilitates Artemis endonuclease activity. The EMBO journal, 25(16), pp.3880–9.

Goodarzi, A.A., Jeggo, P. & Lobrich, M., 2010. The influence of heterochromatin on DNA double strand break repair: Getting the strong, silent type to relax. DNA Repair, 9(12), pp.1273–1282.

Gottlieb, T.M. & Jackson, P., 1993. The DNA-Dependent Protein Ki for DNA Ends and AssocWbn with Ku Ant. , 72, pp.131–142.

Gu, J. et al., 2007. XRCC4:DNA ligase IV can ligate incompatible DNA ends and can ligate across gaps. The EMBO Journal, 26(4), pp.1010–1023.

Guo, Z. et al., 2010. ATM activation by oxidative stress (supp). Science (New York, N.Y.), 330(6003), pp.517–521.

Gurley, K.E. & Kemp, C.J., 2001. Synthetic lethality between mutation in Atm and DNA-PKcs during murine embryogenesis. Current Biology, 11(3), pp.191–194.

Hada, M. & Georgakilas, A.G., 2008. Formation of Clustered DNA Damage after High-LET Irradiation : A Review. J. Radiat. Res., 49(3), pp.203–210.

Haffner, M.C. et al., 2010. Androgen-induced TOP2B-mediated double-strand breaks and prostate cancer gene rearrangements. Nature genetics, 42(8), pp.668–675.

Hagen, U., 1994. Mechanisms of induction and repair of DNA double-strand breaks by ionizing radiation: Some contradictions. Radiation and Environmental Biophysics, 33(1), pp.45–61.

Hammarsten, O., DeFazio, L.G. & Chu, G., 2000. Activation of DNA-dependent protein kinase by single-stranded DNA ends. Journal of Biological Chemistry, 275(3), pp.1541–1550.

Harper, J.W. & Elledge, S.J., 2007. The DNA Damage Response: Ten Years After. Molecular Cell, 28(5), pp.739–745.

Harrison, J.C. & Haber, J.E., 2006. Surviving the Breakup: The DNA Damage Checkpoint. Annual Review of Genetics, 40(1), pp.209–235.

Heck, M.M., Hittelman, W.N. & Earnshaw, W.C., 1988. Differential expression of DNA topoisomerases I and II during the eukaryotic cell cycle. Proceedings of the National Academy of Sciences of the United States of America, 85(4), pp.1086–90.

Helleday, T., Eshtad, S. & Nik-Zainal, S., 2014. Mechanisms underlying mutational signatures in human cancers. Nature reviews. Genetics, 15(9), pp.585–598.

Helmink, B.A. et al., 2011. H2AX Prevents CtIP-Mediated DNA End Resection and Aberrant Repair in G1-Phase Lymphocytes Beth. Nature, 469(7329), pp.245–249.

Heo, J. et al., 2015. TDP1 promotes assembly of non-homologous end joining protein complexes on DNA. DNA Repair, 30, pp.28–37.

Huertas, P. et al., 2008. CDK targets Sae2 to control DNA-end resection and homologous recombination. Nature, 455(7213), pp.689–692.

Huertas, P., 2010. DNA resection in eukaryotes: deciding how to fix the break. Nature structural & molecular biology, 17(1), pp.11–16.

Iliakis, G. et al., 2003. DNA damage checkpoint control in cells exposed to ionizing radiation. Oncogene, 22, pp.5834–5847.

Jackson, A.L. & Loeb, L.A., 2001. The contribution of endogenous sources of DNA damage to the multiple mutations in cancer. Fundamental and Molecular Mechanisms of Mutagenesis, 477(1–2), pp.7–21.

Jeppesen, D.K., Bohr, V.A. & Stevnsner, T., 2011. DNA repair deficiency in neurodegeneration. Progress in Neurobiology, 94(2), pp.166–200.

Ji, G. et al., 2013. Polymorphisms in double-strand breaks repair genes are associated with impaired fertility in Chinese population. Reproduction research, 145(5), pp.463–70.

Jiang, W. et al., 2015. Aberrant TCRδ rearrangement underlies the T-cell lymphocytopenia and t(12;14) translocation associated with ATM deficiency. Blood, 125(17), pp.2665–2668.

Kankanala, J. et al., 2016. Isoquinoline-1,3-diones as Selective Inhibitors of Tyrosyl DNA Phosphodiesterase II (TDP2). Journal of Medicinal Chemistry, 59(6), pp.2734–2746.

Kastan, M.B. & Lim, D.S., 2000. The many substrates and functions of ATM. Nature reviews Molecular cell biology, 1(3), pp.179–186.

Khanna, K.K. & Jackson, S.P., 2001. DNA double-strand breaks: signaling, repair and the cancer connection. Nature genetics, 27(3), pp.247–54.

Kijas, A.W. et al., 2015. ATM-dependent phosphorylation of MRE11 controls extent of resection during homology directed repair by signalling through Exonuclease 1. Nucleic Acids Research, 43(17), pp.8352–8367.

Kim, Y.-C. et al., 2009. Activation of ATM depends on chromatin interactions occurring before induction of DNA damage. Nature cell biology, 11(1), pp.92–96.

King, I.F. et al., 2013. Topoisomerases facilitate transcription of long genes linked to autism. Nature, 501(7465), pp.58–62.

Kinner, A. et al., 2008. Gamma-H2AX in recognition and signaling of DNA double-strand breaks in the context of chromatin. Nucleic acids research, 36(17), pp.5678–5694.

Königer, C. et al., 2014. Involvement of the host DNA-repair enzyme TDP2 in formation of the covalently closed circular DNA persistence reservoir of hepatitis B viruses. Proceedings of the National Academy of Sciences of the United States of America, 111(40), pp.E4244-53.

Kossmann, B.R. et al., 2016. Discovery of selective inhibitors of tyrosyl-DNA phosphodiesterase 2 by targeting the enzyme DNA-binding cleft. Bioorganic and Medicinal Chemistry Letters, 26(14), pp.3232–3236.

Kühne, M. et al., 2004. A Double-Strand Break Repair Defect in ATM-Deficient Cells Contributes to Radiosensitivity A Double-Strand Break Repair Defect in ATM-Deficient Cells Contributes to Radiosensitivity. Cancer research, 64, pp.500–508.

Kurosawa, A. & Adachi, N., 2010. Functions and regulation of Artemis: a goddess in the maintenance of genome integrity. J Radiat. Res., 51(5), pp.503–509.

Kuzminov, A., 2001. Single-strand interruptions in replicating chromosomes cause double-strand breaks. Proceedings of the National Academy of Sciences of the United States of America, 98(15), pp.8241–8246.

Kwan, K.Y. & Wang, J.C., 2001. Mice lacking DNA topoisomerase IIIbeta develop to maturity but show a reduced mean lifespan. Proceedings of the National Academy of Sciences of the United States of America, 98(10), pp.5717–21.

Lam, I. & Keeney, S., 2015. Mechanism and regulation of meiotic recombination initiation,

Lange, J. et al., 2011. ATM controls meiotic double-strand-break formation. Nature, 479(7372), pp.237–40.

Lavin, M. et al., 2015. ATM-Dependent Phosphorylation of All Three Members of the MRN Complex: From Sensor to Adaptor. Biomolecules, 5(4), pp.2877–2902.

Lavin, M.F., 2008. Ataxia-telangiectasia: from a rare disorder to a paradigm for cell signalling and cancer. Nature reviews Molecular cell biology, 9(10), pp.759–769.

Lavin, M.F., 2013. The appropriateness of the mouse model for ataxia-telangiectasia: Neurological defects but no neurodegeneration. DNA Repair, 12(8), pp.612–619.

Lees-Miller, S.P. & Meek, K., 2003. Repair of DNA double strand breaks by non-homologous end joining. Biochimie, 85(11), pp.1161–1173.

Lempiäinen, H. & Halazonetis, T.D., 2009. Emerging common themes in regulation of PIKKs and PI3Ks. The EMBO journal, 28(20), pp.3067–73.

Lewis, S.M. et al., 1997. Cryptic signals and the fidelity of V(D)J joining. Molecular and cellular biology, 17(6), pp.3125–36.

Li, C. et al., 2011. Oncogenic role of EAPII in lung cancer development and its activation of the MAPK-ERK pathway. Oncogene, 30(September 2010), pp.3802–3812.

Li, C. et al., 2011. Pleiotropic functions of EAPII/TTRAP/TDP2: Cancer development, chemoresistance and beyond. Cell Cycle, 10(19), pp.3274–3283.

Li, J. et al., 2012. Nuclear accumulation of HDAC4 in ATM deficiency promotes neurodegeneration in ataxia telangiectasia. Nature medicine, 18(5), pp.783–90.

Li, W. & Wang, J.C., 1998. Mammalian DNA topoisomerase IIIa is essential in early embryogenesis. Biochemistry, 95(February), pp.1010–1013.

Li, Y. et al., 2014. Topoisomerase IIbeta is required for proper retinal development and survival of postmitotic cells. Biology open, 3(2), pp.172–84.

Liao, S., Tammaro, M. & Yan, H., 2016. The structure of ends determines the pathway choice and Mre11 nuclease dependency of DNA double-strand break repair. Nucleic Acids Research, 44(12), pp.5689–5701.

Lindahl, T., 1993. Instability and decay of the `primary structure of DNA. Nature, 363.

Lindahl, T. & Barnes, D.E., 1992. Mammalian DNA ligases. Ann. Rev. Biochem., 61(1), pp.251–281.

Lindahl, T. & Wood, R.D., 1999. Quality Control by DNA Repair. Science, 286(5446), pp.1897–1905.

Liu, L.F. et al., 1983. Cleavage of DNA by mammalian DNA topoisomerase II. J Biol CheM, 258(24), pp.15365–15370.

Löbrich, M. et al., 2010. gammaH2AX foci analysis for monitoring DNA double-strand break repair: strengths, limitations and optimization. Cell cycle (Georgetown, Tex), 9(4), pp.662–669.

Löbrich, M. & Jeggo, P.A., 2007. The impact of a negligent G2/M checkpoint on genomic instability and cancer induction. Nature reviews. Cancer, 7(11), pp.861–9.

Longhese, M.P. et al., 2009. DNA double-strand breaks in meiosis: Checking their formation, processing and repair. DNA Repair, 8(9), pp.1127–1138.

Lou, Z. et al., 2006. MDC1 maintains genomic stability by participating in the amplification of ATM-dependent DNA damage signals. Molecular Cell, 21(2), pp.187–200.

Lovett, B.D. et al., 2001. Etoposide metabolites enhance DNA topoisomerase II cleavage near leukemia-associated MLL translocation breakpoints. Biochemistry, 40(5), pp.1159–1170.

Luciana Chessa, R.M. and A.M., 2016. Focusing New Ataxia Telangiectasia Therapeutic Approaches. Journal of Rare Disorders: Diagnosis and Therapy, pp.1–9.

Lyu, Y.L. et al., 2006. Role of topoisomerase IIbeta in the expression of developmentally regulated genes. Molecular and cellular biology, 26(21), pp.7929–41.

Madabhushi, R. et al., 2015. Activity-Induced DNA Breaks Govern the Expression of Neuronal Early-Response Genes. Cell, 161(7), pp.1592–1605.

Mahaney, B.L. et al., 2012. XRCC4 and XLF form long helical protein filaments suitable for DNA end protection and alignment to facilitate DNA double strand break repair. National Institutes of Health, 29(6), pp.997–1003.

Malyarchuk, S. et al., 2013. Artemis is required to improve the accuracy of repair of double-strand breaks with 5'-blocked termini generated from non-DSB-clustered lesions. Mutagenesis, 28(3), pp.357–366.

Mao, Z. et al., 2008. DNA repair by nonhomologous end joining and homologous recombination during cell cycle in human cells. Cell cycle (Georgetown, Tex.), 7(18), pp.2902–6.

Marchand, C. et al., 2016. Deazaflavin Inhibitors of Tyrosyl-DNA Phosphodiesterase 2 (TDP2) Specific for the Human Enzyme and Active against Cellular TDP2. ACS Chemical Biology, 11(7), pp.1925–1933.

Marnett, L.J., 2000. Oxyradicals and DNA damage. Carcinogenesis, 21(3), pp.361–370.

McBlane, J.F. et al., 1995. Cleavage at a V(D)J recombination signal requires only RAG1 and RAG2 proteins and occurs in two steps. Cell, 83(3), pp.387–395.

McGrath-Morrow, S.A. et al., 2010. Evaluation and management of pulmonary disease in ataxia-telangiectasia. Pediatric Pulmonology, 45(9), pp.847–859.

McKinnon, P.J., 2012. ATM and the molecular pathogenesis of ataxia telangiectasia. Annual review of pathology, 7, pp.303–321.

McKinnon, P.J. & Caldecott, K.W., 2007. DNA strand break repair and human genetic disease. Annual review of genomics and human genetics, 8, pp.37–55.

McVey, M. & Lee, S.E., 2008. MMEJ repair of double-strand breaks (director's cut): deleted sequences and alternative endings. Trends in Genetics, 24(11), pp.529–538.

Meek, K. et al., 2007. trans Autophosphorylation at DNA-dependent protein kinase's two major autophosphorylation site clusters facilitates end processing but not end joining. Molecular and cellular biology, 27(10), pp.3881–90.

Meek, K., Dang, V. & Lees-Miller, S.P., 2008. DNA-PK. The Means to Justify the Ends? Advances in Immunology, 99(8), pp.33–58.

Mehte, A. & Haber, J.E., 2014. Sources of DNA Double-Strand Breaks and Models of Recombinational DNA repair. , 6(a01428), pp.1–19.

Melorose, J. et al., 2008. DNA repair pathways as targets for cancer therapy. Nat Rev Cancer, 14(3), pp.1291–1295.

Michels, E. et al., 2007. Detection of DNA copy number alterations in cancer by array comparative genomic hybridization. Genetics in medicine : official journal of the American College of Medical Genetics, 9(9), pp.574–584.

Mills, K.D., Ferguson, D.O. & Alt, F.W., 2003. The role of DNA breaks in genomic instability and tumorigenesis. Immunological reviews, 194, pp.77–95.

Morham, S.G. et al., 1996. Targeted Disruption of the Mouse Topoisomerase I Gene by Camptothecin Selection. Molecular and cellular biology, 16(12), pp.6804–6809.

Moshous, D. et al., 2001. Artemis, a novel DNA double-strand break repair/V(D)J recombination protein, is mutated in human severe combined immune deficiency. Cell, 105(2), pp.177–186.

Murai, J. et al., 2012. Tyrosyl-DNA phosphodiesterase 1 (TDP1) repairs DNA damage induced by topoisomerases I and II and base alkylation in vertebrate cells. Journal of Biological Chemistry, 287(16), pp.12848–12857.

Muslimovic, A. et al., 2011. Numerical Analysis of Etoposide Induced DNA Breaks Aida. Plos One, 101(11), pp.1435–1439.

Neale, M.J., Pan, J. & Keeney, S., 2005. Endonucleolytic processing of covalent protein-linked DNA double-strand breaks. Nature, 436(7053), pp.1053–7.

Nitiss, J.L., 2009. Targeting DNA topoisomerase II in cancer chemotherapy. Nature reviews. Cancer, 9(5), pp.338–350.

Nitiss, K.C. et al., 2006. Tyrosyl-DNA phosphodiesterase (Tdp1) participates in the repair of Top2-mediated DNA damage. Pnas, 103(24), pp.8953–8958.

Noon, A.T. et al., 2010. 53BP1-dependent robust localized KAP-1 phosphorylation is essential for heterochromatic DNA double-strand break repair. Nat Cell Biol, 12(2), pp.177–184.

Nordstrand, L.M. et al., 2007. Genome instability and DNA damage accumulation in gene-targeted mice. Neuroscience, 145(4), pp.1309–1317.

Notarangelo, L.D. et al., 2016. Human RAG mutations: biochemistry and clinical implications. Nature reviews. Immunology, 16(4), pp.234–46.

Nowak-Wegrzyn, A. et al., 2004. Immunodeficiency and infections in ataxia-telangiectasia. Journal of Pediatrics, 144(4), pp.505–511.

Nur-E-Kamal, A. et al., 2007. Role of DNA topoisomerase IIB in neurite outgrowth. Brain Research, 1154(1), pp.50–60.

O'Driscoll, M. et al., 2001. DNA ligase IV mutations identified in patients exhibiting developmental delay and immunodeficiency. Molecular Cell, 8(6), pp.1175–1185.

Ochi, T. et al., 2015. DNA repair. PAXX, a paralog of XRCC4 and XLF, interacts with Ku to promote DNA double-strand break repair. Science, 347(6218), pp.185–188.

Olive, P.L. & Banath, J.P., 2006. The comet assay: a method to measure DNA damage in individual cells. Nat. Protocols, 1(1), pp.23–29.

P. Hornyak et al., 2016. Mode of action of DNA-competitive small molecule inhibitors of tyrosyl DNA phosphodiesterase 2. Biochemical Journal, 0, pp.1869–1879.

Panier, S. & Boulton, S.J., 2014. Double-strand break repair: 53BP1 comes into focus. Nature reviews. Molecular cell biology, 15(1), pp.7–18.

Paull, T.T., 2015. Mechanisms of ATM activation. Annual Review of Biochemistry, 84(December), pp.711–738.

Pei, H. et al., 2003. EAPII interacts with ETS1 and modulates its transcriptional function. Oncogene, 22, pp.2699–2709.

Pendleton, M. et al., 2014. Topoisomerase II and leukemia. Annals of the New York Academy of Sciences, 1310(1), pp.98–110.

Petiniot, L.K. et al., 2002. RAG-Mediated V (D) J Recombination Is Not Essential for Tumorigenesis in Atm -Deficient Mice. Molecular and Cellular Biology, 22(9), pp.3174–3177.

St. Pierre, J. et al., 2002. DNA topoisomerase II is essential for preimplantation mouse development. Molecular Reproduction and Development, 61(3), pp.347–357.

Polo, S. & Jackson, S., 2011. Dynamics of DNA damage response proteins at DNA breaks: a focus on protein modifications. Genes and development, 25(5), pp.409–33.

Pommier, Y. et al., 2010. DNA topoisomerases and their poisoning by anticancer and antibacterial drugs. Chemistry and Biology, 17(5), pp.421–433.

Pommier, Y. et al., 2016. Roles of eukaryotic topoisomerases in transcription, replication and genomic stability. Nature Reviews Molecular Cell Biology.

Postow, L., 2011. Destroying the ring: Freeing DNA from Ku with ubiquitin. FEBS Letters, 585(18), pp.2876–2882.

Povirk, L.F., 2012. Processing of Damaged DNA Ends for Double-Strand Break Repair in Mammalian Cells. ISRN Molecular Biology, 2012, pp.1–16.

Quennet, V. et al., 2011. CtIP and MRN promote non-homologous end-joining of etoposide-induced DNA double-strand breaks in G1. Nucleic Acids Research, 39(6), pp.2144–2152.

Raghavan, S.C. & Raman, M.J., 2004. Nonhomologous end joining of complementary and noncomplementary DNA termini in mouse testicular extracts. DNA Repair, 3(10), pp.1297–1310.

Ramsden, D.A., 2011. Polymerases in nonhomologous end joining: building a bridge over broken chromosomes. Antioxidants & redox signaling, 14(12), pp.2509–19.

Ramsden, D.A., Paull, T.T. & Gellert, M., 1997. Cell-free V (D) J recombination. Nature, 388(July).

Reddy, Y.V.R. et al., 2004. Non-homologous end joining requires that the DNA-PK complex undergo an autophosphorylation-dependent rearrangement at DNA ends. Journal of Biological Chemistry, 279(38), pp.39408–39413.

Reynolds, J.J. & Stewart, G.S., 2013. A nervous predisposition to unrepaired DNA double strand breaks. DNA Repair, 12(8), pp.588–599.

Riballo, E. et al., 2004. A pathway of double-strand break rejoining dependent upon ATM, Artemis, and proteins locating to gamma-H2AX foci. Molecular cell, 16(5), pp.715–724.

Richmond, T.J. & Davey, C.A., 2003. The structure of DNA in the nucleosome core. Nature, 423(6936), pp.145–50.

Roos, W.P. & Kaina, B., 2013. DNA damage-induced cell death: From specific DNA lesions to the DNA damage response and apoptosis. Cancer Letters, 332(2), pp.237–248.

Roos, W.P., Thomas, A.D. & Kaina, B., 2015. DNA damage and the balance between survival and death in cancer biology. Nature reviews. Cancer, 16(1), pp.20–33.

Roth, D.B., 2003. Restraining the V(D)J recombinase. Nature reviews. Immunology, 3(8), pp.656–666.

Rothkamm, K. et al., 2003. Pathways of DNA Double-Strand Break Repair during the Mammalian Cell Cycle Pathways of DNA Double-Strand Break Repair during the Mammalian Cell Cycle. Molecular and cellular biology, 23(16), pp.5706–5715.

Rouse, J. & Jackson, S.P., 2002. Interfaces between the detection, signaling, and repair of DNA damage. Science, 297(5581), pp.547–551.

Saenz Robles, M.T. et al., 1994. Induction versus progression of brain tumor development: differential functions for the pRB- and p53-targeting domains of simian virus 40 T antigen. Molecular and Cellular Biology, 14(4), pp.2686–2698.

Sasaki, T. et al., 1998. ATM mutations in patients with ataxia telangiectasia screened by a hierarchical strategy. Human mutation, 12(3), pp.186–95.

Savitsky, K. et al., 1995. A Single Ataxia Telangiectasia Gene with a Product Similar to P1-3 Kinase. , 268(June), pp.1749–1753.

Schatz, D.G. & Swanson, P.C., 2011. V(D)J Recombination: Mechanisms of Initiation. Annual Review of Genetics, 45(D), pp.167–202.

Schellenberg, M.J. et al., 2012. Mechanism of repair of 5α-topoisomerase II–DNA adducts by mammalian tyrosyl-DNA phosphodiesterase 2. Nature Structural & Molecular Biology, 19(12), pp.1363–1371.

Seluanov, A. et al., 2004. DNA end joining becomes less efficient and more error-prone during cellular senescence. Proceedings of the National Academy of Sciences of the United States of America, 101(20), pp.7624–7629.

Sfeir, A. & Symington, L.S., 2015. Microhomology-Mediated End Joining: A Back-up Survival Mechanism or Dedicated Pathway? Trends in Biochemical Sciences, 40(11), pp.701–714.

Shen, J. et al., 2010. Mutations in PNKP cause microcephaly, seizures and defects in DNA repair. Nature genetics, 42(3), pp.245–9.

Shi, K. et al., 2012. Structural basis for recognition of 5'-phosphotyrosine adducts by Tdp2. Nature Structural & Molecular Biology, 19(12), pp.1372–7.

Shiloh, Y. & Ziv, Y., 2013. The ATM protein kinase: regulating the cellular response to genotoxic stress, and more. Nature reviews. Molecular cell biology, 14(4), pp.197–210.

Shiotani, B. & Zou, L., 2009a. ATR signaling at a glance. Journal of Cell Science, 122(3), pp.301–304.

Shiotani, B. & Zou, L., 2009b. Single-Stranded DNA Orchestrates an ATM-to-ATR Switch at DNA Breaks. Molecular Cell, 33(5), pp.547–558.

Shroff, R. et al., 2004. Distribution and Dynamics of Chromatin Modification Induced by a Defined DNA Double-Strand Break. Current Biology, 14, pp.1703–1711.

Smith, J. et al., 2001. The influence of DNA double-strand break structure on end-joining in human cells. Nucleic acids research, 29(23), pp.4783–92.

Smith, M.L. et al., 2009. snapCGH: Segmentation, normalisation and processing of aCGH data. Bioconductor, 18, pp.1–12.

Stavnezer, J., Jeroen E.J. G & E.Schrader, C., 2008. Mechanism and regulation of class switch recombination. Annual Review of Immunology, 26, pp.261–92.

Stiff, T. et al., 2004. ATM and DNA-PK Function Redundantly to Phosphorylate H2AX after Exposure to Ionizing Radiation. Cancer Research, 64(7), pp.2390–2396.

Strande, N.T., Waters, C.A. & Ramsden, D. a, 2012. Resolution of complex ends by Nonhomologous end joining - better to be lucky than good? Genome integrity, 3(1), p.10.

Sun, T. & Hevner, R.F., 2014. Growth and folding of the mammalian cerebral cortex: from molecules to malformations. Nature reviews. Neuroscience, 15(4), pp.217–32.

Sunter, N.J. et al., 2010. Role of Topoisomerase IIα in DNA Damage Response following IR and Etoposide. Journal of Nucleic Acids, 2010, pp.1–8.

Surova, O. & Zhivotovsky, B., 2013. Various modes of cell death induced by DNA damage. Oncogene, 32(33), pp.3789–3797.

Taylor, A.M.R. et al., 1975. Ataxia telangiectasia: a human mutation with abnormal radiation sensitivity. Nature, 258, pp.427–429.

Taylor, A.M.R. et al., 2015. Ataxia telangiectasia: More variation at clinical and cellular levels. Clinical Genetics, 87(3), pp.199–208.

Taylor, A.M.R., 1996. Leukemia and Lymphoma in Ataxia Telangiectasia. Blood, 87(2), pp.423–438.

Taylor, A.M.R., Groom, A. & Byrd, P.J., 2004. Ataxia-telangiectasia-like disorder (ATLD) - Its clinical presentation and molecular basis. DNA Repair, 3(8–9), pp.1219–1225.

Thai, T.H. & Kearney, J.F., 2005. Isoforms of terminal deoxynucleotidyltransferase: Developmental aspects and function. Advances in Immunology, 86, pp.113–136.

Thomas O. Crawford, 1998. Ataxia Telangiectasia. Seminars in Pediatric Neurology, 5(4), pp.287–294.

Thompson, L.H., 2012. Recognition, signaling, and repair of DNA double-strand breaks produced by ionizing radiation in mammalian cells: The molecular choreography. Mutation Research - Reviews in Mutation Research, 751(2), pp.158–246.

Uematsu, N. et al., 2007. Autophosphorylation of DNA-PKCS regulates its dynamics at DNA double-strand breaks. Journal of Cell Biology, 177(2), pp.219–229.

Ünal, E. et al., 2004. DNA damage response pathway uses histone modification to assemble a double-strand break-specific cohesin domain. Molecular Cell, 16(6), pp.991–1002.

Uziel, T. et al., 2003. Requirement of the MRN complex for ATP activation by DNA damage. The EMBO journal, 22(20).

van den Boom, J. et al., 2016. VCP/p97 Extracts Sterically Trapped Ku70/80 Rings from DNA in Double-Strand Break Repair. Molecular Cell, 64(1), pp.189–198.

Verhagen, M.M.M. et al., 2012. Neuropathology in classical and variant ataxia-telangiectasia. Neuropathology, 32(3), pp.234–244.

Vilenchik, M.M. & Knudson, A.G., 2003. Endogenous DNA double-strand breaks: production, fidelity of repair, and induction of cancer. Proceedings of the National Academy of Sciences, 100(22), pp.12871–12876.

Virgen-slane, R. et al., 2012. An RNA virus hijacks an incognito function of a DNA repair enzyme. , pp.1–6.

Ward, I.M. & Chen, J., 2001. Histone H2AX Is Phosphorylated in an ATR-dependent Manner in Response to Replicational Stress. Journal of Biological Chemistry, 276(51), pp.47759–47762.

Ward, J.F., 1988. DNA Damage Produced by Ionizing Radiation in Mammalian Cells: Identities, Mechanisms of Formation, and Reparability. Progress in nucleic acid research and molecular biology, 35, pp.95–125.

Weill, J.-C. & Reynaud, C.-A., 2008. DNA polymerases in adaptive immunity. Nature reviews. Immunology, 8(4), pp.302–312.

Williams, R.S., Williams, J.S. & Tainer, J.A., 2007. Mre11–Rad50–Nbs1 is a keystone complex connecting DNA repair machinery, double-strand break signaling, and the chromatin templateThis paper is one of a selection of papers published in this Special Issue, entitled 28th International West Coast Chromatin a. Biochemistry and Cell Biology, 85(4), pp.509–520.

Woodbine, L. et al., 2013. PRKDC mutations in a SCID patient with profound neurological abnormalities. Journal of Clinical Investigation, 123(7), pp.2969–2980.

Woodbine, L., Gennery, A.R. & Jeggo, P.A., 2014. The clinical impact of deficiency in DNA non-homologous end-joining. DNA Repair, 17, pp.9–20.

Xu, G. lan et al., 2008. TTRAP is a novel PML nuclear bodies-associated protein. Biochemical and Biophysical Research Communications, 375(3), pp.395–398.

Yamamoto, K. et al., 2012. Kinase-dead ATM protein causes genomic instability and early embryonic lethality in mice. The Journal of cell biology, 198(3), pp.305–313.

Yang, X. et al., 2000. DNA Topoisomerase IIα and Neural Development. Science, 287(5450), pp.131–134.

You, Z. et al., 2007. Rapid activation of ATM on DNA flanking double-strand breaks. Nature cell biology, 9(11), pp.1311–1318.

Zeng, Z. et al., 2011. TDP2/TTRAP is the major 5'-tyrosyl DNA phosphodiesterase activity in vertebrate cells and is critical for cellular resistance to topoisomerase II-induced DNA damage. The Journal of biological chemistry, 286(1), pp.403–409.

Zeng, Z. et al., 2012. TDP2 promotes repair of topoisomerase I-mediated DNA damage in the absence of TDP1. Nucleic Acids Research, 40(17), pp.8371–8380.

Zha, S. et al., 2010. ATM-deficient thymic lymphoma is associated with aberrant tcrd rearrangement and gene amplification. The Journal of experimental medicine, 207(7), pp.1369–1380.

Zhang, A. et al., 2006. A Protease Pathway for the Repair of Topoisomerase II-DNA Covalent Complexes. Journal of Biological Chemistry, 281(47), pp.35997–36003.

Zhang, J. qi et al., 2009. Cellular protein TTRAP interacts with HIV-1 integrase to facilitate viral integration. Biochemical and Biophysical Research Communications, 387(2), pp.256–260.

Zhang, M. & Swanson, P.C., 2008. V(D)J recombinase binding and cleavage of cryptic recombination signal sequences identified from lymphoid malignancies. Journal of Biological Chemistry, 283(11), pp.6717–6727.

Zheng, J., 2013. Oncogenic chromosomal translocations and human cancer. Oncology Reports, 30(5), pp.2011–2019.

Zhou, C.H., Xue, J.G. & Chen, J.Z., 2013. Overexpression of TTRAP inhibits cell growth and induces apoptosis in osteosarcoma cells. Biochemistry and Molecular Biology Reports, 46(2), pp.113–118.

VIII. APPENDIX

nature COMMUNICATIONS

ARTICLE

Received 20 Aug 2013 | Accepted 30 Jan 2014 | Published 27 Feb 2014

DOI: 10.1038/ncomms4347 OPEN

ATM specifically mediates repair of double-strand breaks with blocked DNA ends

Alejandro Álvarez-Quilón[1], Almudena Serrano-Benítez[1], Jenna Ariel Lieberman[1], Cristina Quintero[1], Daniel Sánchez-Gutiérrez[2], Luis M. Escudero[2] & Felipe Cortés-Ledesma[1]

Ataxia telangiectasia is caused by mutations in *ATM* and represents a paradigm for cancer predisposition and neurodegenerative syndromes linked to deficiencies in the DNA-damage response. The role of ATM as a key regulator of signalling following DNA double-strand breaks (DSBs) has been dissected in extraordinary detail, but the impact of this process on DSB repair still remains controversial. Here we develop novel genetic and molecular tools to modify the structure of DSB ends and demonstrate that ATM is indeed required for efficient and accurate DSB repair, preventing cell death and genome instability, but exclusively when the ends are irreversibly blocked. We therefore identify the nature of ATM involvement in DSB repair, presenting blocked DNA ends as a possible pathogenic trigger of ataxia telangiectasia and related disorders.

[1] Centro Andaluz de Biología Molecular y Medicina Regenerativa (CABIMER), CSIC-Universidad de Sevilla (Departamento de Genética), Sevilla 41092, Spain. [2] Instituto Biomedicina Sevilla (IBiS), Hospital Virgen del Rocío-CSIC-Universidad de Sevilla (Departamento de Biología Celular), Sevilla 41013, Spain. Correspondence and requests for materials should be addressed to F.C.-L. (email: felipe.cortes@cabimer.es).

Deficiencies in the DNA-damage response (DDR) are the cause of several human genetic syndromes[1]. Common hallmarks of these disorders include neurodegeneration and/or cancer predisposition, which are a probable consequence of deficient and inaccurate repair of DNA damage. Ataxia telangiectasia (A-T), a rare autosomal recessive syndrome that results from inactivation of the PIKK family Ser/Thr protein kinase ATM (A-T Mutated), is perhaps the paradigm for diseases of this type[2,3]. It is characterized by a symptomatology that includes progressive cerebellar ataxia, immunodeficiency, radiosensitivity, hypogonadism and increased cancer incidence (mainly leukaemia and lymphoma). Multiple functions have been assigned to ATM and its list of phosphorylation substrates is extensive[4]. Despite this versatility, its main function, or at least the best understood, is to trigger the initial phosphorylation wave of the DDR to double-strand breaks (DSBs). This fact, together with the exquisite radiosensitivity displayed by ATM-deficient cells and individuals and the symptomatological overlap of A-T with other break repair-defective human syndromes, strongly suggests a link between DSBs and pathology in A-T patients[3,5].

On the basis of all of this, one could anticipate that ATM would be essential, or at least important, for the repair of DSBs. Strikingly, this is not the case, as ATM loss does not result in obvious defects in the DSB repair rate. It has therefore been proposed that the radiosensitivity and chromosomal instability observed in ATM-deficient cells more likely arises from deficient checkpoint allowing cell cycle progression in the presence of damaged DNA[6]. However, there is a subset of DSBs, 10–20% depending on the DNA-damaging agent used[7,8], which do require ATM. The current understanding is that these DSBs correspond to damage occurring in heterochromatin, where ATM is required to open the chromatin structure, allowing access of the repair machinery[9]. Interestingly, in addition to this, ATM is involved in specialized DSB-repair mechanisms that are not heterochromatin associated, such as V(D)J, class-switching and meiotic recombination[10–12]. These processes are related to important aspects of A-T pathogenesis such as immunodeficiency, increased incidence of lymphoma and sterility. Fully understanding the nature of DSBs that specifically require ATM for repair could therefore provide important clues into disease pathogenesis.

DSBs can harbour different types of chemical moieties that differ from the canonical 5′ phosphate and 3′ hydroxyl at the ends[13]. Cells are therefore endowed with a wide variety of enzymatic activities that can 'unblock' DSBs preparing them for repair. However, under certain circumstances, such as the presence of complex or staggered lesions, these activities may be compromised or overwhelmed, resulting in breaks that are 'blocked,' in which case the only possibility to allow repair involves the action of nucleases to 'process' the ends by cleaving DNA sequence. It is therefore conceivable that clean and blocked DSBs can have different repair requirements and consequences. However, the study of how DNA-end complexity influences the DDR and repair has been traditionally impeded by the heterogeneity in the breaks induced by most DNA-damaging agents.

A particular source of DNA breaks is the abortive activity of DNA topoisomerase II (TOP2, α and β isoforms)[14], which are essential homodimeric enzymes that relax, unknot and/or decatenate DNA molecules[15]. The α isoform is specific to cycling cells, having essential functions during replication and chromosome condensation and segregation. In contrast, the TOP2β is the main TOP2 isoform in quiescent cells and acts mainly in transcription. Despite the important function of TOP2 in essential processes of chromosome metabolism, its mechanism of action can be dangerous, as it involves the passage of duplex DNA through a transient DSB created by the enzyme. This key intermediate of TOP2 activity (termed cleavage complex), in which two topoisomerase subunits are covalently linked to each 5′-terminus of a DSB via a phosphodiester bond between the active-site tyrosine and the 5′-phosphate, is normally very short-lived, because the topoisomerase rapidly religates the DSB once DNA strand passage through the gap has occurred. However, under certain circumstances, such as the presence of nearby DNA lesions, cleavage complexes can be stabilized and interfere with the transcription or replication machinery. If this is the case, trapped TOP2 is degraded, leading to the formation of irreversible DSBs with peptidic blockages at the 5′ ends of the DNA. This mechanism underlies the clinical efficacy of a widely used class of antitumour agents that 'poison' topoisomerase activity (for example, etoposide)[16], thereby prolonging the half-life of the intermediate and increasing the possibility of DSB formation[16].

Etoposide can therefore be used to generate DSBs homogeneously characterized by covalent peptide blockage of the 5′ ends. Tyrosyl DNA phosphodiesterase 2 (TDP2) is the only known enzyme in higher eukaryotes with the physiological capacity to unblock this type of DNA ends, converting them into 5′ phosphate/3′ hydroxyl ligatable termini[17–19]. This scenario offers a unique opportunity for the specific induction of clean and blocked DSBs (Fig. 1a). Following etoposide treatment, the majority of the induced DSBs will be efficiently unblocked by TDP2 in wild-type cells. However, when TDP2 is not present, the blockage will be irreversible and will necessarily require alternative nucleolytic processing to allow repair to proceed. This way, clean and blocked DSBs can be specifically induced by etoposide treatment of wild-type and TDP2-deficient cells, respectively.

In this study, we exploit this genetic tool to demonstrate that ATM functions specifically in the rejoining of blocked DSBs, in a manner that is independent of the chromatin status of the lesions.

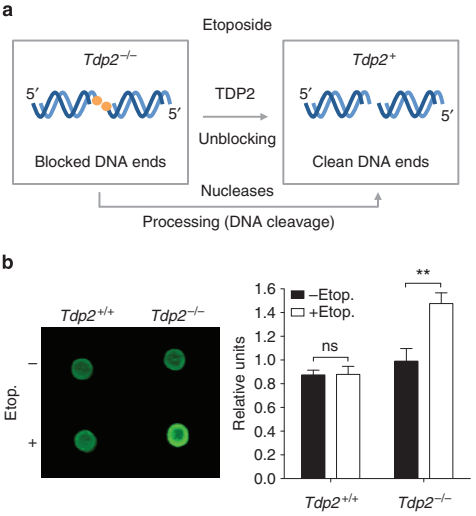

Figure 1 | Protein-blocked DSBs accumulate in *Tdp2*-deficient background upon TOP2 poison treatment. (**a**) Scheme of the strategy used to generate breaks with specific structure. (**b**) SLOPE assay performed in $Tdp2^{+/+}$ and $Tdp2^{-/-}$ confluency-arrested primary MEFs. Average ± s.e.m. of signal from three independent experiments and statistical significance by two-way ANOVA test with Bonferroni post-test is shown (*$P \leq 0.05$; **$P \leq 0.01$; ***$P \leq 0.001$).

We determine that this novel ATM-dependent repair pathway is particularly relevant for cell survival and the maintenance of genome stability upon induction of blocked DSBs. Finally, we confirm these results using a molecularly defined system and determine that ATM functions in promoting appropriate processing of blocked DSBs. These results put forwards DNA-end structure as a key factor determining ATM involvement during DSB repair, something that could have important implications on our understanding of A-T pathogenesis.

Results

Protein-blocked DSBs accumulate in the absence of TDP2. As mentioned above, we can use TOP2 poisons such as etoposide to induce DSBs that are homogeneous in structure. Furthermore, theoretically, we can modulate the ends of these DSBs by working in different genetic backgrounds (Fig. 1a): 3′-hydroxyl 5′-phosphate clean ends will be formed in cells containing TDP2 activity, while breaks with a peptide block on 5′ ends will accumulate in TDP2-deficient cells. To validate this experimental setup, we aimed at developing a methodology to specifically measure protein-blocked DSBs, which we have named SLOPE (Selective Labelling Of Protein-blocked Ends). It is based on a previously described assay that has been used to identify genomic regions of TOP2 cleavage[20]. Following isolation of genomic DNA with standard Proteinase K treatment and silica columns, tyrosine residues will remain covalently linked to DNA at the sites of TOP2-blocked DSBs. Biotin is then specifically conjugated to these residues, and finally, the amount of biotin conjugation is measured in dot blots, and used as a specific indicator of protein covalently linked to DNA. To specifically detect irreversible TOP2-blocked DSBs resulting from etoposide treatment, cells are incubated in the absence of the drug to allow cleavage complex reversal before DNA isolation. As can be seen in Fig. 1b, incubation of wild-type primary mouse embryonic fibroblasts (MEFs) with etoposide did not detectably change the amount of protein covalently linked to DNA compared with untreated samples, while a clear and significant increase was observed in $Tdp2^{-/-}$ cells. These results experimentally demonstrate that, upon etoposide treatment, protein-blocked DSBs accumulate in TDP2-deficient cells, validating our genetic approach for inducing DSBs with different structure.

ATM facilitates repair of TOP2-blocked but not clean DSBs. We decided to apply the experimental setup described above to analyse the impact of ATM loss on the repair of either clean or blocked DSBs. As an indicator of DSB repair, we followed the time course of Ser139-phosphorylated H2AX (γH2AX) foci disappearance in primary MEFs after etoposide treatment. Since TOP2 activity is subject to cell cycle variations[21,22], cells were confluency arrested to avoid discrepancies in DSB induction. In addition, this simplifies the interpretation of the results, as DSB repair during G0/G1 is limited to non-homologous end-joining[23]. We found that the absence of ATM caused a marked reduction in the intensity of etoposide-induced γH2AX foci (Supplementary Fig. 1a); this is not surprising given the key involvement of ATM in H2AX phosphorylation in response to DSBs. However, the number of γH2AX foci per cell was not affected, validating the use of this parameter as a DSB-scoring tool in our setup. In addition, consistent with identical DSB induction, cleavage complexes of TOP2β (the main source of TOP2 activity in quiescent cells[22]) were also accumulated at similar levels

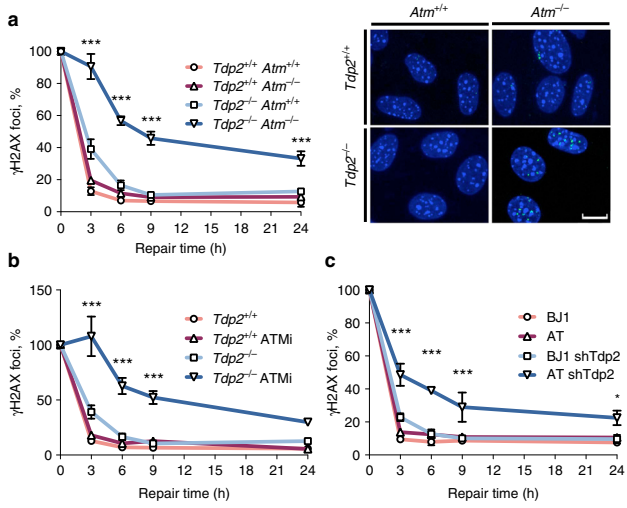

Figure 2 | ATM facilitates repair of TOP2-blocked DSBs. (**a**) Time course of γH2AX foci disappearance after 30 min 10 μM etoposide treatment and repair at different times following drug removal in $Tdp2^{+/+}$ $Atm^{+/+}$, $Tdp2^{+/+}$ $Atm^{-/-}$, $Tdp2^{-/-}$ $Atm^{+/+}$ and $Tdp2^{-/-}$ $Atm^{-/-}$ confluency-arrested primary MEFs. Representative images of γH2AX foci (green) and DAPI counterstain (blue) for the 24 h repair time point are shown. Scale bar, 10 μm. (**b**) As above, in $Tdp2^{+/+}$ and $Tdp2^{-/-}$ confluency-arrested primary MEFs with or without 10 μM ATM inhibitor (KU55933). (**c**) As above, in confluency-arrested primary fibroblast derived from A-T patients (AT) and wild-type controls (BJ1) depleted (shTDP2) or not for TDP2. In this case 20 μM etoposide treatment was applied. In all cases, average ± s.e.m. of the percentage of foci remaining from at least three independent experiments and the minimal statistical significance between cells deficient in both TDP2 and ATM and all other cells by two-way ANOVA test with Bonferroni post-test is shown (*$P \leq 0.05$; **$P \leq 0.01$; ***$P \leq 0.001$).

(Supplementary Fig. 1b), ruling out an effect of ATM in the generation and processing of TOP2 cleavage complexes.

As can be seen in Fig. 2a, the difference in repair rate between $Tdp2^{+/+}$ and $Tdp2^{-/-}$ cells was only minor at the etoposide dose used, which was chosen to avoid artefacts of overwhelming cellular repair capacity. Furthermore, the absence of ATM did not affect the rate of etoposide-induced DSB repair in a TDP2-proficient background. This is consistent with previous observations of a limited DSB-repair defect for IR- but not for etoposide-induced DSBs[8]. ATM, therefore, does not influence repair of clean DSBs. In contrast, a striking drop in the repair kinetics was observed in double $Tdp2^{-/-}$ $Atm^{-/-}$ cells, with ~40% of the breaks remaining unrepaired even 24 h after induction (Fig. 2a and Supplementary Fig. 2a), suggesting that ATM facilitates repair when DSBs are blocked. A single copy of the *Tdp2* gene was enough to eliminate blockages, as $Tdp2^{+/+}$ and $Tdp2^{+/-}$ cells were indistinguishable in ATM-deficient background (Supplementary Fig. 3). Importantly, the effect of ATM was specific to TOP2-mediated breaks, not being observed with ionizing radiation (Supplementary Fig. 2b), in which case, repair of ~10% of the breaks was ATM dependent, as previously described[7], but was not affected by TDP2 deficiency. It is worth noting that, as mentioned above, signalling in response to etoposide strongly relies on ATM (Supplementary Fig. 1a), but it only has an impact on repair efficiency in the absence of TDP2. Consistent with this independence between signalling and repair, ATM and downstream checkpoint proteins were equally activated in $Tdp2^{+/+}$ and $Tdp2^{-/-}$ cells (Supplementary Fig. 4).

To confirm the synergism between *Tdp2* and *Atm* in the repair of etoposide-induced damage during G0/G1, we repeated the analysis but using ATM chemical inhibition instead of deletion (Fig. 2b and Supplementary Fig. 2c). As expected, incubation with an ATM inhibitor affected repair of TOP2-induced DSBs in a $Tdp2^{-/-}$ but not in a $Tdp2^{+/+}$ background. This suggests that the role of ATM in the repair of blocked DSBs depends on its kinase activity and rules out artefacts caused by heterogeneity in MEFs. A similar DSB-repair defect was observed when confluency-arrested primary fibroblasts derived from A-T patients were depleted for TDP2 and not in neither wild type nor non-depleted controls (Fig. 2c and Supplementary Fig. 2d). In this case, however, the effect was milder, perhaps due to an incomplete knockdown of TDP2, as determined by residual 5′ tyrosyl DNA phosphodiesterase activity (Supplementary Fig. 2e). Finally, the effect was not restricted to quiescent cells and was also observed in cycling conditions, both in G1 and G2 stages (Supplementary Fig. 5). Overall, these results constitute strong evidence of an involvement of ATM in DSB repair and suggest that it is specifically linked to DSBs with blocked ends.

ATM function on blocked DSBs is heterochromatin independent. In the currently accepted model, ATM is specifically required to repair DSBs occurring at heterochromatic regions where it promotes decompaction and facilitates access of the repair machinery[24]. Since TOP2-mediated breakage requires on-going transcription[25], it should therefore rarely occur within heterochromatin. Thus, we reasoned that the function of ATM in opening chromatin would unlikely account for its involvement in the repair of TOP2-blocked DSBs. In any case, to rule out this possibility, we decided to analyse the location of etoposide-induced γH2AX foci with respect to heterochromatin in $Tdp2^{-/-}$ $Atm^{-/-}$ confluency-arrested primary MEFs, by three-dimensional confocal microscopy (Fig. 3). As expected, none of the γH2AX foci induced with etoposide colocalized with highly dense chromocenters and only 15.45% (34 out of 220 foci scored) were located at less than 0.4 μm (Fig. 3a), which we considered to be heterochromatin associated. In these same conditions, a significantly higher percentage of the breaks (~40%) required ATM activity for their repair (Fig. 2a), indicating that the chromatin status of a TOP2-blocked DSB is not a major determinant of ATM requirement for repair. Furthermore, the overall distribution of heterochromatin-associated foci was not significantly changed following 24 h of repair (Fig. 3b), with 81.92% of unrepaired foci (154 out of 188) being located within euchromatin (Fig. 3a). We conclude that the involvement of ATM in the repair of TOP2-blocked DSBs is largely independent of the reported role of this protein in facilitating repair at heterochromatin regions.

ATM function on blocked DSBs has consequences for the cell. The incapacity to properly repair a small number or even a single DSB can lead to cell death and/or genome rearrangements. It is therefore conceivable that the DSB-repair defect caused by ATM loss, although affecting a minor fraction of the lesions, underlies the profound radiosensitivity and chromosomal instability observed in A-T patients and cells. We exploited $Tdp2^{-/-}$ $Atm^{-/-}$ cells to directly address the cellular implications of ATM-linked DSB-repair deficiencies, first by monitoring cell survival in response to etoposide treatment (Fig. 4a). *Atm* deletion in transformed MEFs had a negligible effect on etoposide sensitivity in a wild-type ($Tdp2^{+/+}$) background. In contrast, sensitivity of $Tdp2^{-/-}$ cells, which was mild at this low etoposide doses, was significantly increased by ATM loss, correlating with the observed DSB-repair defect (Fig. 2a). An even larger effect was observed if ATM inhibition was used instead of deletion (Fig. 4b), confirming the requirement of ATM kinase activity and ruling out differences being caused by heterogeneity intrinsic to the MEFs or the cellular transformation process. Furthermore, the difference observed between deletion and chemical inhibition suggests a possible negative effect of inactive ATM and is consistent with recently observed enhanced phenotypes of catalytically dead ATM[26,27].

Furthermore, we addressed the impact of ATM loss on genome integrity following etoposide treatment in $Tdp2^{+/+}$ and $Tdp2^{-/-}$ transformed MEFs. First, we monitored micronuclei formation, which arise from the mis-segregation of chromosomes or acentric chromosomal fragments, and is a well-established indicator of genome instability. To restrict our analysis to micronuclei arising during the cell cycle in which treatment was applied, cytokinesis was blocked with cytochalasin B and only binucleated cells were scored (Fig. 5a). Independent deletion of either *Atm* or *Tdp2* caused an increase in etoposide-induced micronuclei. Interestingly, however, the levels were further increased when both genes were simultaneously deleted, doubling the frequency observed in either single mutant. It is worth noting that the frequency observed corresponds to extremely high levels of instability, with many of the cells displaying multiple micronuclei, a qualitative difference compared with single mutants. To confirm these results, we scored chromosomal aberrations in metaphase spreads (Fig. 5b). Following etoposide treatment, $Tdp2^{-/-}$ $Atm^{-/-}$ cells displayed a marked increase in the number of chromosomal aberrations observed. On average, these cells showed a striking 15% aberrant chromosomes, which represent a 7.5-fold and 3-fold increase when compared with single $Tdp2^{-/-}$ and $Atm^{-/-}$ mutants, respectively. A wide variety of aberration types was observed, including breaks, radial chromosomes and fusions. Overall, these results demonstrate that ATM-mediated repair promotes cell survival and the maintenance of genome integrity in response to blocked DSBs, presenting this particular structure as a possible molecular trigger of important A-T symptoms. One must bear in

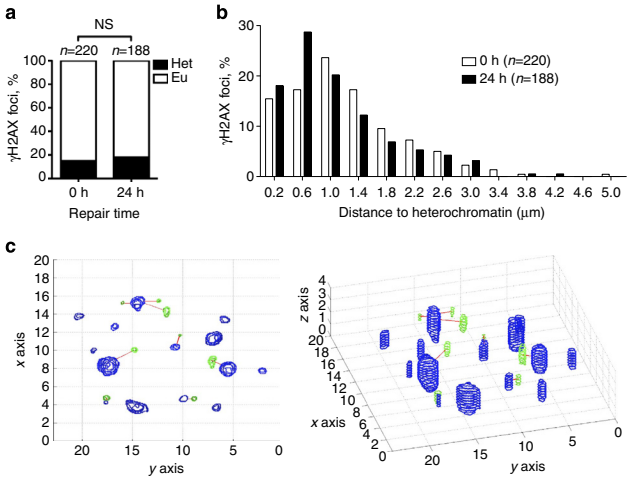

Figure 3 | Unrepaired TOP2-blocked DSBs are not associated with heterochromatin. Confluency-arrested *Atm*$^{-/-}$ *Tdp2*$^{-/-}$ primary MEFs were treated as described in Fig. 1. (**a**) Percentage of γH2AX foci that are located within heterochromatin (Het) or euchromatin (Eu) following 0 and 24 h repair after etoposide treatment. A cutoff distance of 0.4 μM from the centroid of each focus to the nearest euchromatin/heterochromatin boundary was applied. Statistical significance by Chi Square test is indicated. (**b**) Distribution of distances between γH2AX foci and heterochromatin as determined above. Bins of 0.4 μm centred on the indicated distance were used for representation. (**c**) Example of the automatic calculation of distances between γH2AX foci (green) and densely DAPI-stained chromocenters (blue) used for the data shown above. Both a z-stack projection (left) and a 3D reconstitution (right) are shown.

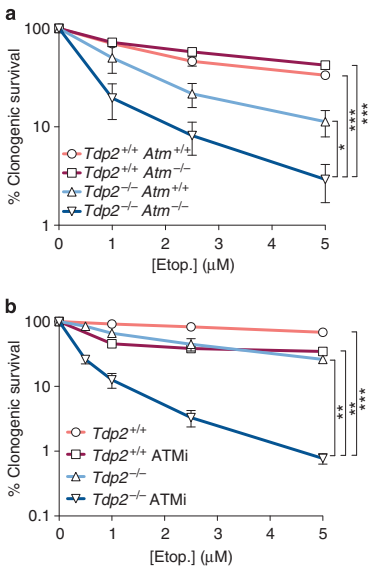

Figure 4 | ATM promotes survival upon induction of blocked DSBs. (**a**) Clonogenic survival of the indicated transformed MEFs following acute treatment with the indicated concentrations of etoposide. Average ± s.e.m. of at least three independent experiments and statistical significance at the highest indicated dose by one-way ANOVA with Bonferroni post-test are shown (*$P \leqslant 0.05$; **$P \leqslant 0.01$; ***$P \leqslant 0.001$). (**b**) As above, with or without incubation with 10 μM ATM inhibitor (KU55933).

mind, however, that the cell death and genome instability phenotypes may not be uniquely caused by the blocked DSB-repair defect, but by its combination with a defective checkpoint that allows cell cycle progression in the presence of DNA lesions.

ATM function on blocked DSBs prevents loss of DNA sequence. TOP2-blocked DSBs are only one type of many possible blockages occurring *in vivo*. We therefore aimed at confirming the involvement of ATM in the repair of blocked DSBs using a different, TOP2-independent, system in which the structure of DNA ends could be molecularly controlled. We started by searching for a 5′ modification that could block DNA ends *in vitro*. We found that a commercially available 5′-biotin modification was not removed from duplex oligonucleotides *in vitro* by HEK293T cellular extracts, while clear a 5′ tyrosyl DNA phosphodiesterase activity was observed under the same conditions (Supplementary Fig. 6a,b). We decided to use this modification to block the ends of the pEGFP-Pem1 system, which uses reconstitution of GFP expression to measure recircularization of a linear plasmid following transfection into mammalian cells[28] (Fig. 4a). Using PCR-mediated amplification with primers with different 5′ end structure, we were able to generate DNA substrates that harboured either clean 5′-phosphates or blocked 5′-biotins at their ends, something that was confirmed by streptavidin-mediated pull-down (Supplementary Fig. 3c). As can be seen in Fig. 6b, repair of pEGFP-Pem1 plasmids containing clean 5′-phosphate ends was not significantly affected by incubation of HEK293T cells with an ATM inhibitor, as measured by either the percentage of GFP-expressing cells or the total accumulated GFP fluorescence. In contrast, repair of 5′-biotin containing plasmids was significantly decreased by ATM inhibition, regardless of the quantification method used. As an additional control, we found that ATM was

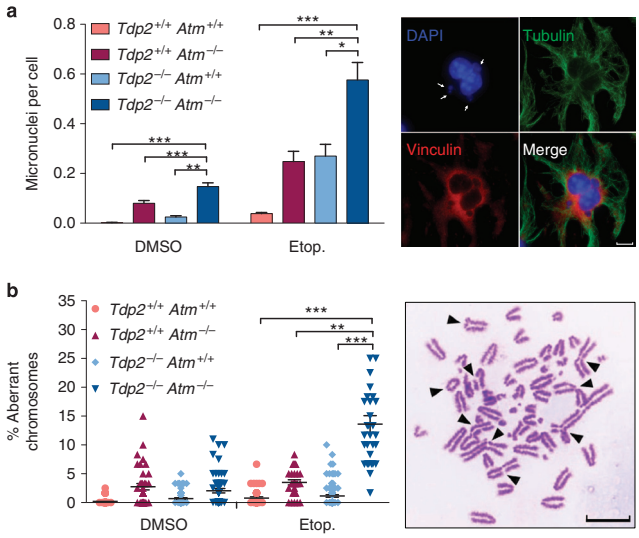

Figure 5 | ATM promotes the maintenance of genome integrity upon induction of blocked DSBs. (**a**) Micronuclei were scored in the indicated binucleated transformed MEFs following acute treatment with 2.5 μM etoposide. Histogram bars (left) represent the average ± s.e.m. of $n \geq 600$ cells from three independent experiments. Statistical significance by one-way ANOVA with Bonferroni post-test is indicated (*$P \leq 0.05$; **$P \leq 0.01$; ***$P \leq 0.001$). Representative image (right) of a treated *Tpd2*$^{-/-}$ *Atm*$^{-/-}$ cell containing multiple micronuclei is shown. Scale bar, 7.5 μm. (**b**) Chromosomal aberrations (both break and exchange type) were scored following acute treatment with 2.5 μM etoposide. Plot (left) shows the number of aberrations per 100 chromosomes from individual metaphase spreads obtained in at least 6 independent experiments. Average ± s.e.m. and statistical significance by Kruskal-Wallis test with Dunn's post-test is indicated (*$P \leq 0.05$; **$P \leq 0.01$; ***$P \leq 0.001$). Representative image (right) of a *Tpd2*$^{-/-}$ *Atm* $^{-/-}$ metaphase containing multiple chromosomal aberrations is shown. Scale bar, 10 μm.

not required to repair a modification such as 5′ hydroxyl that should not result in end blockage due to the existence of cellular machinery to solve the problem (PNKP) (Supplementary Fig. 6d). Therefore, by using a molecularly defined system, we confirm that ATM specifically facilitates repair of DSBs that are blocked.

The system also allows partial loss of sequence at the repair junction thanks to the Pem1 intron (see Fig. 6a). Thus, not only the quantity, but also the quality of repair can be monitored, something that can provide insights into the mechanisms involved. For this purpose, a minimum of 46 individual events for each condition were cloned in bacteria and subjected to restriction analysis to determine the accuracy of the repair process (Supplementary Fig. 7). Interestingly, ATM inhibitors caused a qualitative change in repair of the 5′-biotin but not the 5′-phosphate substrates, with a marked decrease (from 20% to 5%) in the percentage of repair events not harbouring detectable loss of sequence (Fig. 6c). However, in the clones showing DNA loss, the average size of this deleted sequence was unchanged by ATM inhibition (Fig. 6d). This demonstrates that ATM prevents excessive sequence loss from DNA ends, which is indicative of its involvement in blocked DSB end processing.

Discussion

Our study demonstrates that ATM is specifically required for the repair of blocked DSBs. With these results in mind, it is tempting to speculate that the observed existence of two subpopulations of DSBs, according to their ATM dependency or independency for repair[8], to some extent might be based on the structural heterogeneity in the ends induced by DNA-damaging agents. Thus, ATM would not impact in the repair of DSBs with 3′-hydroxyl 5′-phosphate ligatable ends, or those that can be converted into these structures by direct unblocking, while it would greatly facilitate rejoining of DSBs with ends that are blocked and require processing.

In addition, we observe that the role of ATM in blocked DSB repair is independent of the chromatin status of the broken DNA, in apparent contradiction with previous observations of a specific role of ATM in the repair of DSBs occurring in heterochromatin[24]. We understand, however, that blocked end and heterochromatin models for ATM involvement in DSB repair are not conflicting, and it is therefore possible to unify both observations if one thinks that ATM is specifically required in conditions in which repair is suboptimal, regardless of the particular molecular reason. Alternatively, it is also possible that heterochromatin, due to its densely packed structure, is more prone to suffer blocked damage, such as clustered DNA lesions and/or DNA-protein crosslinks, than more open regions. It is worth noting that progressive cerebellar ataxia, which is perhaps the most enigmatic (and also debilitating) symptom of A-T, could hardly be explained based on a heterochromatin hypothesis, since the clearest target population in the cerebellum, Purkinje cells, possess a mostly euchromatic nucleus[29]. Our findings change this picture, as blocked DSBs could also occur in Purkinje cells, and could therefore potentially contribute to this aspect of pathology.

We would like to clarify that TOP2-mediated DSBs, although successfully used as a tool in this study, may constitute only one particular type of many possible physiological blockages requiring ATM *in vivo*, and which could, altogether, contribute to A-T pathogenesis. In this sense, ATM has already been

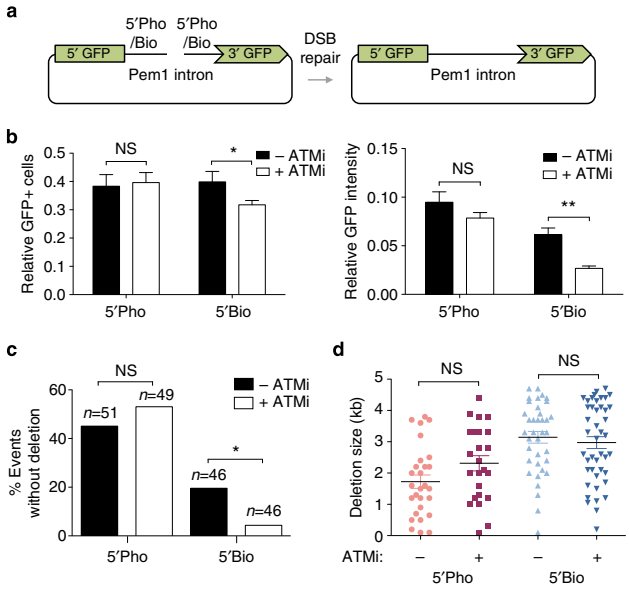

Figure 6 | ATM facilitates repair of biotin-blocked DSBs. (**a**) Scheme of the modified pEGFP-Pem1 system harbouring 5′-phosphate or 5′-biotin ends (left) and the expected repair product (right). (**b**) HEK293T cells were transfected in the presence or absence of 10 μM ATM inhibitor (KU55933) with the substrates described above, and analysed by FACS for GFP-positive cells (left) and average GFP intensity (right). In both cases, data are relative to transfection with a control pEGFP-Pem1 circular plasmid. Average ± s.e.m. of four independent experiments and statistical significance by two-way ANOVA with Bonferroni post-test are shown (*$P \leq 0.05$; **$P \leq 0.01$; ***$P \leq 0.001$). (**c**) Percentage of plasmid-repair events not associated with detectable sequence loss. Statistical significance by Chi Square test is shown (*$P \leq 0.05$; **$P \leq 0.01$; ***$P \leq 0.001$). (**d**) Deletion size in plasmid repair events. Substrates as described above. Average ± s.e.m. and statistical significance by Kruskal-Wallis test with Dunn's post-test is indicated.

directly implicated in two examples of blocked DSB repair with consequences for A-T symptomatology. First, during V(D)J recombination induced by the RAG endonucleases, ATM promotes the stability of coding ends, which are hairpin-blocked, but not of signal ends, which are clean[30]. This deficit likely contributes to immunodeficiency and the development of lymphoid malignancies in A-T[31]. Second, meiotic recombination, which involves the repair of DSBs covalently blocked by the SPO11 protein, is severely compromised in the absence of ATM and is likely the cause of sterility in A-T[10,11]. Our results put forward end blockage as a possible molecular explanation for the particular sensitivity of these systems to ATM loss. Finally, it is worth noting that the extreme etoposide sensitivity of double $Tdp2^{-/-}$ $Atm^{-/-}$ cells opens the door for the use of TDP2 inhibitors, which are currently under development, in sporadic ATM-deficient cancers[32–34].

We envision mainly two complementary manners in which ATM can regulate processing of blocked DSBs (Fig. 7). First, it can promote nucleolytic activity to eliminate the blockage through the action of nucleases such as the MRN complex, CtIP and/or Artemis[8,35,36], some of which have already been reported to affect cellular response to etoposide[37,38]. Second, it can restrict excessive nucleolytic degradation of DNA ends[39]. This can actually operate by a direct inhibitory action on these same nucleases[40] or others such as EXO1[41], and/or by promoting modifications at the DSB, such as for example γH2AX, which can protect from nucleolytic action[42]. This dual impact of ATM on DSB ends, exerted through its wide range of phosphorylation targets, makes it an ideal candidate to orchestrate blocked DSB processing, so it is restricted to the minimal resection necessary to allow rejoining.

In summary, we demonstrate that ATM does indeed function in DSB repair, but specifically to limit the potentially detrimental consequences of blocked DNA ends. If not properly dealt with, these lesions can impact cell survival and genome integrity, which can contribute to the development of A-T symptomatology. Determining the identity of physiologically occurring blockages and their specific influence on pathogenesis should therefore attract future efforts to unravel the aetiology of this devastating disease.

Methods

Cells and cell culture. Primary MEFs were isolated from crosses between $Tdp2^{-/-}$ and $Atm^{-/-}$ mice[19,43] at day 13 p.c. and cultured at 37 °C, 5% CO_2, 3% O_2 in Dubelcco's Modified Eagle's Medium (DMEM) supplemented with penicillin, streptomycin, 15% FCS and non-essential amino acids. All experiments were carried out between P1 and P5. MEFs were transformed by retroviral delivery of T121, a fragment of the SV40 large T antigen that antagonizes the three Rb family members but not p53 (ref. 19). Transformed MEFs and HEK293T cells were maintained at 37 °C, 5% CO_2 in DMEM supplemented with penicillin, streptomycin and 10% FCS. A-T (Coriell's Repository GM05823D) and BJ1 primary fibroblasts were cultured at 37 °C, 5% CO_2, in DMEM supplemented with penicillin, streptomycin and 15% FCS.

Selective labelling of protein-blocked DNA ends. The selective labelling of protein-blocked DNA ends (SLOPE) assay is a modification of selective labelling of TOP2 cleavage sites (SLOT) protocol[20]. Cells were treated 30 min with 100 μM etoposide or vehicle (DMSO), and 30′ after drug removal (to allow reversal of

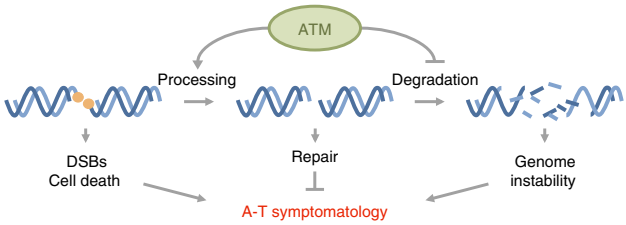

Figure 7 | Model for ATM involvement in blocked DSB repair. ATM promotes processing of blocked DSBs and inhibits excessive degradation. This promotes efficient and accurate repair, preventing the accumulation of unrepaired DSBs, cell death and genome instability, which can trigger the development of A-T symptomatology.

cleavage complexes) genomic DNA was extracted with the Qiagen Blood and Tissue Kit, which includes proteinase K treatment. Tyrosine residues that remain covalently linked to DNA were labelled with biotin using EDC and amine-PEG3-biotin (Thermo Scientific). DNA was precipitated to eliminate unreacted amine-PEG3-biotin and resuspended in TE buffer. Five hundred nanograms of DNA were dotted on a Hybond-H^+ (Amersham Bioscience) membrane and cross-linked with 70,000 µJ cm^{-2} UV. The membrane was blocked with Odyssey blocking buffer (LI-COR Biosciences) with 1% SDS, incubated with IRDye Streptavidin 800CW, 1/10,000 (LI-COR Biosciences) in the same buffer, washed (three times in TBS-0.1% Tween20) and allowed to dry. Dots were analysed and quantified in Odyssey CLx with ImageStudio Odyssey CLx Software. The results are related to an internal control of the same labelling protocol performed on plasmid DNA.

Immunofluorescence. Cells were grown on coverslips for 7 days until confluency-arrested, treated as indicated and fixed 10 min in ice-cold methanol or 4% PFA-PBS. Cells were then permeabilized (2 min in PBS-0.2% Triton X-100), blocked (30 min in PBS-5% BSA) and incubated with the required primary antibodies (1–3 h in PBS-1% BSA). Cells were then washed (three times in PBS-0.1% Tween 20), incubated for 30 min with the corresponding AlexaFluor-conjugated secondary antibodies (1/1,000 dilution in 1% BSA-PBS) and washed again as described above. Finally, they were counterstained with DAPI (Sigma) and mounted in Vectashield (Vector Labs). γH2AX foci were manually counted (double-blind) in 40 cells from each experimental condition. Primary antibodies were used at the indicated dilution: γH2AX (Millipore, 05-636), 1/1,000; α-Tubulin (Abcam, ab18251), 1/2,000; Vinculin hVIN-1 (Sigma, V9131) 1/2,000.

TOPIIβ cleavage complexes. Confluency arrested primary MEFs were treated 1 h with 100 µM etoposide or vehicle (DMSO), immediately lysed in 1% Sarkosyl (Sigma) and processed according to the *in vivo* complex of enzyme (ICE) assay[44]. Samples were centrifuged at 57,000 r.p.m. for 20 h at 25 °C using 3.3 ml 13 × 33 mm polyallomer Optiseal tubes (Beckman Coulter) in a TLN100 rotor (Beckman Coulter). 2.5 µg of precipitated DNA was transferred onto Hybond ECL membranes (GE Healthcare) using a Bio-Dot SF Microfiltration Apparatus (Biorad). Membranes were blocked 1 h with Odyssey Blocking Buffer (LI-COR Biosciences), incubated with 1/1,000 anti-TOP2β antibody (Santa Cruz, sc-13059), in Odyssey Blocking Buffer-0.1% Tween20, washed (three times with TBS-0.1% Tween20), incubated with 1/15,000 IRDye 800CW Goat anti-Rabbit IgG (LI-COR) and finally washed (three times with TBS-0.1%-Tween20 and three times with TBS). Once the membranes were dry, slots were analysed and quantified in Odyssey CLx using ImageStudio Odyssey CLx Software.

TDP2 knockdown. Lentiviral vectors for TDP2 knockdown (pLKO.1-puro-Tdp2-2; SIGMA, clone TRCN0000003072) and empty control (pLKO.1-puro) were generated in HEK293T transfected with the packaging vectors pCMVDR8.91 and pMDG. A-T and BJ1 primary fibroblasts were infected with pLKO.1-puro-Tdp2-2 or pLKO.1-puro lentiviruses in 100 mm dishes, incubated for 3 days and then placed under puromycin selection (1 µg ml^{-1}) for 7 days.

5′ activity *in vitro*. For the preparation of labelled double-stranded 5′-phospho-tyrosyl, 5′-phosphobiotin and 5′-phosphate substrates, 5′- TAT ACT TCT CTT TCC AGG GCT ATG T-3′ oligonucleotides with tyrosine (Midland Certified Reagents), biotin (Sigma) or phosphate (Sigma) modifications at the 5′ end were annealed to 5′-AGA CAT AGC CCT GGA AAG AGA AGT ATA-3′ (Sigma) and labelled in the presence of [α-32P]-dCTP, ddTTP and Klenow polymerase. Cell extracts were prepared by mild sonication in Lysis Buffer (40 mM Tris–HCl, pH 7.5, 100 mM NaCl, 0.1% Tween-20, 1 mM DTT) supplemented with 1 mM PMSF and protease inhibitor cocktail (Sigma) followed by clarification 10 min 16,500 *g* 4 °C. Protein concentration was measured with Bradford reagent (Sigma). 5′ reactions contained 50 nM substrate, 80 µM competitor single-stranded oligonucleotide and the indicated amount of cellular extract in a total volume of 6 µl Reaction Buffer (50 mM Tris–Cl, pH 7.5, 50 mM KCl, 1 mM $MgCl_2$, 1 mM DTT, 100 µg ml^{-1} BSA). Reactions were stopped by the addition of 3 µl 3 × Formamide Loading Buffer and 5 min 95 °C incubation. Samples were resolved by denaturing polyacrylamide gel electrophoresis and analysed by phosphorimaging in a Fujifilm FLA5100 device (GE Healthcare).

γH2AX foci in specific cell cycle stages. Immunofluorescence was performed as described above with the following modifications. Fixation was performed 10 min at room temperature in 4% PFA-PBS. Cyclin A staining was used to distinguish G1 and S/G2 cells. To exclude replicating cells, 5-ethynyl-2′-deoxyuridine (EdU, Invitrogen) was added throughout treatment and repair at a final concentration of 10 µM. Click chemistry reaction was performed by incubating (30 min r.t.) with 1 µM AlexaFluor 647-conjugated azide (Invitrogen) in reaction cocktail (100 mM TrisHCl pH 8.5, 1 mM $CuSO_4$, 100 mM ascorbic acid). γH2AX foci were manually counted (double-blind) in 40 G1 cells (Cyclin A negative) or 20 G2 cells (Cyclin A positive EdU negative) from each experimental condition. Antibodies were used at the indicated dilution: γH2AX (Millipore, 05-636), 1/1,000; Cyclin A (Santa Cruz, sc-751), 1/200.

Western blot. Confluency-arrested primary MEFs were resuspended on ice using a cell scraper 30 min after treatment with the indicated concentration of etoposide. They were lysed in Laemli buffer and boiled at 96 °C for 5 min. Protein concentration was measured by Pierce 660 nm Protein Assay with Ionic detergent compatibility reagent (Thermo Scientific). Thirty micrograms of sample was run in NuPAGE Tris-Acetate Mini gels 3–8% (Novex) and transferred to Immobilon-FL Transfer Membranes (Millipore). Membranes were blocked in Odyssey Blocking Buffer (LI-COR Biosciences) incubated with primary antibodies in Odyssey Blocking Buffer-0.1% Tween20 and washed (three times in TBS-0.1% Tween20). They were then incubated with the corresponding IRDye-conjugated secondary antibodies in Odyssey Blocking Buffer-0.02% to 0.1% Tween20 and washed (three times in TBS-0.1% Tween20 and 1 × in TBS buffer). Membranes were analyzed in Odyssey CLx with ImageStudio Odyssey CLx Software. Primary antibodies were used at the indicated dilution: ATM (Sigma, MAT3-4G10/8), 1/1,000; ATM pS1981 (Cell Signaling, #4526), 1/1,000; p-CHK2 Thr68 (Cell Signaling, #2661), 1/1,000; p-p53 Ser15 (Cell Signaling, #9284), 1/1,000; p-CHK1 Ser345 (Cell Signaling, #2341), 1/1,000; α-tubulin (Sigma, T9026), 1/50,000.

Image processing. An in-house MATLAB R2012a-based application was designed to segment nuclei images. For each nucleus, a series of Z-sections (0.21 µm step) were obtained using a Leica TCS-SP5 confocal microscope with a HCX PL APO 63x/1.40λBL objective. These series were segmented to obtain the number, position, intensity and volume values of γH2AX foci and heterochromatin (G and B components of the RGB image, respectively). The segmentation from the different sections was integrated to reconstitute the 3D information of each entire nucleus. Using this reconstitution, the distance between each focus and the nearest euchromatin/heterochromatin boundary in the 3D space was determined.

Clonogenic survival assays. Survival assays were carried out seeding 2,000 cells in 100 mm dishes, in duplicate for each experimental condition. After 12 h, cells were preincubated with 10 µM ATM inhibitor KU55933 (Tocris) or vehicle for 1 h. The indicated concentration of etoposide was added and cells were incubated for additional 3 h. Following one wash with PBS, fresh medium was added and cells were incubated for 10–14 days. Dishes were fixed and stained for colony scoring in Crystal Violet solution (0.5% Crystal violet in 20% ethanol). The surviving fraction at each dose was calculated by dividing the average number of visible colonies in treated versus untreated dishes.

Cytogenetic analysis. Micronuclei were analysed in transformed MEFs previously seeded onto coverslips. Following treatment, cytochalasin B (Sigma) was added at 4 μg ml^{-1}. Twenty-two hours post treatment, cells were fixed and subjected to DAPI staining as described above. Only binucleated cells were scored, which was confirmed by visualization of the cytoplasm with Tubulin and Vinculin immunofluorescence (performed as described above). Chromosomal aberrations were scored in Giemsa-stained metaphase spreads. Following treatment, recovery in fresh medium was allowed for 2 h, and demecolcine (Sigma) was added at a final concentration of 0.2 μg ml^{-1}. Four hours later, cells were collected by trypsinization, subjected to hypotonic shock for 1 h at 37 °C in 0.3 M sodium citrate, and fixed in 3:1 methanol:acetic acid solution. Cells were dropped onto acetic acid-humidified slides and stained 20 min in Giemsa-modified (Sigma) solution (5% v/v in H_2O).

Validation of pEGF-Pem1 substrates. The structure of 5′ DNA ends was analysed by streptavidin-mediated precipitation. Dynabeads (10 μg) M-270 Streptavidin magnetic beads (Invitrogen) were prewashed (3 × in 5 mM Tris–HCl pH 7.5, 0.5 mM EDTA in the presence of 1 M NaCl) and incubated with 100 ng of purified PCR products in the same buffer for 1 h. Beads were then washed 4 × in the same buffer, gradually decreasing NaCl concentration to 0. Finally, DNA was eluted by 2 h incubation with *Bgl*II restriction enzyme (New England Biolabs) in the recommended buffer. Input, unbound and bound DNA was analysed by agarose gel electrophoresis.

Plasmid-circularization assays. Substrates were generated by PCR-mediated amplification of plasmid pEGFP-Pem1-Ad2[28] with primers 5′-AAT TCT TCT CTT TCC AGG GCT AT GT-3′ and 5′- AAT TCA TCC CCA GAA ATG TAA CTT G-3′ harbouring phosphate or biotin moieties at 5′ ends (Sigma). DNA of the correct size was then gel-purified and transfected into HEK293T cells, pretreated for 30 min with 10 μM ATM inhibitor KU55933 (Tocris) or vehicle. Sixteen hours later, cells were analysed by FACS. Individual repair events were cloned in *E. coli* by plasmid rescue from transfected cells and analysed by digestion with *Dra*I.

Statistical analysis. In all cases the indicated statistical test was applied using Prism 5 package (Graphpad).

References

1. McKinnon, P. J. & Caldecott, K. W. DNA strand break repair and human genetic disease. *Ann. Rev. Genomics. Hum. Genet.* **8,** 37–55 (2007).
2. Lavin, M. F. Ataxia-telangiectasia: from a rare disorder to a paradigm for cell signalling and cancer. *Nat. Rev. Mol. Cell. Biol.* **9,** 759–769 (2008).
3. McKinnon, P. J. ATM and the molecular pathogenesis of ataxia telangiectasia. *Ann. Rev. Pathol.* **7,** 303–321 (2012).
4. Shiloh, Y. & Ziv, Y. The ATM protein kinase: regulating the cellular response to genotoxic stress, and more. *Nat. Rev. Mol. Cell. Biol.* **14,** 197–210 (2013).
5. Reynolds, J. J. & Stewart, G. S. A nervous predisposition to unrepaired DNA double strand breaks. *DNA Repair (Amst)* **12,** 588–599 (2013).
6. Löbrich, M. & Jeggo, P. A. The two edges of the ATM sword: co-operation between repair and checkpoint functions. *Radiother. Oncol.* **76,** 112–118 (2005).
7. Kühne, M. *et al.* A double-strand break repair defect in ATM-deficient cells contributes to radiosensitivity. *Cancer Res.* **64,** 500–508 (2004).
8. Riballo, E. *et al.* A pathway of double-strand break rejoining dependent upon ATM, Artemis, and proteins locating to gamma-H2AX foci. *Mol. Cell.* **16,** 715–724 (2004).
9. Goodarzi, A. A., Jeggo, P. & Löbrich, M. The influence of heterochromatin on DNA double strand break repair: Getting the strong, silent type to relax. *DNA Repair (Amst)* **9,** 1273–1282 (2010).
10. Xu, Y. *et al.* Targeted disruption of ATM leads to growth retardation, chromosomal fragmentation during meiosis, immune defects, and thymic lymphoma. *Genes Dev.* **10,** 2411–2422 (1996).
11. Barlow, C. *et al.* Partial rescue of the prophase I defects of Atm-deficient mice by p53 and p21 null alleles. *Nat. Genet.* **17,** 462–466 (1997).
12. Bednarski, J. J. & Sleckman, B. P. Lymphocyte development: integration of DNA damage response signaling. *Adv. Immunol.* **116,** 175–204 (2012).
13. Caldecott, K. W. Single-strand break repair and genetic disease. *Nat. Rev. Genet.* **9,** 619–631 (2008).
14. Deweese, J. E. & Osheroff, N. The DNA cleavage reaction of topoisomerase II: wolf in sheep's clothing. *Nucleic Acids Res.* **37,** 738–748 (2009).
15. Nitiss, J. L. DNA topoisomerase II and its growing repertoire of biological functions. *Nat. Rev. Cancer* **9,** 327–337 (2009).
16. Nitiss, J. L. & Targeting, D. N. A. topoisomerase II in cancer chemotherapy. *Nat. Rev. Cancer* **9,** 338–350 (2009).
17. Cortes Ledesma, F., Khamisy El, S. F., Zuma, M. C., Osborn, K. & Caldecott, K. W. A human 5′-tyrosyl DNA phosphodiesterase that repairs topoisomerase-mediated DNA damage. *Nature* **461,** 674–678 (2009).
18. Zeng, Z., Cortes Ledesma, F., Khamisy El, S. F. & Caldecott, K. W. TDP2/TTRAP is the major 5′-tyrosyl DNA phosphodiesterase activity in vertebrate cells and is critical for cellular resistance to topoisomerase II-induced DNA damage. *J. Biol. Chem.* **286,** 403–409 (2011).
19. Gómez-Herreros, F. *et al.* TDP2-dependent non-homologous end-joining protects against topoisomerase II-induced dna breaks and genome instability in cells and *in vivo*. *PLoS Genet.* **9,** e1003226 (2013).
20. Haffner, M. C. *et al.* Androgen-induced TOP2B-mediated double-strand breaks and prostate cancer gene rearrangements. *Nat. Genet.* **42,** 668–675 (2010).
21. Olive, P. L. & Banáth, J. P. Detection of DNA double-strand breaks through the cell cycle after exposure to X-rays, bleomycin, etoposide and 125IdUrd. *Int. J. Radiat. Biol.* **64,** 349–358 (1993).
22. Woessner, R. D., Mattern, M. R., Mirabelli, C. K., Johnson, R. K. & Drake, F. H. Proliferation- and cell cycle-dependent differences in expression of the 170 kilodalton and 180 kilodalton forms of topoisomerase II in NIH-3T3 cells. *Cell Growth Differ.* **2,** 209–214 (1991).
23. Rothkamm, K., Krüger, I., Thompson, L. H. & Löbrich, M. Pathways of DNA double-strand break repair during the mammalian cell cycle. *Mol. Cell. Biol.* **23,** 5706–5715 (2003).
24. Goodarzi, A. A. *et al.* ATM signaling facilitates repair of DNA double-strand breaks associated with heterochromatin. *Mol. Cell.* **31,** 167–177 (2008).
25. Zhang, A. *et al.* A protease pathway for the repair of topoisomerase II-DNA covalent complexes. *J. Biol. Chem.* **281,** 35997–36003 (2006).
26. Daniel, J. A. *et al.* Loss of ATM kinase activity leads to embryonic lethality in mice. *J. Cell Biol.* **198,** 295–304 (2012).
27. Yamamoto, K. *et al.* Kinase-dead ATM protein causes genomic instability and early embryonic lethality in mice. *J. Cell Biol.* **198,** 305–313 (2012).
28. Seluanov, A., Mittelman, D., Pereira-Smith, O. M., Wilson, J. H. & Gorbunova, V. DNA end joining becomes less efficient and more error-prone during cellular senescence. *Proc. Natl. Acad. Sci. USA* **101,** 7624–7629 (2004).
29. Kriaucionis, S. & Heintz, N. The nuclear DNA base 5-hydroxymethylcytosine is present in purkinje neurons and the brain. *Science* **324,** 929–930 (2009).
30. Bredemeyer, A. L. *et al.* ATM stabilizes DNA double-strand-break complexes during V(D)J recombination. *Nature* **442,** 466–470 (2006).
31. Liao, M. J. & Van Dyke, T. Critical role for Atm in suppressing V(D)J recombination-driven thymic lymphoma. *Genes Dev.* **13,** 1246–1250 (1999).
32. Vorechovský, I. *et al.* Clustering of missense mutations in the ataxia-telangiectasia gene in a sporadic T-cell leukaemia. *Nat. Genet.* **17,** 96–99 (1997).
33. Schaffner, C., Idler, I., Stilgenbauer, S., Döhner, H. & Lichter, P. Mantle cell lymphoma is characterized by inactivation of the ATM gene. *Proc. Natl. Acad. Sci. USA* **97,** 2773–2778 (2000).
34. Stankovic, T. *et al.* Inactivation of ataxia telangiectasia mutated gene in B-cell chronic lymphocytic leukaemia. *Lancet* **353,** 26–29 (1999).
35. Wu, X. *et al.* ATM phosphorylation of Nijmegen breakage syndrome protein is required in a DNA damage response. *Nature* **405,** 477–482 (2000).
36. Wang, H. *et al.* The interaction of CtIP and Nbs1 connects CDK and ATM to regulate HR-mediated double-strand break repair. *PLoS Genet.* **9,** e1003277 (2013).
37. Quennet, V., Beucher, A., Barton, O., Takeda, S. & Löbrich, M. CtIP and MRN promote non-homologous end-joining of etoposide-induced DNA double-strand breaks in G1. *Nucleic Acids Res.* **39,** 2144–2152 (2011).
38. Kurosawa, A. *et al.* The requirement of Artemis in double-strand break repair depends on the type of DNA damage. *DNA Cell Biol.* **27,** 55–61 (2008).
39. Rahal, E. A. *et al.* ATM mediates repression of DNA end-degradation in an ATP-dependent manner. *DNA Repair (Amst)* **7,** 464–475 (2008).
40. Rahal, E. A. *et al.* ATM regulates Mre11-dependent DNA end-degradation and microhomology-mediated end joining. *Cell Cycle* **9,** 2866–2877 (2010).
41. Bolderson, E. *et al.* Phosphorylation of Exo1 modulates homologous recombination repair of DNA double-strand breaks. *Nucleic Acids Res.* **38,** 1821–1831 (2010).
42. Helmink, B. A. *et al.* H2AX prevents CtIP-mediated DNA end resection and aberrant repair in G1-phase lymphocytes. *Nature* **469,** 245–249 (2011).
43. Barlow, C. *et al.* Atm-deficient mice: a paradigm of ataxia telangiectasia. *Cell* **86,** 159–171 (1996).
44. Nitiss, J. L., Soans, E., Rogojina, A., Seth, A. & Mishina, M. Topoisomerase assays. *Curr. Protoc. Pharmacol* **57,** 3.3.1–3.3.27 (2012).

Acknowledgements

Work in F.C.-L. laboratory is funded with grants from the Spanish Government (SAF2010-21017 and BFU2010-11042-E, Ministerio de Ciencia e Innovación), the regional Andalusian Government (CVI-7948) and the European Union (PERG07-2010-268466) and with the following fellowships: Formación Personal Investigador (BES-2011-047351, Ministerio de Ciencia e Innovación) for A.A.-Q., Beca Predoctoral AEFAT

(Asociación Española Familia Ataxia Telangiectasia) for A.S.-B., Personal Investigador en Formación (Universidad de Sevilla) for J.A.L. and Ramón y Cajal (RYC-2009-03928, Ministerio de Ciencia e Innovación) for F.C.-L. L.M.E. is supported by the Miguel Servet program, (Instituto Carlos III) and the Spanish Government grant (BFU2011-25734, Ministerio de Ciencia e Innovación). We thank O. Fernández-Capetillo, P. Huertas, T. Stracker, V. Gorbunova, J.A. Pintor-Toro and R.M. Ríos for reagents; M. Haffner for technical advice; A. Aguilera, K. Caldecott and F. Prado for comments.

Author contributions

A.A.-Q. performed most of the experiments, data analysis and interpretation. A.S.-B. performed G1/G2 repair kinetic analysis. J.A.L. analysed TOP2 cleavage complexes. C.Q. performed micronuclei analysis and provided technical support. D.S.-G. and L.M.E. performed the automated analysis of confocal microscopy images. F.C.-L. designed the experiments, interpreted the data and wrote the paper.

Additional information

Supplementary Information accompanies this paper at http://www.nature.com/naturecommunications

Competing financial interests: The authors declare no competing financial interests.

Reprints and permission information is available online at http://npg.nature.com/reprintsandpermissions/

How to cite this article: Álvarez-Quilón, A. *et al.* ATM specifically mediates repair of double-strand breaks with blocked DNA ends. *Nat. Commun.* 5:3347 doi: 10.1038/ncomms4347 (2014).

OPEN ACCESS Freely available online

PLOS | GENETICS

TDP2–Dependent Non-Homologous End-Joining Protects against Topoisomerase II–Induced DNA Breaks and Genome Instability in Cells and *In Vivo*

Fernando Gómez-Herreros[1☯], Rocío Romero-Granados[2☯], Zhihong Zeng[1], Alejandro Álvarez-Quilón[2], Cristina Quintero[2], Limei Ju[1], Lieve Umans[3], Liesbeth Vermeire[3], Danny Huylebroeck[3], Keith W. Caldecott[1]*, Felipe Cortés-Ledesma[2]*

1 Genome Damage and Stability Centre, University of Sussex, Falmer, United Kingdom, **2** Centro Andaluz de Biología Molecular y Medicina Regenerativa (CABIMER), CSIC–Universidad de Sevilla (Departamento de Genética), Sevilla, Spain, **3** Laboratory of Molecular Biology (Celgen), Department of Development and Regeneration, University of Leuven, Leuven, Belgium

Abstract

Anticancer topoisomerase "poisons" exploit the break-and-rejoining mechanism of topoisomerase II (TOP2) to generate TOP2-linked DNA double-strand breaks (DSBs). This characteristic underlies the clinical efficacy of TOP2 poisons, but is also implicated in chromosomal translocations and genome instability associated with secondary, treatment-related, haematological malignancy. Despite this relevance for cancer therapy, the mechanistic aspects governing repair of TOP2-induced DSBs and the physiological consequences that absent or aberrant repair can have are still poorly understood. To address these deficits, we employed cells and mice lacking tyrosyl DNA phosphodiesterase 2 (TDP2), an enzyme that hydrolyses 5′-phosphotyrosyl bonds at TOP2-associated DSBs, and studied their response to TOP2 poisons. Our results demonstrate that TDP2 functions in non-homologous end-joining (NHEJ) and liberates DSB termini that are competent for ligation. Moreover, we show that the absence of TDP2 in cells impairs not only the capacity to repair TOP2-induced DSBs but also the accuracy of the process, thus compromising genome integrity. Most importantly, we find this TDP2-dependent NHEJ mechanism to be physiologically relevant, as *Tdp2*-deleted mice are sensitive to TOP2-induced damage, displaying marked lymphoid toxicity, severe intestinal damage, and increased genome instability in the bone marrow. Collectively, our data reveal TDP2-mediated error-free NHEJ as an efficient and accurate mechanism to repair TOP2-induced DSBs. Given the widespread use of TOP2 poisons in cancer chemotherapy, this raises the possibility of TDP2 being an important etiological factor in the response of tumours to this type of agent and in the development of treatment-related malignancy.

Citation: Gómez-Herreros F, Romero-Granados R, Zeng Z, Álvarez-Quilón A, Quintero C, et al. (2013) TDP2–Dependent Non-Homologous End-Joining Protects against Topoisomerase II–Induced DNA Breaks and Genome Instability in Cells and *In Vivo*. PLoS Genet 9(3): e1003226. doi:10.1371/journal.pgen.1003226

Editor: Nancy Maizels, University of Washington, United States of America

Received July 13, 2012; **Accepted** November 21, 2012; **Published** March 7, 2013

Funding: Work in FC-L laboratory is funded with grants from the Spanish Government (SAF2010-21017 and BFU2010-11042-E) and the European Union (PERG07-2010-268466) and with the following fellowships from the Spanish Government: Ramón y Cajal (RYC-2009-03928) for FC-L, JAE-Doc (2010-011) for RR-G, and FPI (BES-2011-047351) for ÁA-Q. Work in the KWC laboratory is funded by MRC grants to KWC (G0901606, G0600776, MR/J006750/1) and supported FG-H, ZZ, and LJ. Generation of the Tdp2 floxed and conditional mice in the DH lab was supported by the EC FP6 Integrated Project EndoTrack, the Interuniversity Attraction Pole IUAP-P6/20 and P7/07 project, and the Queen Elisabeth Medical Foundation (GSKE 1113) and type 3 large-infrastructure support InfraMouse (Hercules Foundation ZW09-03, to DH). The funders had no role in study design, data collection and analysis, decision to publish, or preparation of the manuscript.

Competing Interests: The authors have declared that no competing interests exist.

* E-mail: k.w.caldecott@sussex.ac.uk (KWC); felipe.cortes@cabimer.es (FC-L)

☯ These authors contributed equally to this work.

Introduction

The double-stranded helical structure of DNA creates topological problems in all processes that involve opening of the double helix and accessing the genetic information [1,2]. In particular, the transcription and duplication of DNA and its condensation into chromosomes generates knots and tangles that need to be resolved to avoid interference with diverse cellular processes and to ensure faithful chromosome segregation during mitosis. DNA topoisomerases are enzymes that introduce transient breaks in DNA to solve these topological problems. Type II topoisomerases, such as topoisomerase II in eukaryotes (TOP2) are essential homodimeric enzymes that relax, unknot and decatenate DNA molecules by catalyzing the passage of duplex DNA through a transient DNA double strand break (DSB) created by the enzyme [3]. Two isoforms of TOP2, α and β, exist in higher eukaryotes, with primary roles in replication and chromosome segregation and in transcription, respectively.

A key intermediate of TOP2 activity is the cleavage complex, in which each of two topoisomerase subunits is covalently linked to the 5′-terminus of an enzyme-generated DSB via a phosphodiester bond between the active-site tyrosine and the 5′-phosphate. The cleavage complex is normally a very short-lived intermediate, because the topoisomerase rapidly re-ligates the DSB once DNA strand passage through the DSB has occurred. However, under certain circumstances, such as the presence of nearby DNA lesions, cleavage complexes can be stabilized resulting in an increased likelihood of collision with RNA or DNA polymerases [4]. Such collisions can convert cleavage complexes into potentially clastogenic or lethal DSBs that require cellular DNA repair pathways for their removal.

Author Summary

DNA double-strand breaks (DSBs) are dangerous because they can lead to cellular death and tissue degeneration if not repaired, or to genome rearrangements, which are a common hallmark of cancer, if repaired incorrectly. Although required for all chromosomal transitions in cells, transient DNA cleavage by topoisomerase II (TOP2) is a potential endogenous source of DSBs, which are characteristic in that TOP2 remains covalently bound to the DNA termini. In addition, numerous chemotherapeutic regimes rely on compounds that "poison" TOP2 activity, stimulating the formation of DSBs that target tumour cells. However, these compounds also affect healthy tissue and confer undesirable side effects, including the stimulation of genome rearrangements that can trigger secondary malignancies (mainly acute leukemia). Identifying the factors that participate in the repair of TOP2-induced DSBs and fully understanding their mechanism of action are therefore important for the design of chemotherapeutic regimes that are more effective and safer. Here we demonstrate that TDP2, a recently identified protein that can liberate DSB termini from blocked TOP2, functions as part of established cellular DSB repair processes and is required to safeguard genome integrity upon treatment with TOP2 poisons, both in cells and in mice. These results can therefore have important implications in cancer treatment.

Cleavage complexes are the target of a widely used class of anti-tumor agents that 'poison' topoisomerase activity, thereby prolonging the half-life of the intermediate and increasing the possibility of DSB formation [4,5]. Thus, these drugs kill tumor cells by inducing high levels of TOP2-associated DSBs. Consequently, TOP2 poisons are commonly used antineoplastic drugs in the treatment of a broad range of tumor types including malignant lymphomas, sarcomas, leukemias, and lung, ovarian, breast and testicular cancers [5]. However, similar to other chemotherapeutic agents, TOP2-targeting drugs are only partially selective for tumour cells, resulting in unwanted toxicity in normal tissues and in therapy-associated chromosome translocations and secondary leukemias [6–14]. Moreover, some breakpoints in such translocations have actually been correlated with preferential sites of cleavage by TOP2 [13–17].

A characteristic feature of TOP2-induced DNA breaks is covalent attachment of the enzyme to 5′ ends of the DNA, which must be removed by cellular end-processing enzymes if DSB repair is to occur [18]. Until recently, the only known mechanism for removal TOP2 peptide from DNA 5′-termini in mammalian cells involved excision of the DNA fragment linked to the peptide using nucleases such as the MRN complex, CtIP or Artemis [19–21]. Recently, however, we identified a human 5′-tyrosyl DNA phosphodiesterase (5′-TDP) that can cleave 5′-phosphotyrosyl bonds and thereby release TOP2 from DSB termini without the need to also remove DNA sequence [22]. Consequently, this enzyme, which was previously known as signalling protein and transcription cofactor TTRAP/EAPII [23,24], is now denoted tyrosyl DNA phopshodiesterase-2 (TDP2; Human Gene Nomeclature Organisation). Notably, consistent with its enzyme activity, TDP2 is required for cellular resistance to the anti-cancer TOP2 poison etoposide, but is not required for cellular resistance to ionizing radiation or methylmethane sulphonate [22,25]; agents that induce DNA damage independently of TOP2 activity.

Following DNA end processing, DSBs can be repaired either by homologous recombination (HR) or by non-homologous end joining (NHEJ) [26]. However, these pathways utilize fundamentally different mechanisms for rejoining DSBs and consequently differ in their accuracy. In particular, HR utilizes undamaged sister chromatids to replace any nucleotides removed from DNA termini during DNA end processing and consequently is normally 'error-free'. However, this process is available only during S phase or G2, when sister chromatids are available. In contrast, NHEJ is a 'cut-and-splice' process in which DSB termini are ligated together following DNA end processing without accurate replacement of missing nucleotides, and thus is potentially 'error-prone'.

Here, we employ avian and murine experimental models to show that *TDP2*/*Tdp2* deletion results in hypersensitivity to a structurally diverse range of anti-cancer TOP2 poisons. Moreover, we present genetic, biochemical and cellular evidence for TDP2 functioning in a mechanism of NHEJ that protects genome integrity in response to TOP2-induced damage. Finally, we show that this TDP2 dependent pathway also operates *in vivo*, as, upon exposure to TOP2 poisons, it is required for normal adult mouse lymphopoiesis, intestinal mucosa homeostasis and the maintenance of genome stability in the bone marrow. Collectively, our results suggest that TDP2 defines an error-free mechanism of NHEJ in mammals, which is specialized in the repair of TOP2-induced DSBs and reduces both tissue toxicity and genome instability in response to this particular type of DNA damage. These findings suggest the possibility of TDP2 being a significant etiological factor in the clinical tolerance and response to widely used TOP2 poisons.

Results

TDP2 is required for cellular resistance to clinical TOP2 poisons and is the major 5′-TDP activity in the mouse

The discovery of TDP2 as the first 5′-TDP activity raised the possibility of it being an important factor in the clinical response to TOP2 poisons [22,25]. Indeed, TDP2 deleted avian DT40 cells are hypersensitive to etoposide [22,25]. To address this question further, we examined the sensitivity of $TDP2^{-/-/-}$ cells to two additional, structurally diverse, TOP2 poisons. These drugs, denoted doxorubicin and amsacrine (m-AMSA), are employed widely during cancer therapy but in contrast to etoposide, 'poison' TOP2 by intercalating into DNA [5]. Nevertheless, similarly to etoposide, $TDP2^{-/-/-}$ cells displayed significant hypersensitivity to both doxorubicin and m-AMSA (Figure 1A). Moreover, a functional TDP2 phosphodiesterase domain was required for cellular resistance to this type of drug, because expression of wild-type human TDP2 (hTDP2) rescued the sensitivity of $TDP2^{-/-/-}$ DT40 cells to m-AMSA, whereas $hTDP2^{D262A}$ harbouring an inactivating mutation in the catalytic active site [5] did not (Figure 1A). These results show that TDP2 is required for cellular resistance to a range clinically relevant and structurally diverse TOP2 poisons, and support our contention that this requirement reflects the 5′-TDP activity of this enzyme.

To determine the impact of TDP2 on TOP2-induced DNA damage in mammals, and thus its possible relevance to anti-cancer therapy, we adopted a mouse model in which the first three exons of *Tdp2*, plus the 5′-UTR, were deleted by Cre-mediated excision (Figure 1B; see Materials and Methods). Mice homozygous for the deleted allele ($Tdp2^{flA}$, from here-on denoted $Tdp2^{\Delta 1-3}$) are viable, and so far we have not detected any abnormal pathology (unpublished observations). However, transformed $Tdp2^{\Delta 1-3}$ mouse embryonic fibloblasts (MEFs) were hypersensitive to etoposide (Figure 1C, left, and Figure S1), but were not hypersensitive to DNA damage induced independently of TOP2 by γ-irradiation (Figure 1C, right).

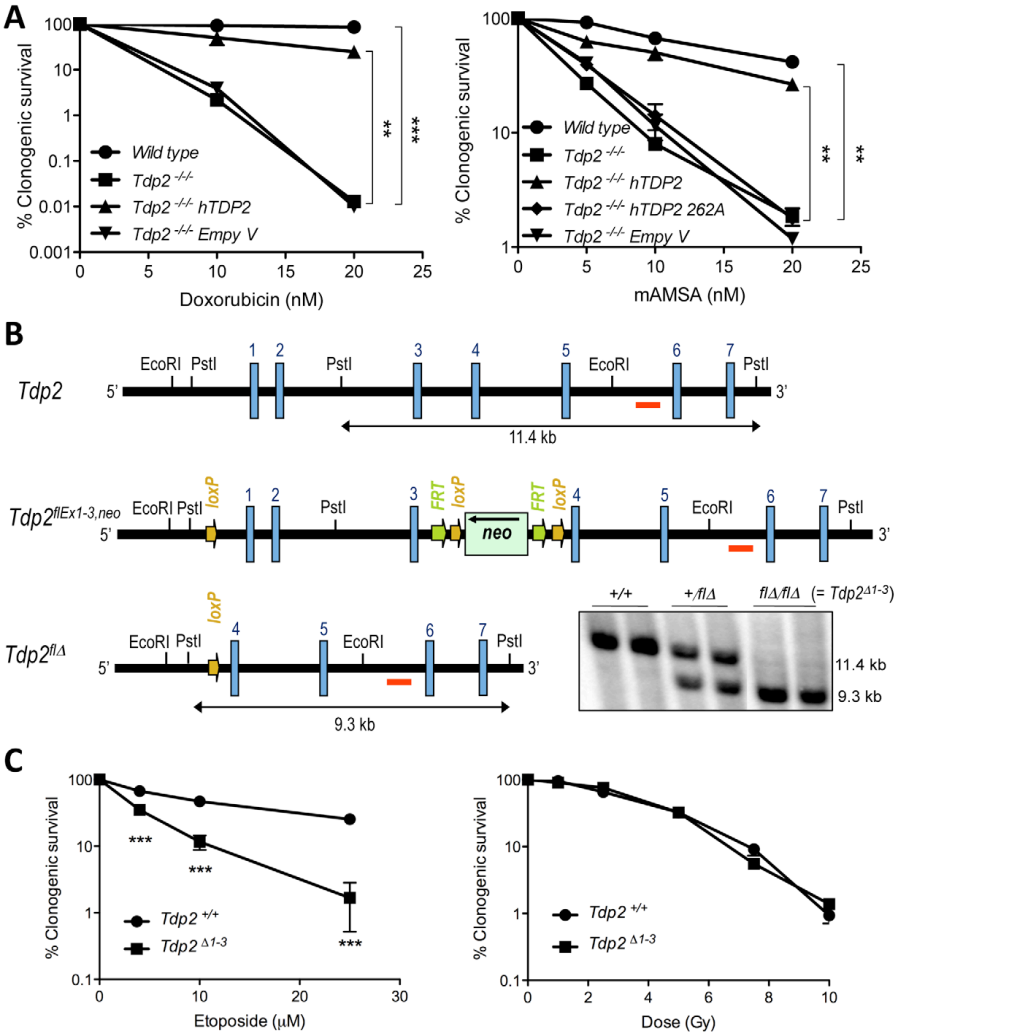

Figure 1. TDP2 promotes survival following TOP2-induced DSBs. A. Clonogenic survival of the indicated DT40 cell line; wild-type, *TDP2*$^{-/-/-}$ and *TDP2*$^{-/-/-}$ complemented with human TDP2 (hTDP2) and catalytic-dead human TDP2 (hTDP2 262A) or empty vector (Empty V); following continuous treatment with the indicated concentrations of doxorubicin (left) or mAMSA (right). Average ± s.e.m. of at least three independent experiments and statistical significance at the highest indicated dose when compared to *TDP2*$^{-/-/-}$ cells by Two-way ANOVA with Bonferroni post-test is shown. B. Scheme showing the strategy for targeted deletion of the first three exons of *Tdp2* in mouse. The wild-type (*Tdp2*$^{+}$), conditional (*Tdp2*$^{flEx1-3,neo}$) and deleted (*Tdp2*$^{fl\Delta}$) alleles are depicted. The *EcoRI-EcoRI* fragment of *Tdp2* was used in the targeting construct. Southern-blot analysis of *PstI*-digested DNA from wild-type (*+/+*), heterozygous (*+/flΔ*) and knock-out (*flΔ/flΔ*, from now on denoted *Tdp2*$^{\Delta 1-3}$) mice, using the indicated probe (red line), is shown (bottom right). C. Clonogenic survival of wild-type and *Tdp2*$^{\Delta 1-3}$ transformed MEFs after 3 h acute exposure to the indicated concentrations of etoposide (left) or the indicated dose of γ-irradiation (right). Average ± s.e.m. of three independent experiments and statistical significance by Two-way ANOVA test with Bonferroni post-test is shown. In all figures (*P≤0.05; **P≤0.01; ***P≤0.005).
doi:10.1371/journal.pgen.1003226.g001

Protein extracts from spleen, thymus, and bone marrow from wild type mice possess robust 5′-TDP activity, but, importantly, this activity was absent in analogous protein extracts from *Tdp2*$^{\Delta 1-3}$ mice, confirming successful inactivation of the enzyme (Figure 2A). Cell extracts prepared from primary *Tdp2*$^{\Delta 1-3}$ MEFs also lacked detectable 5′-TDP activity (Figure 2B). This was true

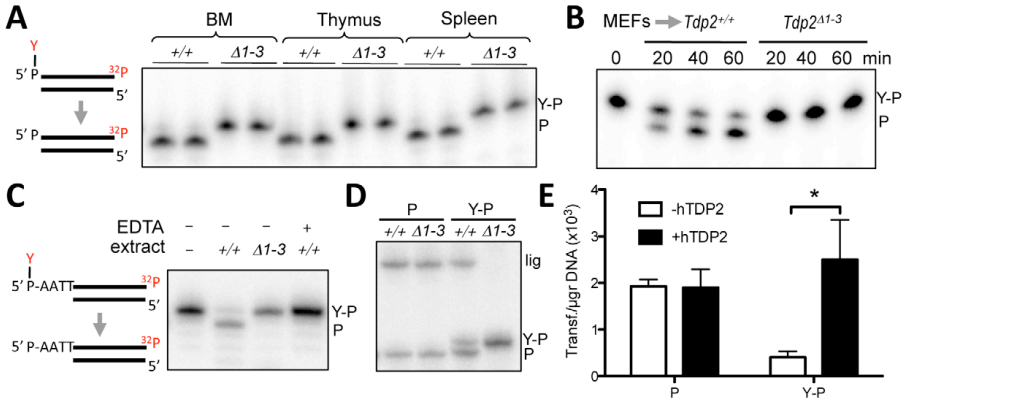

Figure 2. Deletion of *Tdp2* in mouse abolishes 5′-TDP activity and ligation of 5′ phosphotyrosine-blocked ends. A. Duplex substrate harbouring a 5′phosphotyrosine blunt end (left) was incubated with 9 μg $Tdp2^{+/+}$ or $Tdp2^{\Delta 1-3}$ tissue extract from bone marrow (BM), thymus and spleen for 1 h. B. Substrate in "A" was incubated with 1.5 μg of cellular extract from $Tdp2^{+/+}$ or $Tdp2^{\Delta 1-3}$ primary MEFs for the indicated time. C. Duplex substrate harbouring a 5′phosphotyrosine self-complementary overhang end (left) was incubated with 10 μg cellular extract from $Tdp2^{+/+}$ or $Tdp2^{\Delta 1-3}$ transformed MEFs for 2 h in the presence or absence of 50 mM EDTA. D. Self-ligation of 5′ phosphate (P) and 5′ phosphotyrosine (Y–P) overhang substrates as depicted in "C" incubated for 1.5 h with 3.3 μg cellular extract from $Tdp2^{+/+}$ or $Tdp2^{\Delta 1-3}$ transformed MEFs in the presence of T4 DNA ligase. In all cases migration of the 5′ phosphotyrosine substrate (Y–P), 5′ phosphate (P) and ligation (lig) products are indicated. E. Circularization efficiency of a linear plasmid with 5′ phosphotyrosine (Y–P) and 5′ phosphate (P) catalysed by $Tdp2^{\Delta 1-3}$ transformed MEFs extracts in the presence and absence of recombinant human TDP2 (hTDP2). Reaction products were transformed into *E. coli* and the number of transformants obtained per μg of initial substrate DNA (average ± s.e.m. of three independent experiments) is shown. Statistical significance by Two-way ANOVA test with Bonferroni post-test is indicated is shown.
doi:10.1371/journal.pgen.1003226.g002

not only for blunt-ended DSB substrates, but also for DSB substrates harbouring a 4-bp 5′-overhang (Figure 2C), characteristic of TOP2-induced DSBs. Additionally, EDTA-mediated chelation of Mg^{2+}, which is essential for TDP2 function, completely eliminates 5′-TDP activity in wild type MEF extracts. These observations are significant because the related enzyme TDP1, whose activity is Mg^{2+} independent, was recently reported to possess weak activity on this type of substrate [27]. Our data therefore suggest that TDP2 is the primary, if not only, source of 5′-TDP activity in MEF extracts (Figure 2C).

TDP2 creates ligatable DSBs and functions in NHEJ

Based on the mechanism of TOP2 cleavage, we anticipated that TDP2 activity would reconstitute 'clean' DSBs (5′ phosphate and 3′ hydroxyl termini) with 4-bp overhangs, which would be an ideal substrate for ligation by NHEJ. Interestingly, these ligation events would accurately preserve the DNA sequence, suggesting the possibility of an error-free NHEJ mechanism that specifically acts on TOP2-induced DSBs. To test this hypothesis, we examined whether TDP2 action at DSBs typical of those induced by TOP2 creates termini that can be ligated by T4 DNA ligase. Indeed, inclusion of T4 DNA ligase in reactions containing wild type MEF extract resulted in the additional appearance of a product of 46-nt, indicative of the completion of DSB repair by DNA ligation. However, this product was not observed if reactions contained cell extract from $Tdp2^{\Delta 1-3}$ MEFs, confirming that DNA ligation was dependent on TDP2 activity (Figure 2D). Interestingly, the length of the product is consistent with a ligation event in which DNA sequence is preserved. To analyse ligation events directly catalysed by cell extracts, we generated linear plasmids harbouring 5′ phosphate or 5′ phosphotyrosine ends by PCR amplification with the corresponding modified primers. The incubation of these substrates with NHEJ-competent nuclear extracts [28] results in plasmid circularization events that can be scored as colonies following bacterial transformation. As can be seen in Figure 2E, nuclear extracts from $Tdp2^{\Delta 1-3}$ MEFs efficiently circularized linear plasmids with 5′ phosphate ends but not linear plasmids harbouring 5′-phosphotyrosine. This difference was lost upon addition of recombinant TDP2 to the reaction, confirming the TDP2–dependent nature of the repair reaction. Collectively, our data suggest that TDP2 activity facilitates NHEJ of 5′ tyrosine-blocked ends by generating DSBs with ligatable termini, consistent with our hypothesis that this enzyme can support error-free NHEJ of TOP2-induced DNA damage.

To genetically test whether TDP2 functions indeed during NHEJ, we generated $TDP2^{-/-/-}$ DT40 cells harboring a targeted deletion of Ku70, a core component of the NHEJ pathway (Figure S2). Whilst both $TDP2^{-/-/-}$ and $KU70^{-/-}$ cells were hypersensitive to etoposide, cells in which both genes were deleted ($TDP2^{-/-/-}/KU70^{-/-}$) were no more hypersensitive than cells in which Ku70 alone was deleted (Figure 3A). In contrast to this epistatic relationship with a core NHEJ factor, transient knockdown of TDP2 further enhances etoposide sensitivity of HR defective (BRCA2 mutated) human fibroblasts (Figure 3B). Based on these genetic relationships, we conclude that TDP2 functions in a NHEJ-mediated and HR-independent pathway for the repair of TOP2-induced DSBs.

To further assign a role for TDP2 in the NHEJ pathway for DSB repair, we measured DSB repair rates in primary $Tdp2^{\Delta 1-3}$ MEFs by immunodetection of γH2AX, a phosphorylated derivative of histone H2AX that arises at sites of chromosomal DSBs [29]. We measured DSB repair in specific phases of the cell cycle, because whilst NHEJ is operative throughout, HR-mediated DSB repair is operative only in S/G2 [30]. Notably, DSB repair rates were markedly reduced in

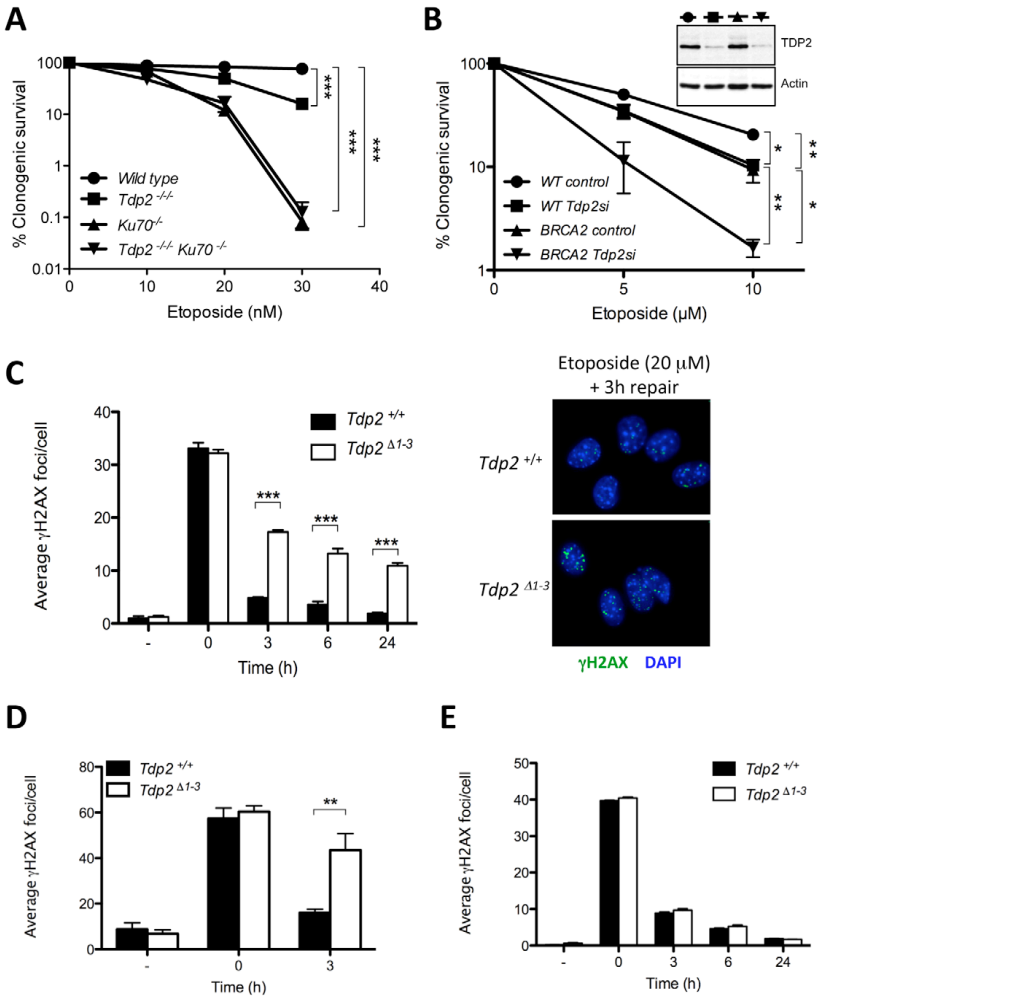

Figure 3. TDP2 promotes repair of TOP2-induced DSBs by NHEJ. A. Clonogenic survival of wild-type, *TDP2*$^{-/-/-}$, *KU70*$^{-/-}$ and *TDP2*$^{-/-/-}$ *KU70*$^{-/-}$ DT40 cells following continuous treatment with the indicated concentrations of etoposide. Average ± s.e.m. of at least three independent experiments and statistical significance at the highest indicated dose by Two-way ANOVA with Bonferroni post-test is shown. B. Clonogenic survival of wild-type and BRCA2-mutant human transformed fibroblasts with (Tdp2si) and without (control) TDP2 depletion following 3 h acute exposure to the indicated concentrations of etoposide. Western blot analysis of TDP2 levels in wild type and BRCA2-mutant cell extracts after 48 h of transfection is indicated (inset). Other details as in "A". C. γH2AX foci induction after 30 min 20 μM etoposide treatment and repair at different times following drug removal in confluency arrested *Tdp2*$^{+/+}$ and *Tdp2*$^{\Delta 1-3}$ primary MEFs. Representative images of the 3 h repair time point including DAPI counterstain (right) and average ± s.e.m. of at least three independent experiments (left) are shown. Statistical significance by Two-way ANOVA test with Bonferroni post-test is indicated. D. G2 primary MEFs (see Matherials and Methods) following 30 min 10 μM etoposide treatment. Other details as in "C". E. Confluency arrested primary MEFs exposed to 2Gy γ-irradiation. Other details as in "C".
doi:10.1371/journal.pgen.1003226.g003

Tdp2$^{\Delta 1-3}$ MEFs following etoposide treatment, both in G0/G1 (Figure 3C) and G2 (Figure 3D), consistent with TDP2 functioning, as NHEJ, independently of cell cycle. These results were not specific to murine cells, since similar results were observed in TDP2-depleted human A549 cells (Figure S4). In contrast to treatment with etoposide, the rate of DSB repair was normal in *Tdp2*$^{\Delta 1-3}$ MEFs following γ-irradiation, consistent with a role for TDP2 specifically at TOP2-induced DSBs (Figure 3E). Collectively, these data demonstrate that TDP2 is required in mammalian cells for rapid repair of TOP2-induced DSBs by NHEJ, and for cellular resistance to these lesions.

TDP2 promotes genome stability following TOP2-induced DNA damage

We hypothesized that this TDP2-mediated error-free NHEJ mechanism would be important to maintain genome integrity upon exposure to TOP2 poisons. To address this possibility, we quantified the frequency of micronuclei (MN), nucleoplasmic bridges (NB), and chromosomal aberrations following etoposide treatment. These events constitute well-established indicators of genome instability caused by misrepair of DSBs in which acentric, dicentric and aberrant chromosomes or chromosome fragments can be formed. As expected, etoposide increased the number of micronuclei and nucleoplasmic bridges in both transformed $Tdp2^{+/+}$ and $Tdp2^{\Delta 1-3}$ MEFs, but this increase was significantly higher (up to three-fold) in $Tdp2^{\Delta 1-3}$ cells (Figure 4A). Primary $Tdp2^{\Delta 1-3}$ MEFs at low passage (P3–4) similarly displayed elevated levels of micronuclei and nucleoplasmic bridges following etoposide treatment, compared to wild type primary MEFs (Figure 4B), although in the case of nucleoplasmic bridges the low number of cells displaying these structures prevented the difference from reaching statistical significance.

An additional indicator of genome instability is elevated frequencies of chromosome aberrations. Consequently, we quantified the frequency of chromosome breaks and exchanges in metaphase spreads of transformed $Tdp2^{+/+}$ and $Tdp2^{\Delta 1-3}$ MEFs. In agreement with the increased cell cycle arrest of $TDP2^{-/-/-}$ DT40 cells in G2 following etoposide treatment [25], we noted an etoposide-dependent reduction in metaphase cells that was particularly severe in $Tdp2^{\Delta 1-3}$ MEFs (unpublished observations). However, of those metaphases observed and scored, both chromosome exchanges and breaks were significantly higher (2 to 5-fold) in $Tdp2^{\Delta 1-3}$ MEFs than in $Tdp2^{+/+}$ MEFs (Figure 4C). A similar increase in these events in $Tdp2^{\Delta 1-3}$ MEFs, compared to wild type cells, was observed if low-passage primary MEFs were employed, ruling out the possibility that the elevated genome instability in $Tdp2^{\Delta 1-3}$ MEFs was an artefact of cellular transformation (Figure 4D). In the latter case, etoposide treatment almost ablated the appearance of mitotic cells in populations of both wild type and $Tdp2^{\Delta 1-3}$ MEFs, necessitating the use of caffeine to prevent G2 arrest. Taken together these results demonstrate that loss of TDP2 results in increased genome instability following TOP2-induced DNA strand breakage.

Loss of TDP2 results in elevated homologous recombination

The above results demonstrate increased genome instability in $Tdp2^{\Delta 1-3}$ MEFs, consistent with a role for TDP2 in error-free NHEJ-mediated repair of TOP2-induced DSBs. In this scenario, we considered the possibility that loss of TDP2 might also result in channelling of DSB repair towards HR. To address this question, we analyzed the formation of RAD51 foci, a well-established indicator of repair by HR. Following treatment with etoposide, the average number of Rad51 foci per cell was ~3-fold higher in $Tdp2^{\Delta 1-3}$ than in wild-type MEFs (Figure 5A), in agreement with an increase in the use of HR to repair TOP2-induced DSBs when TDP2 is not present. Furthermore, we compared the frequency of etoposide-induced sister chromatid exchanges (SCEs), a molecular hallmark of HR [31], in wild type and $Tdp2^{\Delta 1-3}$ MEFs (Figure 5B). Notably, SCE levels increased substantially in transformed MEFs following acute etoposide exposure, being significantly higher in $Tdp2^{\Delta 1-3}$ cells at two etoposide concentrations tested (1 and 2.5 μM). These data confirm that, upon etoposide treatment, the frequency of HR is elevated in $Tdp2^{\Delta 1-3}$ MEFs, consistent with TDP2 functioning in NHEJ.

Elevated hypersensitivity to TOP2-induced DNA damage in $Tdp2^{\Delta 1-3}$ mice

To address the relevance of TDP2-mediated repair of TOP2-induced DSBs *in vivo*, we compared the impact of etoposide on adult (8 wk) wild type and $Tdp2^{\Delta 1-3}$ mice. A single intraperitonal injection of etoposide (75 mg/kg) caused a decrease in body weight in the initial 4 days post-treatment both in wild type and $Tdp2^{\Delta 1-3}$ animals (Figure 6A). However, whereas $Tdp2^{+/+}$ mice exhibited relatively mild and transient weight loss, $Tdp2^{\Delta 1-3}$ littermates lost weight progressively and were sacrificed at day 6 to prevent suffering. No differences in body weight were observed between mock-treated (with DMSO) wild type and $Tdp2^{\Delta 1-3}$ mice. Histopathological analysis of $Tdp2^{\Delta 1-3}$ mice sacrificed 6 days after etoposide treatment revealed marked villous atrophy in the small intestinal mucosa as the likely cause of the drastic weight loss (Figure 6B). This was not observed in either wild-type and/or DMSO treated animals (data not shown), suggesting a protective role for TDP2 against adverse effects of etoposide *in vivo*.

TOP2-induced DNA damage results in increased lymphoid toxicity in $Tdp2^{\Delta 1-3}$ mice

In addition to severe intestinal damage, etoposide administration resulted in elevated splenic and thymic atrophy in $Tdp2^{\Delta 1-3}$ mice, compared to wild type mice (Figure 6C), consistent with the known hypersensitivity of these organs to this drug [32]. Histological analysis of these tissues revealed a marked reduction in the cellular content in $Tdp2^{\Delta 1-3}$ animals (Figure 6C, right, note the low density of dark-stained nuclei). In light of these results, we analysed B-cell and T-cell maturation in wild type and $Tdp2^{\Delta 1-3}$ mice (Figure 6D and Figure S5). In the case of B-cell precursors in bone marrow, treatment with etoposide resulted in a decrease of 30–50% in the fraction of cells that were $CD43^+$ $B220^+$ progenitors (Pro-B cells) and a decrease of >95% in the fraction of cells that were $CD43^-$ $B220^{low}$ (Pre-B cells) or $CD43^-$ $B220^{high}$ (immature B cells) precursors. In all cases the reduction in B-cell precursors was greater in $Tdp2^{\Delta 1-3}$ mice, but the differences were not statistically significant at the administered dose. In contrast, in the case of T-cell maturation, whereas etoposide treatment reduced the fraction of $CD4^+$ $CD8^+$ immature T cells by 30–40% in wild type mice, these cells were almost completely eliminated in $Tdp2^{\Delta 1-3}$ mice (Figure 6A, bottom right). No effect was observed in CD11b/Mac-1^+ myeloid cells in the bone marrow (Figure S6). Taken together, these results suggest that loss of TDP2 increases cellular attrition in the lymphoid system, particularly in the T-cell lineage, in response to TOP2-induced DNA damage.

$Tdp2^{\Delta 1-3}$ mice display increased TOP2-induced genome instability in bone marrow

A major side-effect of cancer therapy employing TOP2 poisons is secondary hematological malignancy, and in particular acute leukemia, resulting most likely from error prone/erroneous repair of TOP2-induced DSBs and chromosome translocations [4,7]. Given our findings that TDP2 limits genome rearrangements induced by etoposide in cells, we examined whether TDP2 also promotes genome stability in bone marrow *in vivo*. We quantified the fraction of micronucleated polychromatic erythrocytes (PCEs) in bone marrow smears from $Tdp2^{\Delta 1-3}$ and $Tdp2^{+/+}$ mice 24 hour after intraperitoneal injection of etoposide (1 mg/kg). The rodent erythrocyte micronucleus test is a standard procedure to detect cytogenetic damage in toxicological studies and is based on the detection of micronuclei in erythrocyte precursors (Hayashi et al 1994). As expected, etoposide increased the fraction of PCEs that were micronucleated in both wild type and $Tdp2^{\Delta 1-3}$ animals

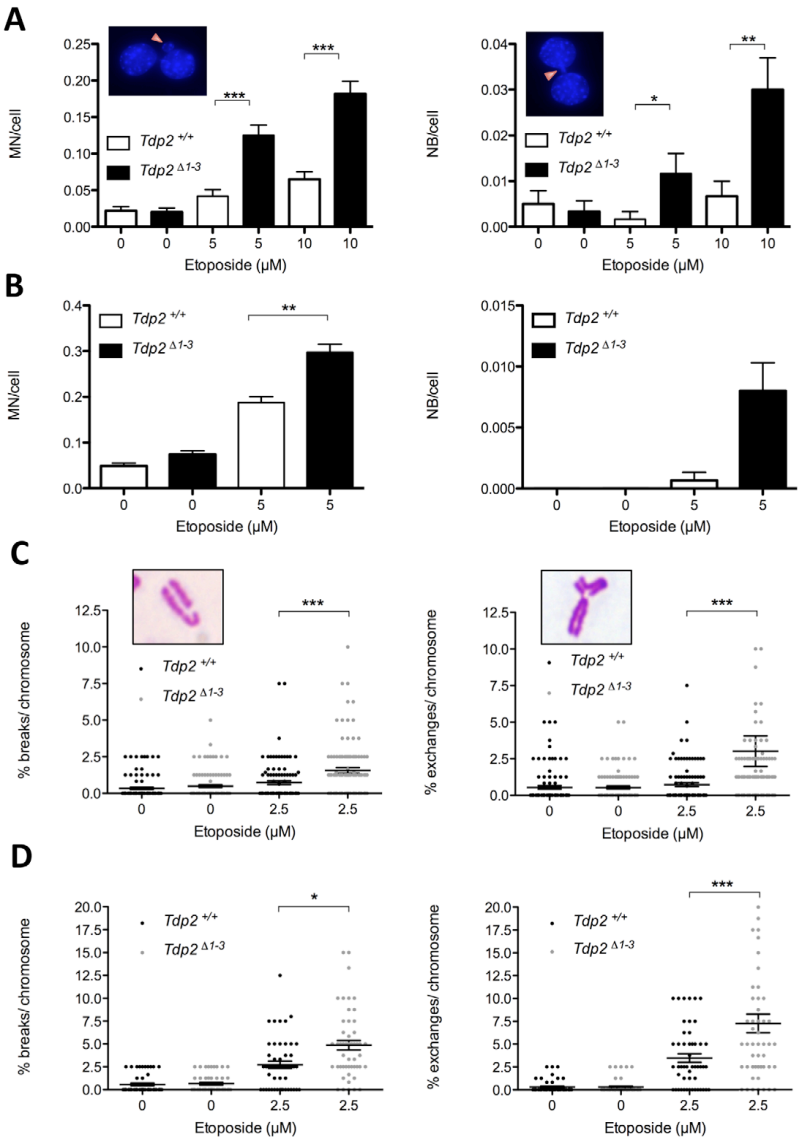

Figure 4. The absence of TDP2 increases etoposide-induced genome instability in mammalian cells. A. Micronuclei (MN, left) and nucleoplasmic bridges (NB, right) in binucleated (following cytochalasin B-mediated cell cycle arrest) *Tdp2*$^{+/+}$ and *Tdp2*$^{\Delta 1-3}$ transformed MEFs following acute treatment (30 min) with indicated dose of etoposide. See insets for representative images. Histogram bars represent the average ± s.e.m. of n≥600 cells coming from three independent experiments. Statistical significance by Mann-Whitney test. B. Primary MEFs in the absence of cytochalasin B treatment (n≥1500). Other details as in "A". C. Break-type (left) and exchange-type (right) chromosomal aberrations in transformed *Tdp2*$^{+/+}$ and *Tdp2*$^{\Delta 1-3}$ MEFs following acute treatment (30 min) with indicated dose of etoposide. See insets for a representative image. Plots show the number of breaks/exchanges per 100 chromosomes from individual metaphase spreads (n = 100) obtained in at least two independent experiments. Average ± s.e.m. and statistical significance by Mann-Whitney test is also indicated. D. Metaphase spreads from primary MEFs (n = 50). Caffeine was added 4 h after etoposide treatment. Other details as in "C".
doi:10.1371/journal.pgen.1003226.g004

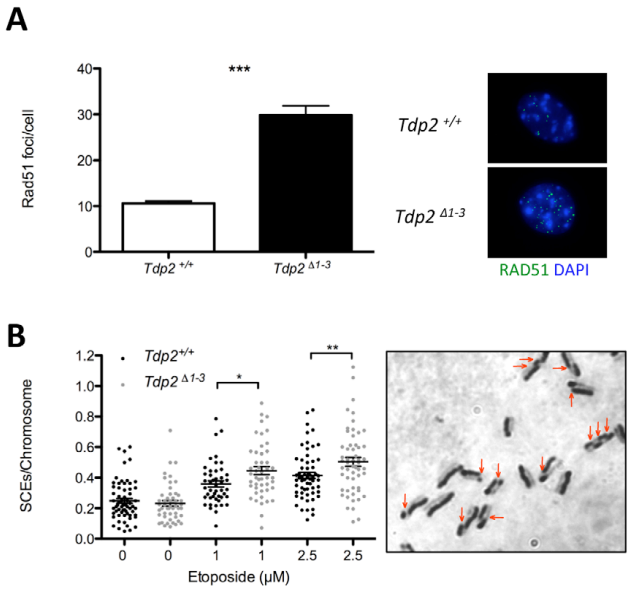

Figure 5. The absence of TDP2 increases etoposide induced homologous recombination. A. Total number of foci per RAD51 foci-containing cell in $Tdp2^{+/+}$ and $Tdp2^{\Delta 1-3}$ primary MEFs following 30 min 10 μM etoposide treatment and 2 h recovery (left). Replicating cells were excluded from the analysis. A representative image is shown (right). Average ± s.e.m. from 3 independent experiments and statistical significance by T test is indicated. B. Sister chromatid exchanges (SCEs) scored in $Tdp2^{+/+}$ and $Tdp2^{\Delta 1-3}$ transformed MEFs after 30 min acute treatment with the indicated concentration of etoposide. Plots show the number of SCEs per chromosome from individual metaphase spreads (n≥50) obtained in at least two independent experiments. Average ± s.e.m. and statistical significance by Mann-Whitney test is also indicated.
doi:10.1371/journal.pgen.1003226.g005

(Figure 7). However, this increase was ~2-fold higher in $Tdp2^{\Delta 1-3}$ mice than in wild type mice, suggesting that TDP2 protects heamatopoietic cells from genome instability induced by anti-cancer TOP2 poisons.

Discussion

TDP2 is the major 5′-tyrosyl DNA phosphodiesterase in mammals

In the current study we observe that *Tdp2* deletion ablates detectable 5′-TDP activity in different mouse tissues and MEFs, consistent with our previous observations in DT40 cells [25]. It is worth noting that other roles have been assigned to this protein, in other cellular processes such as signal transduction and transcriptional regulation [33]. So far, however, we have been unable to detect any spontaneous phenotype caused by TDP2 loss, either at cellular level or *in vivo*, while dramatic effects are observed upon etoposide treatment. This suggests that the most important function of TDP2, following Top2 induced DNA damage at least, is related to the 5′ TDP activity of this enzyme. Additionally, our data suggest that alternative, TDP2–independent, mechanisms of DSB repair are sufficient to cope with the endogenous level of TOP2 damage arising during normal mouse development and life.

A role for human TDP1 in repairing TOP2-induced DSBs was recently suggested by a weak 5′-TDP activity of human recombinant protein on DSBs possessing 4-bp 5′-overhangs, and on a mild sensitivity of $TDP1^{-/-}$ DT40 cells to etoposide [27]. This is also consistent with the increased resistance to etoposide reported in cells highly overexpressing TDP1 [34], and with the reported 5′-TDP activity of Tdp1 in *Saccharomyces cerevisiae* [35]. However, while our standard activity assays employs DSBs with blunt-ended 5′-phosphotyrosyl termini, in the current study we similarly failed to detect residual 5′-TDP activity in $Tdp2^{\Delta 1-3}$ MEF extracts on DSB substrates with 4-bp 5′-overhangs (Figure 2C). In addition, in our hands, $TDP1^{-/-}$ DT40 cells are not hypersensitive to etoposide, and deletion of *TDP1* in $TDP2^{-/-/-}$ DT40 cells does not increase sensitivity to etoposide above that observed by *TDP2* deletion alone [36]. Consequently, we conclude that TDP2 is the major if not only 5′-TDP activity in mammals (as in DT40 chicken cells), at physiologically relevant enzyme concentrations at least.

TDP2 is required for survival and efficient repair upon induction of TOP2-mediated DSBs in mammals

We have shown that *Tdp2*-deleted mouse cells are hypersensitive to TOP2-induced DNA damage, but not to ionizing radiation, in agreement with previous results with $TDP2^{-/-/-}$ DT40 cells [25]. Moreover, we demonstrate that this hypersensitivity correlates with a defect in the repair of etoposide-induced DSBs, as measured by immunostaining for sites of γH2AX, which suggests that TDP2-mediated repair promotes tolerance to TOP2-induced DNA damage in mammalian cells. Remarkably, we observed that TDP2 is required for resistance to TOP2-induced DNA damage not only at the cellular level, but also at the whole-organism level. Indeed, etoposide administration in $Tdp2^{\Delta 1-3}$ mice resulted in both increased mortality due to intestinal damage and in elevated

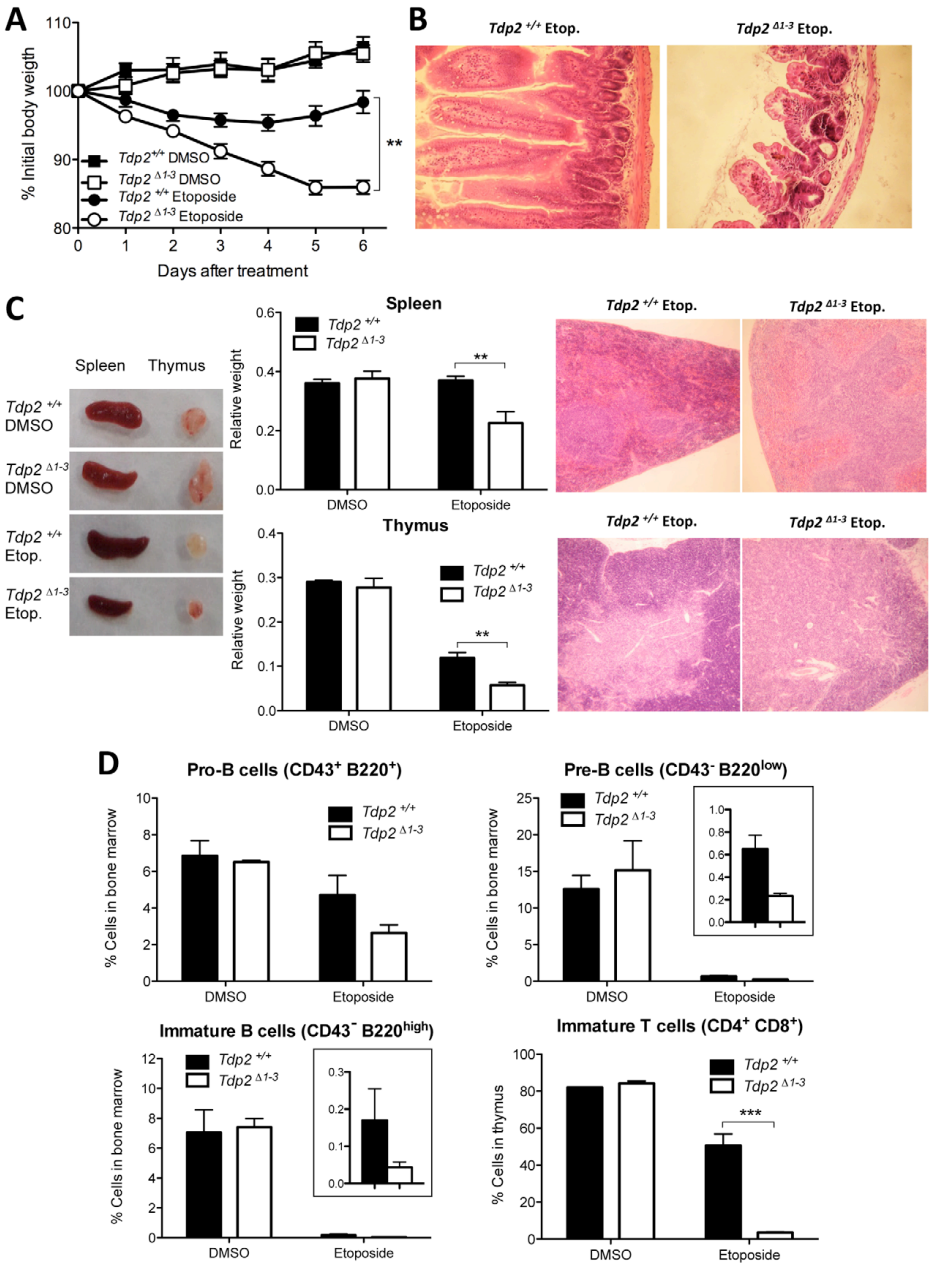

Figure 6. The absence of TDP2 causes etoposide sensitivity *in vivo*. A. 8-week old wild-type and *Tdp2*$^{\Delta 1-3}$ littermates were intraperitoneally injected with a single 75 mg/kg dose of etoposide or vehicle (DMSO) and body weight was recorded in the following 6 days. Average ± s.e.m. of the percentage of initial body weight from at least 8 mice and statistical significance by One-way ANOVA with Bonferroni post-test is shown. B. Representative image of hematoxylin-eosin stained jejunum slices from wild-type and *Tdp2*$^{\Delta 1-3}$ animals 6 days after etoposide treatment. C.

Macroscopic (left) and histological (right) representative image of spleen and thymus from wild-type and *Tdp2*$^{\Delta 1-3}$ animals 6 days after treatment. Average weight of these organs ± s.e.m. and statistical significance by Two-way ANOVA with Bonferroni post-test is shown (centre). D. FACS analysis of B-cells in bone marrow (top and bottom-left) and T-cells in thymus (bottom right) in wild-type and *Tdp2*$^{\Delta 1-3}$ animals 6 days after treatment. See insets to compare etoposide treated samples when required. Average percentage of the indicated cell type among the total number of cells in the corresponding tissue ± s.e.m. of at least 3 animals and statistical significance by Two-way ANOVA with Bonferroni post-test is shown.
doi:10.1371/journal.pgen.1003226.g006

toxicity in lymphoid tissue, established *in vivo* targets of etoposide [32]. TDP2 is therefore a critical factor in the cellular and physiological response to TOP2 poisons.

TDP2 functions in NHEJ and protects genome integrity

One important result of our study was to uncover the relationship between TDP2 and the major DSB-repair pathways, NHEJ and HR. We have shown that TDP2 can convert DSBs with 5′-phosphotyrosyl termini into DSBs that are directly ligatable, and might thus be of particular utility in facilitating an error-free NHEJ pathway for repair of TOP2-induced DSBs. Several of our observations support the idea that TDP2 is a component of NHEJ. First, the contribution of TDP2 to cellular resistance to TOP2 induced DNA damage is dependent on the NHEJ machinery and independent on HR, as, with regards to etoposide sensitivity, *KU70* is epistatic over *TDP2* deletion in DT40 cells while an additive effect is observed when TDP2 is depleted in BRCA2-deficient human fibroblasts. Second, loss of TDP2 results in a DSB repair defect not only in G2 but also in G0/G1, cell cycle stages in which NHEJ is the main if not only DSB repair mechanism available [26,30,37,38]. Third, *Tdp2*$^{\Delta 1-3}$ MEFs exhibit increased levels of HR-mediated DSB repair, as measured by elevated frequencies of RAD51 foci and sister chromatid exchange in response to etoposide treatment, which is a phenotype observed in other cell lines in which NHEJ is defective [39–41]. Additionally, we have been unable to generate DT40 cells in which both *TDP2* and *XRCC3* are deleted, suggesting that loss of both TDP2 and HR-mediated DSB repair is cell lethal (unpublished observations).

Whilst the above observations argue strongly that TDP2 is a component of NHEJ, it is important to note that TDP-independent NHEJ mechanisms to process TOP2-linked termini most likely also exist and employ nucleases such as MRN complex, CtIP or Artemis [5,18–21]. This explains why *KU70*$^{-/-}$ DT40 cells exhibit much greater hypersensitivity to etoposide than *TDP2*$^{-/-/-}$ DT40 cells, and why *Tdp2*$^{\Delta 1-3}$ MEFs still repair a significant fraction of etoposide-induced DSBs in G0/G1 (when NHEJ is the only DSB repair pathway available). Whilst nuclease-mediated NHEJ can support cell survival in response to TOP2-induced DNA damage, they most likely do so at the expense of increased genetic instability. This is because the removal of sequence from 4-bp complementary 5′-overhang during NHEJ will, on the one hand, likely result in chromosome deletions, and on the other hand, increase the propensity for DSB misjoining and chromosome translocation. In contrast, HR provides an error-free pathway to repair TOP2-induced DSBs that have been processed by nucleases, by restoring any missing DNA sequence from and intact sister chromatid in S and G2 [30,37,42]. In this scenario, the increased etoposide-induced genome instability in *Tdp2*$^{\Delta 1-3}$ mice, both in cultured cells from these animals and in bone marrow *in vivo*, likely reflects the use of TDP2–independent NHEJ in cellular contexts in which HR-mediated DSB repair is unavailable (e.g. in cells in G0/G1), or is saturated by the number of etoposide-induced DSBs.

In summary, based on these and our previously published data, we suggest that TDP2 defines a novel error-free NHEJ sub-pathway that converts TOP2-linked 5′-termini into ligatable DNA termini. We suggest that this may be particularly important during G1 and in post-mitotic cells, which lack HR-mediated repair, and thus in which it may be the only mechanism for error-free DSB repair of TOP2-induced DSBs (Figure 8).

TDP2 and cancer therapy

The results presented here can have important implications in the treatment of cancer. Given the widespread use of TOP2 poisons in cancer therapy, and the observed hypersensitivity to TOP2 poisons of cells lacking TDP2, our findings suggest that TDP2 could affect the response of tumour cells to chemotherapy. In this context, TDP2 expression is reportedly elevated in the majority of non-small cell lung cancer cells [43], and mutant-p53-dependent over-expression of TDP2 has been implicated in cellular resistance to etoposide in lung cancer cells [44]. TDP2 might therefore be a valid target for overcoming tumour resistance to TOP2 poisons and/or a useful predictive biomarker for clinical response to these agents.

In addition, our toxicity assays in mice and the increased genome instability in cells and in mouse bone marrow correlate well with known side effects of treatment with TOP2 poisons during cancer therapy. This raises the possibility that heterogeneity in expression levels or activity of TDP2 could be an

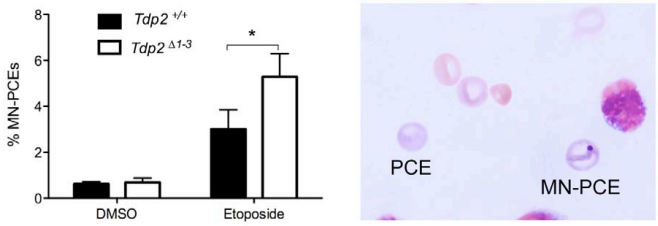

Figure 7. The absence of TDP2 increases etoposide-induced genome instability *in vivo*. Percentage of micronucleated polychromatic erythrocytes (MN-PCE) among the total number of polychromatic erythrocytes (PCE), examples of which are shown (right), in bone marrow smears of wild-type and *Tdp2*$^{\Delta 1-3}$ mice 24 h after intraperitoneal injection of 1 mg/kg etoposide or vehicle (10% DMSO). Average ± s.e.m. of 4 (DMSO) and 6 (VP16) animals and statistical significance by paired T test is shown.
doi:10.1371/journal.pgen.1003226.g007

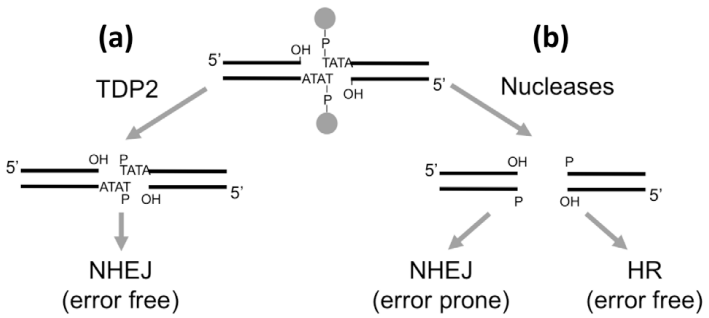

Figure 8. Model for the repair of TOP2-induced DSBs. (a) TDP2-mediated cleavage of the 5′ phosphodiester link between TOP2 peptide and DNA results in 3′ hydroxyl (OH) 5′ phosphste (P) cohesive ends that are easily ligatable by NHEJ resulting in error-free repair. (b) Alternatively, nucleolytic attack on the DNA backbone can also remove the protein adduct from the DSB but genetic information is lost from the ends. Accurate repair of this break would therefore need HR to copy the missing information from the sister chromatid, while NHEJ would result in error-prone repair.
doi:10.1371/journal.pgen.1003226.g008

important etiological factor both in the toxicity that accompanies chemotherapy involving TOP2 poisons [45] and on the incidence of treatment-related hematological malignancy, typically acute leukemia occurring in a relatively high proportion of patients [4,7,8]. Like other acute leukemias, therapy-related malignancies are linked to specific translocations that result in the expression of fusion proteins and contribute in some way to disease development. Intriguingly, in some cases, these translocations map to regions of preferential TOP2 cleavage, supporting a model in which the translocations arise via erroneous repair of TOP2-induced DSBs. These translocations are also surprisingly similar to those found in infant leukemia [46], suggesting that erroneous repair of TOP2-induced DSBs may also be a source of primary malignancy. Consistent with this idea, TOP2-induced DSBs are implicated in translocations commonly associated with prostate cancer [47]. In the light of our findings, it is tempting to speculate that TDP2 activity reduces the likelihood of oncogenic translocations, by ensuring rapid and accurate repair of TOP2-induced DSBs. It is possible, however, that TDP2 might occasionally promote a translocation, by liberating a DSB that engages in erroneous DNA ligation, as might be the case in some extremely conservative rearrangements that have been reported [12,13].

Conclusions

We have shown that TDP2 protects mouse cells from the cytotoxic and clastogenic effects of TOP2 poisons, most likely by functioning in error-free pathway for NHEJ. These results have important implications in the treatment of cancer. For example, development of small molecule inhibitors for TDP2 may provide a way of sensitizing particular types of tumor to chemotherapy, though precaution is necessary to consider the possible consequences of TDP2 inhibition on normal cells and on the generation of secondary malignancies.

Materials and Methods

Ethics statement

All animal procedures were performed in accordance with European Union legislation and with the approval of the Ethical Committee for Animal Experimentation of the University of Leuven and the University of Seville, respectively.

Cells and cell culture

Chicken DT40 B lymphoma cells were cultured at 39°C, 5% CO_2 in RPMI 1640 medium supplemented with 10^{-5} M β-mercaptoethanol, penicillin, streptomycin, 10% fetal calf serum (FCS), and 1% chicken serum (Sigma). *TDP2*$^{-/-/-}$ cell line was previously described [25]. To generate *KU70* deletion constructs, Hygromycin (Hygro^R) or Neomycin (Neo^R) resistance cassettes were inserted between sequences of 1.6 kb and 3.3 kb in length from the *KU70* locus [48]. KU70-Hygro^R and KU70-Neo^R deletion constructs were sequentially transfected into wild-type and *TDP2*$^{-/-/-}$ cells. The gene targeting events were confirmed by Southern blot analysis of *EcoRI* -digested genomic DNA hybridized to an external probe (Figure S1).

Transformed human fibroblast lines 1BR (wild-type) and HSC62 (BRCA2-mutant) were described previously [49]. Cells were cultured in DMEM supplemented with penicillin, streptomycin and 15% FCS.

Primary MEFs were isolated from littermate embryos at day 13 p.c. and cultured at 37°C, 5% CO_2, 3% O_2 in Dubelcco's Modified Eagle's Medium (DMEM) supplemented with penicillin, streptomycin, 10% FCS and non-essential aminoacids. All experiments were carried out between P2 and P4. MEFs were transformed by retroviral delivery of T121, a fragment of the SV40 large T antigen that antagonizes the three Rb family members but not p53 [50]. Transformed MEFs were maintained at 37°C, 5% CO_2 in DMEM supplemented with penicillin, streptomycin and 10% FCS.

Generation of Tdp2 conditional and knockout mice

A targeting construct was generated for *Tdp2* in which the first three exons were flanked by *lox*P sites, followed by an FRT- and *lox*P-flanked neomycin-resistance (neo) cassette. These three exons encode for the N-terminal half of TDP2 and contain mapped interaction domains for e.g. TDP2 itself, CD40 and TRAF6 [23]. The *Tdp2*$^{flEx1-3,neo}$ targeting construct was electroporated in E14 (129Ola) ES cells and correctly recombined ES cell clones were confirmed by Southern blot analysis. The functionality of the *lox*P sites was shown *in vitro* by electroporation of a correctly targeted ES cell clone with a Cre-expressing vector. Several correctly targeted ES cell clones were used for aggregation with CD1 morulae and transferred into pseudo-pregnant recipient females to

obtain chimaeric mice. Three chimaeric males produced heterozygous offspring after breeding with CD1 wild-type females. The obtained offspring was genotyped with both a *lox*P-specific and a neo-specific PCR. Intercrosses between $Tdp2^{flEx1-3,neo/+}$ mice led to the generation of homozygous floxed *Tdp2* mice which were viable and fertile. To delete the critical exons we crossed the heterozygous *Tdp2* mice with an EIIa-Cre mouse (Adenovirus EIIa-promoter driven Cre) and obtained $Tdp2^{flA/+}$ mice. Intercrosses of the latter mice resulted in viable homozygous knockout mice (from now on denoted $Tdp2^{A1-3}$) at the normal 25% Mendelian distribution. Southern blot analysis confirmed the complete recombination of the *lox*P-flanked sequences in the homozygous mice and hence the generation of *Tdp2* knockout mice.

5′-TDP activity *in vitro*

Labelled double-stranded 5′-phosphotyrosyl substrates were generated essentially as previously described [22,22,25]. For 5′ overhang substrates 5′-Y-P-AATTCTTCTCTTTCCAGGGC-TATGT-3′ (Midland Certified Reagents) and 5′-AGACA-TAGCCCTGGAAAGAGAAG-3′ (Sigma) oligonucleotides were annealed. Cell and tissue extracts were prepared by mild sonication in Lysis Buffer (40 mM Tris–HCl, pH 7.5, 100 mM NaCl, 0.1% Tween-20, 1 mM DTT) supplemented with 1 mM PMSF and protease inhibitor cocktail (Sigma) and clarification by centrifugation 10 min 16500 g 4°C. Protein concentration was measured with Bradford reagent (Sigma). 5′-TDP reactions contained 50 nM substrate, 80 µM competitor single-stranded oligonucleotide and the indicated amount of protein extract in a total volume of 6 µl Reaction Buffer (50 mM Tris-Cl, pH 7.5, 50 mM KCl, 1 mM $MgCl_2$, 1 mM DTT, 100 µg/ml BSA). Ligation reactions with oligos contained in addition 5 units of T4 DNA ligase (Fermentas) and 1 mM ATP (Sigma) Reactions were stopped by the addition of 3 µl 3× Formamide Loading Buffer and 5 min 95°C incubation. Samples were resolved by denaturing polyacrylamide gel electrophoresis and analysed by phosphorimaging in a Fujifilm FLA5100 device (GE Healthcare).

Plasmid circularization assays

Substrates were generated by PCR-mediated amplification of plasmid pEGFP-Pem1-Ad2 [51] with primers 5′-AATTCTTCTCTTTCCAGGGCTATGT-3′ and 5′- AATT-CATCCCCAGAAATGTAACTTG-3′ harbouring phosphate (Sigma) or phosphotyrosine (Midland Certified Reagents) moieties at 5′ ends. NHEJ-competent nuclear extracts were prepared as previously described [28]. Reactions were performed by incubating (6 h at 16°C) 100 ng of each substrate with 7 µg of nuclear extracts in NHEJ Buffer (50 mM Tris-HCl pH 7.5, 50 mM KCl, 1 mM DTT, 2 mM MgCl2, 1 mM ATP, 100 µg/ml BSA) in the presence or absence of 50 nM hTDP2 recombinant protein (purified as previously described [22]). Reactions were stopped by addition of EDTA (to a final concentration of 100 mM) and treated 30′ with Proteinase K (0.2 mg/ml). DNA was purified using FavorPrep GEL/PCR Purification Mini Kit (Favorgen) and transformed into MegaX DH10B T1 Electrocompetent Cells (Invitrogen). Positive transformants were selected by plating on LB agar plates containing kanamycin (25 µg/ml).

Clonogenic survival assays

To determine sensitivity in DT40, cells were plated in 5 ml of medium containing 1.5% (by weight) methylcellulose (Sigma) in 6-well plates at 50, 500, and 5000 cells/well per treatment condition. Media also contained the indicated concentration of doxorubicin (Sigma), mAMSA (Sigma) or etoposide (Sigma). In all experiments, cells were incubated for 7–11 days and visible colonies were counted.

Survival assays in MEFs were carried out seeding 2000 cells in 100 mm dishes, in duplicate for each experimental condition. After 6 hours, cells were irradiated or treated with the indicated concentrations of etoposide for 3 hours, washed with PBS and fresh medium was added. Cells were incubated for 10–14 days and fixed and stained for colony scoring in Crystal violet solution (0.5% Crystal violet in 20% ethanol). The surviving fraction at each dose was calculated by dividing the average number of visible colonies in treated versus untreated dishes.

Human fibroblasts were transfected with non-targeting Negative Control and *TDP2* smartpool siRNAs (Thermo Scientific) using HyperFect transfection reagent (Invitrogen). Cells were transfected twice in two consecutive days and used for survival 48 hours after second transfection. Other details as described above.

Immunofluorescence and antibodies

MEFs grown on coverslips for the required time, 7 days for confluency-arrested cells and 2 days for cycling cells, were treated as indicated and fixed (10 min in PBS-4% paraformaldehyde), permeabilized (2 min in PBS-0.2% Triton X-100), blocked (30 min in PBS-5% BSA) and incubated with the required primary antibodies (1–3 h in PBS-1% BSA). Cells were then washed (3×5 min in PBS-0.1% Tween 20), incubated for 30 min with the corresponding AlexaFluor-conjugated secondary antibodies (1/1000 dilution in 1% BSA-PBS) and washed again as described above. Finally, they were counterstained with DAPI (Sigma) and mounted in Vectashield (Vector Labs). Rad51 foci scoring requires 30 sec. pre-extraction in PBS-0.1% Triton X-100 prior to fixation. γH2AX and Rad51 foci were manually counted (double-blind) in 40 cells from each experimental condition. When necessary to identify replicating cells, 5-ethynyl-2′-deoxyuridine (EdU, Invitrogen) was added throughout treatment and repair at a final concentration of 10 µM. Click chemistry reaction was performed before DAPI staining by incubating (30 min r.t.) with 1 µM AlexaFluor-conjugated azide (Invitrogen) in reaction cocktail (100 mM TrisHCl pH 8.5, 1 mM $CuSO_4$, 100 mM ascorbic acid). For the analysis of G0/G1 confluency-arrested cells only Cyclin A negative cells were scored. For G2, as EdU was present (10 µM) during and after treatment, only Cyclin A positive cells without EdU incorporation were scored (see Figure S3). Primary antibodies were used at the indicated dilution: γH2AX (Millipore, 05-636) 1/1000, Cyclin A (Santa Cruz, sc-751) 1/500, Rad51 (Abcam, ab213) 1/200 and Tubulin (Santa Cruz, sc-5286) 1/2500.

Cytogenetic analysis

Micronuclei and nucleoplasmic bridges were analysed in transformed and low passage primary MEFs previously seeded onto coverslips. Following treatment, cytochalasin B (Sigma) was added at 4 µg/ml to transformed but not to primary MEFs. 22 h (transformed) or 30 h (primary) post-treatment, cells were fixed and subject to DAPI staining as described above. In transformed cells only binucleated cells were scored, which was confirmed by visualization of the cytoplasm with anti Tubulin immunofluorescence (performed as described above).

Chromosomal aberrations were scored in Giemsa stained metaphase spreads. Following treatment, recovery in fresh medium was allowed for 2 h (transformed MEFs) or 4 h (primary MEFs) and demecolcine (Sigma) was added at a final concentration of 0.2 µg/ml. Caffeine (Sigma) was also added at a final concentration of 0.1 µg/ml but only to primary cells. 4 h later cells were collected by trypsinisation, subject to hypotonic shock for

1 hour at 37°C in 0.3 M sodium citrate and fixed in 3:1 methanol:acetic acid solution. Cells were dropped onto acetic acid humidified slides and stained 20 minutes in Giemsa-modified (Sigma) solution (5% v/v in H_2O).

For SCEs 10 µM BrdU (Sigma) was added to the medium for two complete cycles (approximately 48 hours) before collection. Drug treatment was applied for 30 minutes 6–8 hours before cell collection. Metaphase spreads were obtained as described above. Before Giemsa staining, slides were incubated in Hoescht 33258 solution (10 µg/ml) for 20 minutes, exposed to UV light (355 nm) for 1 hour and washed for 1 hour at 60°C in 20× SCC.

Animal maintenance

The mouse colony was maintained in an outbred 129Ola, CD1 and C57BL/6 background under standard housing conditions, at 21±1°C with a photoperiod of 12:12 h (lights on at 8:00). They were housed in isolated cages with controlled ventilation trough HEPA-filters and were in flow cabins. Sterile food pellets and water were available *ad libitum*. Breeding pairs between heterozygotes ($Tdp2^{+/flΔ}$×$Tdp2^{+/flΔ}$) were set to obtain wild-type ($Tdp2^{+/+}$) and knock-out ($Tdp2^{Δ1–3}$) littermates for analysis. Mice were genotyped with Phire Animal Tissue Direct PCR Kit (Thermo) following manufacturer instructions and using primers 5′-CCTTCATTACTTCTCGTAGGTTCTGGGTC-3′, 5′-ACCCGCTCTTCACGCTGCTTCC-3′ and 5′-TACACCGTGCCATAATGACCAAC-3′. This results in amplification of a 429 bp fragment from the wild-type allele or 561 bp fragment from the mutant allele.

In vivo etoposide sensitivity

At 8 weeks of age, $Tdp2^{+/+}$ and $Tdp2^{Δ1–3}$ mice underwent intraperitoneal injection with 3 µl/g of body weight of either DMSO (vehicle control) or etoposide at 25 mg/ml in DMSO for a final dose of 75 mg/kg. Weight and general health status was monitored daily from the day of injection (inclusive). 6 days post-treatment mice were sacrificed by cervical dislocation and dissected for histopathological analysis. Weight of spleen and thymus was recorded prior to their histological or cell content analysis. Bone marrow (BM) from femurs and tibias of each mouse was also obtained.

For histological analysis organs were fixed in 4% paraformaldehyde for 2 days, embedded in paraffin, cut in 6 µm slices by microtome, stained with Hematoxylin-Eosin and visualized under the microscope. For cell content analysis by FACS, BM and thymus were homogenized in EDTA Buffer (140 mM NaCL, 1.5 mM KH_2PO_4, 2.7 mM KCl, 8.1 mM Na_2HPO_4, 0.6 mM EDTA). Cells from both tissues were immunolabelled with the appropriate fluorescently-labelled antibodies according to manufacture's recommendations and analyzed using a FACScalibur flow cytometer (Becton Dickinson): B220-APC (17-0452), CD43 FITC (11-0431), CD8 APC (17-0081) and CD4 FITC (11-0043) (eBiosciences); CD11b/Mac-1 PE (550019) (Becton Dickinson). Data was compiled and analysed using CellQuest software (Becton Dickinson).

Micronuclei analysis *in vivo*

At 8 weeks of age, $Tdp2^{+/+}$ and $Tdp2^{Δ1–3}$ mice underwent intraperitoneal injection with 2.5 µl/g of body weight of either 10% DMSO (vehicle control) or etoposide at 400 µg/ml in 10% DMSO for a final dose of 1 mg/kg. Mice were sacrificed by cervical dislocation 24 h after injection and BM from one femur and tibia was extracted and homogenized in 3 ml FBS. Cellular content was concentrated in 150 µl FBS by centrifugation and smears were prepared on glass slides. Following 5 min fixation in methanol, slides were stained 30 min in Giemsa-modified (Sigma) solution (5% v/v in 100 mM Tris-HCl pH 6.8) and visualized under the microscope. 2000 polychromatic erythrocytes (PCE) were scored for the presence of micronuclei (MN-PCE) in each slide.

Supporting Information

Figure S1 TDP2 promotes survival following TOP2-induced DSBs in mammalian cells. Clonogenic survival of wild-type and Tdp2Δ1–3 transformed MEFs after continuous exposure to the indicated concentrations of etoposide. Average ± s.e.m. of three independent experiments and statistical significance by Two-way ANOVA test with Bonferroni post-test is shown.
(TIF)

Figure S2 Targeted deletion of *KU70* in DT40 cells. Southern-blot analysis of *EcoRI*-digested DNA from wild-type (+/+), heterozygous (+/−) and knock-out (−/−) DT40 cells in $TDP2^{+/+/+}$ and $TDP2^{-/-/-}$ background. A probe hybridizing to a region of the *KU70* locus not contained in the deletion construct was used. The 5.5-kb (wild-type) and 2.8-kb (deleted) expected bands are indicated. Note that two clones were selected for further analysis.
(TIF)

Figure S3 Cell cycle dependent induction of DSBs following etoposide treatment in primary MEFs. DSBs detected as γH2AX foci (bottom left), Cyclin A content (Cyc A, top right), 5-ethynyl-2′-deoxyuridine incorporation (EdU, bottom right) and DAPI counterstain (top left) are shown. G1 (Cyc A negative, EdU negative), S-phase (Cyc A positive, EdU positive) and G2 (Cyc A positive, EdU positive) nuclei are indicated (arrows).
(TIF)

Figure S4 TDP2 depletion impairs repair of TOP2-induced DSBs in human A549 cells. A. γH2AX foci induction after 30 min 50 µM etoposide treatment and repair at different times following drug removal in G1 TDP2-depleted (pS-TDP2) and control non-depleted (pS) cells. B. G2 cells with 10 µM etoposide treatment. Other details as in "A". Average ± s.e.m. of at least three independent experiments is shown. Statistical significance by Two-way ANOVA test with Bonferroni post-test is indicated. TDP2 depletion was performed as previously described [22].
(TIF)

Figure S5 The absence of TDP2 sensitizes lymphocyte precursors to etoposide treatment *in vivo*. FACS analysis of B-cells in bone marrow (A) and T-cells in thymus (B) in wild-type and $Tdp2^{Δ1–3}$ animals 6 days after treatment with 75 mg/kg etoposide or vehicle control (DMSO). Pro-B cell ($CD43^+$ $B220^+$), Pre-B cell ($CD43^-$ $B220^{low}$) immature B cell ($CD43^-$ $B220^{high}$) and immature T cell ($CD4^+$ $CD8^+$) populations are indicated (rectangles).
(TIF)

Figure S6 Myeloid cells are not significantly affected by etoposide treatment. FACS analysis of $Mac1^+$ myeloid cells in bone marrow in wild-type and $Tdp2^{Δ1–3}$ animals 6 days after treatment with 75 mg/kg etoposide or vehicle control (DMSO). Scatter plot (A) and quantification (B) are shown. The mild increase correlates with the observed decrease in lymphocite precursors.
(TIF)

Acknowledgments

We thank C. Cruz for technical support in histological analysis, M. J. Sánchez for antibodies and expert advice in hematopoietic study, and P. Jeggo for cell lines.

Author Contributions

Conceived and designed the experiments: FG-H RR-G ZZ AÁ-Q KWC FC-L. Performed the experiments: FG-H RR-G ZZ AÁ-Q CQ. Analyzed the data: FG-H RR-G ZZ AÁ-Q KWC FC-L. Wrote the paper: FG-H KWC FC-L. Designed and generated the mouse model: LU LV DH. Technical support: CQ LJ.

References

1. Champoux JJ (2001) DNA topoisomerases: structure, function, and mechanism. Annu Rev Biochem 70: 369–413. doi:10.1146/annurev.biochem.70.1.369
2. Wang JC (2002) Cellular roles of DNA topoisomerases: a molecular perspective. Nat Rev Mol Cell Biol 3: 430–440. doi:10.1038/nrm831
3. Nitiss JL (2009) DNA topoisomerase II and its growing repertoire of biological functions. Nat Rev Cancer 9: 327–337. doi:10.1038/nrc2608
4. Deweese JE, Osheroff N (2009) The DNA cleavage reaction of topoisomerase II: wolf in sheep's clothing. Nucleic Acids Res 37: 738–748. doi:10.1093/nar/gkn937
5. Nitiss JL (2009) Targeting DNA topoisomerase II in cancer chemotherapy. Nat Rev Cancer 9: 338–350. doi:10.1038/nrc2607
6. Anderson RD, Berger NA (1994) International Commission for Protection Against Environmental Mutagens and Carcinogens. Mutagenicity and carcinogenicity of topoisomerase-interactive agents. Mutat Res 309: 109–142.
7. Felix CA, Kolaris CP, Osheroff N (2006) Topoisomerase II and the etiology of chromosomal translocations. DNA Repair (Amst) 5: 1093–1108. doi:10.1016/j.dnarep.2006.05.031
8. Povirk LF (2006) Biochemical mechanisms of chromosomal translocations resulting from DNA double-strand breaks. DNA Repair (Amst) 5: 1199–1212. doi:10.1016/j.dnarep.2006.05.016
9. Albain KS, Le Beau MM, Ullirsch R, Schumacher H (1990) Implication of prior treatment with drug combinations including inhibitors of topoisomerase II in therapy-related monocytic leukemia with a 9;11 translocation. Gene Chromosome Canc 2: 53–58.
10. Ahuja HG, Felix CA, Aplan PD (2000) Potential role for DNA topoisomerase II poisons in the generation of t(11;20)(p15;q11) translocations. Gene Chromosome Canc 29: 96–105.
11. Andersen MK, Christiansen DH, Jensen BA, Ernst P, Hauge G, et al. (2001) Therapy-related acute lymphoblastic leukaemia with MLL rearrangements following DNA topoisomerase II inhibitors, an increasing problem: report on two new cases and review of the literature since 1992. Br J Haematol 114: 539–543.
12. Lovett BD, Lo Nigro L, Rappaport EF, Blair IA, Osheroff N, et al. (2001) Near-precise interchromosomal recombination and functional DNA topoisomerase II cleavage sites at MLL and AF-4 genomic breakpoints in treatment-related acute lymphoblastic leukemia with t(4;11) translocation. Proc Natl Acad Sci USA 98: 9802–9807. doi:10.1073/pnas.171309898
13. Whitmarsh RJ, Saginario C, Zhuo Y, Hilgenfeld E, Rappaport EF, et al. (2003) Reciprocal DNA topoisomerase II cleavage events at 5"-TATTA-3" sequences in MLL and AF-9 create homologous single-stranded overhangs that anneal to form der(11) and der(9) genomic breakpoint junctions in treatment-related AML without further processing. Oncogene 22: 8448–8459. doi:10.1038/sj.onc.1207052
14. Mistry AR, Felix CA, Whitmarsh RJ, Mason A, Reiter A, et al. (2005) DNA topoisomerase II in therapy-related acute promyelocytic leukemia. N Engl J Med 352: 1529–1538. doi:10.1056/NEJMoa042715
15. Giguère A, Hébert J (2011) Microhomologies and topoisomerase II consensus sequences identified near the breakpoint junctions of the recurrent t(7;21)(p22;q22) translocation in acute myeloid leukemia. Gene Chromosome Canc 50: 228–238. doi:10.1002/gcc.20848
16. Le H, Singh S, Shih S-J, Du N, Schnyder S, et al. (2009) Rearrangements of the MLL gene are influenced by DNA secondary structure, potentially mediated by topoisomerase II binding. Gene Chromosome Canc 48: 806–815. doi:10.1002/gcc.20685
17. Mirault M-E, Boucher P, Tremblay A (2006) Nucleotide-resolution mapping of topoisomerase-mediated and apoptotic DNA strand scissions at or near an MLL translocation hotspot. Am J Hum Genet 79: 779–791. doi:10.1086/507791
18. Connelly JC, Leach DRF (2004) Repair of DNA covalently linked to protein. Mol Cell 13: 307–316.
19. Kurosawa A, Koyama H, Takayama S, Miki K, Ayusawa D, et al. (2008) The requirement of Artemis in double-strand break repair depends on the type of DNA damage. DNA Cell Biol 27: 55–61. doi:10.1089/dna.2007.0649
20. Sartori AA, Lukas C, Coates J, Mistrik M, Fu S, et al. (2007) Human CtIP promotes DNA end resection. Nature 450: 509–514. doi:10.1038/nature06337
21. Quennet V, Beucher A, Barton O, Takeda S, Löbrich M (2011) CtIP and MRN promote non-homologous end-joining of etoposide-induced DNA double-strand breaks in G1. Nucleic Acids Res 39: 2144–2152. doi:10.1093/nar/gkq1175
22. Cortes Ledesma F, Khamisy El SF, Zuma MC, Osborn K, Caldecott KW (2009) A human 5′-tyrosyl DNA phosphodiesterase that repairs topoisomerase-mediated DNA damage. Nature 461: 674–678. doi:10.1038/nature08444
23. Pype S, Declercq W, Ibrahimi A, Michiels C, Van Rietschoten JG, et al. (2000) TTRAP, a novel protein that associates with CD40, tumor necrosis factor (TNF) receptor-75 and TNF receptor-associated factors (TRAFs), and that inhibits nuclear factor-kappa B activation. J Biol Chem 275: 18586–18593. doi:10.1074/jbc.M000531200
24. Pei H, Yordy JS, Leng Q, Zhao Q, Watson DK, et al. (2003) EAPII interacts with ETS1 and modulates its transcriptional function. Oncogene 22: 2699–2709. doi:10.1038/sj.onc.1206374
25. Zeng Z, Cortes Ledesma F, Khamisy El SF, Caldecott KW (2011) TDP2/TTRAP is the major 5′-tyrosyl DNA phosphodiesterase activity in vertebrate cells and is critical for cellular resistance to topoisomerase II-induced DNA damage. J Biol Chem 286: 403–409. doi:10.1074/jbc.M110.181016
26. Shrivastav M, De Haro LP, Nickoloff JA (2008) Regulation of DNA double-strand break repair pathway choice. Cell Res 18: 134–147. doi:10.1038/cr.2007.111
27. Murai J, Huang S-YN, Das BB, Dexheimer TS, Takeda S, et al. (2012) Tyrosyl-DNA phosphodiesterase 1 (TDP1) repairs DNA damage induced by topoisomerases I and II and base alkylation in vertebrate cells. J Biol Chem 287: 12848–12857. doi:10.1074/jbc.M111.333963
28. Baumann P, West SC (1998) DNA end-joining catalyzed by human cell-free extracts. Proc Natl Acad Sci USA 95: 14066–14070.
29. Löbrich M, Shibata A, Beucher A, Fisher A, Ensminger M, et al. (2010) gammaH2AX foci analysis for monitoring DNA double-strand break repair: strengths, limitations and optimization. Cell Cycle 9: 662–669.
30. Huertas P (2010) DNA resection in eukaryotes: deciding how to fix the break. Nat Struct Mol Biol 17: 11–16. doi:10.1038/nsmb.1710
31. Sonoda E, Sasaki MS, Morrison C, Yamaguchi-Iwai Y, Takata M, et al. (1999) Sister chromatid exchanges are mediated by homologous recombination in vertebrate cells. Mol Cell Biol 19: 5166–5169.
32. Takahashi N, Kadota T, Kawano S, Ishikawa K, Kuroyanagi K, et al. (1986) [Toxicity studies of VP 16-213 (I)–Acute toxicity in mice, rats and rabbits]. J Toxicol Sci 11 Suppl 1: 1–16.
33. Li C, Sun S-Y, Khuri FR, Li R (2011) Pleiotropic functions of EAPII/TTRAP/TDP2: cancer development, chemoresistance and beyond. Cell Cycle 10: 3274–3283. doi:10.4161/cc.10.19.17763
34. Barthelmes HU, Habermeyer M, Christensen MO, Mielke C, Interthal H, et al. (2004) TDP1 overexpression in human cells counteracts DNA damage mediated by topoisomerases I and II. J Biol Chem 279: 55618–55625. doi:10.1074/jbc.M405042200
35. Nitiss KC, Malik M, He X, White SW, Nitiss JL (2006) Tyrosyl-DNA phosphodiesterase (Tdp1) participates in the repair of TOP2–mediated DNA damage. Proc Natl Acad Sci USA 103: 8953–8958. doi:10.1073/pnas.0603455103
36. Zeng Z, Sharma A, Ju L, Murai J, Umans L, et al. (2012) TDP2 promotes repair of topoisomerase I-mediated DNA damage in the absence of TDP1. Nucleic Acids Res. doi:10.1093/nar/gks622
37. Symington LS, Gautier J (2011) Double-strand break end resection and repair pathway choice. Annu Rev Genet 45: 247–271. doi:10.1146/annurev-genet-110410-132435
38. de Campos-Nebel M, Larripa I, González-Cid M (2010) Topoisomerase II-mediated DNA damage is differently repaired during the cell cycle by non-homologous end joining and homologous recombination. PLoS ONE 5: e12541. doi:10.1371/journal.pone.0012541
39. Li GC, Ouyang H, Li X, Nagasawa H, Little JB, et al. (1998) Ku70: a candidate tumor suppressor gene for murine T cell lymphoma. Mol Cell 2: 1–8.
40. Pierce AJ, Hu P, Han M, Ellis N, Jasin M (2001) Ku DNA end-binding protein modulates homologous repair of double-strand breaks in mammalian cells. Genes Dev 15: 3237–3242. doi:10.1101/gad.946401
41. Saintigny Y, Delacôte F, Boucher D, Averbeck D, Lopez BS (2007) XRCC4 in G1 suppresses homologous recombination in S/G2, in G1 checkpoint-defective cells. Oncogene 26: 2769–2780. doi:10.1038/sj.onc.1210075
42. Cortes Ledesma F, Prado F, Aguilera A (2007) Sister chromatid recombination. In: Aguilera A, Rothstein R, editors. Top Curr Genet 17 (Molecular Genetics of Recombination). Berlin Heidelberg: Springer-Verlag. pp. 363–380.
43. Li C, Fan S, Owonikoko TK, Khuri FR, Sun S-Y, et al. (2011) Oncogenic role of EAPII in lung cancer development and its activation of the MAPK-ERK pathway. Oncogene 30: 3802–3812. doi:10.1038/onc.2011.94
44. Do PM, Varanasi L, Fan S, Li C, Kubacka I, et al. (2012) Mutant p53 cooperates with ETS2 to promote etoposide resistance. Genes Dev 26: 830–845. doi:10.1101/gad.181685.111
45. Wolff SN, Hainsworth JD, Greco FA (2008) High-dose etoposide: from phase I to a component of curative therapy. J Clin Oncol 26: 5310–5312. doi:10.1200/JCO.2008.19.0892
46. Langer T, Metzler M, Reinhardt D, Viehmann S, Borkhardt A, et al. (2003) Analysis of t(9;11) chromosomal breakpoint sequences in childhood acute leukemia: almost identical MLL breakpoints in therapy-related AML after treatment without etoposides. Gene Chromosome Canc 36: 393–401. doi:10.1002/gcc.10167
47. Haffner MC, Aryee MJ, Toubaji A, Esopi DM, Albadine R, et al. (2010) Androgen-induced TOP2B-mediated double-strand breaks and prostate cancer gene rearrangements. Nat Genet 42: 668–675. doi:10.1038/ng.613

48. Takata M, Sasaki MS, Sonoda E, Morrison C, Hashimoto M, et al. (1998) Homologous recombination and non-homologous end-joining pathways of DNA double-strand break repair have overlapping roles in the maintenance of chromosomal integrity in vertebrate cells. EMBO J 17: 5497–5508. doi:10.1093/emboj/17.18.5497
49. Beucher A, Birraux J, Tchouandong L, Barton O, Shibata A, et al. (2009) ATM and Artemis promote homologous recombination of radiation-induced DNA double-strand breaks in G2. EMBO J 28: 3413–3427. doi:10.1038/emboj.2009.276
50. Sáenz Robles MT, Symonds H, Chen J, Van Dyke T (1994) Induction versus progression of brain tumor development: differential functions for the pRB- and p53-targeting domains of simian virus 40 T antigen. Mol Cell Biol 14: 2686–2698.
51. Seluanov A, Mittelman D, Pereira-Smith OM, Wilson JH, Gorbunova V (2004) DNA end joining becomes less efficient and more error-prone during cellular senescence. Proc Natl Acad Sci USA 101: 7624–7629. doi:10.1073/pnas.0400726101